University of Pavia
Faculty of Engineering
Department of Civil Engineering and Architecture

3D Concrete Printing: a new Era in Construction Industry

Lorenzo Casagrande, M.Sc.

Supervisor: Prof. Ing. Ferdinando Auricchio

This dissertation is submitted for the degree of

Doctor of Philosophy

October 2019

Italian Abstract

La manifattura additiva nel settore delle costruzioni fornisce vantaggi in termini di miglioramento del tasso di produzione, di flessibilità architettonica e di riduzione dei costi, ponendo nuove sfide ingegneristiche. Molte di queste sfide consistono nell'ottimizzare la compatibilità del calcestruzzo con i peculiari aspetti del processo realizzativo, a cui si associano specifici requisiti meccanici. Tuttavia, indagando le procedure di prova, risulta chiaro come fino ad oggi nessuna linea guida sia stata riconosciuta; ne consegue che i ricercatori possono riferirsi o a tipologie di test sviluppate per terreni o per calcestruzzi induriti, dando vita ad una scarsa capacità di predizione. Questo lavoro tratta il monitoraggio dell'evoluzione della resistenza meccanica di calcestruzzi stampabili, monitorando cioè quando il materiale si trasforma dallo stato fresco a quello indurito.

Inizialmente sono stati delineati i fondamenti del 3D Concrete Printing, assieme ad un analisi dettagliata della successione cronologica di letteratura, dove sono state evidenziate le potenzialità e le sfide del metodo. Successivamente un mix stampabile in 3D è stato sviluppato e testato: precisamente, tre tipologie di test sono state prese in considerazione, cioè, prove a compressione uniassiali non confinate, prove a compressione uniassiali per creep e test reologici. Al fine di definire una struttura per i futuri test, sono state considerate quattro variabili che potenzialmente influenzano la buildaiblity e il creep: (i) la maturazione dallo stato fresco, (ii) la percentuale di superfluidificante, (iii) l'utilizzo di una membrana durante la produzione dei provini e (iv) il tasso di spostamento. Contrariamente, i test reologici sono stati effettuati variando unicamente la percentuale di superfluidificante. Infine viene inoltre fornita una struttura analitica per la predizione del collasso.

Abstract

Nowadays, additive manufacturing in construction industry gives advantages in terms of improved production rate, architectural flexibility and cost reduction, posing new engineering challenges. Most of these challenges consist in optimizing the concrete compatibility with the extrusion and the buildup process, resulting in specific mechanical requirements. However, focusing on testing procedure, it is clear that until now no standards are recognized; it comes out that authors may refer either to soil or to hardened testing, giving rise to a scarce prediction capability. As a result, this work deals with the monitoring of 3D printable concrete mechanical strength evolution, i.e., when the early age mix develops from the fresh to the hardened state.

Initially, fundamentals of 3D Concrete Printing are outlined, along with a breakdown of the chronological succession of literature documents where potentials and challenges of the method are highlighted. Subsequently, a 3D printable concrete mix has been developed and tested: in detail, three testing typologies are explored, i.e., uniaxial unconfined compression tests, uniaxial compression creep tests and rheological tests. In order to define a dedicated testing framework, we consider four variables that may affect results influencing buildability and creep: (i) the early age curing time, (ii) the percentage of superplasticizer, (iii) the employment of membrane during the sample casting and (iv) the displacement rate. By contrast, rheological tests are performed by varying only the percentage of superplasticizer. Finally, we provide an analytical framework for failure prediction.

Acknowledgments

This dissertation was written from 2017 to 2019 during my time spent as research scholar at the Department of Civil Engineering and Architecture (DICAr) at the University of Pavia, Italy. I would like to thank sincerly Prof. Ing. Ferdinando Auricchio for giving me the opportunity to work in his research group and for his valuable guidance as my doctoral supervisor.

Moreover, I would like to address my thanks to the reviewers of my dissertation, Prof. Ing. Liberato Ferrara and Prof. Ing. Mirian Velay-Lizancos. Their interest in my work and their helpful recommendations are gratefully appreciated.

In the course of my research project, I spent part of the time at the University of Naples Federico II, Italy. I want to thank Prof. Ing. Domenico Asprone, Prof. Ing. Costantino Menna and Ing. Laura Esposito for their kind hospitality and the good cooperation that we continued also afterwards.

Finally, I want to thank my family for their help and support at all times.

Pavia, October 2019 Lorenzo Casagrande

Contents

Notation and glossary

Throughout the work, the notation, abbreviations and symbols are described when first used. Abbreviations and symbols used across chapters are summarized in following.

Abbreviations

3D	Three-dimensional.
3DCP	3D Concrete Printing.
AM	Additive Manufacturing.
BIM	Building Information Modeling.
CAD	Computer Aided Design.
CAM	Computer Aided Manufacturing.
CC	Contour Crafting.
CCC	Contour Crafting Construction.
CCE	Conventional Construction Equipment.
CNC	Computer Numerically Controlled.
DF	Digital Fabrication.
DFC	Digital Fabrication Concrete.
FEM	Finite Element Method.
GGBFS	Ground-Granulated Blast-Furnace Slag.
GP	Geopolymers.
LE	Layered Extrusion.
n-ZEB	nearly Zero-Energy Buildings.
OPC	Ordinary Portland Cement.
POFA	Palm Oil Fuel Ash.
RCA	Recycled Coarse Aggregate.
RHA	Rice Husk Ash.
RM	Rapid Manufacturing.
RPS	Rapid Prototyping System.
RSD	Relative Standard Deviation.
SCCs	Self Compacting Concretes.
SDA	Saw Dust Ash.
SFF	Solid Freeform Fabrication.
TCT	Triaxial Compressive Test.
UCE	Unconventional Construction Equipment.
UUCT	Uniaxial Unconfined Compressive Test.
WFS	Waste Foundry Sand.

Chapter 1

Introduction

Digital fabrication techniques combined with suitable cementitious materials have successfully led to the implementation of innovative manufacturing processes for concrete-like products. Among the available techniques, significant advantages are expected in layered extrusion (LE) concrete technology, such as the reduction in construction time and cost (for labor and formworks), increase in worker safety, potential of freeform architectures, environmental benefits due to the saving of material waste (especially with respect to formworks), and achievable shape complexity. On the other hand, engineering challenges related to LE are several: larger machines required, design and characterization of materials, implementation of reinforcement, surface finishing, formation of cold joints, etc. Moreover, printed materials should satisfy specific rheological requirements in order to achieve an optimized balance between workability and extrudability on the one hand – which would require reduced pumping forces – and the need for buildability (i.e. ability to stacked concrete layers) on the other hand – which would require an increased strength.

1.1 Motivation

In this perspective, design the pre-print phase consists in optimizing the concrete compatibility with the automated printing system; unfortunately, rheological properties of 3D printed cementitious materials exhibit many dualities.

For instance, pumpability and extrudability require reduced yield stress and a relatively low plastic viscosity, while such parameters should increase to improve the buildability. Another duality lays in the building rate: on one hand, it should be fast enough to guarantee adequate bond strength between layers and to maintain the construction rate viable; on the other hand, it should be slow enough to provide sufficient buildability. Moreover, because of the absence of a rigid mould, high strength and high stiffness are required: after the fresh material deposition, each concrete layer must be able to carry the self-weight and the weight of the layers above it. Therefore, an experimental investigation is necessary to define mechanical properties of the material, in order to optimize the printing process and ensure the stability of the printed element. Furthermore, as mechanical properties change in time, their strength and stiffness are different for each deposited layer: this gap is higher as the time interval between individual layers increases.

As a result, the need to define a standard procedure is indisputable: early age printable

mortars have faster curing rate than classical casting concrete, affected by printability requirements. Hence, in order to test the material referring to a specific resting time, the experimental test must be carried out before the hardening occurs. Above we have qualitatively emphasized main challenges that need to be addressed in order to achieve a robust 3D concrete printing (3DCP) process and to determine minimum performance requirements. Meeting these criteria requires a comprehensive knowledge on early age concrete, incorporating insight on microstructural changes occurring during cement hydration. Therefore, in the present work the emphasis is posed on the evolution of strength and stiffness when the fresh mix develops from deformable to the hardened state: the mechanical behavior of fresh concrete is evaluated during the open and the layer-cycle time (within the range of 0 to 60 min after mixing, the typical duration of a 3D printing process).

1.2 Objectives

The aim of this work is to formulate a standard procedure in order to define mechanical properties of 3D printable cementitious material. To meet this demand, the following objectives are pursued:

- to sum up chronological steps in digital fabrication with concrete, along with a critical review of the available literature;
- to highlight current potential and challenges of 3D concrete printing;
- to define a 3D printable concrete mix;
- to introduce current testing objectives;
- to develop a standard procedure for uniaxial unconfined compression testing;
- to provide an analytical failure predictive model;
- to define a standard method for creep testing;
- to provide a standard procedure for rheological testing.

1.3 Outline

This work is organized in three parts: (i) the first part introduces a critical review of the literature, (ii) the second part summarizes the experimental campaign, (iii) the third part provides future developments and work synopsis. The content of the individual chapters is summarized in the following.

Part I: Concrete 3D printing - a critical review.

In **Chapter 2**, fundamentals of 3D concrete printing are outlined. The main purpose of this chapter is to introduce historical facts occurred in succession, as well as the breakdown of literature documents during the research. In **Chapter 3**, potential and challenges of the method are highlighted, along with hints for promising environmental objectives.

Part II: Experimental exploration of 3D printable cementitious materials.

Chapter 4 starts with a review of adoptable raw materials for mix design purposes and continues with the definition of the adopted 3D printable concrete mix. Motivated by challenges

of Chapter 3, the testing framework is discussed in **Chapter 5** providing a list of performance requirements and testing procedures for 3D printable concretes. To this end, the chapter starts formalizing testing challenges to be addressed. The second part of the chapter describes the testing campaign and provides an analytical failure predictive model.

Part III: Future developments: Circular Economy for a sustainable environments.

In **Chapter 6**, the work introduces a novel research project aimed to develop a sustainable digital manufacturing process, intended to suggest an innovative and environmentally viable 3D printable concrete. This work closes with concluding remarks in **Chapter 7**.

Part I

3D Concrete Printing - a critical review.

Chapter 2

The origins

After water, concrete is the second most consumed material worldwide and undoubtedly the most widespread construction material: on average, almost one ton of concrete is annually manufactured per capita. Such popularity is due to peculiar concrete attributes, i.e., the abundance of its constituent raw materials, the moderate relative cost and the natural tendency to transform from fluid to harden state, its excellent mechanical and durability properties. It follows that concrete represents de facto an engineered material and its applications are manifold.

Normally, concrete is poured into formworks and subsequently vibrated to manufacture structural and nonstructural components. Until the mid '90s, two alternatives had been developed to remove the compaction process: self-compacting and sprayed concretes. Self-compacting concretes (SCCs) were developed in 1988 in order to obtain more durable concrete structures, by means of limited aggregate content, low water-cement ratio and the use of superplasticizer. However, even if SCCs were much less labor-intensive, self-compacting concretes still needed the use of temporary formworks (which moreover could even be more expensive because of the higher pressure exerted by the fluid concrete).

Sprayed concrete was another technique, developed in 1914 and designed to minimize voids (by means of combined scale of aggregates), that utilized a support surface to eliminate or reduce temporary formworks. The mortar was pneumatically projected and therefore it had to be pumpable and sprayable. Nonetheless, as the shape of sprayed concrete components remains unprecise, such approach was mainly used to reinforce tunnel linings and domes.

Concrete 3D printing is a novel construction technique for manufacturing concrete elements without formworks, based on the nexus between concrete and digital fabrication. Indeed, digital fabrication (DF) with concrete is emerging as a set of promising technologies, able to efficiently and quickly create architectural elements, while at the same time contributing towards advancements in construction cost management and sustainability. Focusing on the layered extrusion manufacturing process, the moving head of an automated printing apparatus typically extrudes a fresh and viscous cementitious mixture in the form of layers following a digitalized path divided into several slices; each slice has a pre-defined thickness and it is repetitively placed on the previous layer until the end of the process, which yields the final concrete component. Engineering challenges originated by such digitalized manufacturing process are manifold, and specific mechanical properties are required for concrete printing. In the following, we propose a critical review beyond the origin of concrete 3D printing.

2.1 1995-2000: the Selective Aggregation

The first work concerning additive manufacturing applied to the construction industry is attributable to **Joseph Pegna**, 1995. Pegna [1, 2], addressed the question "Can Solid Freeform Fabrication (SFF) process deliver functional prototypes of meter size and above?". In detail, he reported an experimental process by which an irregular sample structure was built, by deposition and activation of reactive binders (Portland Cement) on a masked bed of powdered matrix material (granular sand), incrementally building-up layers of the structure. The binder was consequently activated by a catalyst (water steam). In this way, Pegna implemented the proof of concept of Solid Freeform Fabrication for large (> 1meter) construction, highlighting selective aggregation as the sole process liable to manufacture large-scale components. In Fig. 2.1 the process steps, the sample design and production are illustrated.

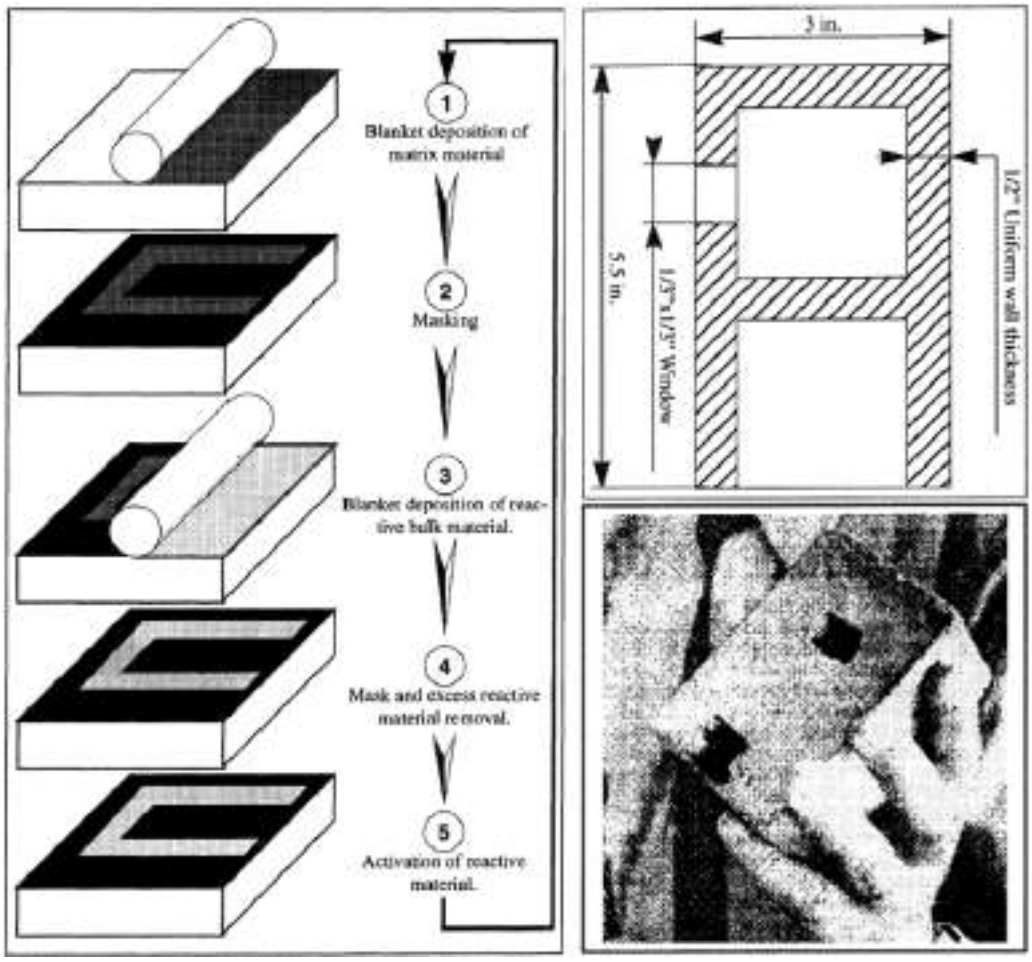

Figure 2.1: Flow diagram of the selective deposition process, after [1].

In 1996, product manufacturing industry was experiencing two crucial challenges: (1) the significant contraction of production time; and (2) the advancement on flexibility for fabricating modest product stocks and a variety of product typologies. Computer-aided design and manufacturing (CAD and CAM) had considerably enhanced the traditional production route, even if a consistent amount of obstacles remained unsolved (such as the fast development of

3D models and cost-effective fabrication). Rapid prototyping systems (RPS) provided the opportunity to manufacture products rapidly and at lower costs respect to traditional methods. **Xue Yan et al.** [3] collected and discussed cutting edge RPSs, each of them based on layer-by-layer material deposition, by which other authors took inspiration for concrete 3d printing applications, resulting in a paradigm shift from manufacturing technology. Just to mention, Stereolithography (1986), Selective laser sintering (mid-1980s), Fused deposition modelling (before mid-1990s), Laminated object manufacturing (before mid-1990s), Three-dimensional printing (before mid-1990s) are typical examples.

A crucial paradigm inherent additive manufacturing processes was born, i.e., that a component could be built by incremental addition of constitutive materials, a procedure that could be easily integrated and automated [4]. As a result, manifold operations such as material removal, processing and assembling could be reduced to a set of identical simple operations. In the same way, large construction components could be substituted with a large amount of elemental component. This is reported in **Pegna** [5], 1997, where an exploratory characterization of the resulting material properties of sample masonry structures was performed. Ultimately, the potential of solid freeform fabrication of large components was assessed.

In 1998 **Pham et al.** [6], presenting an overview of the different rapid prototyping processes, divided those involving the addition of material and those involving its removal. Moreover, another distinction could be made among liquid, discrete particles and solid sheets. For sake of conciseness, we depict in Fig. 2.2 the suggested taxonomy.

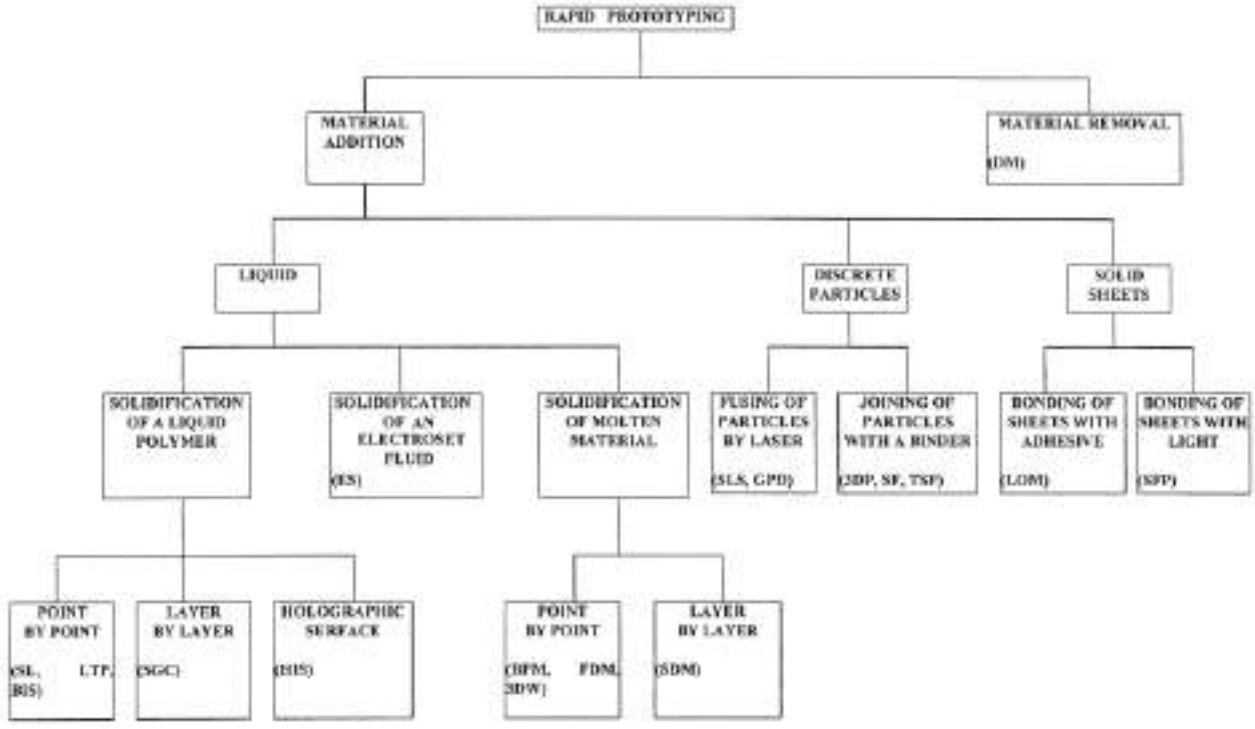

Figure 2.2: Classification of rapid prototyping methods, after [6].

As shown, construction automation and robotics brought much interest in the construction community over the nineties; however, robots in construction were still in an exploratory

stage. This aspect was clearly underlined by **Warszawski et al.** in [7], where a state-of-the-art survey in robotic employment in building construction was performed. He turned out that existing robots: (i) were not adjusted to the building sector; (ii) were difficult to justify economically; (iii) were hampered by managerial barriers; (iv) were not compliant with traditional buildings. Indeed, since the beginning of the twentieth century, automation controlled almost all manufacturing sectors other than construction of civil structures, due to: (a) inappropriateness of accessible digital production technologies for large scale components; (b) traditional structural design rules not suitable for automation; (c) relatively inferior ratio of quantity/type production compared with other industries; (d) narrow variety of materials that could be utilized by an automated system; (e) expensive automated equipment.

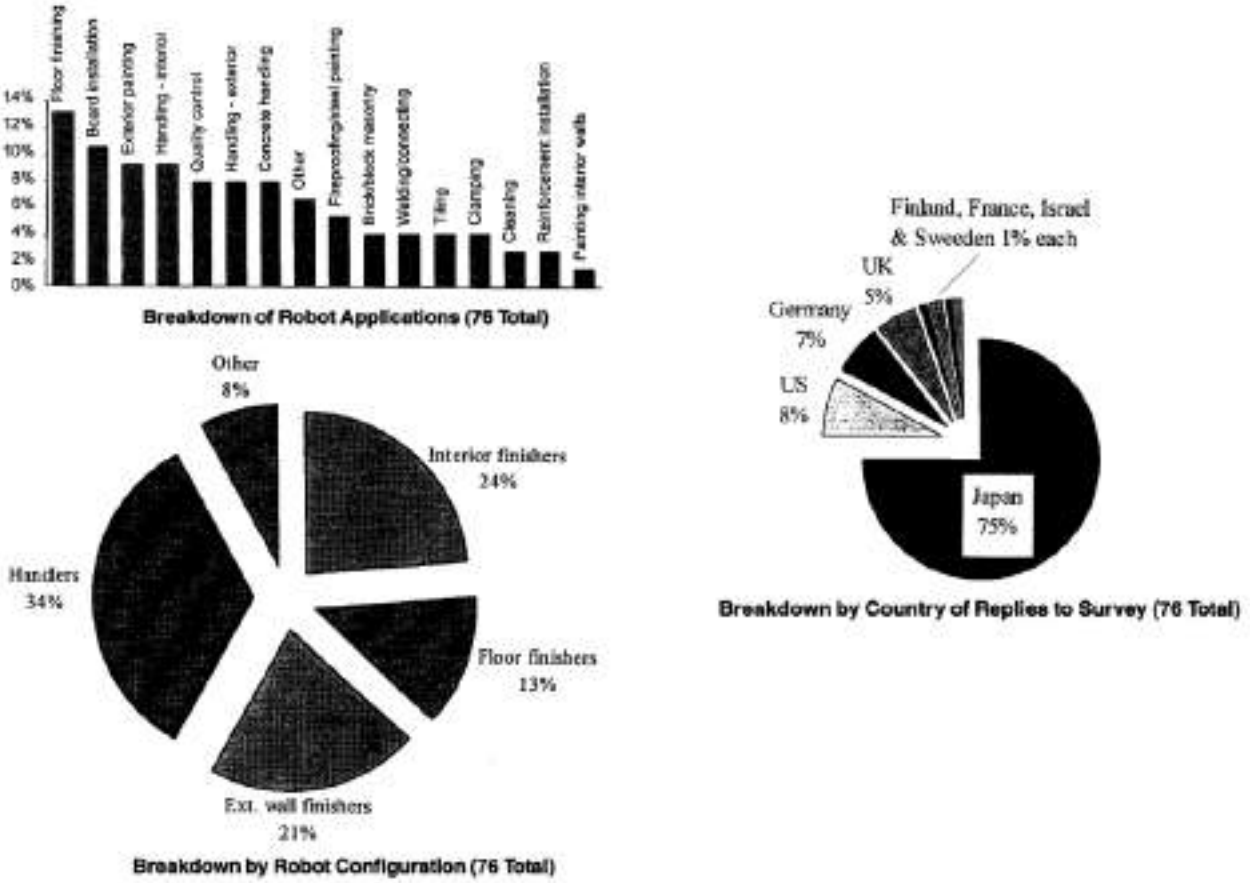

Figure 2.3: Breakdowns of robot applications, after [7].

As a result, up to 1999 additive manufacturing techniques were based on selective aggregation of powders relying on ad-hoc combination of blanket deposition, masks and manual hoppers. A pointwise deposition of multi-material flow powder was still necessary to fully automate the solid free-form fabrication technique. The Sand-Painter Project (**Pegna et al.** 1999 [8]), deriving from the ancestral art, dealt with powder handling, flow characterization, apt to a multi-powder patterned deposition: the main objective of Pegna was accomplish an experimental characterization of two-dimensional powder deposition appliance.

2.2 2001-2006: the Contour Crafting

In 2001 **Kolarevic** [9] asserted that "In a process converse of milling, additive fabrication (often referred to as layered manufacturing, solid freeform fabrication, or rapid prototyping) involves incremental forming by adding material in a layer-by-layer fashion. The digital (solid) model is sliced into two-dimensional layers; the information of each layer is then transferred to the processing head of the manufacturing machine and the physical product is incrementally generated in a layer-by-layer fashion. Because of the limited size of the objects that could be produced, costly equipment, and lengthy production times, the additive fabrication processes have a rather limited application in building design and production. In design, they are mainly used for the fabrication of (massing) models with complex, curvilinear geometries. In construction, they are used to produce components in series, such as steel elements in light truss structures, by creating patterns that are then used in investment casting. Recently, however, several experimental techniques based on sprayed concrete were introduced to manufacture large-scale building components directly from digital data." The time was ripe for a new layered fabrication technology capable to fully employ computer controlled automation: starting from a patented technique, **Khoshnevis et al.** [10] introduced the Contour Crafting (CC), a new promising automation approach applicable to the fabrication of large structures.

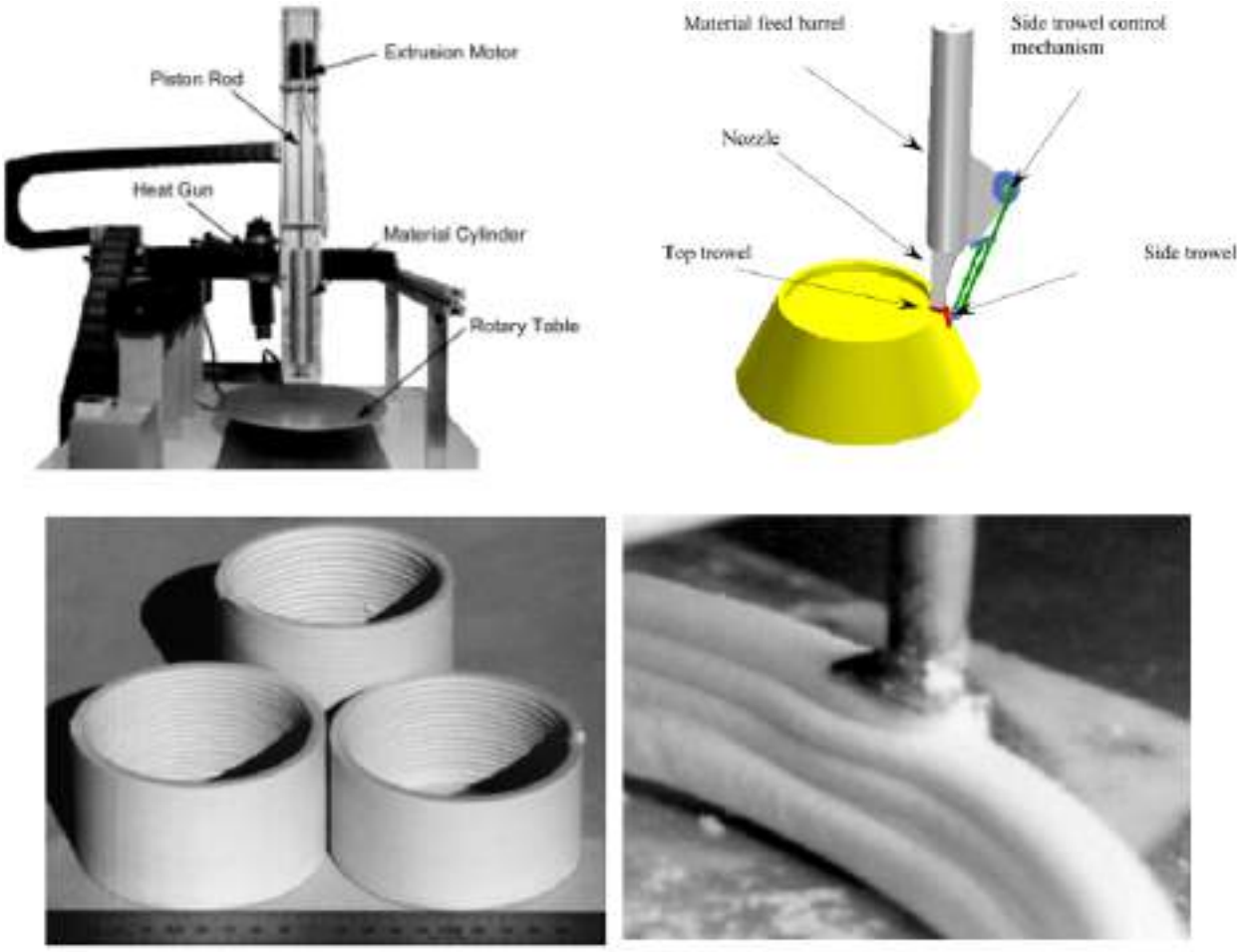

Figure 2.4: The Contour Crafting machine and 3D printed clay parts, after [10].

Today, Contour Crafting is a computer controlled additive fabrication technique that combines an extrusion phase (for reproducing the product surfaces) with a filling phase (to build the product core). The extrusion phase composes the continuous object surface by constraining the extruded flow by the use of trowels: it exhibits a superior surface forming capability by means of bladed trowels to create accurate free-form surfaces. Initially, Khoshnevis [10] provided the process technology, testing spackling compound and clay to gain experimental knowledge on the influence of manifold design parameters on the product quality (e.g., the compressibility of clay, the trowel pressure and the extrusion rate). Most of layered fabrication processes were limited by their incapability to deliver a wide variety of construction materials: in 2002 [11], several fabrication materials were tested, including polymers and various types of ceramics. The trial machine developed for ceramics was able to extrude a wide variety of materials, including concrete.

Digital architectures were deeply changing methods of design and construction, by harmonizing design, analysis, fabrication and assembly of structures around digital technologies: construction by Contour Crafting (CCC) was a visionary integrated approach toward the total automation of on-site construction, including automated modules for tiling, reinforcement, painting, plumbing, achieved with mobile robotics (Khoshnevis 2003 [12]). Finally, in 2004 unique capabilities of Contour Crafting were demonstrated by manufacturing and testing full-scale ($>$ 1m) concrete wall sections (**Dooil Hwang et al.** [13]).

The procedure extruded the internal and external surface of the wall to form a permanent formwork that was then filled with a bulk compound similar to concrete. By means of thixotropic materials, along with rapid curing and low shrinkage properties, the wall layer staking was made feasible. In that period, this approach was leading the automating construction research field in terms of a demonstrated new process.

However, to succeed, Contour Crafting construction automation would require a paradigm shift in technology. Even if CC had the potentiality to automatically build a single house, or a colony of houses, along with their technical installations [14], evidences delayed. Indeed, while

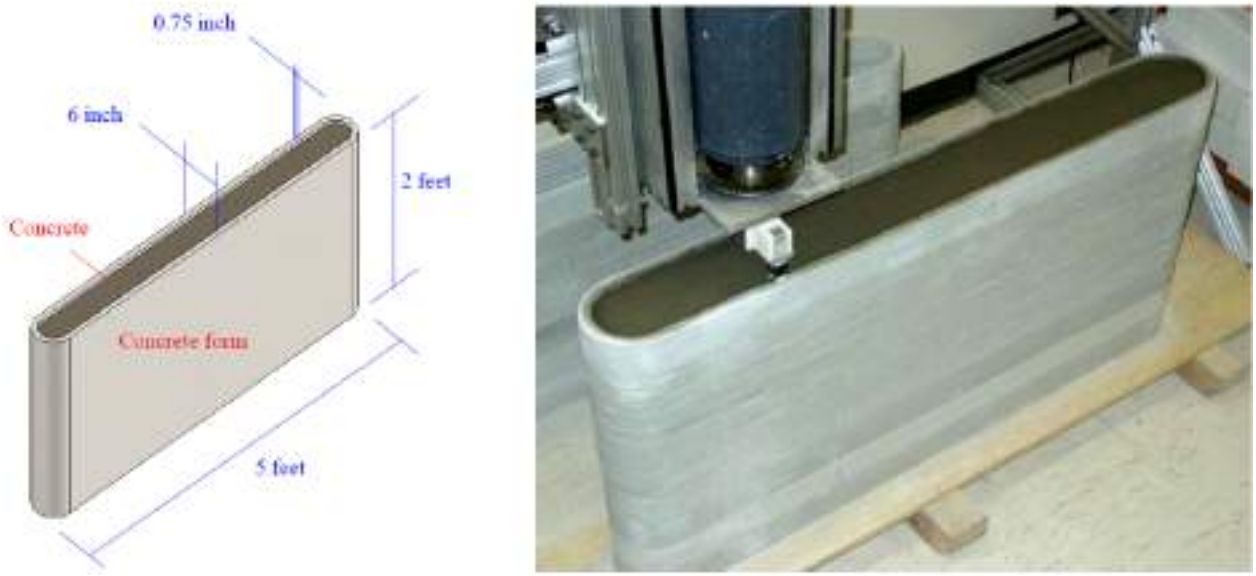

Figure 2.5: A concrete wall made by a CC machine, after [13].

CC theoretically evolved up to design and consider developments for extraterrestrial proposals (Lunar structures, Khoshnevis 2005 [15]), the manufacture of a whole terrestrial building remained largely a manual practice. Although the CC approach was an interesting concept, it still necessitated three different steps, i.e., moulding, reinforcing and placing concrete.

For the first time, considering the use of in situ resources, researchers moved to focus on layer prototyping from the process [16, 17, 18, 19] to the material [20, 21] point of view.

2.3 2007-2011: the Freeform Construction

In 2007 **Bushwell et al.** [22, 23] argued that "In terms of technological development, construction is decades behind other industries such as aerospace, automotive and ship building. The fundamental principles of construction have not changed for hundreds of years; the Romans invented concrete about 100 BC and 2200 years later we are still using it as a primary build material and (more or less) controlling placement with the human hand." As a result, authors defined the new term Freeform Construction as: "Processes for integrated building components which demonstrate added value, functionality and capabilities over and above traditional methods of construction." In detail, Freeform Construction was an emerging concept whose potential was manufacturing full-scale construction components without formworks. Three-dimensional (3D) elements were "sliced" and expressed as a set of two dimensional layers, and then incrementally reassembled to build the desired 3D component. Controlling the material permitted to build any desired shape [24, 25]. Developed from the 90's, Rapid Manufacturing (RM) was a family of layer-based processes: Freeform Construction wanted to scale up these Rapid Manufacturing processes from fabricating 'desktop' sized objects to architectural and construction applications, adopting new materials and processes. However, RM processes could not simply be scaled up: there was a key interdependency among material properties, process function, and design objectives that generated peculiar issues: (i) volume of prints, limited by the machine size; (ii) printing speed, that was much slower than casting; (iii) material constraints, all materials had natural variations in properties that might affect the printed object; (iv) design and control of design; (v) resolution and precision [26].

As stated by **Lim et al.** [26], in 2009 the research and practice of Freeform Construction was limited to three processes worldwide:

Figure 2.6: Contour Crafting, D-shape, and Concrete Printing examples, after [26, 27].

- Contour Crafting (US);
- D-shape (Italy); and
- Concrete Printing (UK).

The D-shape process was presented at the Civils 2007 exhibition in November 2007. The main concept of this method was based on the selective catalysis, i.e., was designed to manufacture architectural artifacts by selective deposition, rapid transformation and than extracting the catalysed object from the bed of un-catalysed material. The process was tested to fabricate a material with properties similar to marble [27].

Concrete printing, born in Loughborough University in 2009, was based on the extrusion process. Data preparation was similar to most Rapid Manufacturing techniques: from a 3D CAD model, sliced layers were generated and saved as a G-Code format. These instructions were delivered to computers that operated all the control commands governing the nozzle position, the movement, the material flow, the extrusion rate, etc.

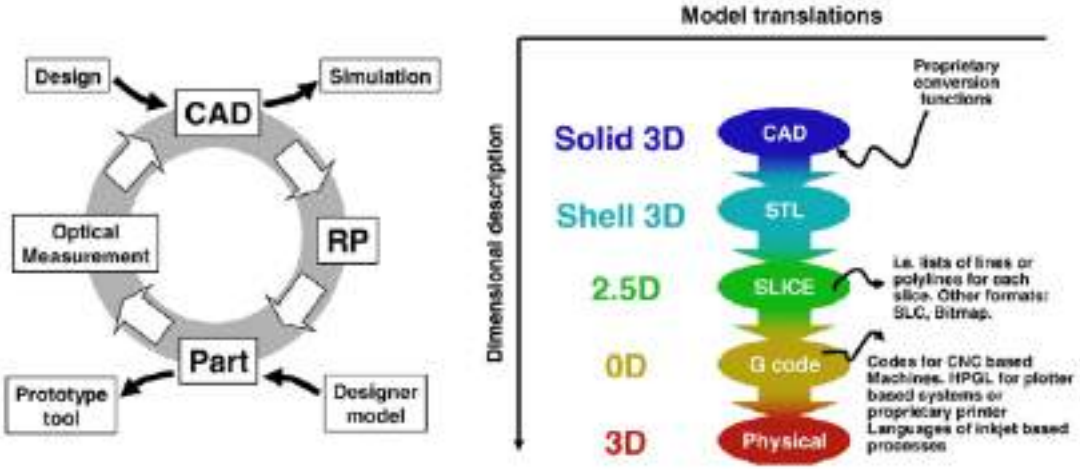

Figure 2.7: Steps in Rapid Manufacturing processes, after [23].

Conveniences of this method were that the direct control on the extrusion diameter gave the appropriated printing resolution, as well as the whole extrusion technique were validated with various materials. The construction process was operated with the deposition of two materials, one was the structural material and one the support material, which was deposited to support overhanging sections and then removed after the construction was completed.

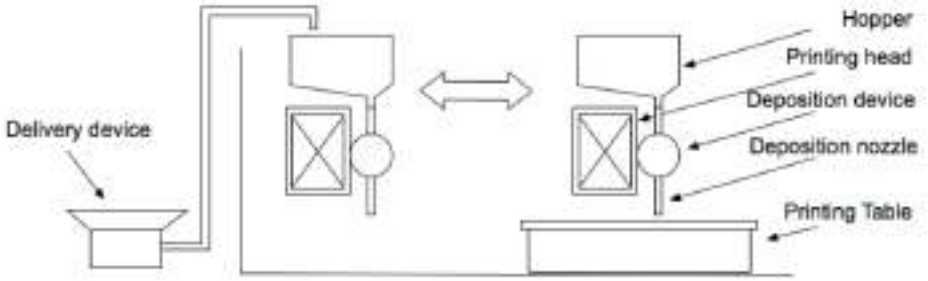

Figure 2.8: Diagram of the material delivery and the refill process, after [26].

Today, this three techniques are similar in that they produce additively, however, they have evolved for distinct applications and materials, resulting in different advantages and disadvantages. Contour Crafting permits high-speed automated construction, depositing the material to create a full-width component with the minimum use of material. In D-Shape each layer has the wanted thickness, is compacted and once a component is completed, the powder bed is removed. Concrete Printing has three-dimensional freedom with a smaller deposition resolution, allowing greater control of geometries. Both Concrete Printing and D-Shape need additional support to build overhangs: D-Shape, as a powder based process adopts the unconsolidated material as a support; Concrete Printing uses a second material [28, 29, 30].

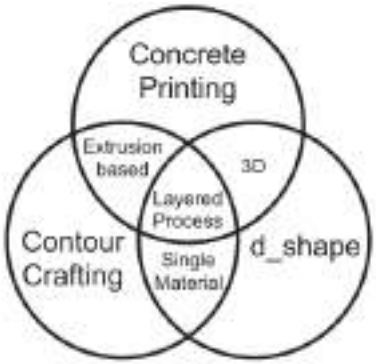

Figure 2.9: Similarities between processes, after [30].

	Contour Crafting	Concrete Printing	D-Shape
Process	Extrusion	Extrusion	3D Printing
Use of mould	Yes (Becomes a part of component)	No	No
Build material	• Mortar mixture for mould • Cementitious material for build	In-house Printable Concrete	Granular material (sand / stone powder)
Binder	None (Wet material extrusion and backfilling)	None (Wet material extrusion)	Chorline-based liquid
Nozzle diameter	15 mm	9–20 mm	0.15 mm
Nozzle number	1	1	6 300
Layer thickness	13 mm	6– 25 mm	4–6 mm
Reinforcement	Yes	Yes	No
Mechanical properties			
Compressive strength	unknown	100 110 MPa	235 242 MPa
Flexural strength	unknown	12–13 MPa	14–19 MPa
Print size	>1 m dimension	>1 m dimension	>1 md dimension
Pre / Post processing	• Reinforcement per 125 mm vertically • Backfill the mould with a cementitious material per 125 mm height	• Reinforcement after printing	• Compression of the powder for next layer by a roller with light pressure prior to the deposition • Removal of unused material
Pros	• Smooth surface by trowel	• High strengths • Minimum printing process; deposition & reinforcement	• High strengths
Cons	• Extra process (moulding) • Weak bonding between batches due to segmented backfilling batches by one hour interval	• Limited printing dimension by the printing frame, 5.4 m (L) × 4.4 m (W) × 5.4 m (H)	• Slow process • Rough surface • Limited printing dimension by the printing frame • Massive material placement • Removal of unused material

Figure 2.10: Existing AM process research related to constructions, after [30].

2.4 2012-2018: 3D Concrete Printing improvements

2.4.1 2012-2015, the material: mix design and fresh-hardened properties

Once the process was roughly defined, the development of a 3D printable concrete was pursued to exploit the potential of this advanced method of construction. Systematic research programs were presented to define optimum mix design proportions and their rheological requirements, both in the hardened [31] and in the fresh [32] state, to guarantee a reliable process.

In 2012 **Le et al.** [31, 32] affirmed that four were the fresh properties to be controlled and measured, namely **extrudability**, **workability**, **open time** and **buildability**.

The material needed to flow and to be extruded by means of a nozzle to produce concrete filaments: such filaments should bond collectively to build each layer, as the fresh mortar was progressively extruded. Le et al. evaluated extrudability by means of simple tests, i.e. extruding 9 mm wide and 300 mm long filaments. Today, traditional techniques to test workability comprise slump, compacting factor and flow tests; however, such tests do not measure fundamental physical properties. Alternatively, a shear vane apparatus can characterize Bingham fluid response in terms of shear strength and viscosity. Authors usually adopt shear vane approach because it provides consistent scientific rheological parameters.

A preliminary definition of open time was "the time period in which the fresh concrete is still reasonably workable" or "the time period in which the workability of fresh concrete was at a level that maintained extrudability" [32, 33]. Moreover, concrete should have adequate buildability properties to remain in position and to sustain further layers without collapsing.

In 2012, the first turning point occured, the amount of entities studying digital fabrication in construction industry exploded: several tentative mixes were explored, investigating the role of structural build-up properties of cement-based materials, i.e., studying the evolution of the mechanical strength of such materials for 3D printing applications. The range of concrete mix trials was broad, varying from Lunar on-site materials [34] to sustainable mix designs [35]; however, custom concrete mixes had recurring components and raw materials, as:

- Portland cement;
- cement replacers;
- water;
- siliceous aggregate with an optimised particle size distribution (< 4 mm);
- limestone filler and/or precise additives (for ease of pumping);
- rheology modifiers (for thixotropic behaviour);
- polypropylene fibres (for plastic shrinkage cracking).

2.4.2 2015-2016, collateral processes

In this family of digital manufacturing methods, disparate alternatives were regularly developed and enhanced, including:

- Dynamic formwork systems;
- Form Filling.

Dynamic formwork systems were:

- Smart Dynamic Casting;

while, the Form Filling was composed by:

- Custom single use formworks;
- Stay-in-place formworks.

For sake of brevity, we summarize such techniques as follows:

Smart Dynamic Casting: this technique was originated by the Slipforming method, developed by Charles Haglin in 1899. In a single-step process, concrete was consecutively poured in a robotically moving formwork, i.e., a robot controlled the formwork velocity and movement. Physical properties of the material were monitored, while complicated geometries were composed by correlating rheological properties, trajectories and the formwork geometry [36].

Custom single use formworks: digital fabrication of high complexity formworks, generally manufactured by means of computer numerically controlled (CNC) mills, facilitated the construction of customized concrete geometries with unique shapes [37].

Stay-in-place formworks: alternatively to CNC milling, this approach was more sustainable since digitally fabricated formworks could have supplementary applications. One example is the Mesh Mould Metal technique invented in ETH Zurich: an industrial robot bended and welded metal rods into a 3D mesh structure, which represented a porous formwork and reinforcement during the casting process [37].

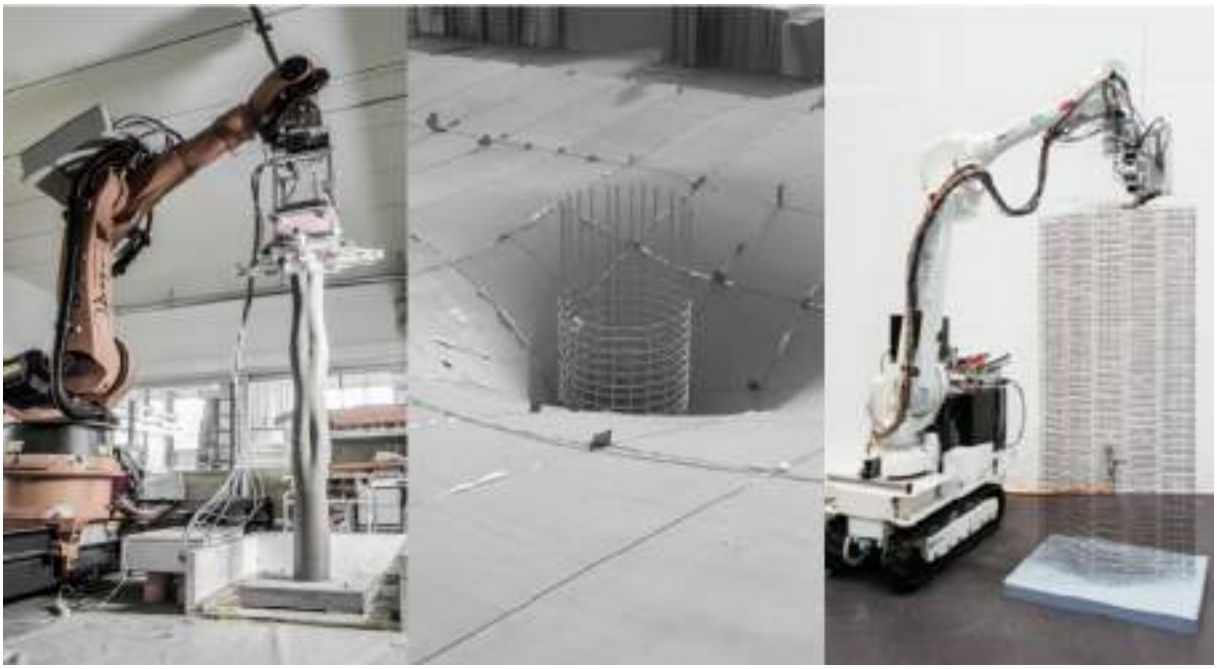

Figure 2.11: Smart Dynamic Casting, Custom single use and Stay-in-place formworks, after [37].

2.4.3 2016, large-scale constructions and components

In 2016, the second turning point occured, the number of companies investing 3D concrete printing boosted, making the linear development into a quasi-exponential one: innovative projects were given on a regular basis. Some significant examples include [38, 39, 40, 41, 42]:

- Two-storey house measuring 400 m^2, China (Beijing-based HuaShang Tengda, 3dprint.com);
- Office building measuring 250 m^2, Dubai (Chinese construction company Winsun, Cnet.com);
- Five-storey apartment building, China (Chinese construction company Winsun, Cnet.com);
- Hotel suite interior measuring 12.5 x 10.5 x 4 m, Philippines (Total Kustom, Totalkustom.com);
- Villa measuring 1100 m^2, China (Chinese construction company Winsun, Cnet.com);
- Children's Castle, USA (Total Kustom, Totalkustom.com).
- Series of 10 houses, China (Chinese construction company Winsun, Cnet.com);
- Multifunctionnal structural wall, France (Gosselin et al. [40]);
- Doubly-curved 4-part sandwich panel measuring 1.5 m x 1.5 m x 0.1m, UK (Lim et al. [42].).

Figure 2.12: Examples of large-scale constructions, after [38, 39, 40, 42].

2.4.4 2017-2018, process and material refinements

While companies gave their support to "make it works" in practice, up to 2017 only few studies contributed to a primary understanding of needed concrete properties: an extensive research and experimental campaign was still necessary. In detail, characterization of the early age response of a printable cementitious mixture demanded a deeper investigation. The accepted definition for workability as "a measure of ease by which fresh concrete can be placed and compacted" [31, 32] was not precise enough: novel measures was needed for describing the early age state of a 3D printable concrete [43]. As stated by **Tay et al.** [44], since 2016 "the two main research interests constituting 45% of the total interest recorded are Printing Technique Analysis and Material Analysis".

When DFC was employed in structural applications, a recurring challenge was the demand in ductility and flexural-tensile capacity. In 2017, **Panda et al.** [45] investigated the mechanical properties of 3D printable geopolymer with disparate fiber lengths and dosages. Evidences from the experimental results demonstrated that fiber additions left almost unvaried the compressive strength, but significantly enhanced the flexural and tensile toughness [46]. An altogether different approach was adopted by **Bos et al.** [47], consisting in an embedded reinforcement cable integrated when filament left the print nozzle.

Another challenge was attaining a mixture with high shape stability in the fresh state: **Kazemian et al.** [48] discussed an experimental program performed to investigate such shape stability. Initially, protracted stoppage time between consequent layers was explored to discover the impacts on the deformations of fresh printing concrete. Subsequently, heat was applied to improve shape stability without cumulating any delay in the construction process.

In 2018, **Bushwell et al.** [49] affirmed that "The material is required to flow and extrude through a nozzle, bond with the previous layer and maintain its shape under increasing hydrostatic pressure generated by subsequent layer deposition. Disturbances during printing, caused by changes in the material or problems with the process, are detrimental to the success of a build and can influence the performance of the component. These issues hamper the robustness of 3DCP, a critical milestone for commercial viability, of which rheological properties of 3DCP materials are fundamentally important". As a result, he discussed: (i) properties of early age 3D printable materials, and (ii) hardened properties of 3D printable materials. Bushwell divided fresh properties in:

- open time, time during which a material remain printable (pumping and extrusion);
- setting and layer cycle-time, time required to complete one layer (vertical building rate);
- deformation of material under successive layers;
- rheological measurements.

while, hardened properties in:

- layer adhesion;
- bulk density and under-filling;
- tensile reinforcement;
- shrinkage and durability;
- measurements of hardened material properties.

correlating such properties with guidance values and providing a roadmap for material research.

A validated Finite Element Modelling (FEM) approach reproducing the printing process was firstly introduced by **Wolfs et al.** [50], considering the experimentally extrapolated time-dependent evolution of mechanical behaviour of early age concrete during printing.

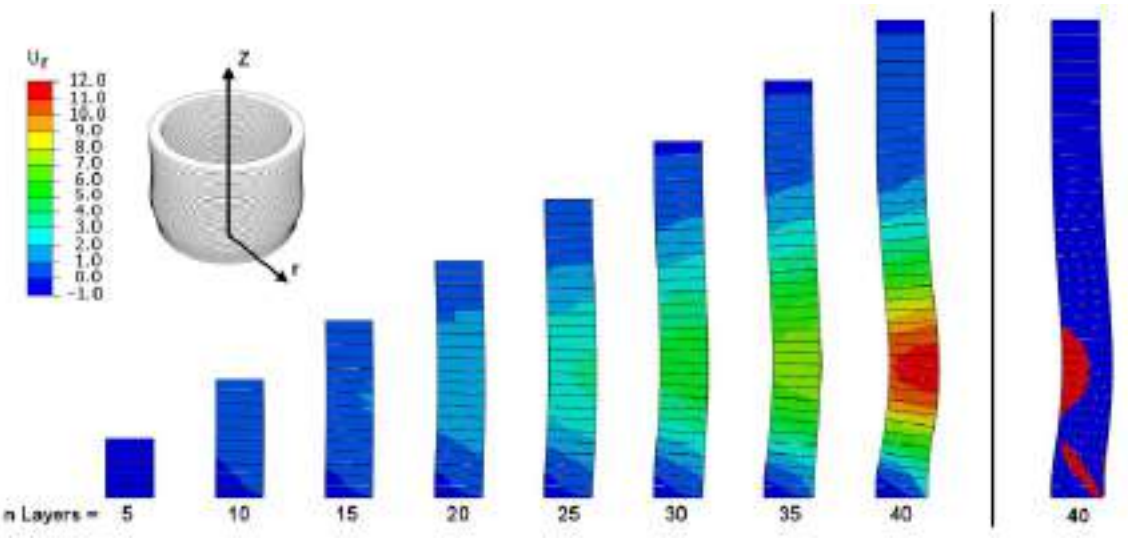

Figure 2.13: Numerical modeling of the 3D printing process, after [50].

Firstly, an appropriate material failure model was selected, i.e. between a Bingham fluid and a proper solid. Subsequently, specific tests were performed deriving stress-strain curves from geotechnical test methods of soils. The next step was developing the FE-model calibrated on the previous tests. Finally, the 3D printing process was modeled and qualitatively validated.

Beside mechanical properties and their numerical simulation, another important issue was to define rheological properties: for any category of flowable material, insights of rheology support in optimizing processing and manufacturing good quality objects. For instance, thixotropy (viscosity reduction when shear is applied), extrudability, shape retention, buildability, thixotropic open time and tensile bond strength were determined for different types of mortar by Panda et al. [51, 52] and **Paul et al.** [53], by means of rheological tests.

We want to conclude this section with some final considerations, as stated by **De Schutter et al.** [54] in late 2018: "Although several showcases of 3D printed concrete structures are available worldwide, many challenges remain at the technical and processing level. The range of printable construction materials is very limited at this moment. Currently available high-performance and very durable cement-based materials cannot be directly processed in a printing technique, because of inadequate rheological and stiffening properties. This holds true also for concrete according to the existing design and construction codes. In future, active rheology control (ARC), active stiffening control (ASC) and other novel approaches will provide solutions of extending the material palette for 3D printing applications."

In Fig. 2.14 we depict the chronological trend of available publication output and research origin over the years. It is possible to observe that, initially, the 3D printing process was investigated; consequently, after 2012 the focus moved to the material definition. It is from 2016 onwards that publications have begun to boost at an exponential rate.

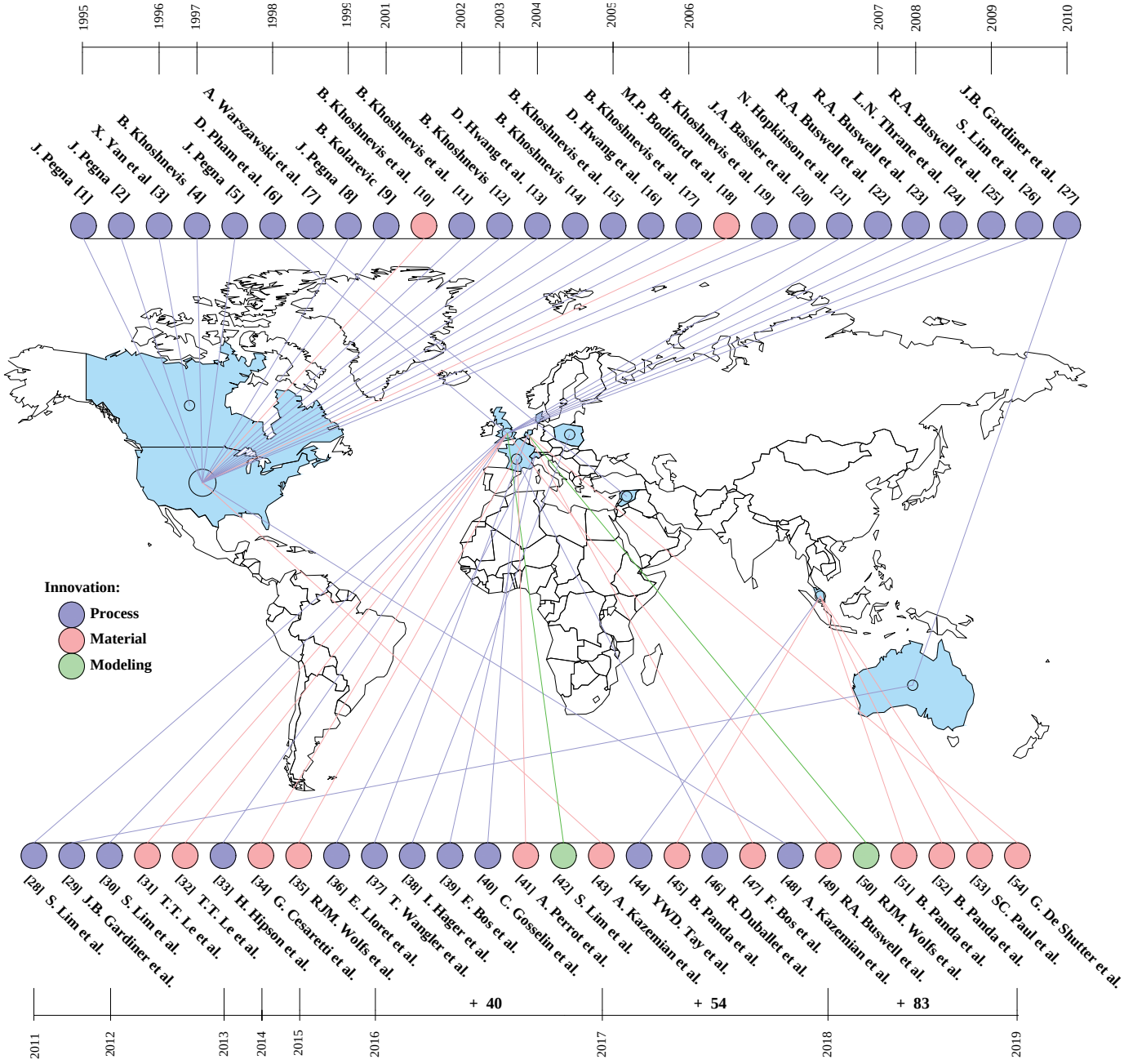

Figure 2.14: Chronological trend of available publication & research origin over the years.

Chapter 3

Potentials and challenges

Digital fabrication techniques combined with suitable cementitious materials have successfully led to the implementation of innovative manufacturing processes for concrete-like products. Even if a regularly increasing amount of researchers and enterprises focuses in this field, 3D concrete printing is still in its infancy and the cumulative body of work is still limited [37]. As a result, we present a synthesis of primary potentials and challenges of 3DCP practical large-scale applications, and we discuss expected progresses of 3DCP in general.

3.1 Potentials

In the European Union, the construction industry represents the 9.7% of the gross domestic product and provides 6.6% of Europe's total employment: however, nowadays developed countries experience stagnation caused by various factors, such as the opposition in bringing changes into a highly conservative sector, scarce industrialization of construction processes, and significant grades of turnover, which makes it difficult to implement new methods [54]. As a result, construction techniques remained unvaried during all along past decades. The principal revolutionary potential of digital fabrication is inherent to the Construction Industry 4.0, as it suggests a logical evolution from the Computer Aided Design (CAD), making construction a fully automated process. It follows that, a contraction of building times and costs, as well as advancements in construction quality, can considerably increment the productivity of the sector. Digitalization of processes, from planning to construction, may potentially shorten errors and support the management of the process itself. Building Information Management (BIM) can supervise digital data from the design to production, maintenance, rehabilitation and recycling. Digital fabrication may determine greater productivity and no additional costs over conventional construction when complex components are fabricated.

Traditional cast in place concrete technique requires the use of formworks; such formworks contribute to significant material, labor and machinery costs: according to [54], formworks can represent from the 28% to half of the total concrete cost. Moreover, formworks increase time delays and negative environmental impacts, particularly for complex structures. In case of digital fabrication with concrete (DFC), control on the evolution of rheological properties can lead to shape retention without any formwork, leading to a considerable cost reduction. Additionally, DFC structure costs are predicted to be broadly complexity independent. The four cost constituents of any construction method are: (i) labor, (ii) machinery, (iii) material

and (iv) design [54]; with DFC is expected that labor costs will be considerably lower than that of conventional construction.

Three principal sub-processes are identifiable in a DFC approach:

- a) pump material toward the printing head;
- b) locate the printing head;
- c) extrusion.

According to [54] machinery utilized for such sub-processes can be summarized in: unconventional construction equipment (UCE), and (adapted) conventional construction equipment (CCE). For the sub-process (a) conventional construction equipment (as piston pumps) can be used; for sub-process (c) unconventional construction equipment (as printing head) is required. This is true if the printing head is adequately designed, equipped with sensors or with multiple nozzles which implement various materials: these sophistications make printing heads a substantial cost factor. On one hand, material costs for digital fabrication can be lower than in case of traditional construction depending on topology optimization and on contraction of wasted material. On the other hand, such costs can significantly increase due to the use of expensive mix design with fine substance additions as nano-clay, nano-silica and special chemical admixtures. Mixes employed for DFC are relatively complicated materials, designed to achieve problem-free processing, high thixotropy, early strength, additionally to other properties expected from the structural concrete [54]. As a result, the mixing process should be characterized by precise dosing, intensive mixing and storage of ingredients according to guidelines provided by material researchers and concrete technologists.

Design costs (which comprises 3D modelling, BIM etc.) are foreseen to steadily diminishing, considering progresses in DFC: the potential cost contraction is more probable in case of large-scale implementation (due to reuse of algorithms, digital data and data base).

Environmental potentials

Worldwide, the building sector is accountable for environmental impacts to the extent of 40% of energy consumption, 40% of solid waste production, 38% of GHG emissions and 12% of water depletion [55]. Growing concern in ecology and sustainability is encouraging innovations in construction, in order to reduce the environmental impacts generated by conventional construction. Particularly, digital fabrication processes have been correlated with cost-effective production techniques that reduce the energy consumption, resource demands and CO_2 emissions [56]. Moreover, 3D printing demonstrates an important potential in decreasing the material usage by means of topology optimization and in generating non conventional geometries without supporting structures. Enforcing structural optimization as well as functional hybridization allows the material to be placed only where it is structurally or functionally needed. Topology optimization adds shape complexity, but also decreases the employment of material with digital fabrication. In AM technologies, as the material is added layer-by-layer, optimized design may virtually lead to zero-waste manufacturing processes. AM has a deep impact on manufacturing processes worldwide, allowing rapid, economic and customized fabrication of parts, based on the idea of modularity and disassemblability of structures, too difficult and expensive to produce with more standard construction procedures.

3.2 Challenges

Albeit disparate trials of 3D printed concrete elements are available worldwide, several challenges persist both at the technical and the processing level. Principal challenges emerged can be summarized as follows [37, 39, 54]:

- Material selection;
- Control of rheology and phase transition;
- Material layering and development of "cold joints";
- Implementation of reinforcement;
- Surface finishing.

One prevailing obstacle is the limited range of 3D printable material palette practical available. Contemporary showcases are produced with concrete mixes, developed more to be capable to stack layers without premature collapses, rather than to guarantee acceptable operability conditions. Indeed, inspecting the structural performance of hardened printed concrete elements, poor properties can frequently be observed: for instance, the curing of 3D printed components without formworks represents a technical challenge, since it can conduct to shrinkage cracking. Although several research teams currently investigate on fresh material properties, hardened mechanical and durability properties remain often inadequate. Therefore, since traditional cement-based mortars can not be directly processed in a 3D printing technique, the conversion of available high-performance cementitious materials to 3D printable materials remains a challenge (that entails specific normative implication). Moreover, the accurate control of rheological characteristics and the physico-chemical composition of the mix guarantee the appropriate structural buildup of the component. Variations in the cement or aggregate type, as well as in the additive nature, may demand a new concrete mix design.

In layered extrusion of concrete components, the role of interfaces becomes substantial. Indeed, between consequent layers an interface area arises, which properties depend on the time elapsed between the extrusion of subsequent layers (cold joints). Even if modern guidelines consider concrete as a homogeneous material, such weaker interfaces affect the overall mechanical performance, the bond and the durability behavior, resulting de facto in an anisotropic behavior. As a result, structural design needs new design models, new procedures for dimensioning structural elements and for estimate deformations, considering, for example, that new reinforcement concepts have to be applied. Additionally, the traditional approaches of cube/cylinder testing are no longer representative for 3D printed cementitious materials, since samples cannot be manufactured in the classical way. Shortcomings in design guidelines and testing protocols will delay progress of digital fabrication in concrete industry.

Another crucial challenge in additive manufacturing with concrete is the reinforcement integration. Even if an adequate solution are not available yet, several tentatives have been investigated. The main opportunities emerged can be summarized as follows [54]:

- dispersing short steel or polymer fibers as dispersed reinforcement, shrinkage reducers and early strength enhancers;
- extruding concrete around vertically placed steel reinforcement;
- automating free forming 3D printed steel reinforcement;
- installation of external reinforcement;

- autonomous installation of reinforcing rods, dynamically located consequent to singular filament extrusion.

These solutions are not yet completely developed nor validated at large scale: however, in order to implement large-scale digital fabrication at industrial level, such challenges must be addressed.

Part II

Experimental exploration of 3D printable cementitious materials.

Chapter 4

Mix Design

4.1 Introduction

Normally, concrete is arranged in formworks and then cured to construct building components. To date, to overcome the compaction stage two alternatives have been proposed: self-compacting and sprayed concretes [32]. 3D concrete printing is a novel additive manufacturing process, capable to reproduce architectural elements without formworks: a digitally controlled printing head extrudes the cementitious mixture in layers, building the structural component. Related engineering challenges are manifold, since specific rheological properties are required. In general, printability (i.e. the physical integrity of the element during printing) is defined in [32, 49] by means of:

- **Pumpability**, is the capability to reach the printing head through the pumping system;
- **Extrudability**, is the capacity to be extruded by the nozzle with a stable material flow;
- **Buildability**, is the capability to withstand the weight of consecutive layers.

Additionally, meet strength-base performance requirements generally means to increase the cement amount: however, this increment will necessarily introduce shrinkage due to the heat rise in cement hydration [56].

Although it is clear that the concrete rheology must be optimized in order to balance different needs, no relevant guidelines exist to define test methods, performance requirements and acceptance criteria for the early age behavior of the printing concrete. Moreover, previous studies on 3D printed concrete exhibited that pre- and post-print properties are highly dependent on raw material selection and early age printing material requirements [54, 57].

As a result, since the awareness in rheology improve flow-able material processing, the goal of **Part II** is to conduct a concise and comprehensive review on raw materials, select an appropriate compound and examine the mechanical behavior of fresh concrete (in the range of 0 to 60 min after mixing), through a simple and systematic approach that provides an exhaustive framework for performance-based laboratory testing. In detail, the time-dependent evolution of concrete mechanical properties will be investigated by means of compressive, creep and rheological tests, i.e., quantitatively associating a strength-based failure criterion to compression strength and a deformation-based failure principle to creep (buildability), as well as the workability (pumpability and extrudability) to rheological tests.

4.2 Raw materials for concrete 3D printing

In order to achieve high performance materials and therefore to obtain an easy-flowing and easy-extrudable mix, concrete must be accurately designed to meet critical criteria and ensure compatibility with the printing system. Hence, particular care should be paid in the raw material selection, since such materials influence fresh and hardened properties of the composite: for instance, increase the cement amount and reduce the water/binder ratio is a standard procedure executed to meet target high-strength performances; however, this will necessarily result into increased shrinkage. Therefore, cement can be partially replaced with mineral constituents that feature cementitious properties and pozzolanic reactions, such as silica fume, fly ashes, blast furnace slag, fillers and nano-silica. Incorporation of such materials lend mechanical benefits to the early age concrete, reducing porosity and improving fluidity, dimensional stability, as well as durability properties (but detrimental to early age strength). Considering that aggregates and coarse sand are not suitable to guarantee a flowable and extrudable mixing, minerals are required, added in powder scale [58].

Accordingly, in the following we briefly summarize the principal dry constituents eligible as partial replacement of Ordinary Portland Cement in 3D printing. We provide a compendium of latest researches, therefore, for further details, the reader may refer to proposed references.

- **Silica fume**, derived from silicon metal and ferrosilicon alloy production, due to the ultra-fine powder and to 85-90% silica content it contributes to give additional strength, lower porosity, permeability and bleeding, reacting with the calcium hydroxide of Portland Cement [59].
- **Fly ash**, is a coal combustion by-product, generally in spherical shape and distincts in two main typologies, class F and class C. The first one is produced burning anthracite (SiO_2>70%), the second one burning lignite (CaO>15-30%). It provides significant mechanical benefits to concrete, including lower heat of hydration, strength and durability performance [60], reducing the global cost of concrete production.
- **Blast furnace slag**, is a by-product of steel manufacturing industry. It can be used as a partial replacement of cement (up to 40%) [61], giving higher compressive and flexural strength, due to the high composition in silicates and aluminates, as well as to its ultra-fineness.
- **Limestone fillers**, is obtained by the grinding of limestone. It contains high amounts of calcium carbonate ($CaCO_3$) and permit to obtain a more compact structure by pore-filling effect, improving the workability of concrete mixtures and increasing the early strength. Economic benefits arise due to the possibility to develop similar strength with lower cement [62].
- **Nano-silica**, consists in amorphous silicon dioxide with nanoscale particle size; due to its notable surface area it provides the potential for strong reactivity, enhancing compressive strength and durability, filling up pores and promoting cement hydration. It requires more water resulting in less flowability [63].

Chemical additives can also be selected to modify the hydration of Portland cement, adjusting the workability of the concrete mix in early age stages and thus influencing the rheological properties of fresh mix. To satisfy the required workability, various additives are used. A brief summary is outlined in the following.

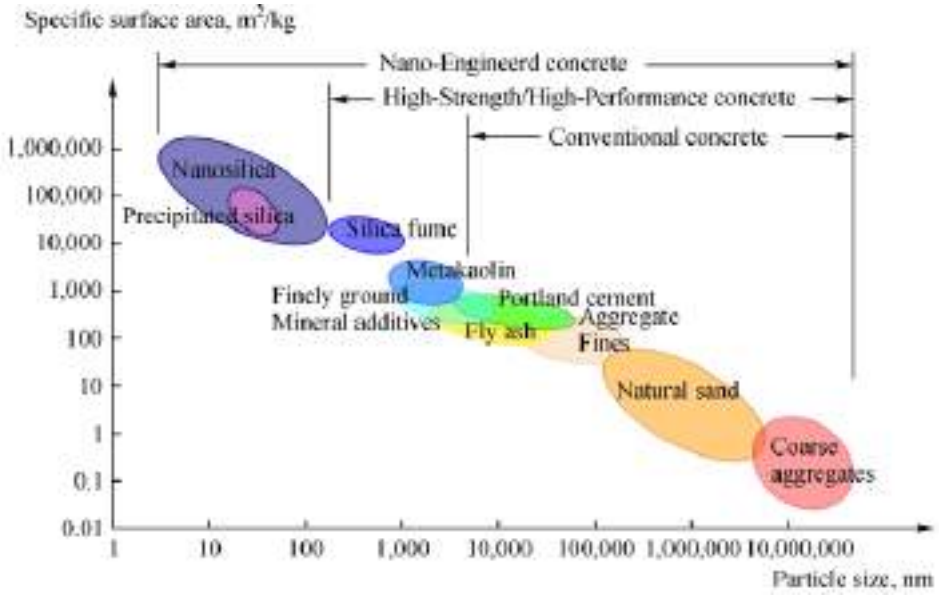

Figure 4.1: Particle size and specific surface area related of concrete components, after [58]

- **Superplasticizer**, reduces the water-to-binder ratio increasing the workability. It can be classified in lignosulfonic acid (LS), melamine form-aldehyde sulfonic acid (SMF), naphthalene formaldehyde sulfonic acid (SNF) and poly-carboxylic acid (CE). The water, that is usually entrapped by cement particles (a), is released (c) thanks to the negatively charged superplasticizer particles that procure repulsive forces among cement particles (b) (Fig. 4.2, [58]). New generation SPs also work by means of steric repulsion concept
- **Accelerator**, is a category of additives normally adopted to shorten the setting time of concrete, developing a rapid cement hydration and producing early stiffness-strength evolution. It can be either alkaline or alkali-free [58].
- **Retarder**, delays the hydration of cement particles. It can be classified in Sodium gluconate (SG), tartaric acid (TA) and citric acid (CA) [58].
- **Viscosity modifying agent**, is a polymer that adjusts the rheological performance of concrete mortars, enhancing the dimensional stability. Due to the VMA polymer chains that obstruct the free water movement, the compound plastic viscosity increases [58].

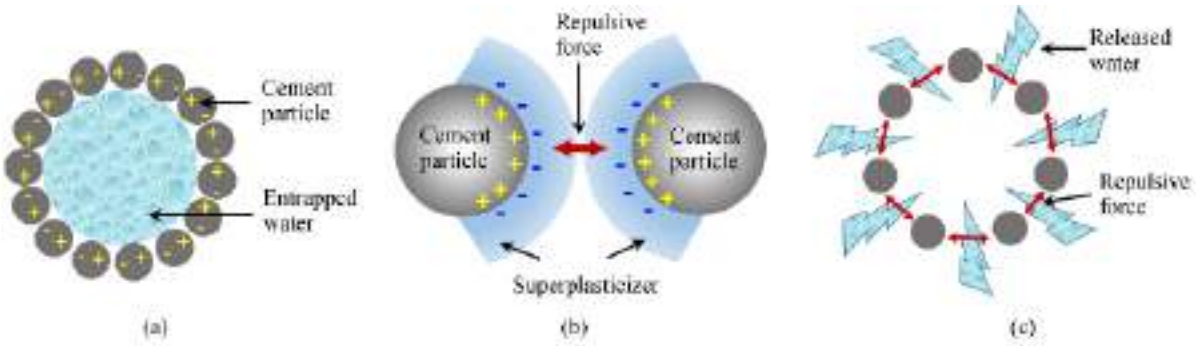

Figure 4.2: Effect of superplasticizer on cement particles, after [58].

4.3 Adopted mix design

The chosen mix design is optimized to meet performance requirements, both in fresh and hardened concrete. Fresh printed materials should satisfy specific rheological requirements, in order to achieve an optimized balance between workability and extrudability on the one hand – which would require reduced pumping forces – and the need for buildability (i.e. ability to stacked concrete layers) on the other hand – which would require an increased strength. Hardened requirements are the compressive and flexural strengths of the material. Since an opportune balance of all components has to be achieved to ensure the proper compatibility between the process and the mix, several trials are performed in order to discover the optimum amount of materials. Finally, we select sand with a maximum size of 2mm, in agreement with the diameter of the nozzle (i.e. 25mm) and to guarantee a high printing resolution; CEM type I 42.5N is adopted as binder (water-to-binder ratio w/b=0.35) and limestone fillers ($CaCO_3$) is added as inert. Solid components are mixed for 60 seconds at low speed (140 rpm). Subsequently, dry components are mixed with 25/0.18 mm length/diameter polypropylene fibres to reduce shrinkage and deformation in the plastic state (140 rpm – 30 seconds). Next water is added, mixing again for 60 seconds (140 rpm). Afterwards, different amounts of polycarboxylic (CE) superplasticizer are assumed to increase the workability (and thus allowing to reduce the water-to-binder ratio), mixing for 120 seconds at high speed (285 rpm). In Fig. 4.3 we summarize the definitive mix design.

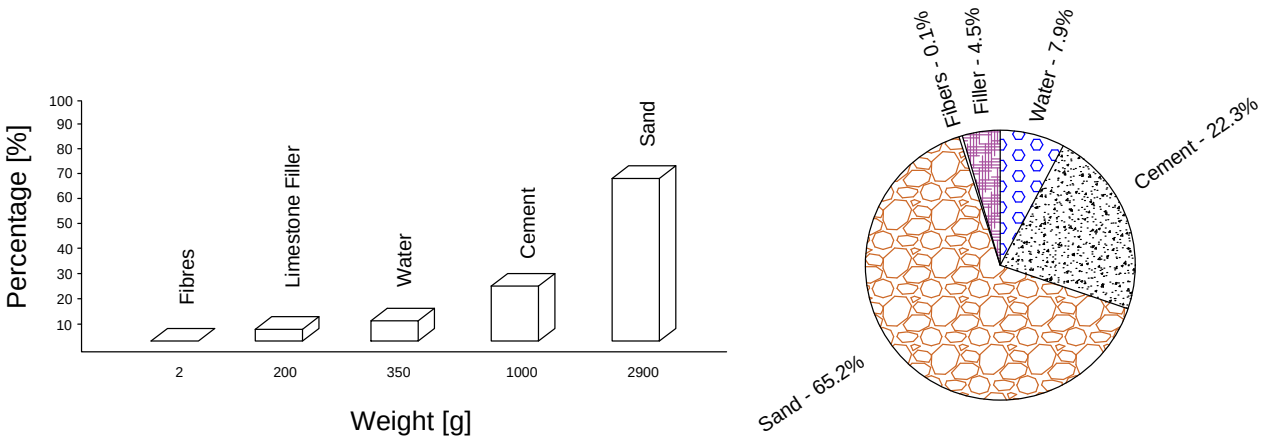

Figure 4.3: Reference mix design.

Chapter 5

Experimental Programme

5.1 Test Challenges

The development and the validation of experimental frameworks for testing printing mixtures presents manifold challenges. Although several studies have investigated the peculiar properties of printing mixtures, both in the hardened [31] and in the fresh [32] state, a complete list of performance requirements and testing procedures has not been recommended yet. Moreover, to date, 3D printing processes are unstandardized, requiring expert robotic operators and exceptional care in concrete mixing [54]. Indeed, unreliability of the process emerges from the strict dependency on operational parameters, such as the generation of computing instructions (G-code), the appropriateness of materials (rheological properties) and hitches during printing, parameters that may hamper the robustness of the process [37]. This work intends to supply both a state-of-the-art review and an effective testing procedure, in order to identify a robust framework for performance-based laboratory testing able to address minimum material performance requirements (qualitatively expressed by pumpability, extrudability and buildability descriptors).

According to [49], we want to focus on the following crucial themes:

- **Open time** (that directly influences pumpability and extrudability);
- **Setting and layer cycle-time** (correlated to the buildability);
- **Deformation under self-weight** (correlated to the shape stability).

5.1.1 Open time

In 3D concrete printing the open time is defined as the printability window where a certain amount of material can be pumped and extruded by the nozzle; this is correlated to the preservation of the viscosity and the yield stress, and therefore to the onset of cement hydration. Indeed, printable concretes behave as visco-plastic Bingham materials: they flow only when subjected to stresses higher than the yield strength. Le et al. [32] obtained that the yield stress range that prevent obstruction during pumping/extrusion is between 0.3 to 0.9 kPa. **Thrane et al.** [64] focused on CEM I - Fly Ash and CEM I - and limestone filler compounds, showing that a plastic viscosity and yield stress equal to (38.7 $\pm$ 4.5) Pa.s - (0.59 $\pm$ 0.08) kPa and (21.1 $\pm$ 2.4) Pa.s - (0.27 $\pm$ 0.03) kPa, respectively, were appropriate for pumping/extrusion from

the specific apparatus used by the authors. Therefore, an extensive experimental program is designed to assess time-dependent rheological properties of the chosen mixture.

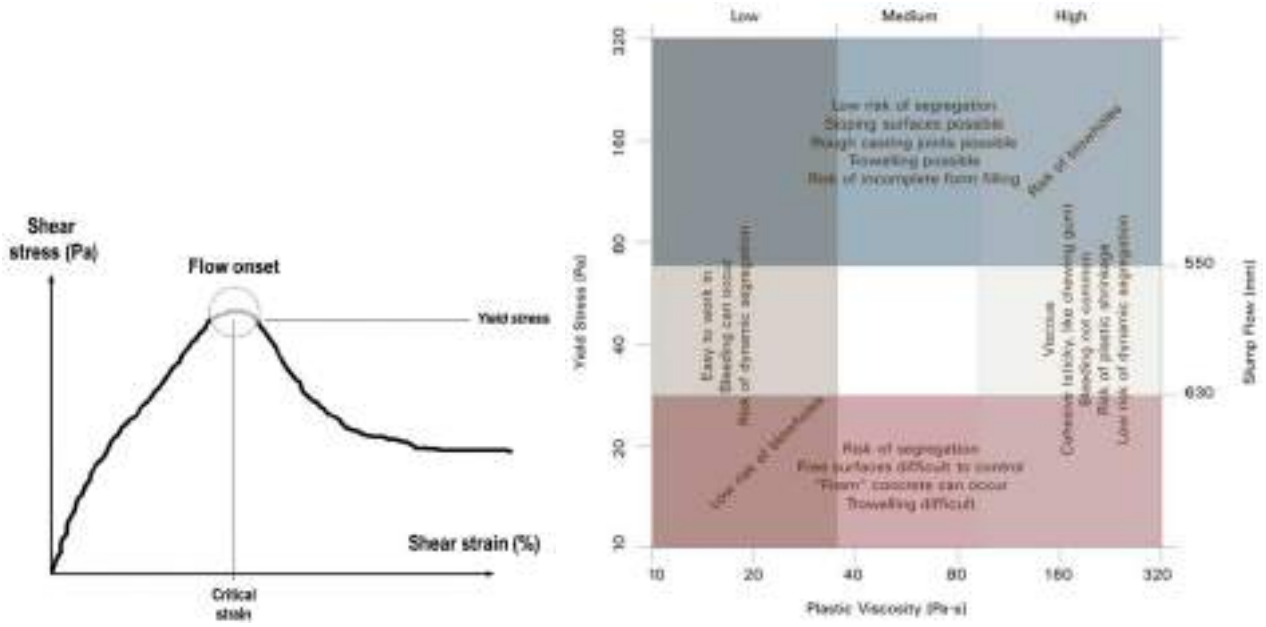

(a) (b)

Figure 5.1: Example of rheological functional diagrams, after [64].

5.1.2 Layer cycle time

The time required to deposit one layer is called layer cycle time: this affects the vertical building rate, since it represents the time delay between overlapped fresh layers. Layer cycle time is determined by the length of the extrusion and the printing speed, influencing both the interlayer bond strength (cold joints) and the early age compressive strength (since hydration of concrete is still evolving during overlaying) [37, 39]. As a result, the layer cycle time is directly correlated with potential strength-based failures: on one hand, relatively small yield stresses needed for pumping are juxtaposed with the demand in yield stresses to maintain the layer geometry and to allow interlayer bond strength; on the other hand, as the printed height rises, so does the hydrostatic compression experienced under self-weight, requiring an increasing compressive strength in the fresh state (commonly called green strength) [65].

Figure 5.2: Different curing state in a 3D concrete printing process, after [39].

This work aims to examine strength-base failures through the evolution of the compressive strength, i.e., when the early age mixed mortar progressively evolves from plastic-deformable to the hardened state. Therefore, the time-dependent compressive strength is explored by means of uniaxial unconfined compression tests, while hints on interlayer bond strength are deducted from rheological tests. Finally, a set of requirements for 3D printable mortars are introduced to prevent strength-based failures.

5.1.3 Deformation under self-weight

The shape stability is the capacity to withstand deformations during the layer-by-layer printing process, maintaining the filament geometry. Three are main sources of deformation when a layer is deposited: the layer self-weight, the weight of higher layers (element self-weight) and the extrusion pressure. The hydrostatic pressure increases with the built height, causing incremental deformations: therefore, since commonly the height of the layer is kept constant during printing, the distance between the nozzle and the working surface incrementally increases. Moreover, each layer has a distinctive stiffness and strength, function of its age: this potentially alters the shape stability and the adhesion to the previous layer; combining this with printing imperfections, the staking is partially governed by the effective stiffness of overlapped layers [37]. As a result, the shape stability is directly correlated with deformation-based failures. Accordingly, we investigate two buildup rate deformative problems: the instantaneous compressive stability (related with the curing time) and the time-dependent early age creep.

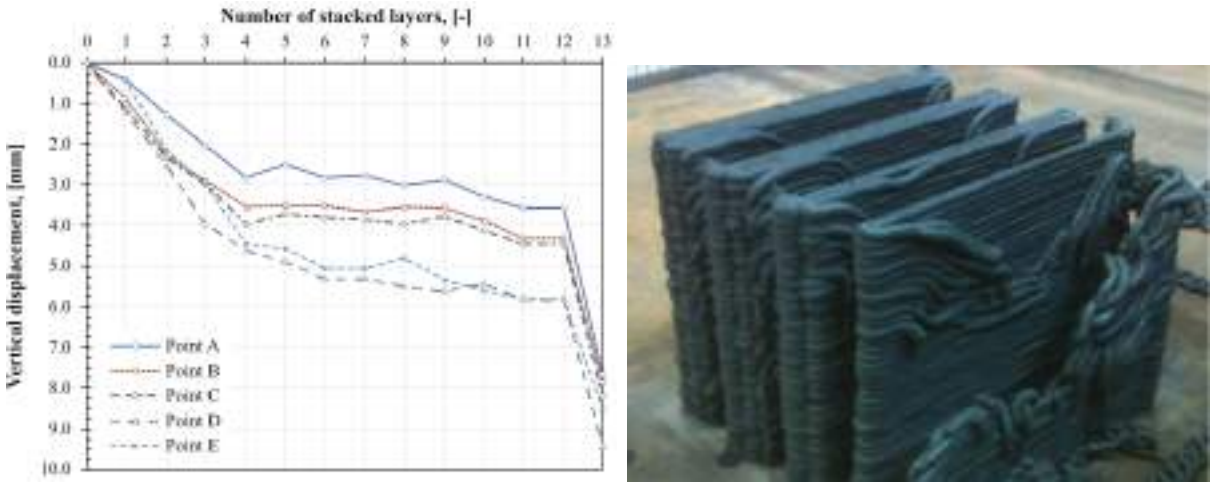

(a) (b)

Figure 5.3: Buildability tests, after [49].

5.2 Testing procedures

In the previous section we have qualitatively emphasized the main challenges that need to be addressed in order to achieve a robust 3D concrete printing process and to determine minimum performance requirements. Meet these criteria means to grow a comprehensive knowledge on the early age concrete, incorporating insight on microstructural changes occurring during

cement hydration. Therefore, in the present work, the emphasis is posed on the evolution of stiffness and strength when the fresh mix develops from the deformable to the hardened state: the mechanical behavior of fresh concrete is evaluated during the open and the layer-cycle time (within the range of 0 to 60 min after mixing, the typical duration of a 3D printing process). In general, experimental tests on standard cast concrete cannot be executed until the first setting has occurred. Consequently, to date, response results before initial setting are sparse and scattered [41, 50]. As the mortar is in fresh state, even after the first setting it is extremely challenging to extract specimens from their mold without affecting their integrity.

To overcome this issue, we design a plastic 3D printed openable mould (Fig. 5.4) by which we can reproduce cylindrical specimens with good shape retention, even if concrete is in fresh state: the measurement of the performances at early ages allows the development of these performances to be monitored since the very beginning. Since a temporary mould is used, part of gravity-induced stresses are sustained by this support through interface friction stresses, due to adhesion to internal surfaces: sensitivity of experimental results to such interface friction is investigated, equipping the mold with an internal nylon membrane (interposed between the mold and the specimen) that actively reduce the interface friction (Fig. 5.4).

Furthermore, to increase workability and compensate low water-to-binder ratio, it is a common practice to add superplasticizer; however, quantities exceeding the optimum might conduct to unwanted flowability, affecting buildability. Therefore, another crucial outcome is to give insight on the sensitivity of the applied superplasticizer amount to the early age stiffness and strength development. All samples are tested at room temperature T$\approx 22^{o}$C.

As a result, **315** tests are executed, as summarized in the following.

	Uniaxial unconfined compression tests (fresh)	**Uniaxial unconfined compression test (mature)**	**Creep tests**	**Rheological tests**
Age [min]	0, 15, 30, 60	40320 (28 days)	0, 15, 30, 60	0, 15, 30, 60
Superplasticizer [%]	0.0, 0.1, 0.15	0.0, 0.1, 0.15	0.0, 0.1, 0.15	0.1, 0.15
Number of samples per set	5	5	5	1
Membrane	With & Without	-	With	-
Buildup rate [steps]	-	-	1, 2, 3	-
Duration [sec]	-	-	300, 900	180
Shear rate [1/sec]	-	-	-	1, 2.5, 5, 7.5, 10
Tot. number of samples	**120**	**15**	**140**	**40**

Table 5.1: Test matrix.

(a) (b) (c)

Figure 5.4: The 3D printed openable mould for concrete sample preparation.

5.3 Uniaxial unconfined compression tests

5.3.1 Introduction

In order to obtain a comprehensive characterization of the early age constitutive behaviour of 3D printable concrete (i.e. the stress-strain curves), compressive tests should be performed within a proper time-frame that ideally emulates the time delay between the material release from the nozzle and the consequent printing step. Unfortunately, until now compressive tests have no standard procedures for early age printable concrete samples. However, an appropriate test framework is desired in order to enhance the knowledge about the mechanical behaviour of printable concrete during the printing process. Considering the physical state of early age printable mortars, possible testing standards may be adapted from those valid for soil or fresh concrete; however, in some specific cases, these could be not applicable and require completely new test methods. Nonetheless, key aspects that need to be addressed include representative sample size, testing equipment, loading/displacement rate, specimen preparation in terms of pouring procedure and material compaction, measurement devices, etc.

In the available literature, limited research has been carried out on early age compression properties of 3D printable concrete [41, 43, 50] whereas many authors [53, 67, 68] have investigated the hardened state (with minimum test age of 24 hours) which, in practice, is not useful to predict the mechanical performance of the structural element during the printing process. With the aim of predicting buildability performances of cementitious printable mortars, Perrot et al. [41] proposed a strength-based failure criterion based on the comparison of the vertical stress acting on the first printed layer with the critical stress related to the plastic deformation that is linked to the material yield stress. Such a model was validated using squeeze flow tests performed on very early age concrete. In detail, in order to simulate a layer-by-layer construction, authors loaded a cylindrical sample by applying 1.5 N load increments (i.e. corresponding to the increasing weight of the layer-by-layer deposition). The time elapsed between load increments was also varied to simulate different building rates (in the range of 1 to 6.2 m/h). The experimental campaign was appropriate to detect the sample failure; however, no stress-strain relationships were provided in the study.

Kazemian et al. [43] investigated shape stability (also called shape retention or "green" strength) through two different test methods, namely "layer settlement test" and "cylinder stability". These techniques evaluated the compression response of layered samples. Indeed, in the cylinder stability test, a cylindrical sample with total height of 80 mm (composed by two concrete layers of 40mm) was loaded with 5.5 kg (i.e. 4.77 kPa): any possible change in the height as a result of self-weight and applied load was then measured and recorded for different concrete mixtures. Hence, no stress-strain relationships were reported in this type of test method.

By contrast, constitutive laws related to early age printable concrete material were provided by Wolfs et al. [50, 69]. A customised triaxial compressive test (TCT) was carried out on cylindrical concrete samples according to ASTM D2850. The samples were not compacted during the preparation and then subjected to triaxial compression in displacement-controlled conditions and at distinct concrete ages (i.e. 15, 30, 60 and 90 minutes). The displacement rate of 15 mm/min (i.e. 30% strain/min) was fast enough to neglect effects of thixotropic build-up/aging during individual tests. Results of TCT related to confining pressure equal to zero can be compared with those of uniaxial unconfined compressive tests (UUCT) performed

by same authors [50, 69]. In particular, UUC tests were carried out on cylindrical concrete samples, with a diameter of d = 70 mm and height of h = 140 mm, designed according to ASTM D2166 [69]. In this case, the preparation procedure was directed to obtain a homogeneous sample and consisted in using steel cylindrical moulds lined with a thin sheet of Teflon in combination with compaction for 5 s on a 30 Hz vibration table The same concrete age range (t = 5, 15, 30, 60 and 90 minutes) was adopted for tests, as well as the same displacement rate of 42 mm/min, i.e. 30% strain/min, allowing for a proper comparison with the TCT in terms of stress-strain relationships. The comparison of the two test results, UUCT and TCT, highlighted discrepancies in terms of strength and stiffness values, probably associated with the better compaction of the samples in the UUCT, which improved the concrete mechanical proprieties. Indeed, the imperfection density is typically much larger in the case of fresh concrete without compaction; moreover, the impact of such imperfections is generally amplified for small size specimens (i.e. TCT).

From what above said, it appears that the need to define standard testing procedures is indisputable. On one hand, establishing universal acceptance criteria for printable concrete would require a large number of relevant studies to encompass the performance of different printing mixtures used in digital fabrication projects. On the other hand, mechanical parameters (e.g. compressive stress-strain laws, stiffness, yield stress etc.) of the printable mortar in the un-layered state represent the starting point for the implementation of any predictive model, simulating the printing process itself and related mechanical phenomena. Following this motivation, the present work aims to investigate the effects of compression test parameters on the mechanical behaviour of a printable cementitious mortar; in particular, the following aspects are considered:

- Material and sample preparation: during an automated printing process, it is possible to experience variations in the compaction of the extruded material, due to random changes in water content, different conditions of the stocked dry material, human errors, etc. Furthermore, since the material is in an early age (or fresh) state when it comes out from the printing nozzle, there are practical difficulties in simulating these conditions during the laboratory specimen preparation (i.e. pouring, compaction and demoulding).
- Compressive test setup: to properly run the experiments, representative samples should be subjected to compression load/displacement. Since printable cement-based materials roughly behave as visco–plastic Bingham materials, their mechanical response is strongly influenced by the loading rate, which could significantly affect the measured strength.
- Evolution in time of compression stress/strain: compressive strength and stiffness of early age concrete inevitably changes during the printing process. Since early age mechanical properties evolve in time, during the printing process each layer behaves differently than other ones, especially for high value of the cycle-time (i.e. time required to complete one build layer) [49].

In order to investigate these aspects, results of uniaxial compressive tests performed on a printable cementitious material already used in [70] are compared with the results obtained by varying: (i) the percentage of superplasticizer, (ii) the sample preparation procedure, (iii) the displacement rate adopted during the test. Furthermore, compressive tests are carried out at distinct concrete age of t = 0, 15, 30 and 60 minutes in order to define the evolution in time of the constitutive stress-strain law.

5.3.2 Material and methods

In this section we provide details of a reference 3D printable mix (already used in [70]). Results of uniaxial compressive tests performed on this material, used as reference mix (REF), are compared with results obtained by varying:

- material and sample preparation;
- displacement rate adopted during the test.

Furthermore, compressive tests are performed at distinct concrete age, t = 0, 15, 30 and 60 minutes, in order to define the time evolution of the stress-strain constitutive law.

5.3.2.1 Material

Printable cementitious mortars should be designed in order to meet specific performance requirements, both in the fresh and in the hardened state. In early age, fresh materials should satisfy specific rheological requisites in order to achieve an optimized balance among workability, extrudability and buildability. In the hardened state, the structural performance is correlated to strength and stiffness material proprieties.

The reference mix contains sand with a maximum size of 4mm, in agreement with the diameter of the nozzle used in [70] (i.e. 25mm), CEM type I 42.5N and limestone fillers ($CaCO_3$). A percentage value of 0.5% in cement weight of polypropylene fibres is also added to the mixture to prevent plastic shrinkage cracking (in the early age stage and after the deposition process). Nonetheless, since the viscosity of the printing material is affected by the presence of fibres and by the water-to-binder ratio (i.e. w/c=0.35), the mix has to be adjusted with polycarboxylate superplasticizer (0.10% by weight of cement) in order to achieve an optimal rheological balance with respect to material pumpability. The reference mix is named with the acronym SP0.10 (i.e. the percentage value of Super Plasticizer is equal to 0.10%) and its components are reported in Tab. 5.2. Starting from the reference mix we consider superplasticizer variations in order to entail variations of material consistency during the printing process; in particular, the following conditions are examined: (i) absence of superplasticizer (i.e. 0.00% - SP0.00) and (ii) 0.15% of superplasticizer (i.e. SP0.15).

Mixture ID	**Fine aggregate [kg/m3]**	**Cement [kg/m3]**	**Water [kg/m3]**	**Limestone Filler [kg/m3]**	**Fibers [kg/m3]**	**SuperPlasticizer %**
REF-SP0.10	1456	497	174	101	1	**0.10**

Table 5.2: Reference mix design.

5.3.2.2 Specimen preparation

Compression tests are performed on cylindrical samples, having the diameter (d) of 60mm and the height (h) of 120mm: the geometry is chosen to exclude size effects due to particle size distribution and to have h/d=2, i.e., to allow diagonal shear failure (this may also depends on the friction between the specimen end faces). Initially, the fine aggregate, cement and filler are mixed for 60 seconds at low speed (140 rpm). Subsequently, such dry components are mixed

with polypropylene fibers (140 rpm – 30 seconds). Afterwards, water is added mixing again for 60 seconds (140 rpm). Finally, poly-carboxylic superplasticizer (CE) is added gradually, mixing for 120 seconds at high speed (285 rpm).

As aforementioned, experimental tests on standard cast concrete cannot be executed until the first setting has occurred. However, layered extrusion technique is a process by which subsequent fresh concrete layers are stacked on top of each other: as a result, the vertical stress and strain due to compressive loads may potentially lead to strength- and deformation-based failures of 3D printed layers. Even after the first setting, it is complex to extract specimens from the mould without affecting their integrity. In order to overcome this issue, we design a plastic 3D printed openable mould, by which we can reproduce cylindrical specimens with good shape retention.

Since a temporary mould is used, part of gravity-induced stresses is sustained by this support through interface adhesion: after the demoulding, the sample could be affected by residual stresses and imperfection. Improvements in the sample preparation are achieved using an internal nylon membrane (interposed between the mould and the specimen) that actively reduce the interface friction (Fig. 5.4). After casting, the samples are demoulded and the membrane is removed: in this way the curing takes place in the same condition both for sample cast with membrane and sample cast without membrane. Hence, also the influence of the specimen preparation is studied, by comparing results obtained with (M - Membrane) or without (NM – No Membrane) the use of the membrane during casting.

Before testing, samples are demuolded and the membrane is removed in order to start cement hydration.

5.3.2.3 Compressive tests

Specimens are tested in an electromechanical Universal Testing Machine, with 10kN capacity in displacement-control condition at room temperature T$\approx 22^oC$. Tests are performed up to a vertical strain of 12%, i.e. 15 mm in displacement.

Since no physical measurement on the sample are considered feasible without altering the specimen, stress and strain are deduced from force-displacement diagrams. In particular, the stress is computed by dividing the recorded load for the cross-sectional area of the sample (i.e. 2826 mm^2), whereas the strain is obtained by dividing the displacement of the loading head for the initial height of the sample. The Young's modulus is computed as secant modulus from 0% to 2% of the strain. In order to achieve the evolution in time of the stress-strain law, compressive tests are carried out at distinct concrete ages of t = 0, 15, 30 and 60 minutes with displacement rate of 3mm/min (Displacement Rate – DR). Since mechanical properties of cementitious materials are rate sensitive, compressive tests are performed, only for the reference mix, together with a higher value of displacement rate (i.e. 30mm/min), in order to compare the results.

5.3.2.4 Summary of tests

Uniaxial unconfined compressive tests are carried out, for five samples, by varying: (i) the concrete age (i.e. t=0, 15, 30 and 60 minutes), (ii) the percentage of Superplasticizer (i.e. 0.00, 0.10 and 0.15% in weight of cement), (iii) the sample casting procedure (with or without the membrane) and (iv) the displacement rate (i.e. 3mm/min and 30mm/min). In Tab.

5.3 such variables are summarized. Each specimen set is identified by the acronym "SPxx-yM-DRzz", where "SPxx" represents the percentage of superplasticizer (SP0.00, SP0.10 and SP0.15), "yM" indicates if the membrane is used during the casting (M and NM, respectively if the nylon membrane is used or not) and "DRzz" is the value of displacement rate in mm/min (DR3 or DR30). The reference test is indicated by the acronym "REF-SP0.10-M-DR3".

Variables	**Uniaxial unconfined compression tests**					
Acronym	**REF-SP0.10-M-DR3**	**SP0.00-M-DR3**	**SP0.15-M-DR3**	**SP0.00-NM-DR3**	**SP0.10-NM-DR3**	**SP0.10-M-DR30**
1. Age [min]	0, 15, 30, 60	0, 15, 30, 60	0, 15, 30, 60	0, 15, 30, 60	0, 15, 30, 60	0, 15, 30, 60
2. Superplasticizer [%]	0.1	0.0	0.15	0.0	0.1	0.1
3. Membrane	Yes	Yes	Yes	No	No	Yes
4. Displacement rate [mm/min]	3.0	3.0	3.0	3.0	3.0	30.0
Samples per set	5	5	5	5	5	5
Tot. samples	20	20	20	20	20	20

Table 5.3: Test matrix.

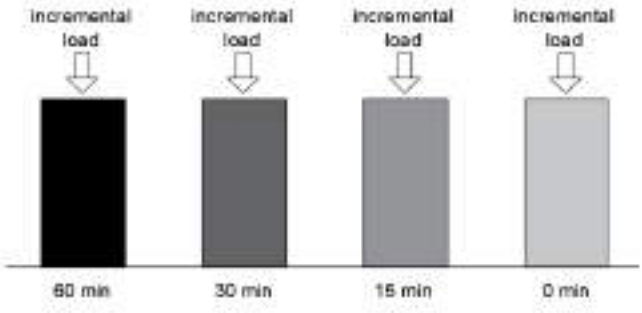

Figure 5.5: Schematic of early age sample set with different curing time.

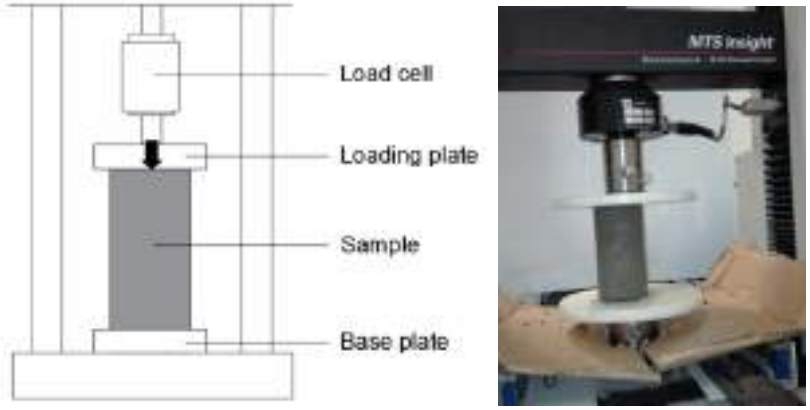

(a) (b)

Figure 5.6: Sketch of uniaxial unconfined compression test.

5.3.2.5 Analytical model

Since the material is in the early age state, which implies low resistance and stiffness values, during printing stability checks of the structural element are necessary, including:

- A compression check;

- A self-buckling check.

The structural performance of early age material strictly depends on the temporal evolution of some mechanical parameters; therefore, an experimental characterization is necessary. In the following section, uniaxial compressive test results for (different concrete age) are shown, by varying the percentage of superplasticizer (i.e. 0, 0.1, 0.15% in cement weight), the casting condition (with or without a nylon membrane interposed between the sample and the mould) and the displacement rate (low and high rate, i.e. 3mm/min or 30mm/min).

The obtained constitutive laws $\sigma - \epsilon$, carried out for different concrete age, provide the temporal evolution of the strength $\sigma_{c,max}$(t) and Young's Modulus E(t). Such laws are obtained through a linear regression of data, related to each tested sample. Starting from $\sigma_{c,max}$(t) and E(t), an analytical model is developed to predict the compressive failure, at the first layer, and the self-buckling failure of the printed element, due to its own weight during the printing process. The hypothesis of instantaneous deposition of each layer is made. The time elapsed between the deposition of a layer and the subsequent (i.e. the cycle-time) depends on the layer height and the building rate, as follows:

$$T_{print} = \frac{h_{layer}}{B_R} \tag{5.1}$$

The success of the printing process is strongly correlated to the building rate B_R [mm/min], being fundamental the time variation between consecutive layers [41]. The maximum number of layers which could be stacked before the collapse due to the compression of the first layer, can be obtained by comparing the vertical stress in the first layer σ_V and the developed strength $\sigma_{c,max}$:

$$\textbf{Compression failure} : \sigma_V(t) = H(t)\rho g \leq \sigma_{c,max}(t) \tag{5.2}$$

where H is the total height of the printed element, ρ is the material density and $\sigma_{c,max}$(t) is the linear law obtained from experimental data.

The elastic self-buckling failure check is determined according to the Greenhill's equation (1981); a free-standing vertical column buckles under its own weight if its height exceeds the following critical value:

$$H_{crit}(t) = (7.8373\frac{E(t)I_{min}}{\rho g A})^{1/3} \tag{5.3}$$

where E(t) is the law of the elastic modulus, I_{min} is the minimum moment of inertia (depending to the shape of the printed element), A is the horizontal cross-sectional area and ρ is the density of the material. Considering the simple geometry of a wall, especially by referring to its linear meter, the previous expression becomes:

$$H_{crit}(t) \approx (0.65\frac{E(t)\delta^2}{\rho g})^{1/3} \tag{5.4}$$

being the minimum moment of inertia equal to $I_{min} = \delta^3/12$ and cross-section area $A = \delta$. The self-buckling failure could be approximately predicted by comparing the printed element height to the critical height (according to Greenhill's equation). Though, the stability check is currently made [57] by the comparison between the elastic modulus obtained experimentally and its critical value E_{crit} (t):

$$\textbf{Self-Buckling failure} : E(t) \leq E_{crit}(t) \approx 0.65 \frac{H^3(t)\rho g}{\delta^2} \tag{5.5}$$

Expressions 5.2 and 5.5 are used in the following section to predict the compressive and self-buckling failure, adopting results obtained from each examined testing condition (see summary of the test matrix – Tab. 5.3). In this way it is possible to study the influence of a specific testing procedure on the prediction of the structural performance of the element during the printing process.

5.3.3 Results

Experimental testing results are reported in this section in terms of force-displacement and stress-strain curves for each concrete age examined. In particular, the data are grouped and compared in order to study the influence of: (i) the concrete age, (ii) the material and sample preparation and (iii) the displacement rate. In the following stress-strain charts, the curve related to each sample is reported in grey, whereas the average curve is black. Due to the imperfect flatness of the top surface of samples, the force of the loading cell begins to stabilize around 5N; so does the stress-strain curves, starting from 2kPa (i.e. 2kPa is the stress at 0% of strain). Results condensed in the following pages are structured in this way: the force-displacement and stress-strain curve related to the reference mix are reported and compared for each value of the curing time; then the influence of the material consistency and sample preparation is investigated. Finally the results achieved with different displacement rate are compared.

5.3.3.1 Influence of age

Experimental force-displacement curves are converted into stress-strain curves: the comparison between stress-strain average curves - related to distinct concrete ages - is reported in Fig. 5.10. It is possible to observe that, as the resting time increases, there is a transition from plastic to brittle behaviour, in addition to an increase in strength and stiffness. After an initial linear-elastic behaviour (the strain limit of the elastic range is approximately 2%), the stress reaches a peak value (i.e., the compressive strength $\sigma_{c,max}$) and then decreases again along the softening branch. The average compressive strength is equal to 8kPa at 0 minutes and grows until 22kPa at 60 minutes. Curves increase roughly linearly in the elastic range; after this initial range, the force decreases as the vertical strain increases (softening). The second branch of force-displacement curves reveals that softening is more evident for older specimens (i.e. t= 30 and 60 min) respect to younger ones (i.e. t= 0 and 15 min). This difference depends to lateral deformations: since fresh concrete is more fluid, lateral deformation are hampered by a relatively low stiffness (that increase with curing time), failing by bulging. By contrast, older samples expand less, having a more definite failure plane evolution.

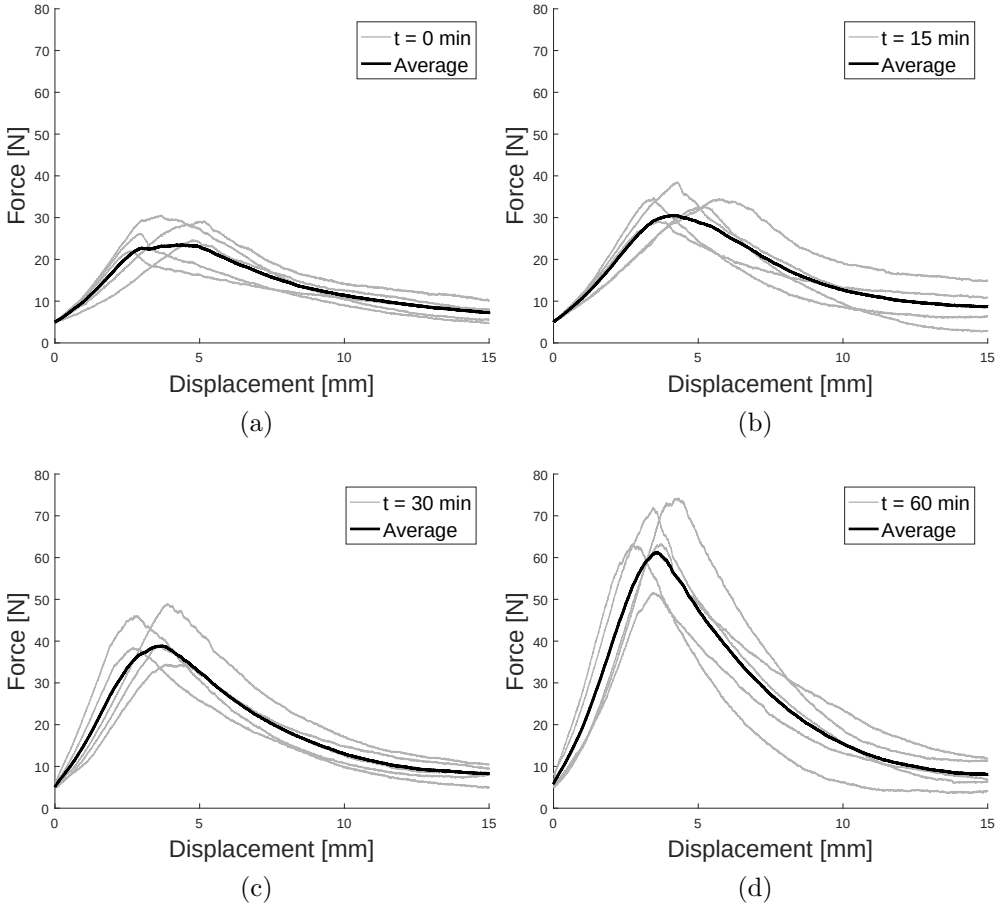

Figure 5.7: Compression tests, 0.1% plasticizer with membrane. Average and individual results at different time - (a) 0 minutes, (b) 15 minutes, (c) 30 minutes, (d) 60 minutes.

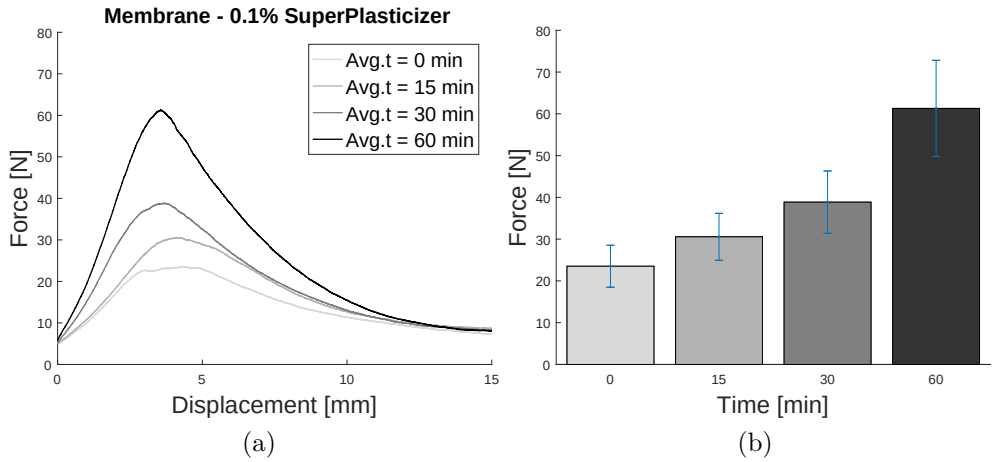

Figure 5.8: Compression tests, 0.1% plasticizer with membrane. Average comparisons at different time - 0 minutes, 15 minutes, 30 minutes, 60 minutes - (a) trend & (b) peaks with standard deviation.

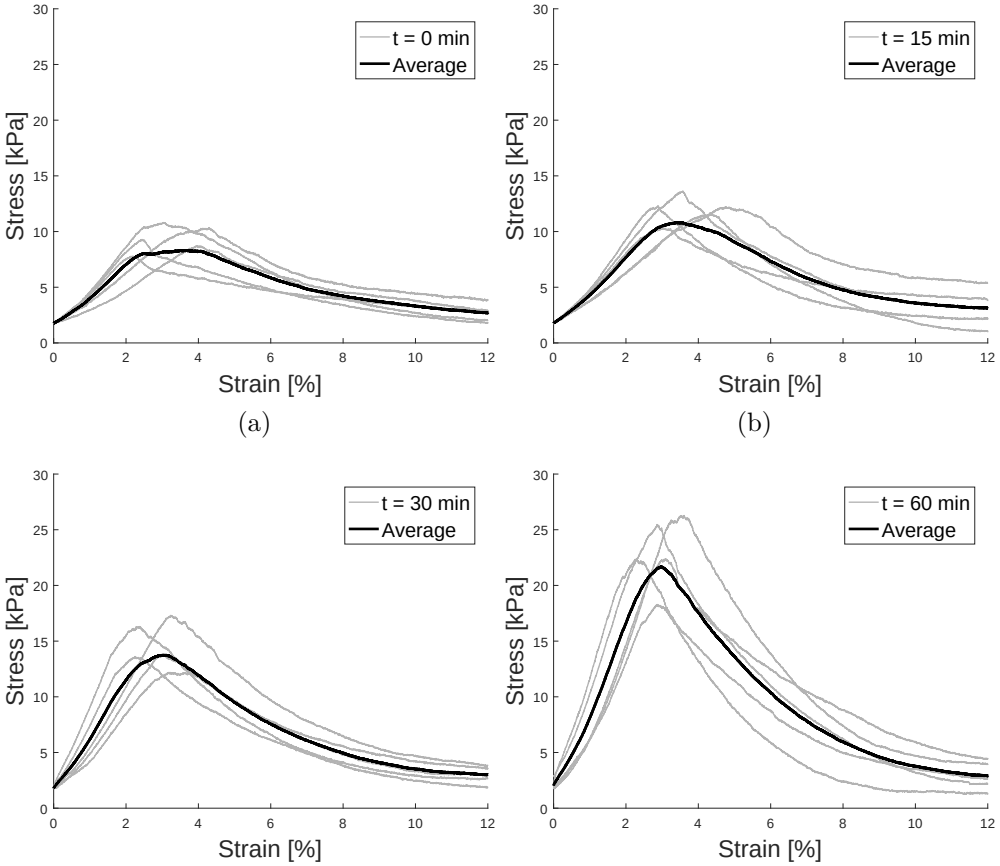

Figure 5.9: Compression tests, 0.1% plasticizer with membrane. Average and individual results at different time - (a) 0 minutes, (b) 15 minutes, (c) 30 minutes, (d) 60 minutes.

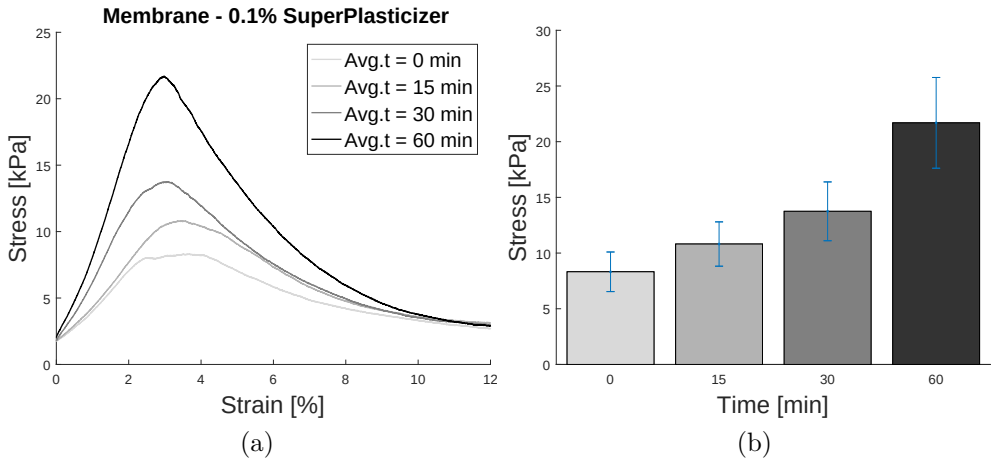

Figure 5.10: Compression tests, 0.1% plasticizer with membrane. Average comparisons at different time - 0 minutes, 15 minutes, 30 minutes, 60 minutes - (a) trend & (b) peaks with standard deviation.

5.3.3.2 Influence of the material

During the sample preparation, the absence of superplasticizer (i.e. SP0.00) results in a workability loss, and related samples are characterized by more imperfections and voids. By contrast, an increment of superplasticizer (i.e. SP0.15), compared to the reference mix, leads to an excessive fluidity of the material, resulting in particle segregation. In Fig. 5.11 stress-strain average curves of the reference mix (a) are compared with average curves obtained with 0.00% (b) and 0.15% (c) of superplasticizer: in both cases there is a decrement of compressive strength. In Fig. 5.24, the average value of compressive strength is reported in function of time and percentage of superplasticizer: 0.00% of SP or 0.15% of SP provide lower values of compressive strength (at t=0 the compressive strength is 8kPa for the reference mix, and its value drops around 5kPa both for SP0.00 and SP0.015) and higher values of relative standard deviation (RSD). At t=0 the RSD is 21.73% for the reference mix, whereas its value grows to 44.86% and 40.42% for 0.00% and 0.15% of SP, respectively. A summary of average compressive strength and Young's modulus values are reported in Tabs. 5.4-5.6.

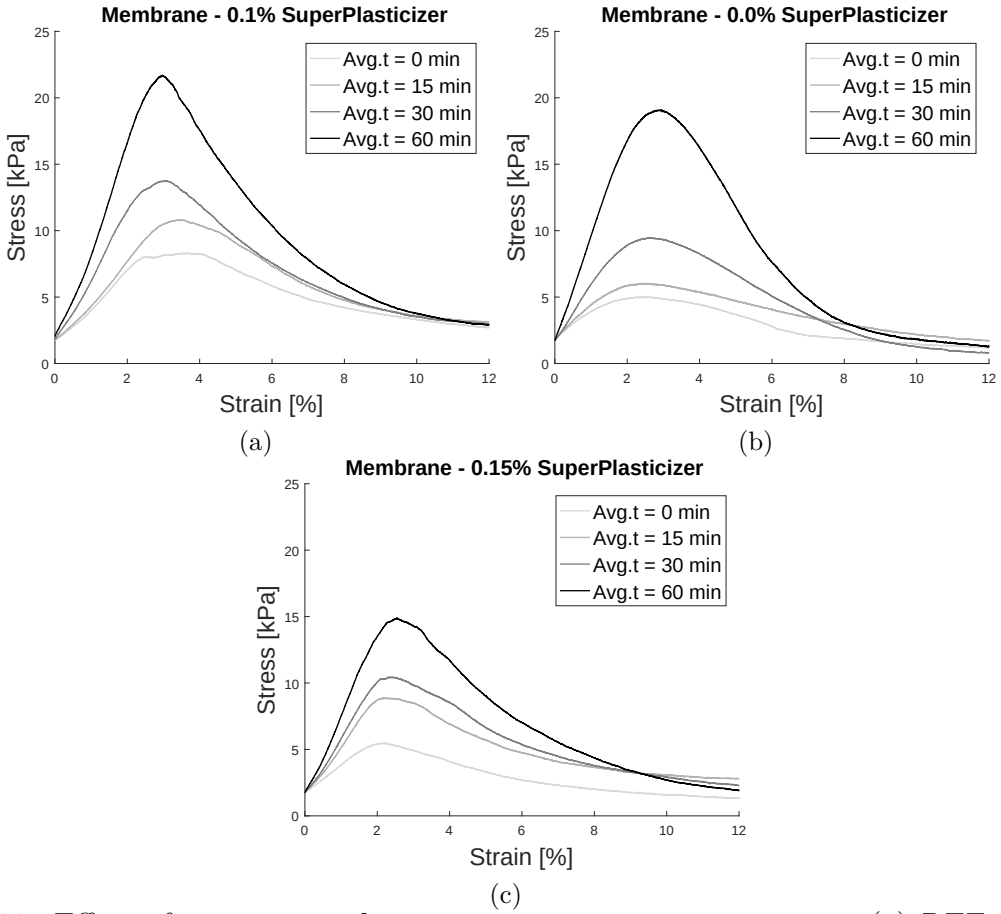

Figure 5.11: Effect of printing conditions, average stress-strain curves: (a) REF-SP0.10-M-DR3, (b) SP0.00-M-DR3 & (c) SP0.15-M-DR3.

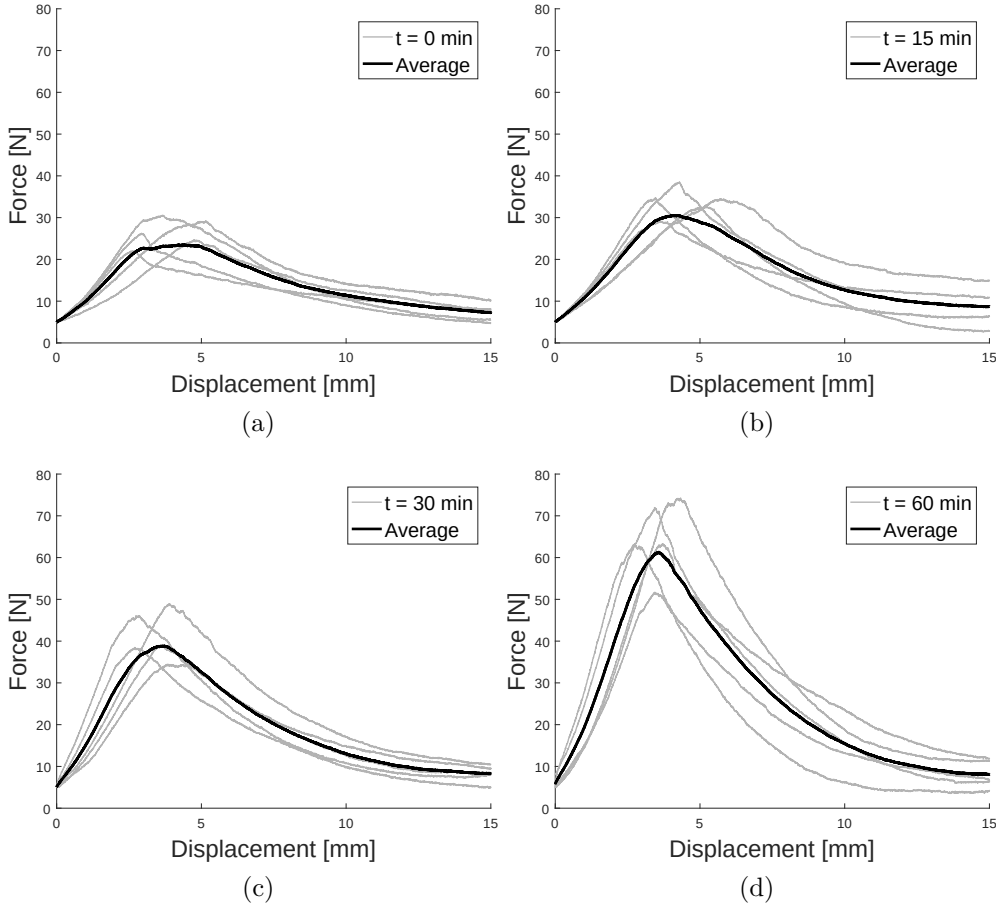

Figure 5.12: Compression tests, 0.1% plasticizer with membrane. Average and individual results at different time - (a) 0 minutes, (b) 15 minutes, (c) 30 minutes, (d) 60 minutes.

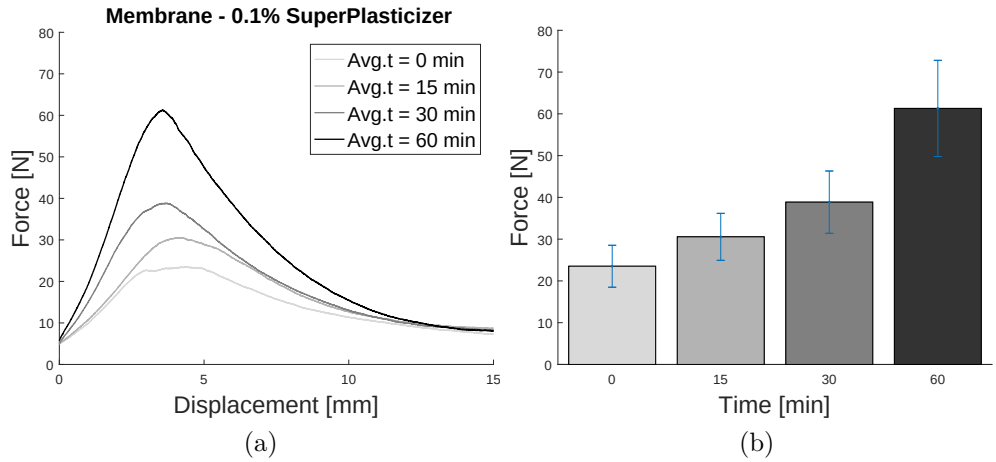

Figure 5.13: Compression tests, 0.1% plasticizer with membrane. Average comparisons at different time - 0 minutes, 15 minutes, 30 minutes, 60 minutes - (a) trend & (b) peaks with standard deviation.

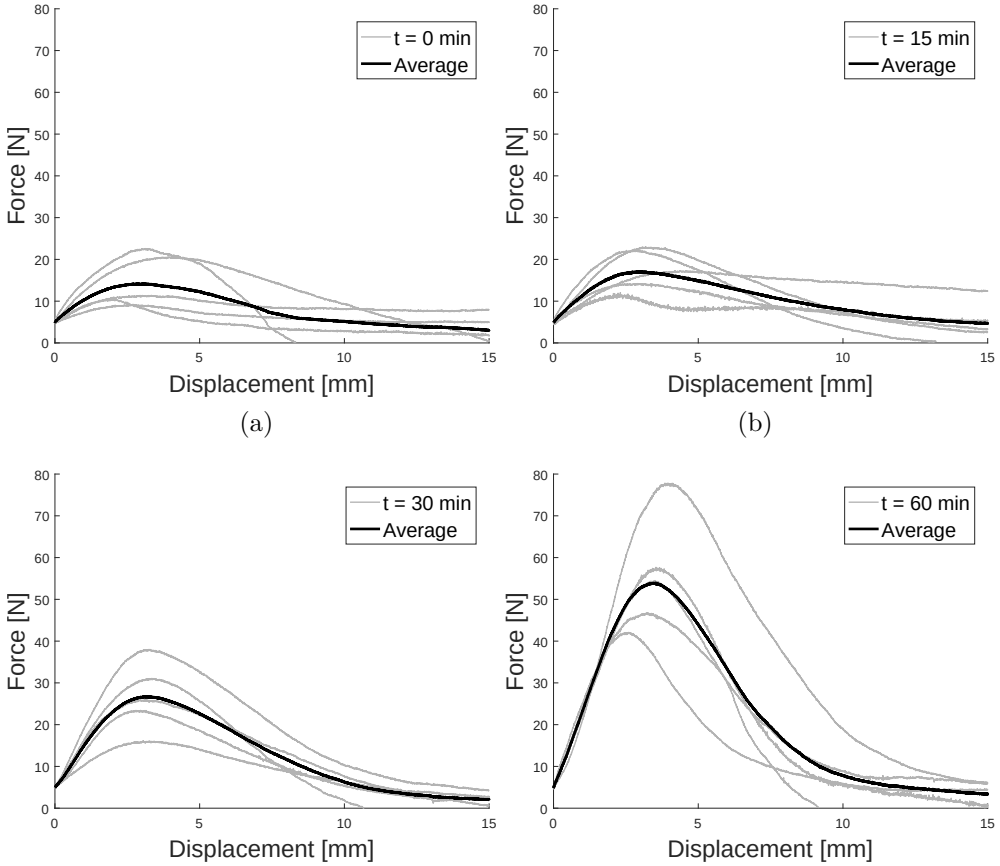

Figure 5.14: Compression tests, 0.0% plasticizer with membrane. Average and individual results at different time - (a) 0 minutes, (b) 15 minutes, (c) 30 minutes, (d) 60 minutes.

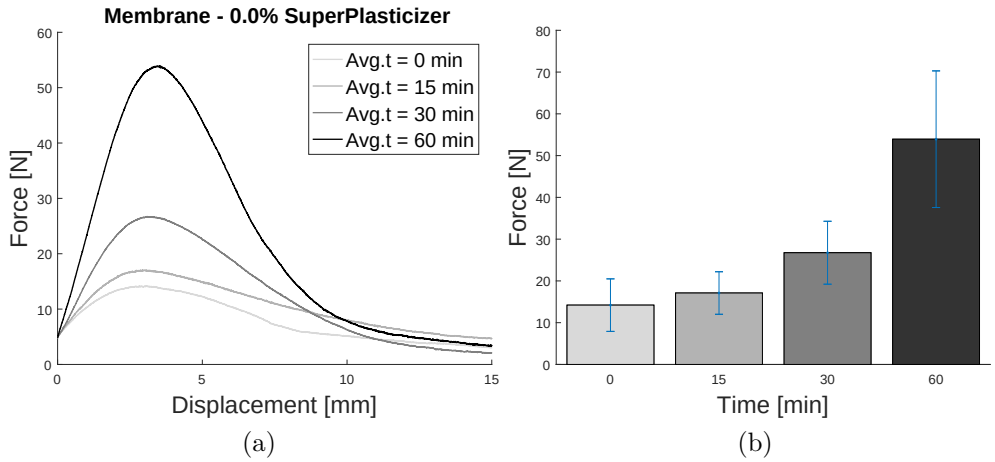

Figure 5.15: Compression tests, 0.0% plasticizer with membrane. Average comparisons at different time - 0 minutes, 15 minutes, 30 minutes, 60 minutes - (a) trend & (b) peaks with standard deviation.

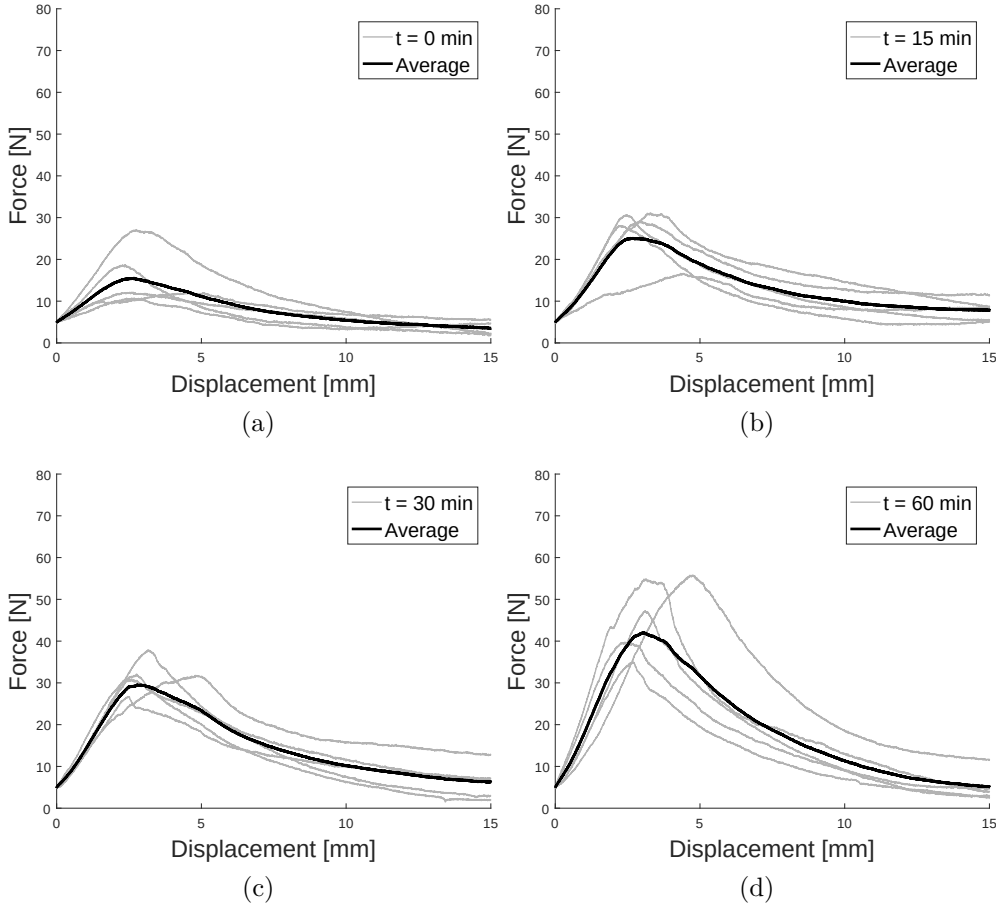

Figure 5.16: Compression tests, 0.15% plasticizer with membrane. Average and individual results at different time - (a) 0 minutes, (b) 15 minutes, (c) 30 minutes, (d) 60 minutes.

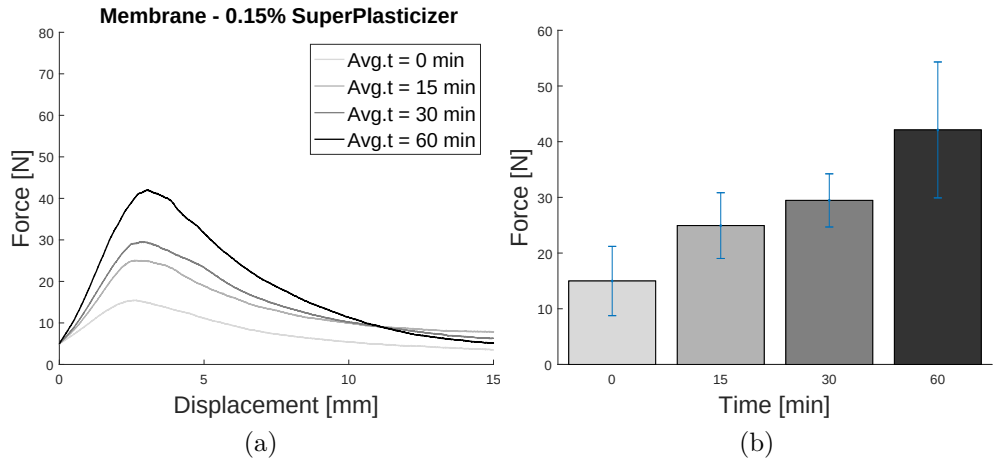

Figure 5.17: Compression tests, 0.15% plasticizer with membrane. Average comparisons at different time - 0 minutes, 15 minutes, 30 minutes, 60 minutes - (a) trend & (b) peaks with standard deviation.

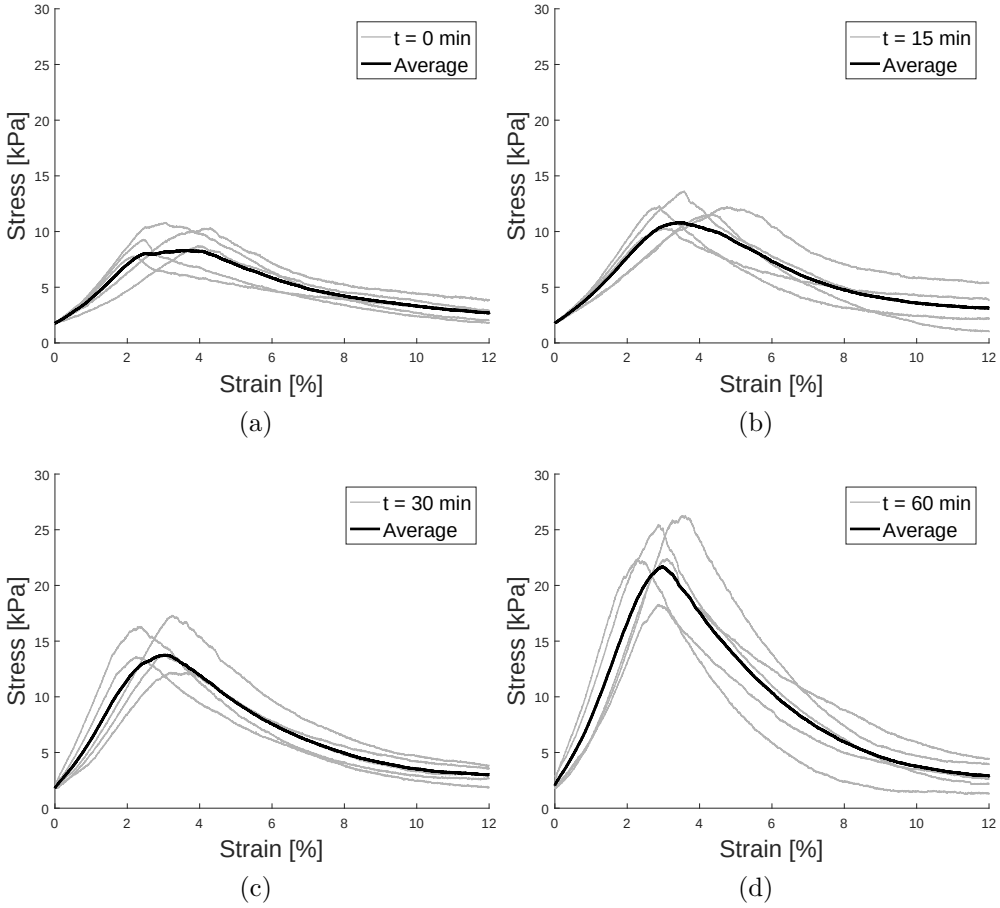

Figure 5.18: Compression tests, 0.1% plasticizer with membrane. Average and individual results at different time - (a) 0 minutes, (b) 15 minutes, (c) 30 minutes, (d) 60 minutes.

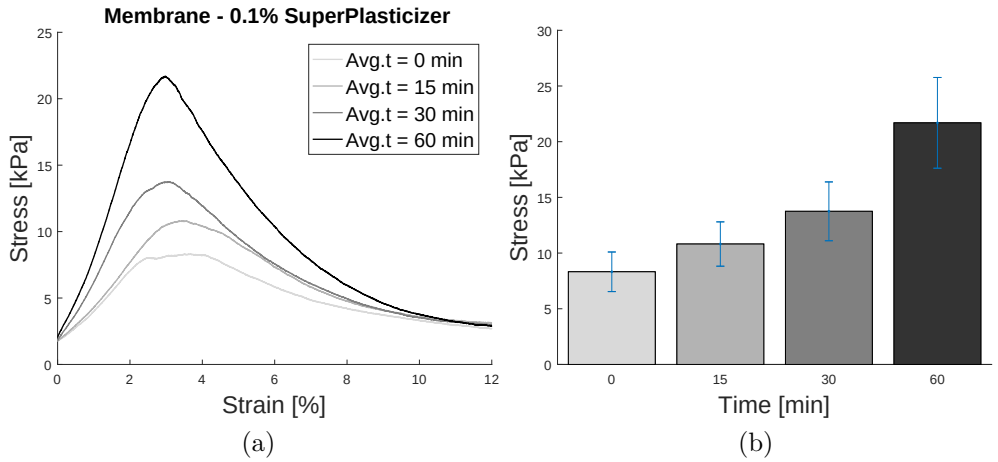

Figure 5.19: Compression tests, 0.1% plasticizer with membrane. Average comparisons at different time - 0 minutes, 15 minutes, 30 minutes, 60 minutes - (a) trend & (b) peaks with standard deviation.

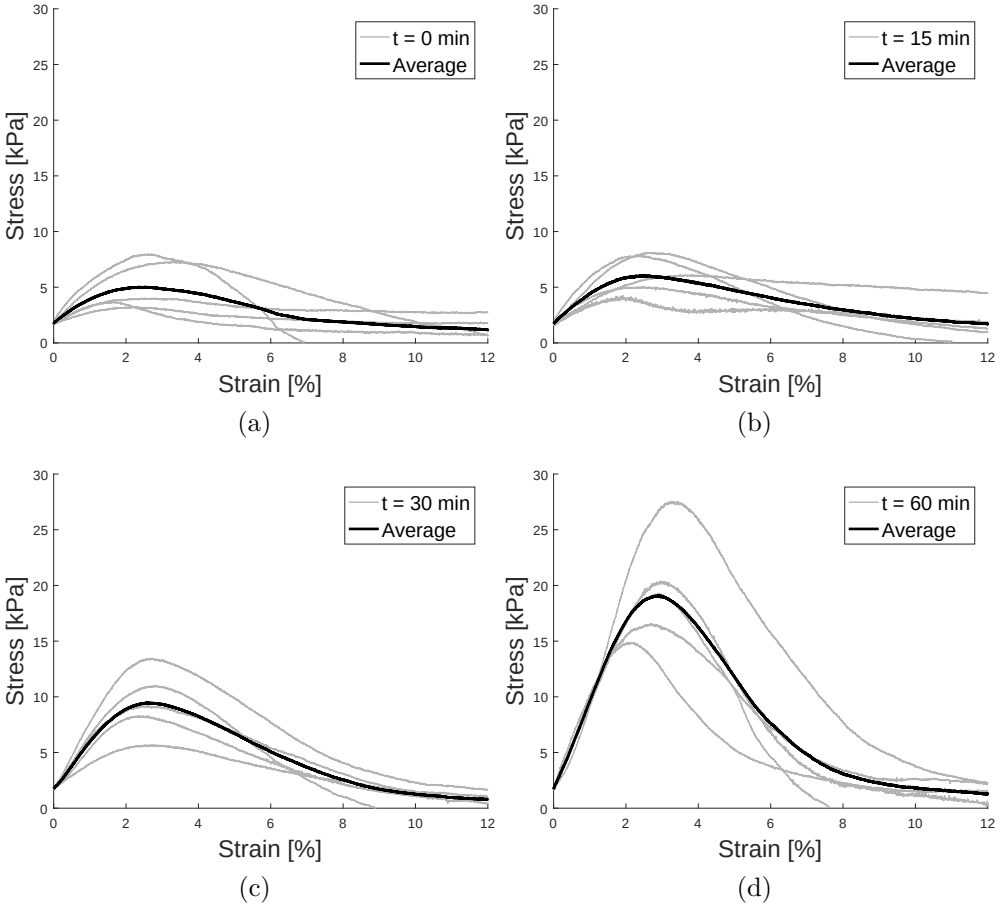

Figure 5.20: Compression tests, 0.0% plasticizer with membrane. Average and individual results at different time - (a) 0 minutes, (b) 15 minutes, (c) 30 minutes, (d) 60 minutes.

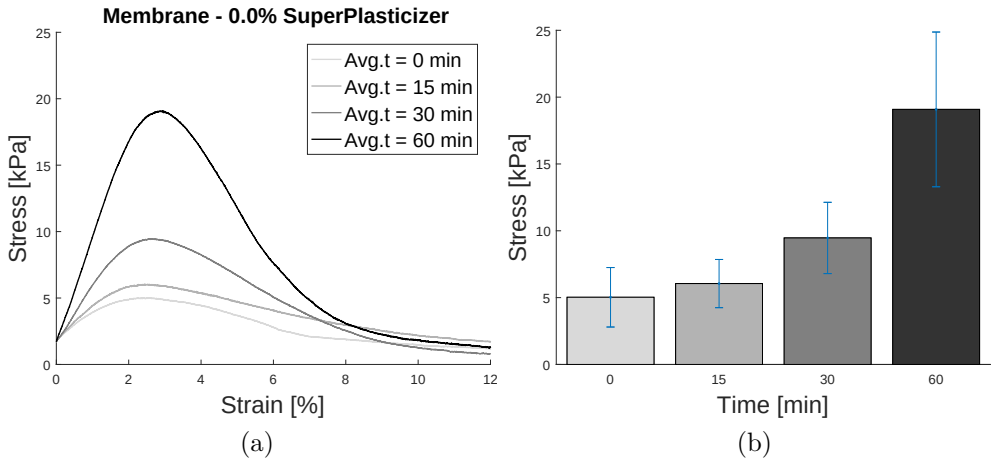

Figure 5.21: Compression tests, 0.0% plasticizer with membrane. Average comparisons at different time - 0 minutes, 15 minutes, 30 minutes, 60 minutes - (a) trend & (b) peaks with standard deviation.

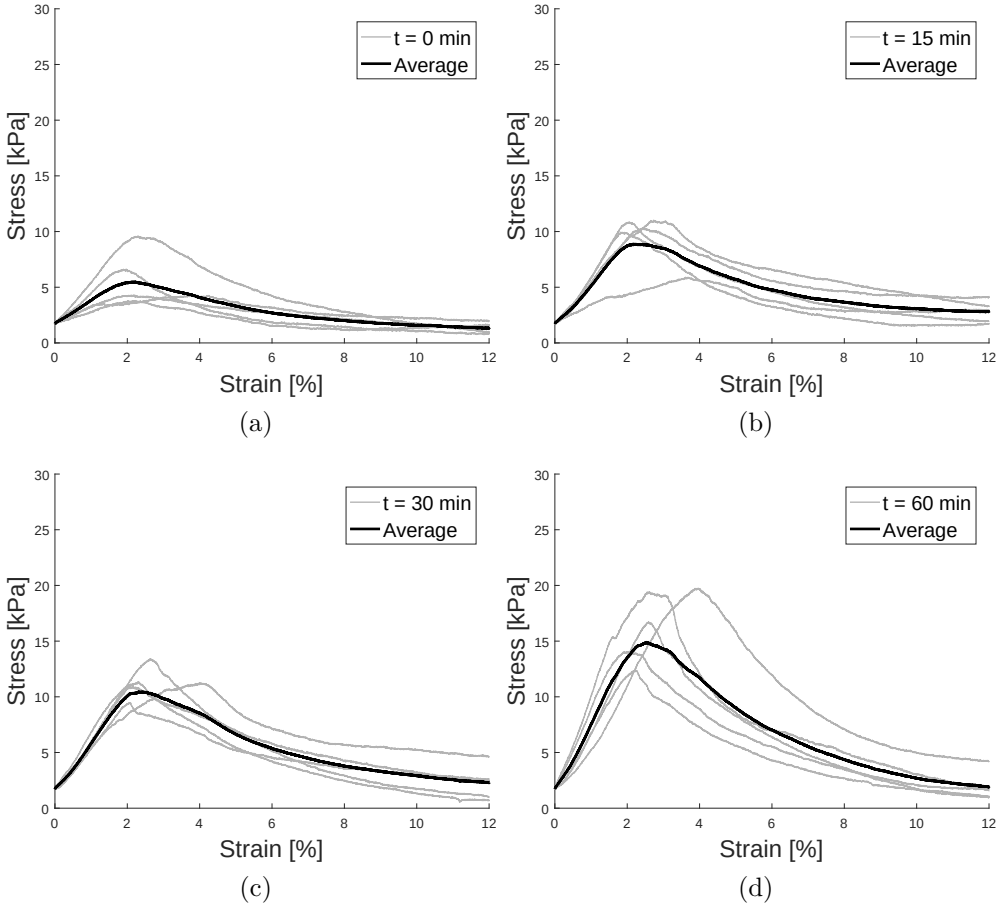

Figure 5.22: Compression tests, 0.15% plasticizer with membrane. Average and individual results at different time - (a) 0 minutes, (b) 15 minutes, (c) 30 minutes, (d) 60 minutes.

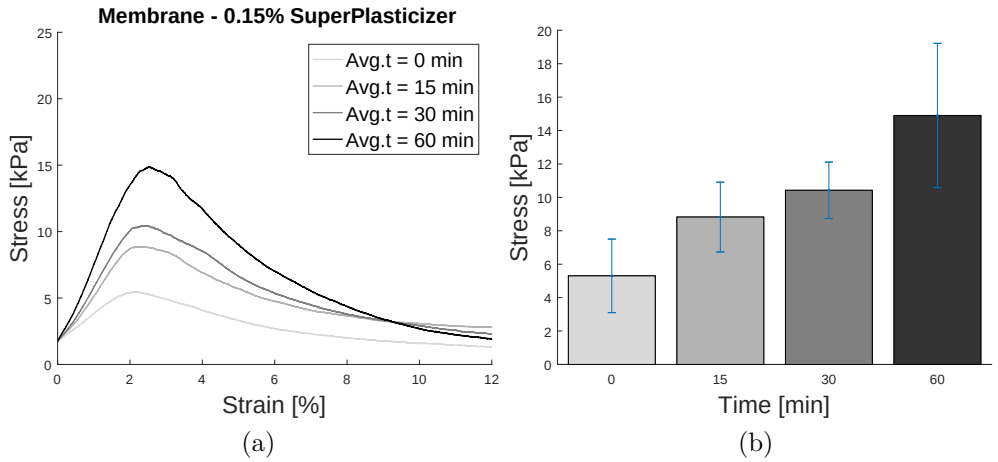

Figure 5.23: Compression tests, 0.15% plasticizer with membrane. Average comparisons at different time - 0 minutes, 15 minutes, 30 minutes, 60 minutes - (a) trend & (b) peaks with standard deviation.

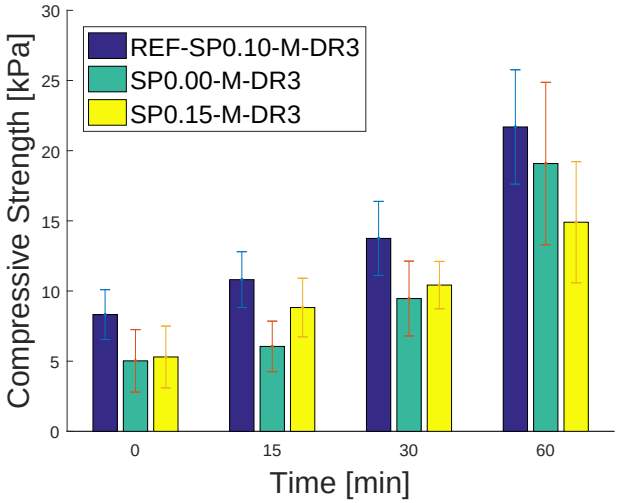

Figure 5.24: Effect of printing conditions, peaks with standard deviation.

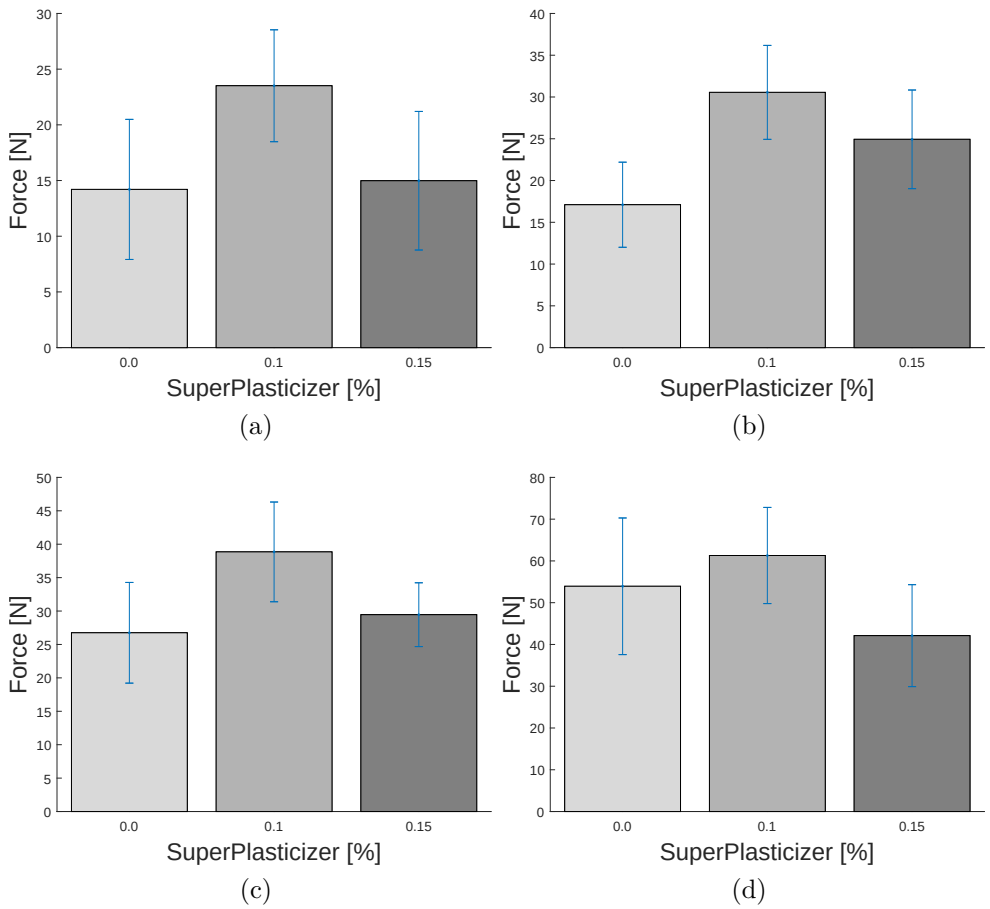

Figure 5.25: Compression tests, 0.0%, 0.1% and 0.15% plasticizer with membrane. Average peak results with standard deviation at different time - (a) 0 minutes, (b) 15 minutes, (c) 30 minutes, (d) 60 minutes.

	Concrete Age			
Compressive Strength	**0 min**	**15 min**	**30 min**	**60 min**
REF-SP0.10-M-DR3	**8.32 kPa**	**10.81 kPa**	**13.75 kPa**	**21.69 kPa**
SP0.00-M-DR3	5.03 kPa	6.05 kPa	9.47 kPa	19.08 kPa
SP0.15-M-DR3	5.30 kPa	8.82 kPa	10.42 kPa	14.90 kPa

Table 5.4: Effect of printing conditions, peak stress at different concrete ages.

	Concrete Age			
Young's Modulus	**0 min**	**15 min**	**30 min**	**60 min**
REF-SP0.10-M-DR3	**210 kPa**	**252 kPa**	**430 kPa**	**607 kPa**
SP0.00-M-DR3	116 kPa	164 kPa	320 kPa	600 kPa
SP0.15-M-DR3	137 kPa	212 kPa	358 kPa	510 kPa

Table 5.5: Effect of printing conditions, Young's Modulus at different concrete ages.

	Concrete Age			
Relative Standard Deviation	**0 min**	**15 min**	**30 min**	**60 min**
REF-SP0.10-M-DR3	**21.73 %**	**16.90 %**	**19.11 %**	**19.12 %**
SP0.00-M-DR3	44.86 %	30.03 %	28.57 %	30.54 %
SP0.15-M-DR3	40.42 %	23.64 %	20.23 %	29.20 %

Table 5.6: Effect of printing conditions, relative standard deviation at different concrete ages.

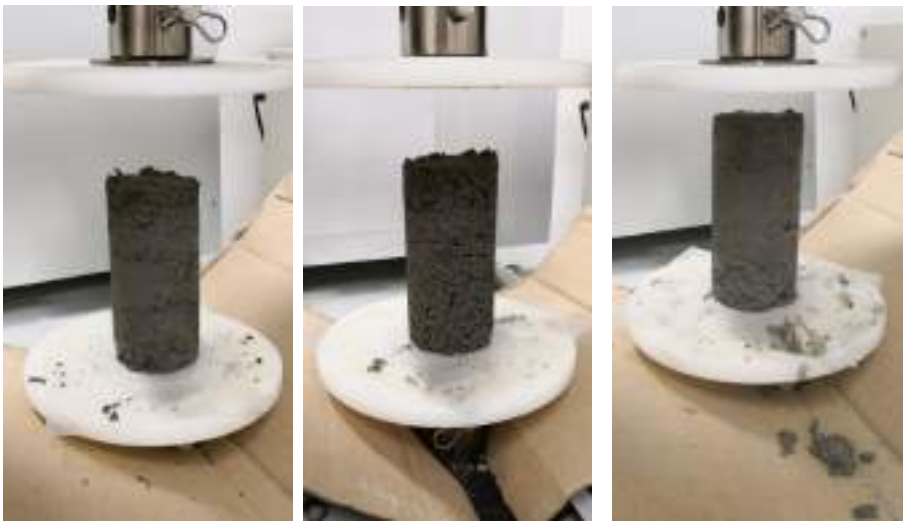

(a) (b) (c)

Figure 5.26: Samples prepared with different percentage of superplasticizer: (a) REF-SP0.10-M-DR3, (b) SP0.00-M-DR3 & (c) SP0.15-M-DR3 .

5.3.3.3 Influence of sample preparation

As mentioned above, also the effect of casting procedures is investigated. Indeed, the influence of the membrane emerges by comparing curves in Fig. 5.27. On one hand, it is evident that the combination of 0.1% superplasticizer amount with the membrane leads to the highest stiffness and strength values, with the lowest relative standard deviation among results. On the other hand, results without membrane present the lowest strength and stiffness (3.54 kPa – 68 kPa); furthermore, such results are the most inaccurate with a maximum of 49.06% and 35.37% as relative standard deviation, respectively for 0.0 and 0.1% superplasticizer amounts. These results are probably due to the adhesion between the 3D printed plastic mould and the fresh concrete specimen: as aforementioned, when the mould is open, part of gravity-induced stresses moves from the mould to the specimen as tangential stresses, causing an initial deterioration of the specimen itself. Hence, if the casting occurs without membrane, the demoulding phase can alter the specimen and a residual stress state can arise in the material.

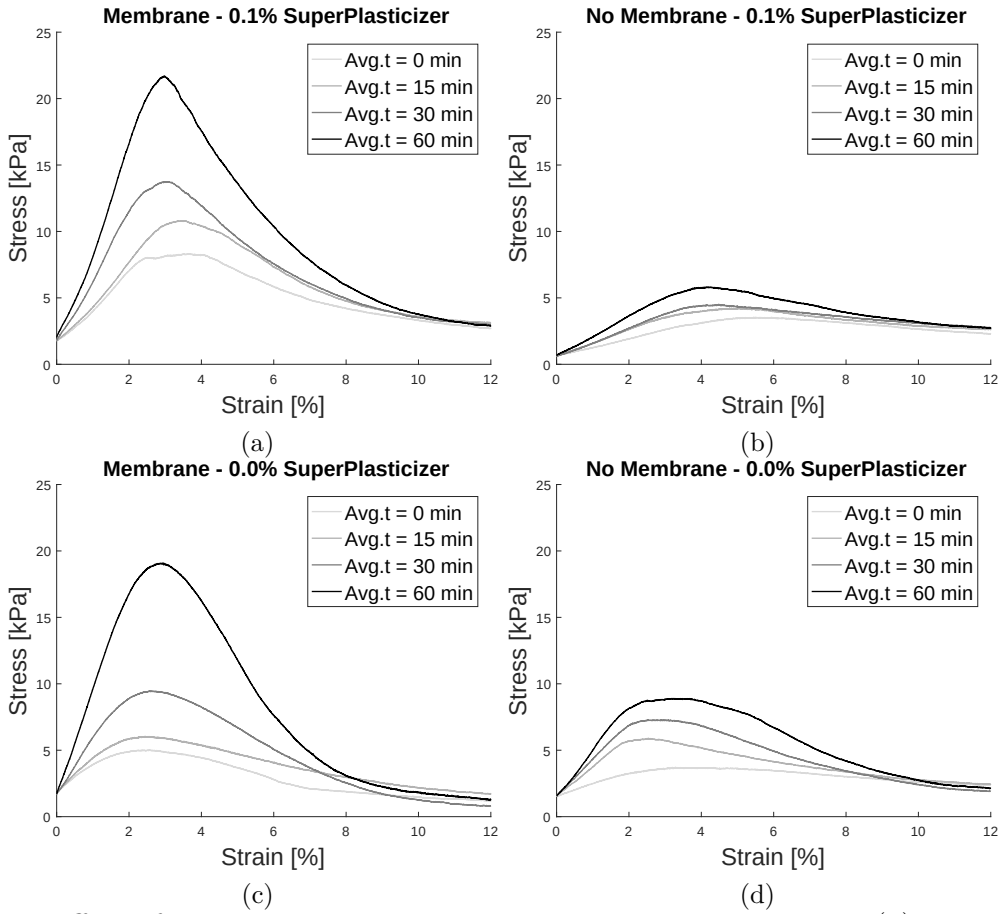

Figure 5.27: Effect of specimen preparation, average stress-strain curves: (a) REF-SP0.10-M-DR3, (b) SP0.10-M-DR3, (c) SP0.00-M-DR3 & (d) SP0.00-NM-DR3.

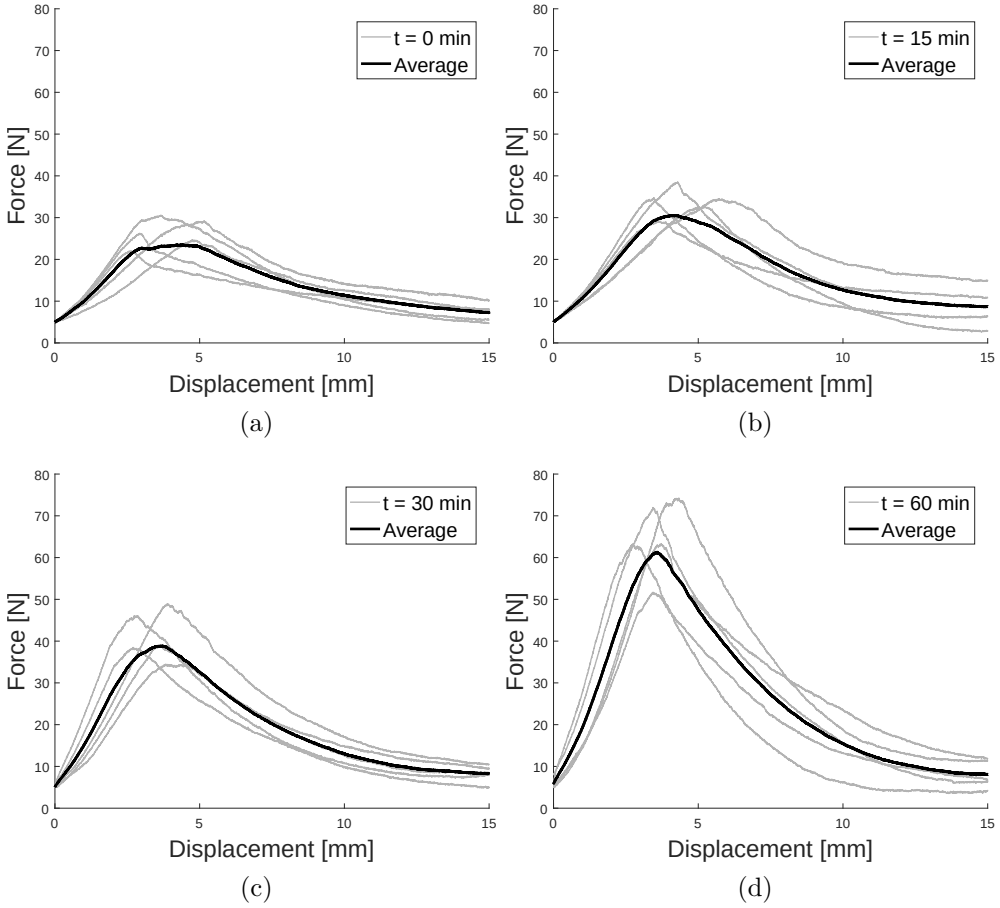

Figure 5.28: Compression tests, 0.1% plasticizer with membrane. Average and individual results at different time - (a) 0 minutes, (b) 15 minutes, (c) 30 minutes, (d) 60 minutes.

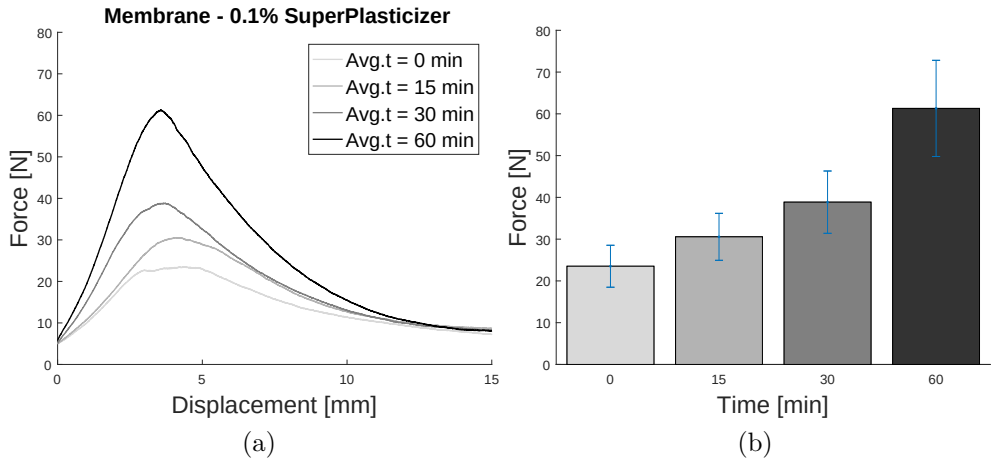

Figure 5.29: Compression tests, 0.1% plasticizer with membrane. Average comparisons at different time - 0 minutes, 15 minutes, 30 minutes, 60 minutes - (a) trend & (b) peaks with standard deviation.

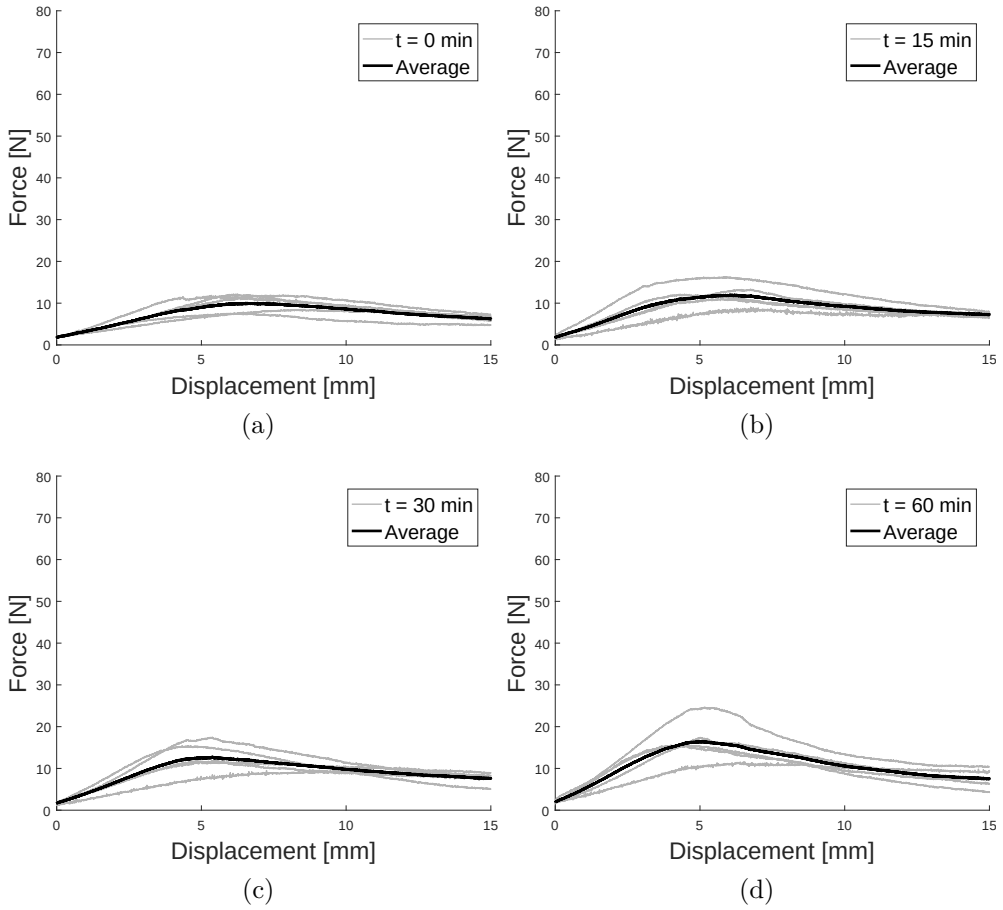

Figure 5.30: Compression tests, 0.1% plasticizer without membrane. Average and individual results at different time - (a) 0 minutes, (b) 15 minutes, (c) 30 minutes, (d) 60 minutes.

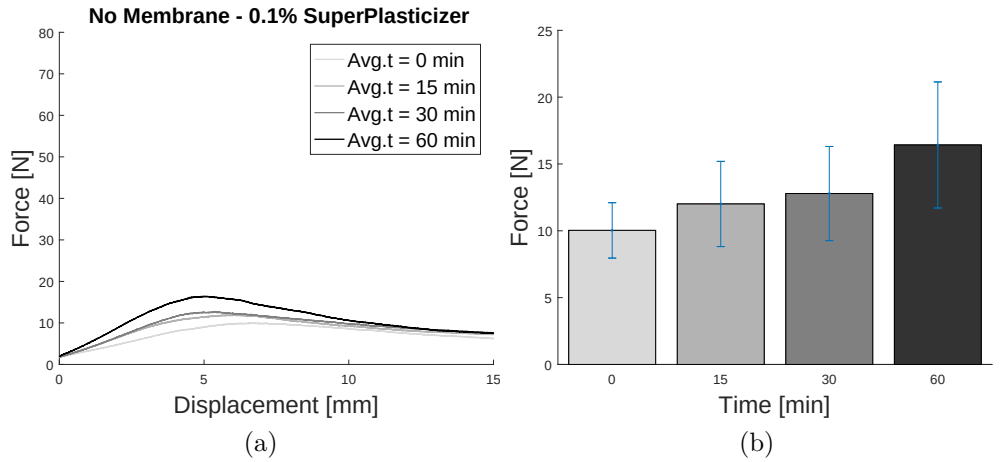

Figure 5.31: Compression tests, 0.1% plasticizer without membrane. Average comparisons at different time - 0 minutes, 15 minutes, 30 minutes, 60 minutes - (a) trend & (b) peaks with standard deviation.

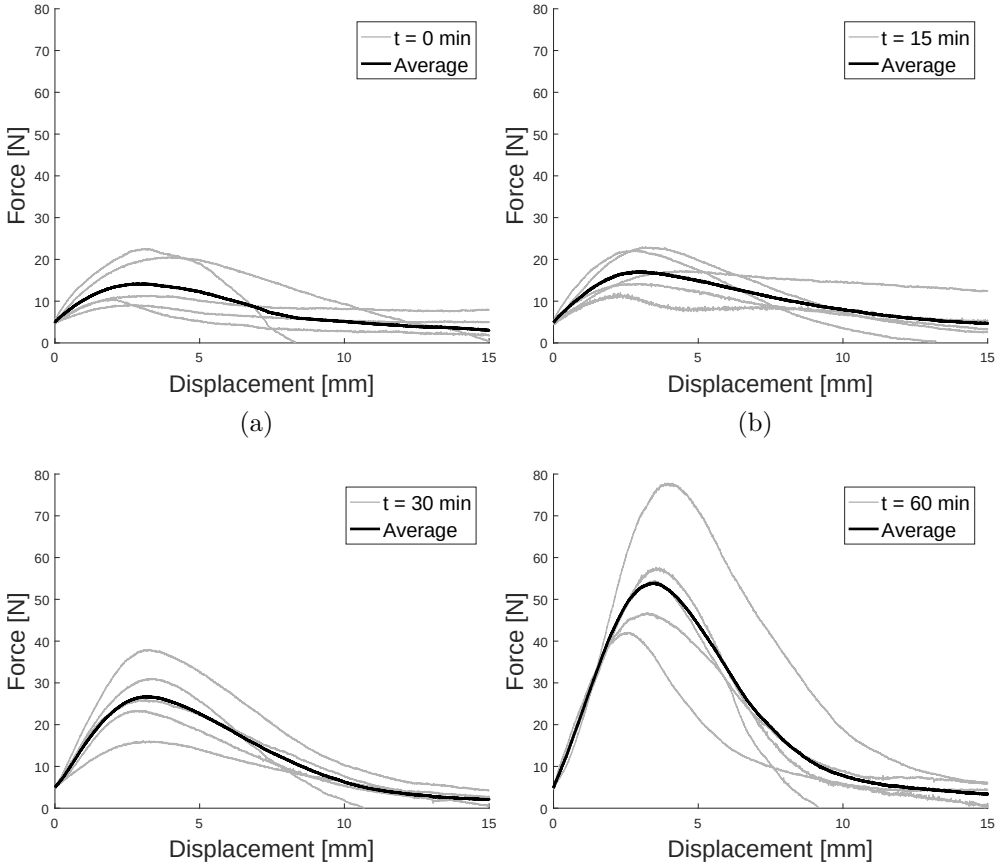

Figure 5.32: Compression tests, 0.0% plasticizer with membrane. Average and individual results at different time - (a) 0 minutes, (b) 15 minutes, (c) 30 minutes, (d) 60 minutes.

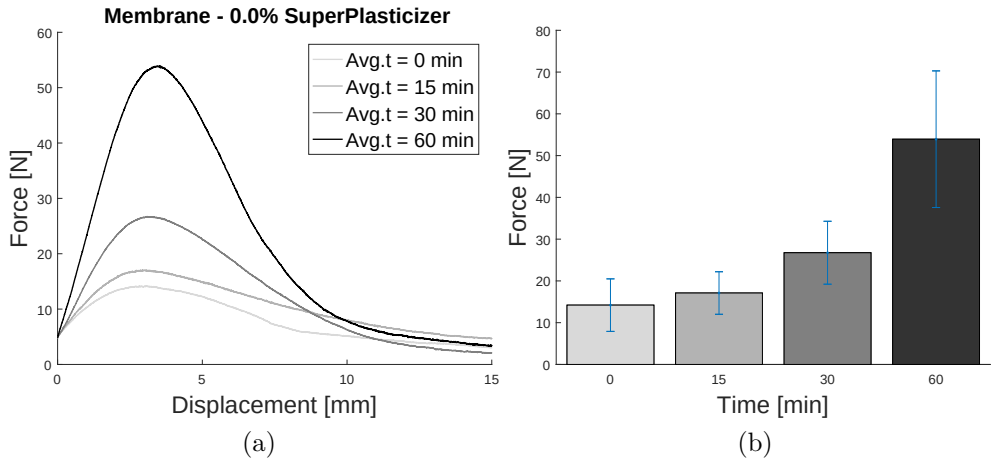

Figure 5.33: Compression tests, 0.0% plasticizer with membrane. Average comparisons at different time - 0 minutes, 15 minutes, 30 minutes, 60 minutes - (a) trend & (b) peaks with standard deviation.

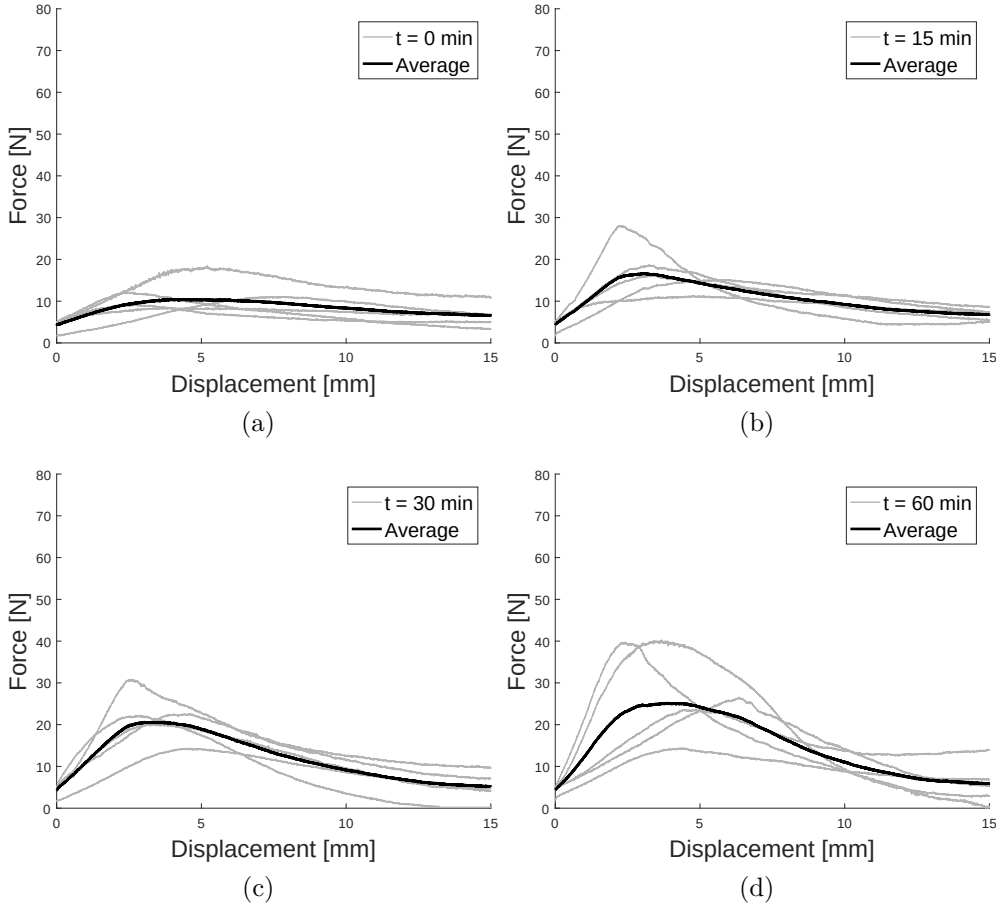

Figure 5.34: Compression tests, 0.0% plasticizer without membrane. Average and individual results at different time - (a) 0 minutes, (b) 15 minutes, (c) 30 minutes, (d) 60 minutes.

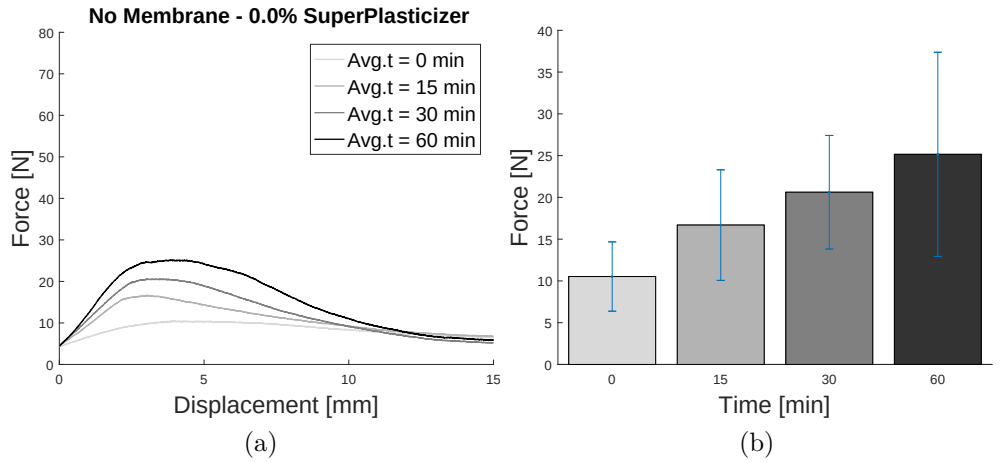

Figure 5.35: Compression tests, 0.0% plasticizer without membrane. Average comparisons at different time - 0 minutes, 15 minutes, 30 minutes, 60 minutes - (a) trend & (b) peaks with standard deviation.

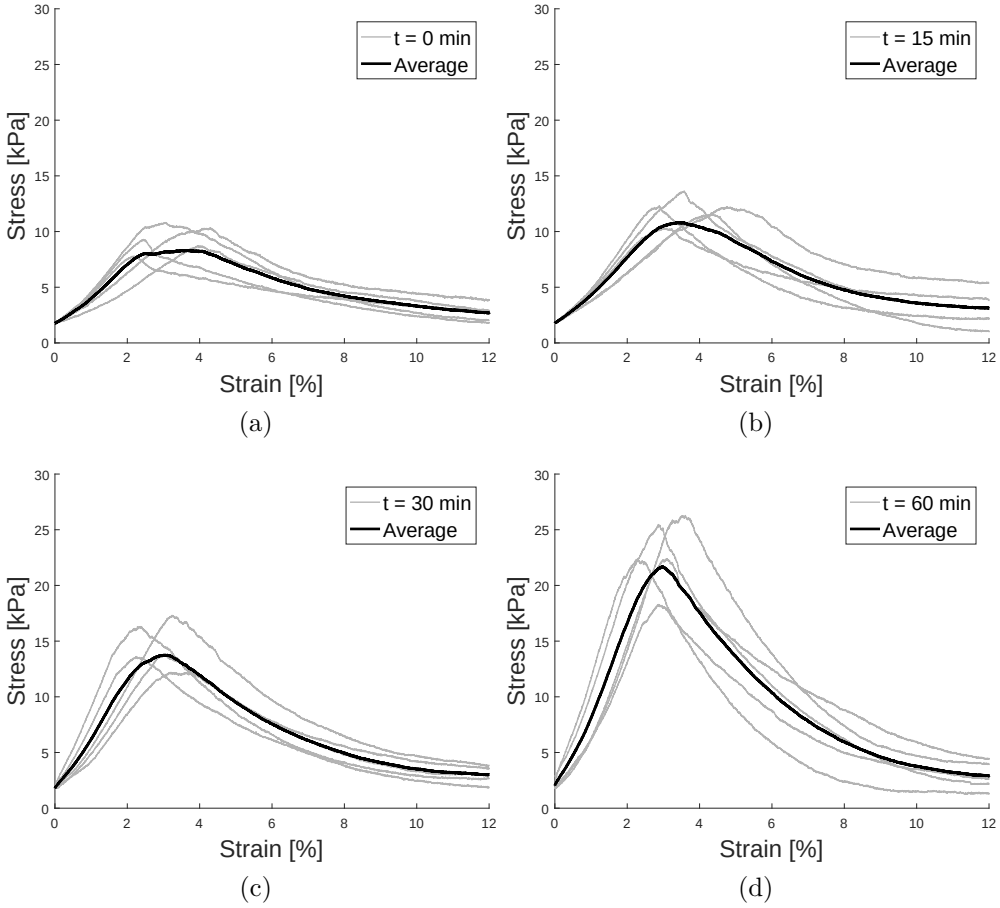

Figure 5.36: Compression tests, 0.1% plasticizer with membrane. Average and individual results at different time - (a) 0 minutes, (b) 15 minutes, (c) 30 minutes, (d) 60 minutes.

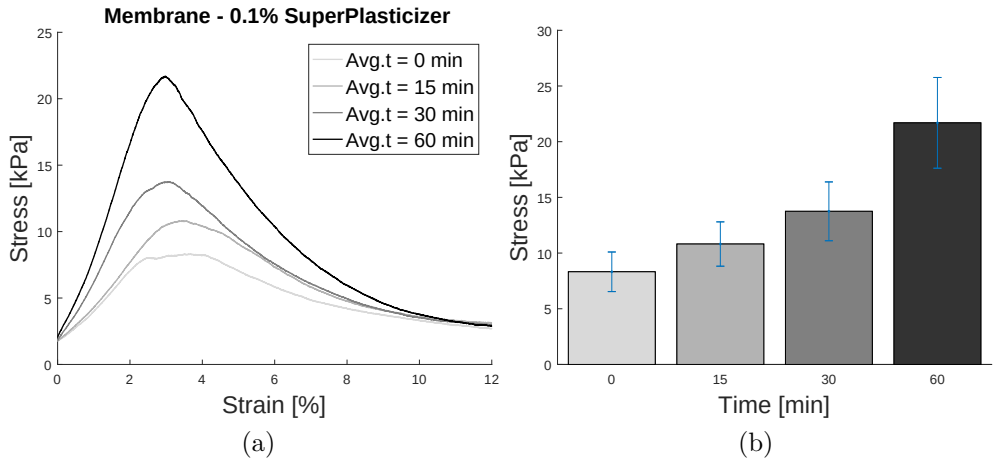

Figure 5.37: Compression tests, 0.1% plasticizer with membrane. Average comparisons at different time - 0 minutes, 15 minutes, 30 minutes, 60 minutes - (a) trend & (b) peaks with standard deviation.

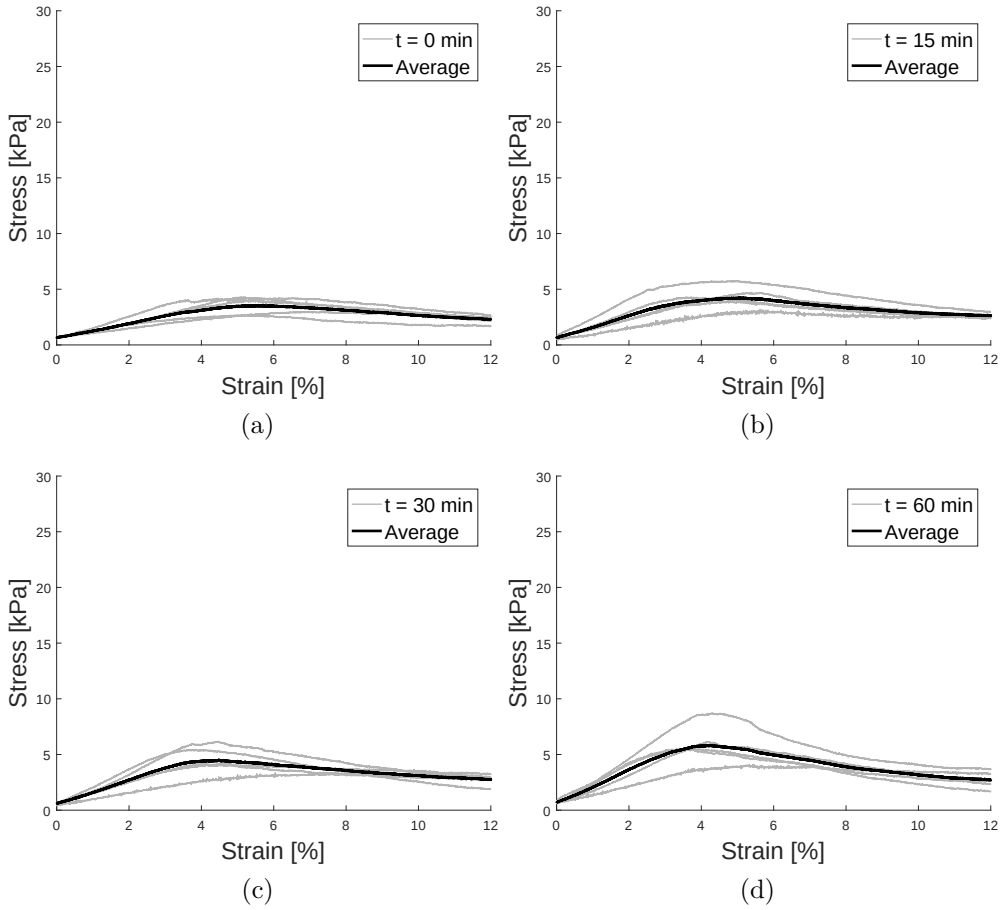

Figure 5.38: Compression tests, 0.1% plasticizer without membrane. Average and individual results at different time - (a) 0 minutes, (b) 15 minutes, (c) 30 minutes, (d) 60 minutes.

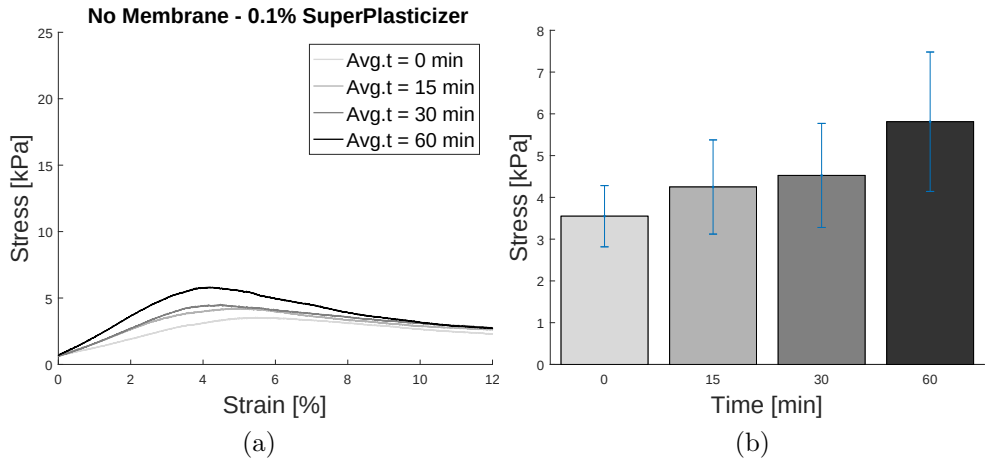

Figure 5.39: Compression tests, 0.1% plasticizer without membrane. Average comparisons at different time - 0 minutes, 15 minutes, 30 minutes, 60 minutes - (a) trend & (b) peaks with standard deviation.

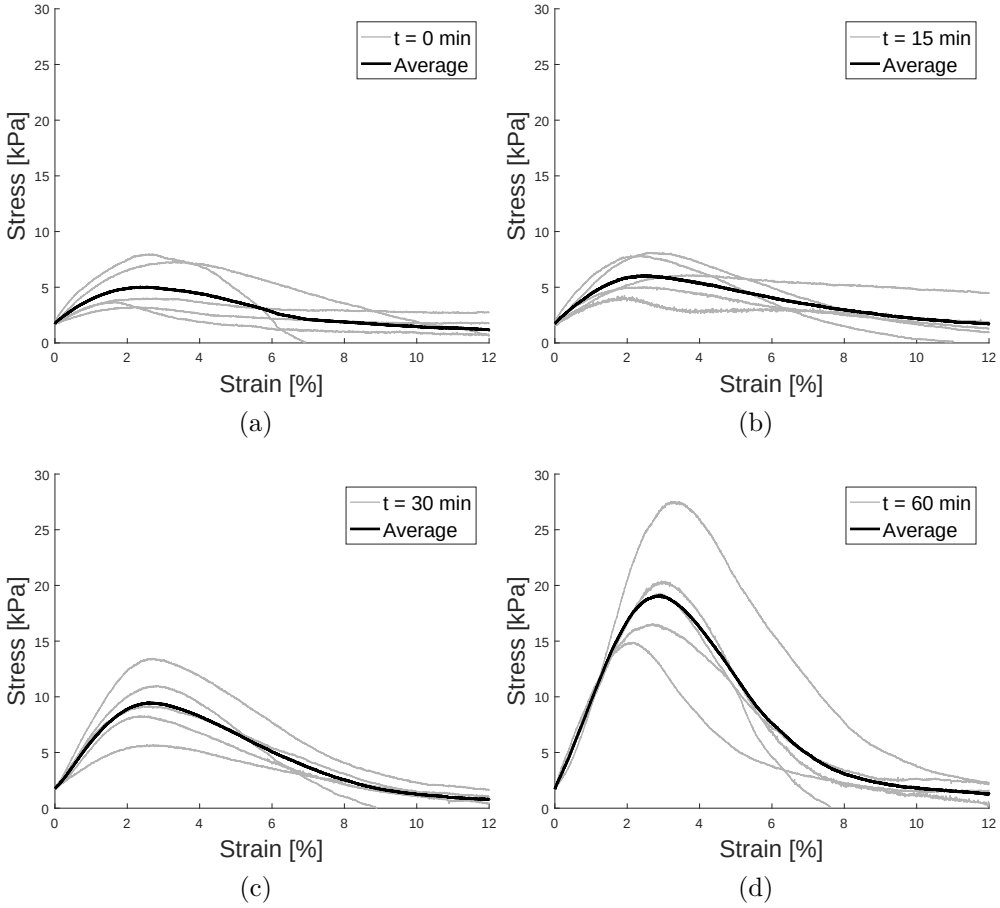

Figure 5.40: Compression tests, 0.0% plasticizer with membrane. Average and individual results at different time - (a) 0 minutes, (b) 15 minutes, (c) 30 minutes, (d) 60 minutes.

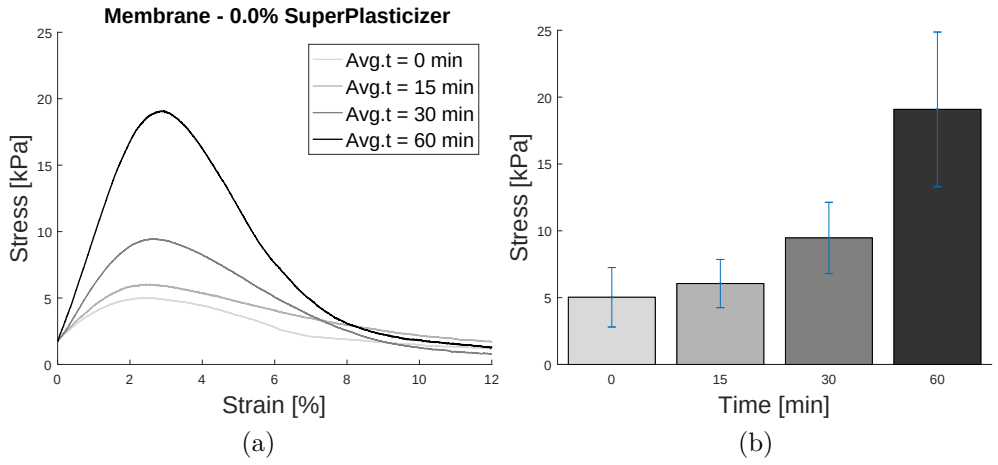

Figure 5.41: Compression tests, 0.0% plasticizer with membrane. Average comparisons at different time - 0 minutes, 15 minutes, 30 minutes, 60 minutes - (a) trend & (b) peaks with standard deviation.

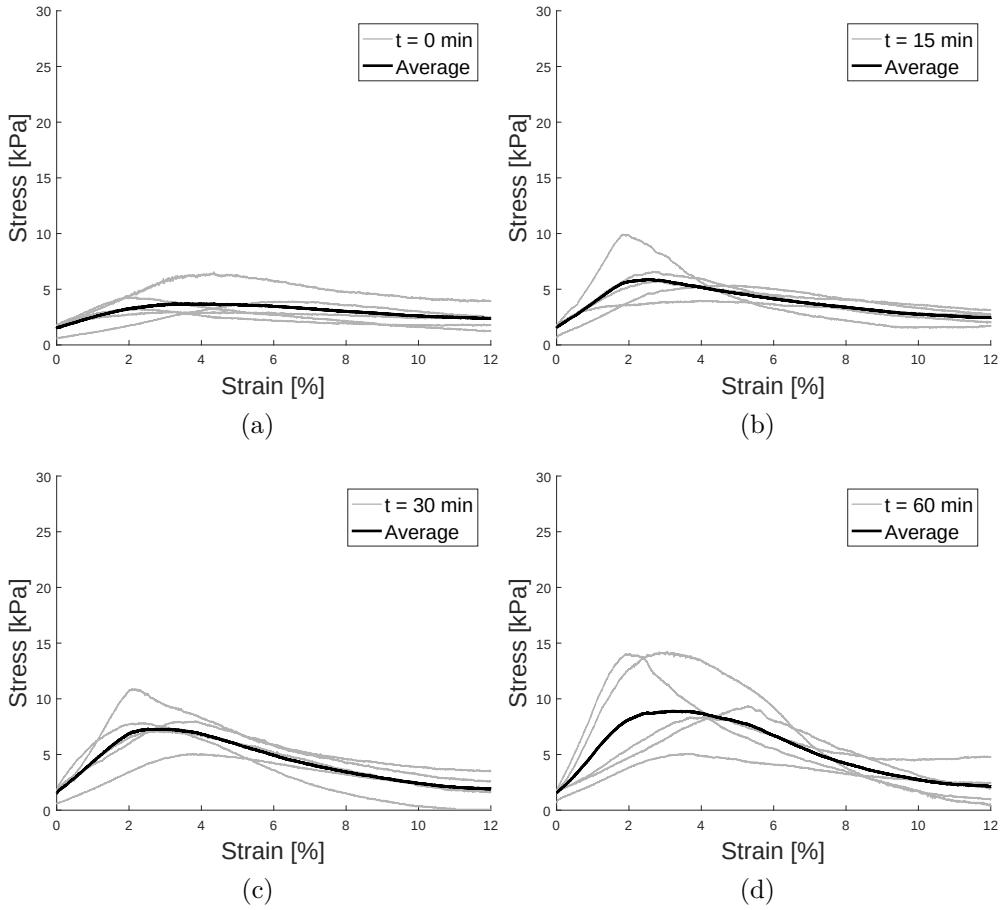

Figure 5.42: Compression tests, 0.0% plasticizer without membrane. Average and individual results at different time - (a) 0 minutes, (b) 15 minutes, (c) 30 minutes, (d) 60 minutes.

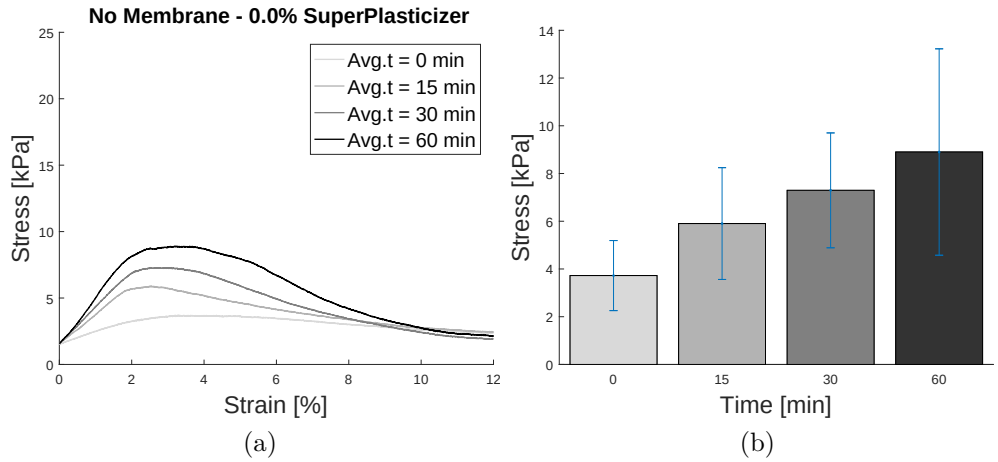

Figure 5.43: Compression tests, 0.0% plasticizer without membrane. Average comparisons at different time - 0 minutes, 15 minutes, 30 minutes, 60 minutes - (a) trend & (b) peaks with standard deviation.

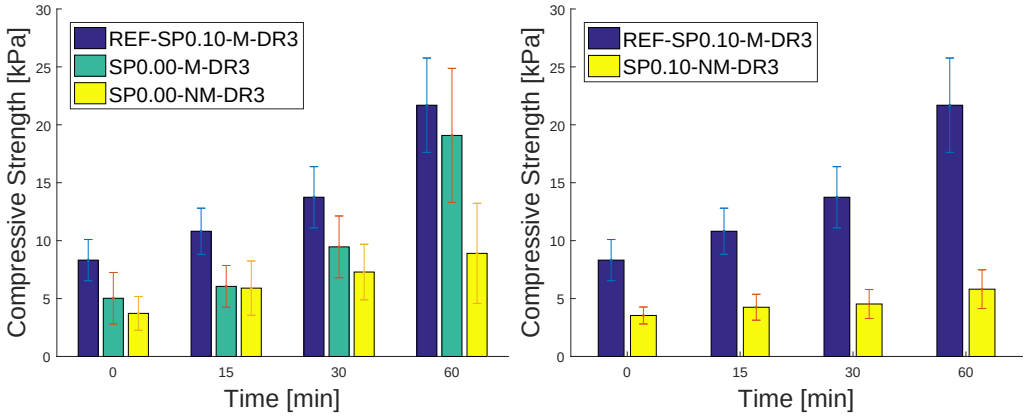

(a) (b)

Figure 5.44: Effect of specimen preparation, peaks with standard deviation: (a) REF-SP0.10-M-DR3, SP0.00-M-DR3 and SP0.00-NM-DR3, (b) REF-SP0.10-M-DR3 and SP0.10-NM-DR3.

	Concrete Age			
Compressive Strength	**0 min**	**15 min**	**30 min**	**60 min**
REF-SP0.10-M-DR3	**8.32 kPa**	**10.81 kPa**	**13.75 kPa**	**21.69 kPa**
SP0.00-M-DR3	5.02 kPa	6.05 kPa	9.46 kPa	19.08 kPa
SP0.00-NM-DR3	3.72 kPa	5.90 kPa	7.29 kPa	8.90 kPa
SP0.10-NM-DR3	3.54 kPa	4.25 kPa	4.53 kPa	5.81 kPa

Table 5.7: Effect of specimen preparation, peak stress at different concrete ages.

	Concrete Age			
Young's Modulus	**0 min**	**15 min**	**30 min**	**60 min**
REF-SP0.10-M-DR3	**210 kPa**	**252 kPa**	**430 kPa**	**607 kPa**
SP0.00-M-DR3	116 kPa	164 kPa	320 kPa	600 kPa
SP0.00-NM-DR3	88 kPa	182 kPa	212 kPa	305 kPa
SP0.10-NM-DR3	68 kPa	94 kPa	95 kPa	124 kPa

Table 5.8: Effect of specimen preparation, Young's Modulus at different concrete ages.

	Concrete Age			
Relative Standard Deviation	**0 min**	**15 min**	**30 min**	**60 min**
REF-SP0.10-M-DR3	**21.73 %**	**16.90 %**	**19.11 %**	**19.12 %**
SP0.00-M-DR3	44.86 %	30.03 %	28.57 %	30.54 %
SP0.00-NM-DR3	48.15 %	40.34 %	33.14 %	49-06 %
SP0.10-NM-DR3	21.91 %	26.39 %	28.27 %	35.37 %

Table 5.9: Effect of specimen preparation, relative standard deviation at concrete ages.

5.3.3.4 Influence of the displacement rate

Stress-strain curves reported in Fig. 5.45 are obtained with two different value of displacement rate, i.e., 3mm/min and 30mm/min. As expected, the compressive strength grows with the strain rate, especially when the material is more brittle. Indeed, at t=60 minutes, the compressive strength is equal to 22kPa with 3mm/min of displacement rate, whereas its value grows until to 33kPa with 30mm/min. Therefore, there is a percentage grows of about 53% in terms of compressive strength (at 60 minutes). However, although a higher strain-rate has beneficial effects in terms of compressive strength, the experimental data seem to be less reliable: DR30 results show higher values of relative standard deviation (see Tab. 5.12). The elastic modulus seems to be no sensitive to the strain rate: the difference in elastic modulus related to REF-SP0.10-M-DR3 and SP0.10-M-DR30 is contained in the range of the experimental scatter (see Tab. 5.11).

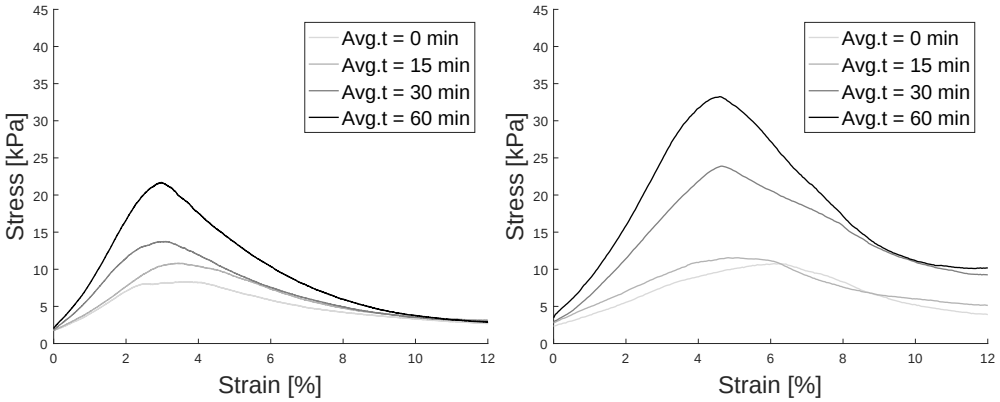

Figure 5.45: Effect of displacement rate, average stress-strain curves: (a) REF-SP0.10-M-DR3 & (b) SP0.10-M-DR30.

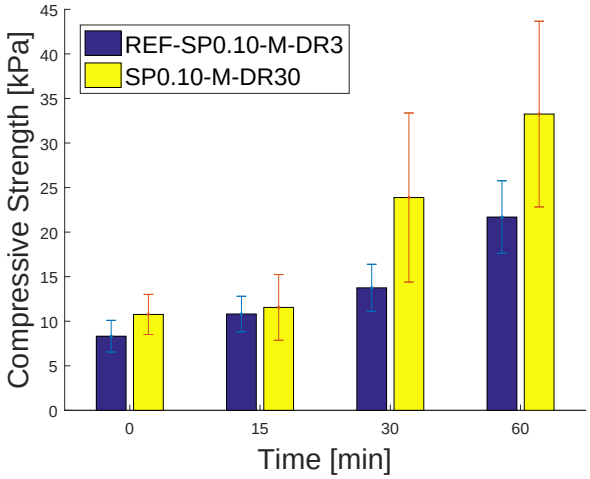

Figure 5.46: Effect of displacement rate, peaks with standard deviation.

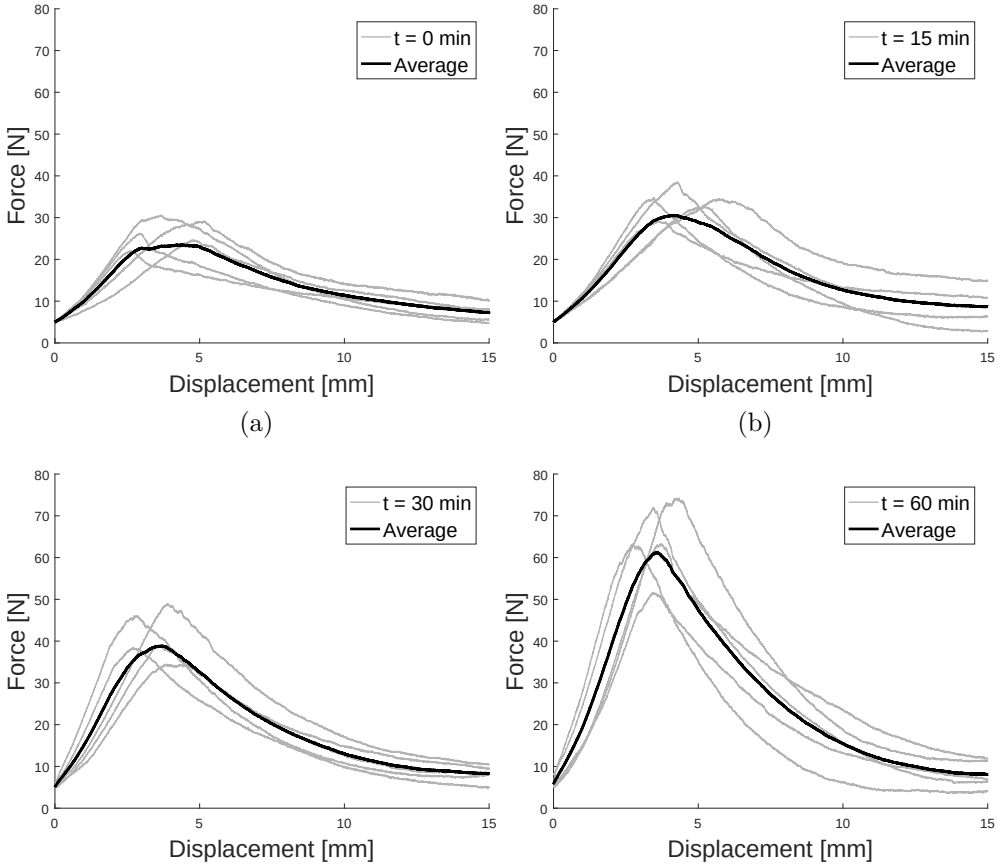

Figure 5.47: Compression tests, 0.1% plasticizer with membrane. Average and individual results at different time - (a) 0 minutes, (b) 15 minutes, (c) 30 minutes, (d) 60 minutes.

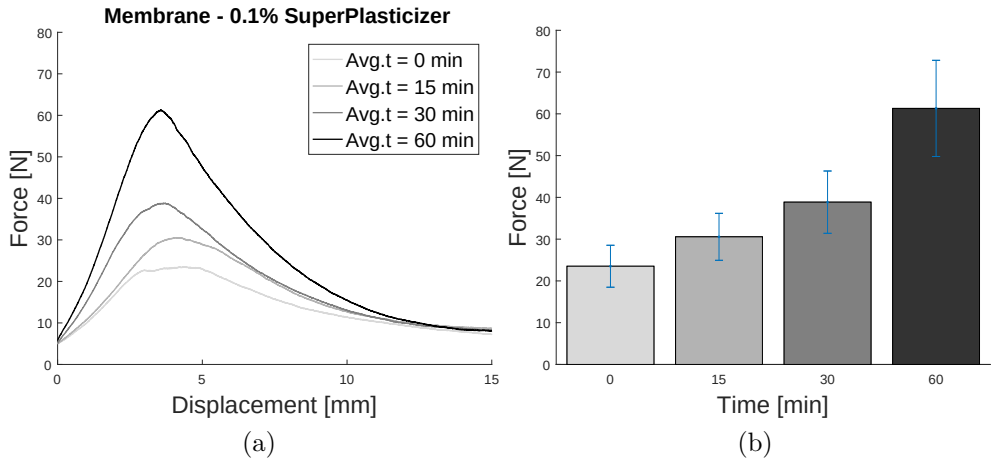

Figure 5.48: Compression tests, 0.1% plasticizer with membrane. Average comparisons at different time - 0 minutes, 15 minutes, 30 minutes, 60 minutes - (a) trend & (b) peaks with standard deviation.

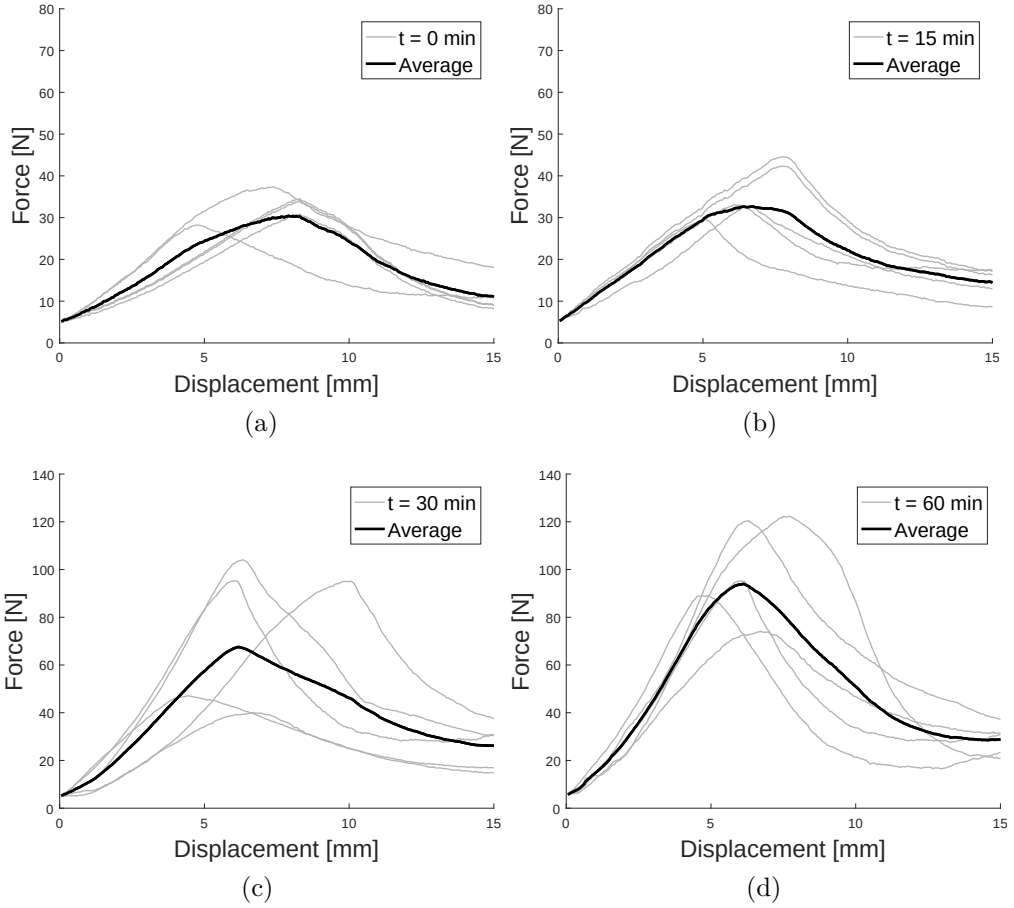

Figure 5.49: Compression tests, 0.1% plasticizer with membrane, DR 30mm/min. Average and individual results at different time - (a) 0 minutes, (b) 15 minutes, (c) 30 minutes, (d) 60 minutes.

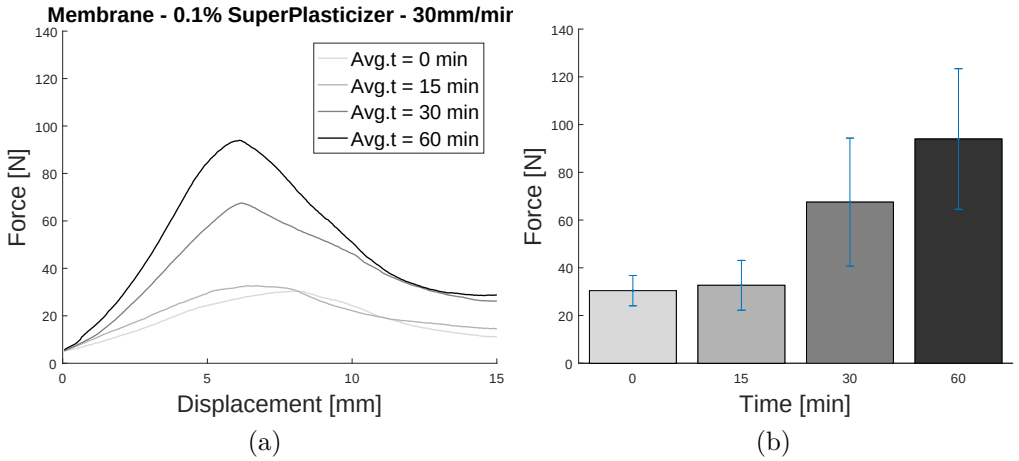

Figure 5.50: Compression tests, 0.1% plasticizer with membrane, DR 30mm/min. Average comparisons at different time - 0 minutes, 15 minutes, 30 minutes, 60 minutes - (a) trend & (b) peaks with standard deviation.

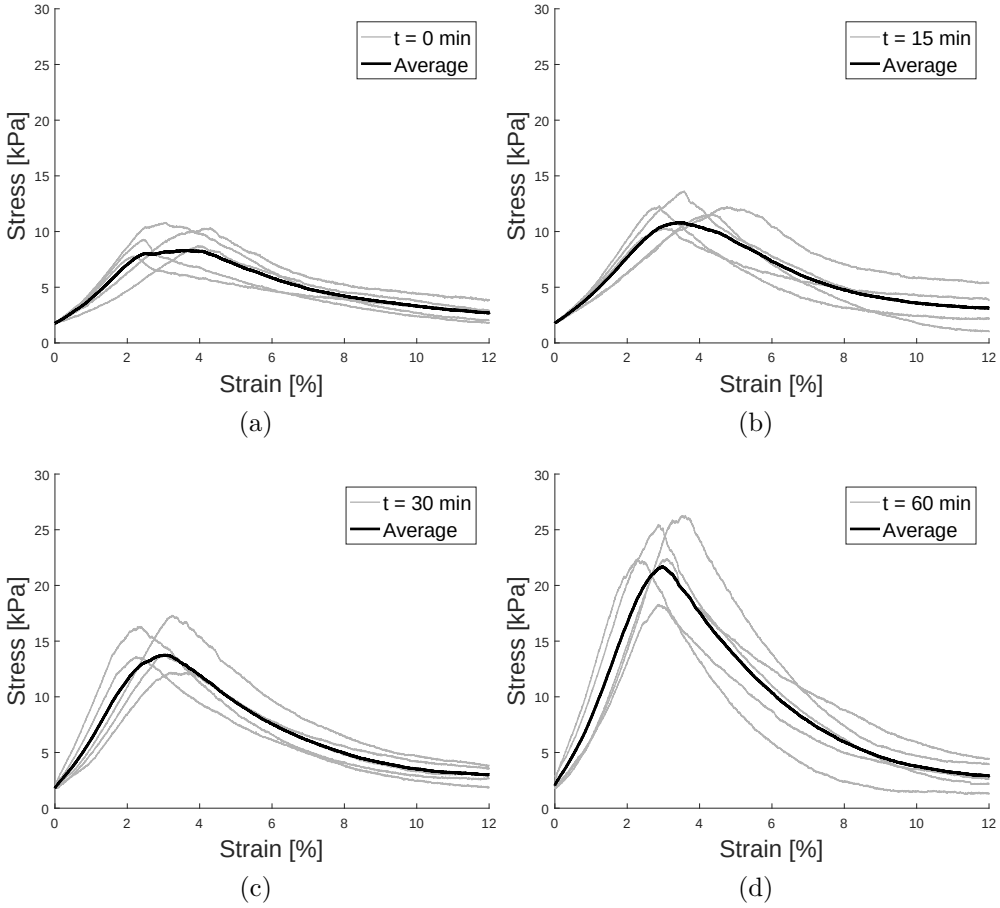

Figure 5.51: Compression tests, 0.1% plasticizer with membrane. Average and individual results at different time - (a) 0 minutes, (b) 15 minutes, (c) 30 minutes, (d) 60 minutes.

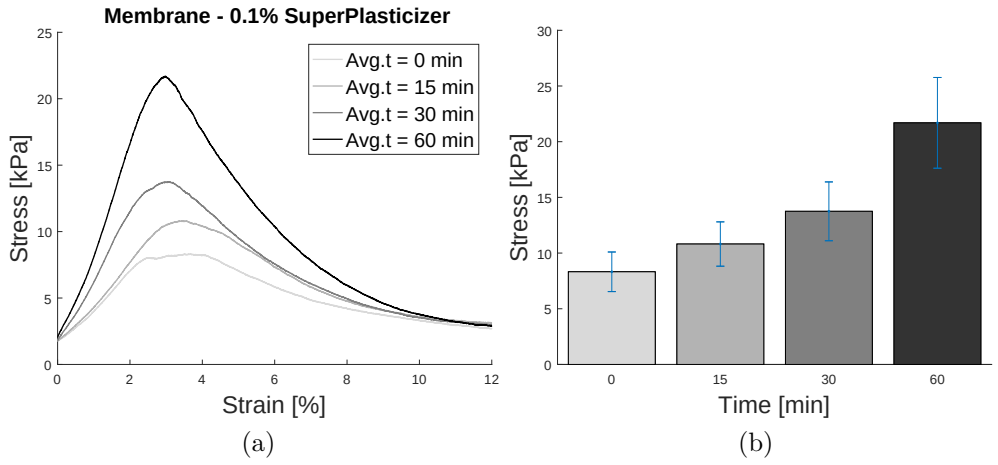

Figure 5.52: Compression tests, 0.1% plasticizer with membrane. Average comparisons at different time - 0 minutes, 15 minutes, 30 minutes, 60 minutes - (a) trend & (b) peaks with standard deviation.

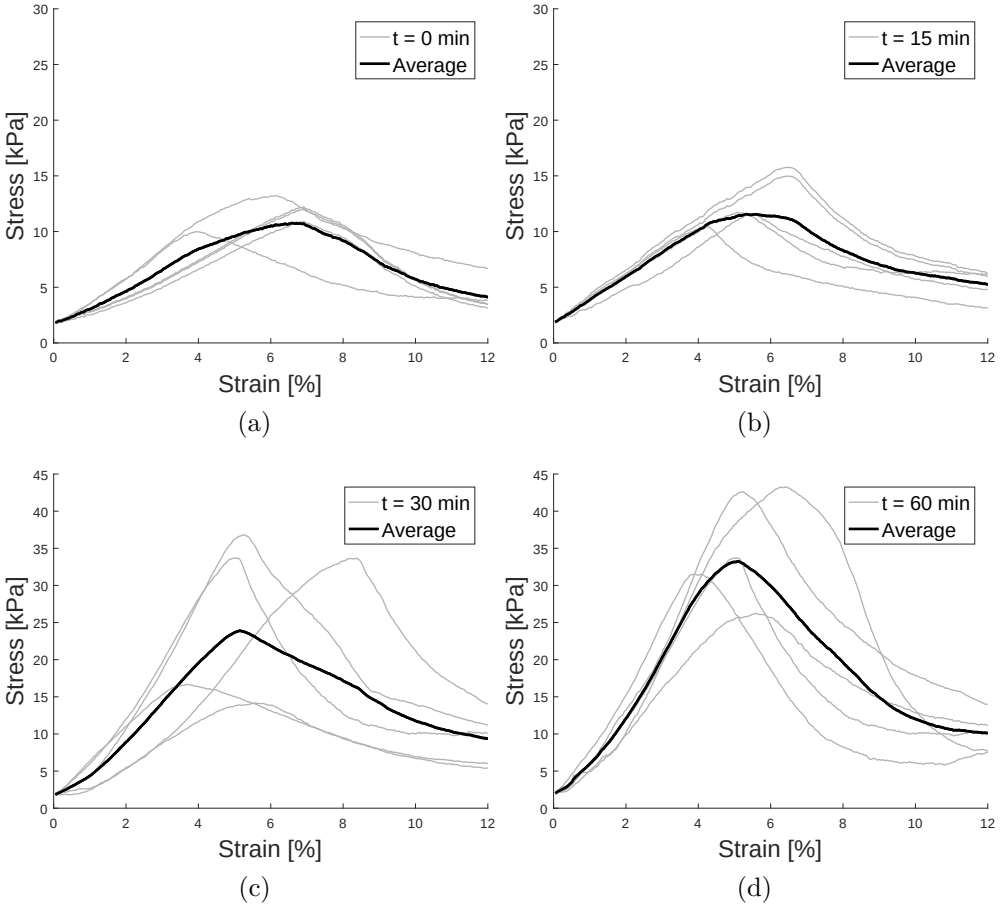

Figure 5.53: Compression tests, 0.1% plasticizer with membrane, DR 30mm/min. Average and individual results at different time - (a) 0 minutes, (b) 15 minutes, (c) 30 minutes, (d) 60 minutes.

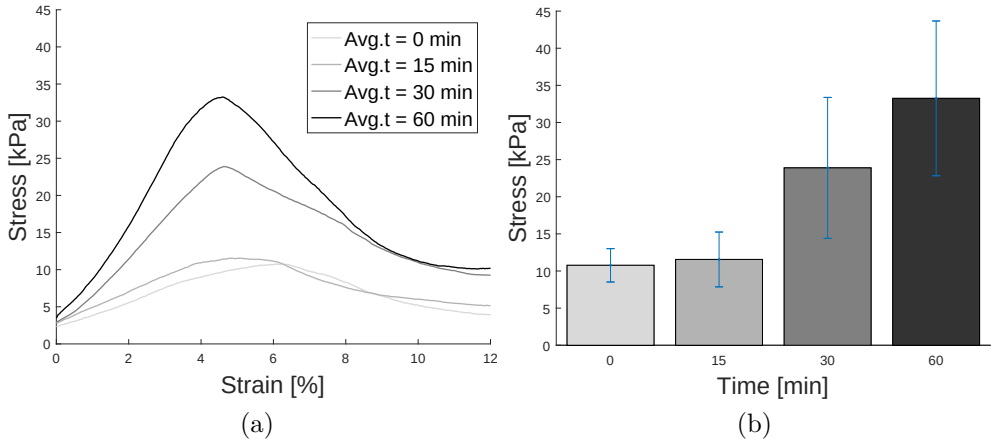

Figure 5.54: Compression tests, 0.1% plasticizer with membrane, DR 30mm/min. Average comparisons at different time - 0 minutes, 15 minutes, 30 minutes, 60 minutes - (a) trend & (b) peaks with standard deviation.

	Concrete Age			
Compressive Strength	**0 min**	**15 min**	**30 min**	**60 min**
REF-SP0.10-M-DR3	8.32 kPa	10.81 kPa	13.75 kPa	21.69 kPa
SP0.10-M-DR30	**10.76 kPa**	**11.55 kPa**	**23.88 kPa**	**33.25 kPa**

Table 5.10: Effect of displacement rate, peak stress at different concrete ages.

	Concrete Age			
Young's Modulus	**0 min**	**15 min**	**30 min**	**60 min**
REF-SP0.10-M-DR3	210 kPa	252 kPa	430 kPa	607 kPa
SP0.10-M-DR30	**212 kPa**	**256 kPa**	**488 kPa**	**763 kPa**

Table 5.11: Effect of displacement rate, Young's Modulus at different concrete ages.

	Concrete Age			
Relative Standard Deviation	**0 min**	**15 min**	**30 min**	**60 min**
REF-SP0.10-M-DR3	**21.73 %**	**16.90 %**	**19.11 %**	**19.12 %**
SP0.10-M-DR30	21.87 %	31.95 %	39.73 %	31.35 %

Table 5.12: Effect of displacement rate, relative standard deviation at different concrete ages.

5.3.4 Discussion

In this section, the temporal evolution of the compressive strength $\sigma_{c,max}$(t) and stiffness E_c (t) are reported for each specimen set, in order to more accurately investigate the influence of specific testing procedures on mechanical properties. In detail, compressive strength and stiffness laws (as function of concrete age) are obtained through a linear regression of experimental data, related to each tested sample. The experimental data are grouped and compared as a function of concrete age in order to study the influence of the material, the sample preparation and the displacement rate on mechanical properties. In detail, the comparison is made by studying the influence of percentage of superplasticizer (see Fig. 5.56), the use of the membrane during casting (see Fig. 5.57 and Fig. 5.58 respectively for 0.00% of SP and 0.10% of SP) and the displacement rate (see Fig. 5.59).

In Fig. 5.55 we report linear fit laws of compressive strength and Young's Modulus related to the reference mix (i.e. SP0.10-M-DR3).

$$\sigma_{c,max}(t) = 0.23t + 8.2[kPa] \quad ; \quad E_c(t) = 7t + 190[kPa] \tag{5.6}$$

Fig. 5.56 shows that the mix with low or with high percentage value of superplasticizer (i.e. SP0.00-M-DR3 and SP0.15-M-DR3, respectively) provides worse mechanical performance, especially in terms of compressive strength. In Fig. 5.57 and Fig. 5.58 the influence of membrane is shown for SP0.00 and SP0.10, respectively. If the demoulding phase takes place without the membrane, the sample is strongly altered. Such effect is more evident for the mix with 0.1% of SP, in which the specimen appears homogeneous after the casting and the only

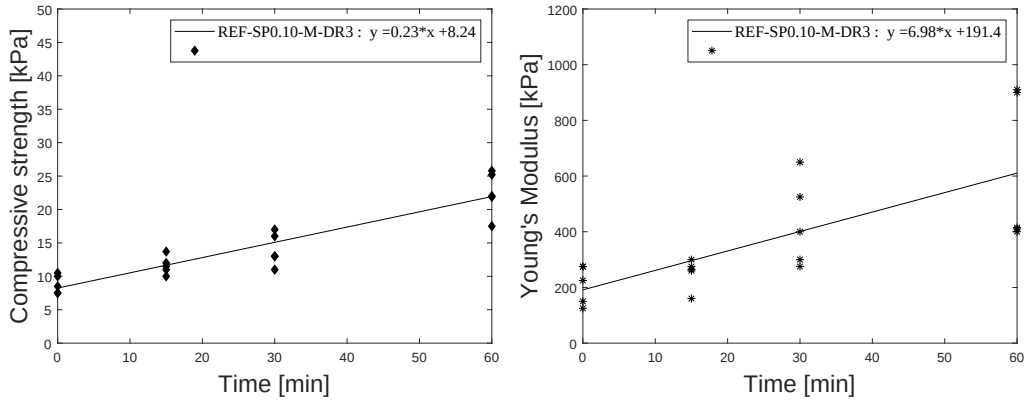

(a) (b)

Figure 5.55: Compressive strength (a) and Elastic modulus (b) for reference mix.

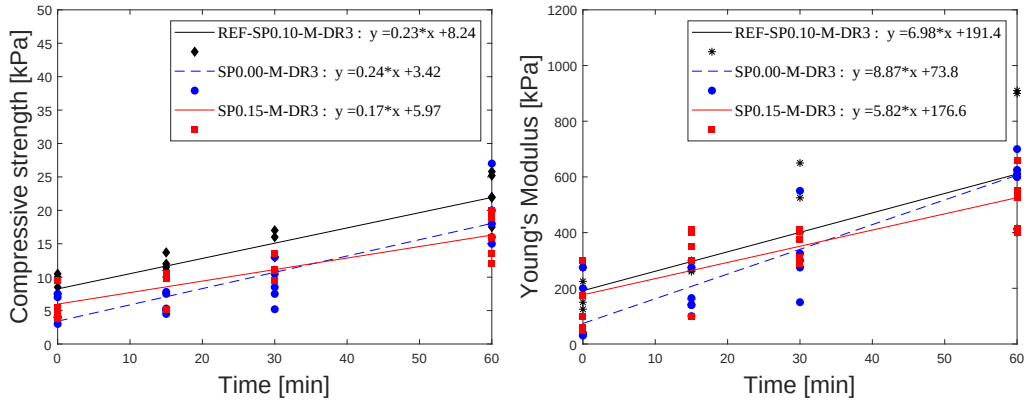

(a) (b)

Figure 5.56: Influence of superplasticizer percentage (0, 0.1 and 0.15% of cement weight - respectively SP0, SP0.1 and SP0.15): (a) compressive strength and (b) elastic modulus.

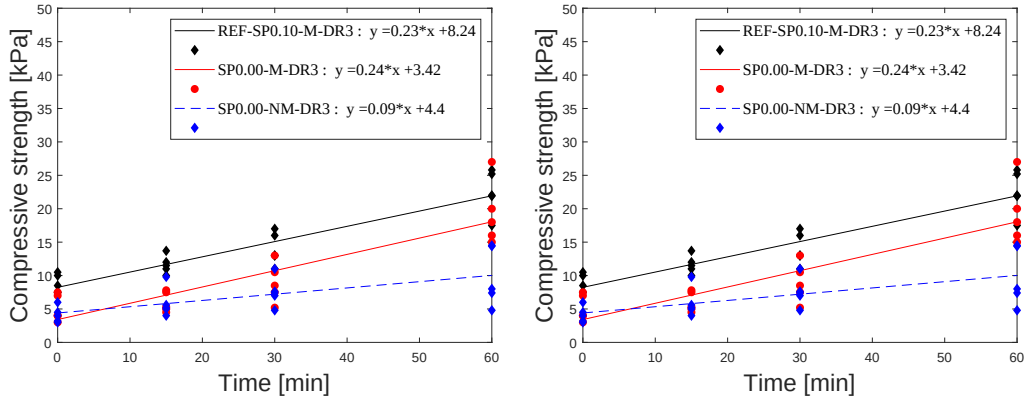

(a) (b)

Figure 5.57: Influence of sample preparation with 0%SP (casted with –M- or without nylon membrane -NM):(a) compressive strength and (b) elastic modulus.

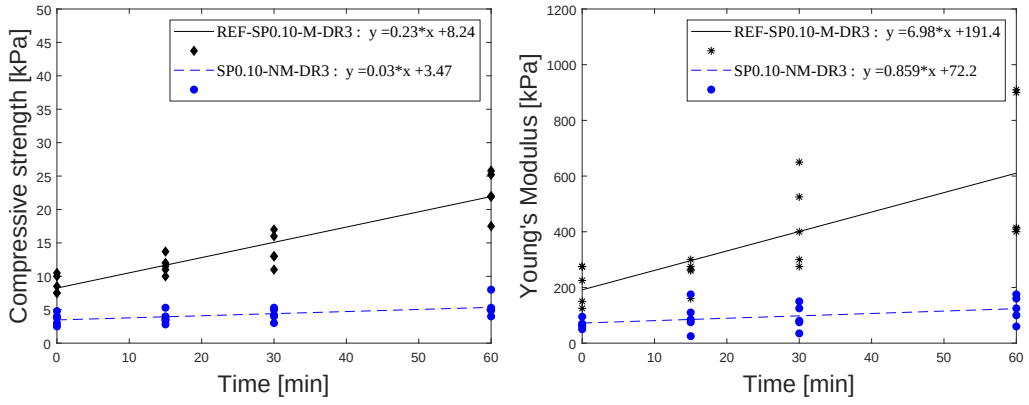

(a) (b)

Figure 5.58: Influence of sample preparation with 0.1%SP (casted with –M- or without nylon membrane -NM):(a) compressive strength and (b) elastic modulus.

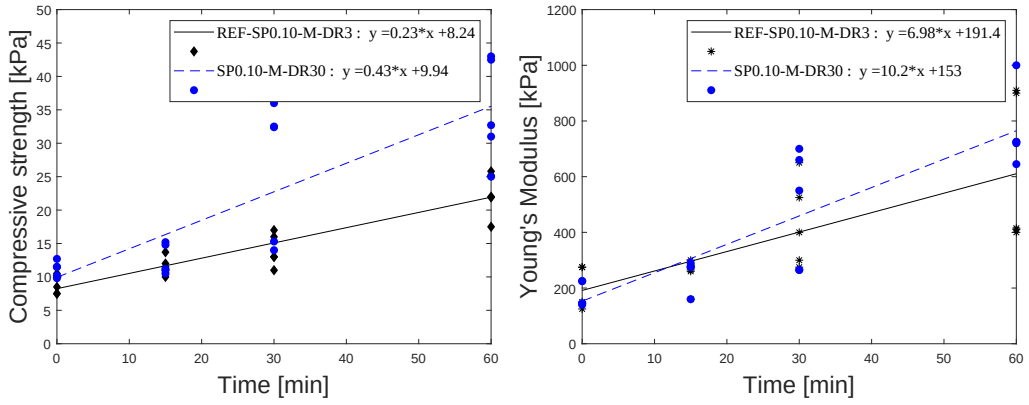

(a) (b)

Figure 5.59: Influence of displacement rate with 0.1%SP (3mm/min VS 30mm/min, respectively DR3 and DR30): (a) compressive strength and (b) elastic modulus.

source of disturbance is due to the demoulding. Indeed, when the sample is prepared with 0% of SP there are more voids inside it than that with 0.1% of SP, and the demoulding disturbance appears lower. Furthermore, by observing Fig. 5.57 and Fig. 5.58, the influence of the membrane is more evident as concrete age increases; indeed, as the concrete hardened over time, geometrical imperfections and voids, which increase in the absence of the nylon membrane, are potentially detrimental for strength development, especially when the material became more brittle. Finally, the comparison between tests carried out at distinct values of displacement rate (i.e. 3mm/min and 30mm/min) is reported in Fig. 5.59. An improvement of mechanical properties is recorded when the test is carried out at higher displacement rate, especially in terms of compressive strength. Indeed, mechanical properties of cementitious materials in the hardened state are known to be rate sensitive, based on three prevalent hypotheses in literature [71]: (i) the Stefan effect, which links the rate sensitivity to the presence of viscous pore fluid inside the cementitious material; (ii) the rate sensitivity of crack propagation, which can alter the fracture mechanism, attenuate crack velocity, and cause preferential cracking through regions of higher strength;(iii) inertial effects. It is known that the failure of brittle materials depends on cracking processes, while the fracture energy

increases rising strain rate [72]. Consequently, the increment of compressive strength with displacement rate grows when the mechanical behaviour becomes more brittle: the distance between the two interpolating lines in Fig. 5.59a increases with resting time of concrete. In detail, the strength increment at t=0 min (from 8kPa to 10kPa, i.e., the percentage of increment equal to 25%) is probably only due to viscous behaviour (point (i) above), while, as the time increases, there is a further strength increment that is probably correlated to the rate sensitivity crack propagation (point (ii) above): at t=60 min, the total strength increment is equal to 15kPa (with a percentage increment of about 75%). Instead, there are no appreciable changes in the Young's Modulus values for the resting time examined: the difference of elastic modulus values related to REF-SP0.10-M-DR3 and SP0.10-M-DR30 is contained in the range of experimental scatter. The interpolating laws (see graphic legend Figs. 5.55-5.59) of strength and stiffness founded are used in the analytical model of failure prediction (compressive and self-buckling failure).

5.3.5 Analytical failure prediction

The need to define an adequate testing procedure for the mechanical characterization of the material is correlated to the correct prediction of the critical height of the printed element. In this paper an analytical model is developed to predict the compressive failure at the first layer, or the self-buckling failure of the whole element; however, the printing process can be compromised by other issues, as the shear stress failure, excessive deformations, geometry imperfections etc. The developed model is used to quantify the failure prediction capability as a function of the testing procedure variability (i.e, in the absence of a standardised testing procedure). The failure prediction is based on the following conditions, based on the hypothesis of wall geometry:

5.2) **Compression failure** : $\sigma_V(t) = H(t)\rho g \leq \sigma_{c,max}(t)$

5.5) **Self-Buckling failure** : $E(t) \leq E_{crit}(t) \approx 0.65\frac{H^3(t)\rho g}{\delta^2}$

The analytical laws of compressive strength $\sigma_{c,max}$(t) and Young's Modulus E(t) are obtained and discussed in the previous section. In the following table, a summary of adopted printing parameters is reported. The value of the building rate is chosen in the range of 1 – 6.2 m/h, as studied by Perrot et al. [41].

Layer wide δ [m]	Layer height h [m]	Building rate [m/h]	Density [kg/m3]
0.04	0.01	2.00	2411

In Fig. 5.60, the comparison between the compressive strength and the vertical stress, and between the Young's modulus and the critical elastic modulus is shown, for the reference mix. For a better representation, the vertical axis is expressed in a semilogarithmic scale. Variables

are reported as a function of the number of stacked layers "n", which is correlated to the time (t) through the following expression:

$$n = \frac{tB_R}{h_{layer}} \tag{5.7}$$

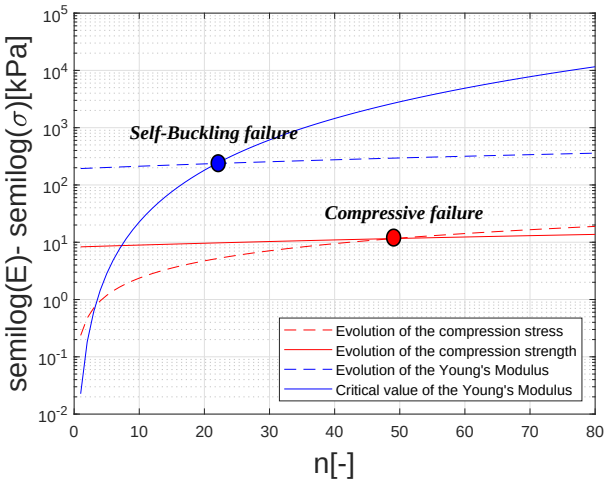

Figure 5.60: Comparison between the compressive strength and the vertical stress (red curves), between the Young's modulus and the critical elastic modulus (blue curves) for Reference Mix.

For the reference mix, the compressive strength at the first layer is reached when 49 layers are stacked above it, while the self-buckling failure occurs after the deposition of 22 layers; hence, the self-buckling occurs firstly, and 22 layers is the failure prediction. The same procedure is made by using the experimental data obtained from each testing condition. In Fig. 5.61 a summary of the obtained results is shown. In all cases, the failure is due to the self-buckling. Even though results can change with the building rate, the critical height (i.e. the maximum number of layers) changes depending on specific test results adopted in the analytical model, varying from the maximum value of 22 (i.e. for reference testing procedure and for SP0.15-M-DR3) to the minimum of 15 layers (i.e. SP0.10-NM-DR3). From the obtained results, it is possible to observe that a small variation within the material (i.e. variation of consistency, presence of voids, previous stress-state) seems to affect the compressive failure prediction: indeed, the maximum number of layers changes from a minimum value of 15 to maximum of 49 (reference mix). By contrast, the displacement rate used during compressive tests can lead to relevant errors in the compressive failure prediction: results show that, by varying the displacement rate from 3mm/min to 30mm/min, there is an increment of the predicted number of layers, from 49 to 91. Consequently, (i) the use of the external membrane during the casting improves the repeatability of test results, due to the lower disturbance induced on the sample during the demoulding - the failure prediction is more trustworthy when the external membrane is used; (ii) the lower or higher percentage of superplasticizer (see the SP0.00-M-DR3 and SP0.15-M-DR3 compared with REF-SP0.10-M-DR3) changes the maximum number from 20 to 49 and from 18 to 22, respectively, for compressive and self-buckling failure. Furthermore, the failure prediction of the reference mix (i.e. 22 layers) is an

upper limit related to achieved results. The variability which characterize the printing process and the material could strongly influence the failure prediction; until now, no accordance exists between numerical/analytical modelling and experimental printing tests. Indeed, also the numerical simulation of the printing process, carried out by Wolfs et al. 2018 [50], diverges from the printing process validation: the maximum number of layers reached during the printing process deviates of 27.5% from the number of layers predicted through the numerical analysis. Obtained results underline the need to define standard procedures for the mechanical characterization of the material, in order to have greater confidence in analytical/predictive models.

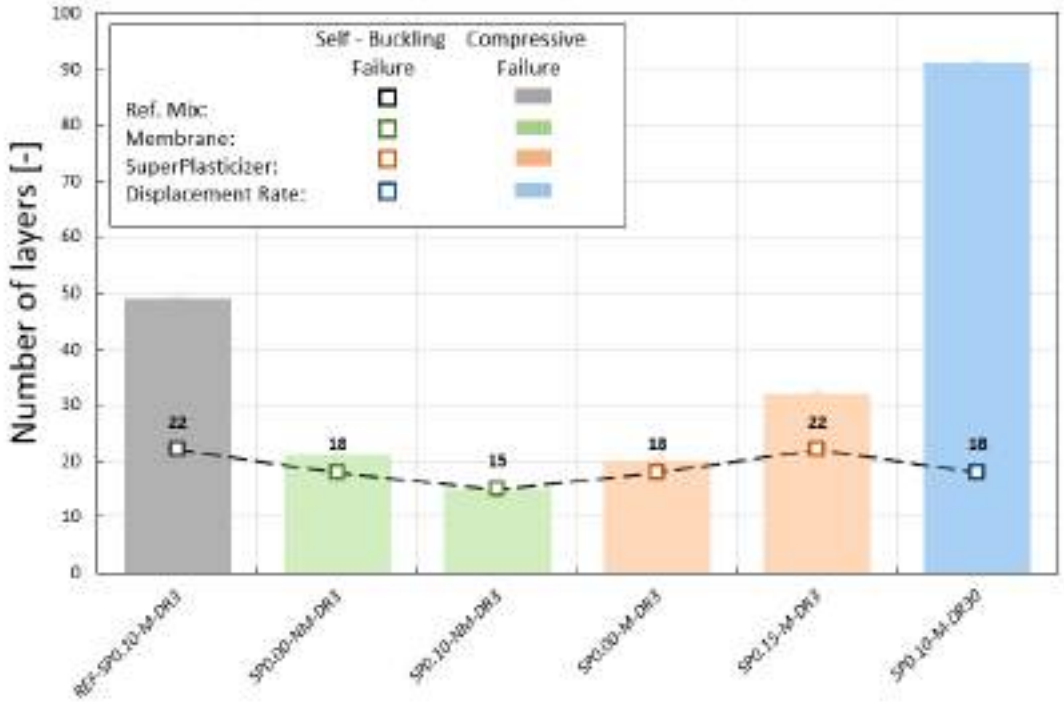

Figure 5.61: Summary of analytical failure prediction – maximum layers' number - for each case examined.

5.4 Creep tests

5.4.1 Introduction

Time-dependent volume changes in cement-based materials can be classified in a stress-independent part, constituted by shrinkage and thermal deformations, and in a stress-dependent part, called creep [73]: these phenomena are correlated, affecting the concrete curing from the very beginning and modifying its long-term performance. However, although the effect of early age shrinkage and thermal cracking is well recognized in literature [74, 75], no consensus is reached on early age creep [76].

Recently, early age creep gained importance due to the development of new concretes and the need in highly creep sensitive structures (dams, nuclear power plant containments, tunnels, etc.). Indeed, such massive structures are particularly affected by volume changes, caused by the heat released during cement hydration. It follows that, if restrained, concrete volume changes provoke early age tensile/compressive overstresses that may lead to self-induced creep strains. Authors [76, 77, 78] argue that creep at early age is more significant than that in hardened concrete; however, since the phenomenon of creep is defined as the evolution of strain under a constant load, the interest has been mainly oriented to those cement pastes capable to sustain such loads, i.e., traditional pastes in a mature phase, expressed in days after casting. For instance, Atrushi (2003) [79], focusing on the determination of creep model parameters, investigated early age concrete properties through an extensive tensile test program developed for six loading ages (1, 2, 3, 4, 6 and 8 days). Bing Han et al (2017) [78], exploring the definition of viscoelastic–plastic models for the early age concrete creep, tested in compression 2 days old prism-shaped specimens. Khan et al (2018) [80], studying the influence of tensile creep on internally-restrained reinforced concrete members, considered two different mixes for determining tensile creep at 0.75, 1, 2, 3, 7 and 28 days. Tab. 5.13 shows a literature review of the most recent experimental investigations carried out for early age basic creep, along with a concise summary of testing conditions and the loading age. It is clear that the current research mainly investigates on the creep response, either in hardened or in early age concretes, both in days after casting.

Nowadays, additive manufacturing in construction industry gives advantages in terms of

Authors	**Concrete Parameters**		**Testing Conditions**	**Loading Age (days)**
	w/c	Admixtures		
Atrushi (2003)	0.4	Silica Fume	Tension	1,2,3,4,6 and 8
Briffaut (2010)	0.45	Superplasticizer	Tension	5
Masse (2010)	0.22	Silica fume, superplasticizer	Tension	7
Darquennes et al. (2011)	0.45	Superplasticizer, Blast slag	Tension/Compression	1
Ni et al. (2019)	0.3	Portland, Fly ash	Tension	1,2,3,5,7
Li et al. (2002)	0.3	Portland, Silica Fume, Blast slag	Tension/Compression	3
Bing Han et al (2017)	0.39	Portland	Compression	2
Khan et al (2018)	0.45	Portland	Tension	0.75,1,2,3,7
Wyrzykowski et al (2019)	0.5	Portland	Compression	1.5,3,7
Ranaivomanana et al. (2013)	0.45	Superplasticizer	Tension/Compression	28
Briffaut et al. (2012)	-	Portland, Superplasticizer	Compression	1

Table 5.13: Literature review of early age tension/compression creep.

improved production rate, architectural flexibility and cost reduction [70], posing new engineering challenges. In detail, most of these challenges consists in optimizing the concrete compatibility with the printing system. Indeed, the 3D printing process consists in extruding and depositing fresh concrete filaments without formworks, usually adopted to confine and stabilize the material: hence, the fresh admixture should be adequately strong, stiff, and stable to sustain its self-weight and the weight of the filaments above it, limiting deformations. Unfortunately, early age concrete is a transient material, whose rheological properties exhibit manifold peculiarities. For instance, the admixture is generally characterized by a high paste volume, a low water-to-cement ratio (w/c), a high dosage of mineral additions and superplasticizer, often mixed with a viscosity-modifying agent [58]. Such peculiarities affect viscoelastic properties of concretes: on one hand, low water-to-cement ratios conduct to a higher strength; on the other hand, high paste volumes are more sensitive to creep and shrinkage [77, 81, 82]. Since the degree of hydration strongly influences the early age creep [83], higher creep strains are experienced if concrete is demoulded and loaded at ages inferior to 1 day [84, 85, 86]. Moreover, as the height of the printed element increases, so does the hydrostatic pressure and the layer compression under the self-weight [49]. As a consequence, we believe that to guarantee the dimensional control and to avoid stability problems, a comprehensive insight on the early age compressive behaviour of 3D printable admixtures is necessary, including creep-induced time-dependent volume changes (that may assume a prominent role during the 3D printing buildup process). However, no data are available in literature.

As a result, we propose a characterization procedure for 3D printable cementitious mortars, apt to investigate basic creep under compressive loads: (i) qualitatively, focusing on main differences between creep in cast and in 3D printable concretes; (ii) quantitatively, defining the temporal evolution of the deformation-based response at multiple fresh concrete curing ages. Hence, in order to achieve an exhaustive characterization of 3D printable concrete response as a function of early age, uniaxial compressive creep tests are performed within an appropriate time-frame, which simulate the elapsed time between the material extrusion and the staking process. Accordingly, such tests are executed at distinct loading ages, t = 0, 15, 30 and 60 minutes, in order to define the time-dependent evolution of the basic creep and to reproduce buildup loading applications that would be expected from a common 3D printing layered extrusion process. In particular, the following aspects are considered:

- Material and sample preparation;
- Uniaxial compressive creep testing conditions;
- Evolution in time of the creep response.

Initially, a 3D printable concrete material is characterized in order to satisfy peculiar rheological requirements, i.e., achieving an optimized balance between pumpability, extrudability and buildability (Section 5.4.2.1). Subsequently, specimens are manufactured and subjected to multiple constant step loads, simulating one-, two- and three-layer weight for two printing rates, 900 and 300 seconds (Section 5.4.3). Finally, a theoretical framework is developed in order to predict the accumulated creep strain achieved during the buildup process (Section 5.4.3.2). Concluding remarks are given.

5.4.2 Material and methods

In this section we develop a characterization procedure for 3D printable concrete mixes (the reference mix and the specimen preparation are provided in Section 5.3.2). Such characterization focuses the on early age compressive creep response: specifically, given that differently from cast concrete the material behavior evolves during the buildup process, we investigate on such time-dependent curing properties that may affect buildability. Accordingly, in the following we discuss:

- the influence of the material and the sample preparation on testing results;
- the creep experimental testing conditions (testing time and displacement rate);
- the simulation of the stacking process.

5.4.2.1 Compressive creep tests

Specimens are tested in an electromechanical Universal Testing Machine, with 10kN capacity in displacement-control condition, at room temperature T $\approx 22^oC$ and controlled relative humidity RH $\approx 60\%$. Tests are performed applying displacements of the loading head up to achieve 8N of vertical force reaction, i.e. the self-weight of the specimen. Once such threshold is reached, we start recording the creep evolution under the constant load. Samples are subjected to target multiple constant step loads simulating one-, two- and three-layer stacking. Since no physical measurement on the sample are considered feasible without altering the specimen, stress and strain are deduced from force-displacement diagrams. In particular, the stress is computed by dividing the recorded load for the cross-sectional area of the sample (i.e. 2826 mm^2), whereas the strain is obtained by dividing the displacement of the loading head for the initial height of the sample. In order to achieve the time-dependent evolution of the creep strain law, tests are carried out at distinct concrete ages of t = 0, 15, 30 and 60 minutes, with a displacement rate of 3mm/min (Displacement Rate – DR). Therefore, since creep is a slow test, defined by applying a constant load for a certain period, specimens are effectively curing under the testing machine. Hence, to evaluate also the curing evolution, two testing times are considered, i.e., 900 and 300 seconds (identified, respectively, as long- and short-term creep, LC- and SC-). Since mechanical properties of cementitious materials are rate sensitive, compressive creep tests are performed, only for the reference mix, also with a higher value of displacement rate (i.e. 30mm/min), in order to assess result variations.

5.4.2.2 Summary of tests

Uniaxial compressive creep tests are carried out by varying: (i) the concrete age (i.e. t=0, 15, 30 and 60 minutes), (ii) the testing time (i.e., 900 and 300 seconds), (iii) the percentage of Superplasticizer (i.e. 0.00, 0.10 and 0.15% in weight of cement) and (iv) the displacement rate (i.e. 3mm/min and 30mm/min). In Tab. 5.14 such variables are summarized. Each specimen set is identified by the acronym "SPxx-yC-DRzz", where "SPxx" represents the percentage of superplasticizer (SP0.00, SP0.10 and SP0.15), "yC" indicates if testing time considered is 900 or 300 seconds (long- and short-term creep, LC- and SC-) and "DRzz" is the value of displacement rate in mm/min (DR3 and DR30). The reference test is indicated by the acronym "REF-SP0.10-LC-DR3". Reference sample is subjected to target multiple constant step loads simulating one-, two- and three-layer stacking.

Variables	**Uniaxial unconfined compression tests**				
Acronym	**REF-SP0.10-LC-DR3**	**SP0.10-LC-DR30**	**SP0.10-SC-DR3**	**SP0.00-SC-DR3**	**SP0.15-SC-DR3**
1. Age [min]	0, 15, 30, 60	0, 15, 30, 60	0, 15, 30, 60	0, 15, 30, 60	0, 15, 30, 60
2. Superplasticizer [%]	0.10	0.10	0.10	0.00	0.15
3. Testing Time [sec]	900	900	300	300	300
4. Displacement rate [mm/min]	3.0	30.0	3.0	3.0	3.0
Samples per set	5	5	5	5	5
Tot. samples	20	20	20	20	20

Table 5.14: Test matrix.

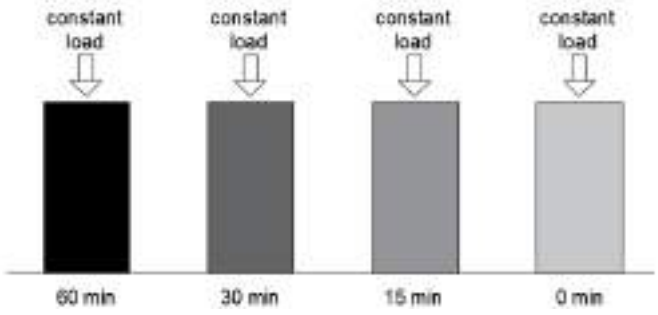

Figure 5.62: Schematic of early age sample set with different curing time.

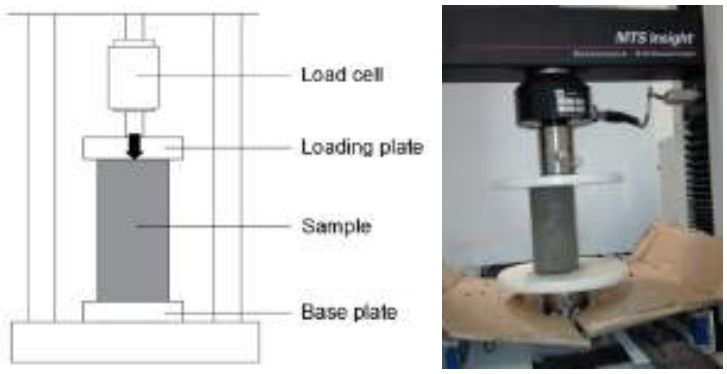

(a) (b)

Figure 5.63: Sketch of uniaxial unconfined creep test.

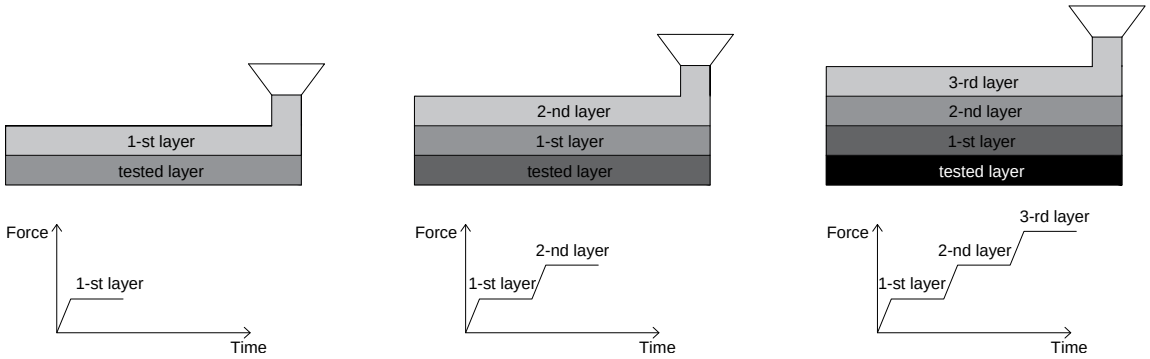

Figure 5.64: Simulation of one-, two- and three-layer stacking.

5.4.3 Results and discussions

We investigate on the basic compressive creep response of fresh concrete: main results, achieved from the set of experimental analysis, are outlined in this section. A general overview of the performance is summarized here, while crucial aspects are referenced when needed to explain key points. Special interest is paid to the influence of mechanical response on printability criteria. As a result, four are the main variables of our study: (i) the early age curing time (t = 0, 15, 30 and 60 min), (ii) the testing time (900 and 300s), (iii) the amount of superplasticizer (0.0, 0.1 and 0.15%) and (iv) the displacement rate (3mm/min and 30mm/min). Subsequently, samples are subjected to multiple constant step loads simulating one-, two- and three-layer stacking, in order to get knowledge on the creep evolution during the buildup process. Results are exhibited in terms of time, averages and standard deviations.

5.4.3.1 Reference long-term creep

Results referred to the long-term compressive creep (900s) are condensed in the following pages, organized in this way: initially, we show a set of four diagrams that represent the time-dependent response (in terms of force, displacement and force-displacement curves) in early age curing time, i.e., for t = 0, 15, 30 and 60 min. Each diagram of this set shows five test results (grey) with their average (black). Subsequently, in the same page, comparisons among averages are presented in order to measure the extent of the specimen response evolution in curing time. Afterwards, average peaks are depicted in a bar chart along with their standard deviation, in order to understand the repeatability of the test; finally, force-displacement results are translated in stress-strain data. Note that the value of long-term creep timespan (900 sec - 15 min) is intentionally selected to investigate the transition among curing ages (i.e., t = 0, 15, 30 and 60 min) during the testing time. The adopted amount of superplasticizer is 0.1% of cement weight.

A displacement-controlled test is performed until the self weight is applied (8N - 2.8kPa), then the load is maintained constant up to 900 sec, and consequently increased again doubling the self weight (16N - 5.6 kPa). In Figs. 5.65 and 5.71, the load application is displayed: it is possible to observe that oscillations, due to the responsiveness of MTS loading machine (up to 8±1.2N and 16±1.8N), become more accentuated as the sample stiffness increases.

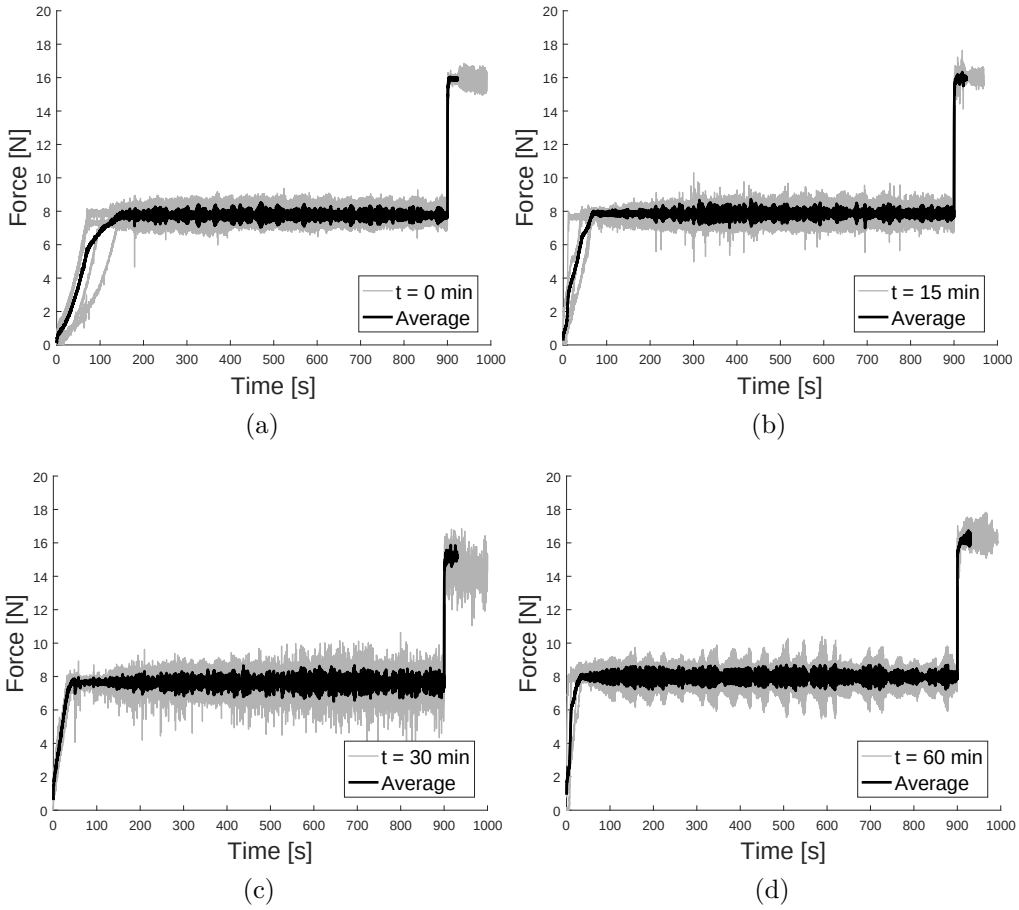

Figure 5.65: Long-term creep tests, 0.1% plasticizer with membrane. Average and individual results at different time - (a) 0 minutes, (b) 15 minutes, (c) 30 minutes, (d) 60 minutes.

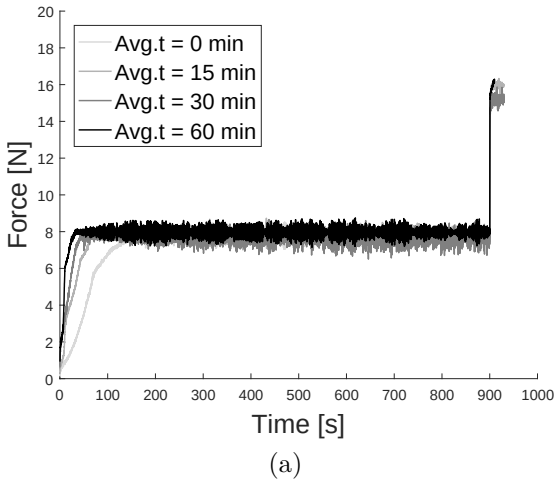

Figure 5.66: Long-term creep tests, 0.1% plasticizer with membrane. Average comparisons at different time - 0 minutes, 15 minutes, 30 minutes, 60 minutes - (a) trend - REF-SP0.10-LC-DR3.

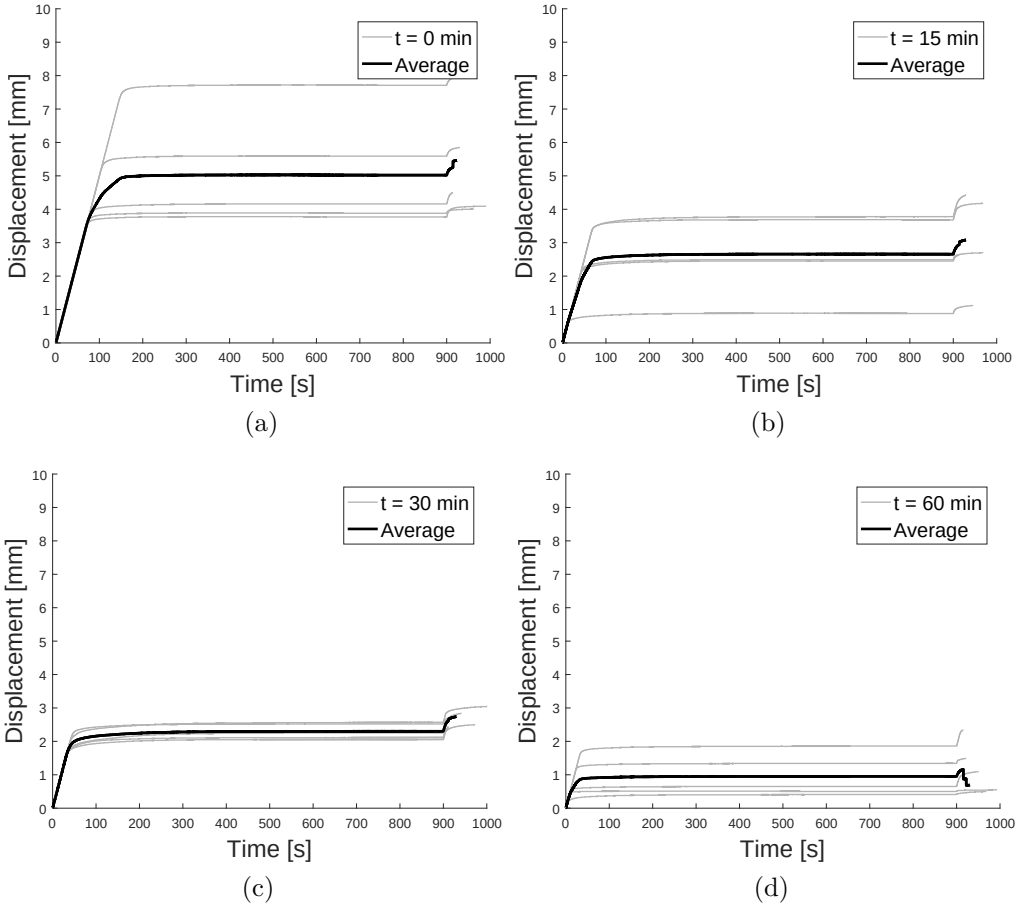

Figure 5.67: Long-term creep tests, 0.1% plasticizer with membrane. Average and individual results at different time - (a) 0 minutes, (b) 15 minutes, (c) 30 minutes, (d) 60 minutes.

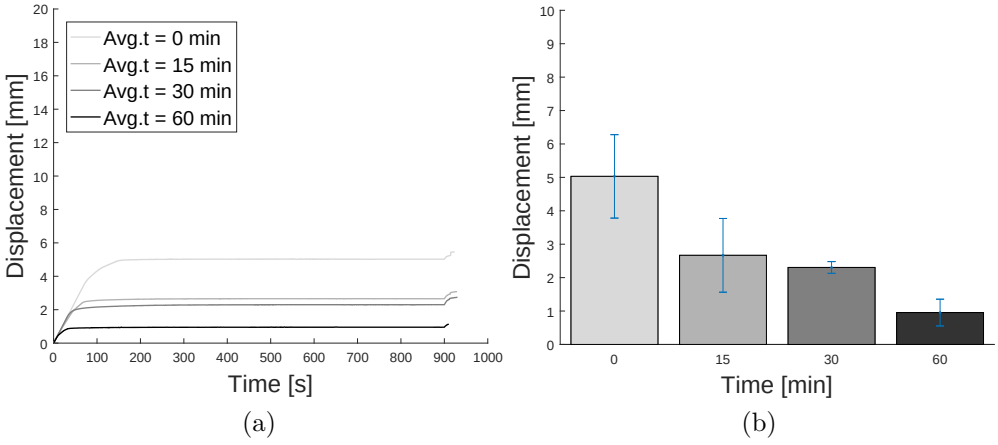

Figure 5.68: Long-term creep tests, 0.1% plasticizer with membrane. Average comparisons at different time - 0 minutes, 15 minutes, 30 minutes, 60 minutes - (a) trend & (b) peaks with standard deviation - REF-SP0.10-LC-DR3.

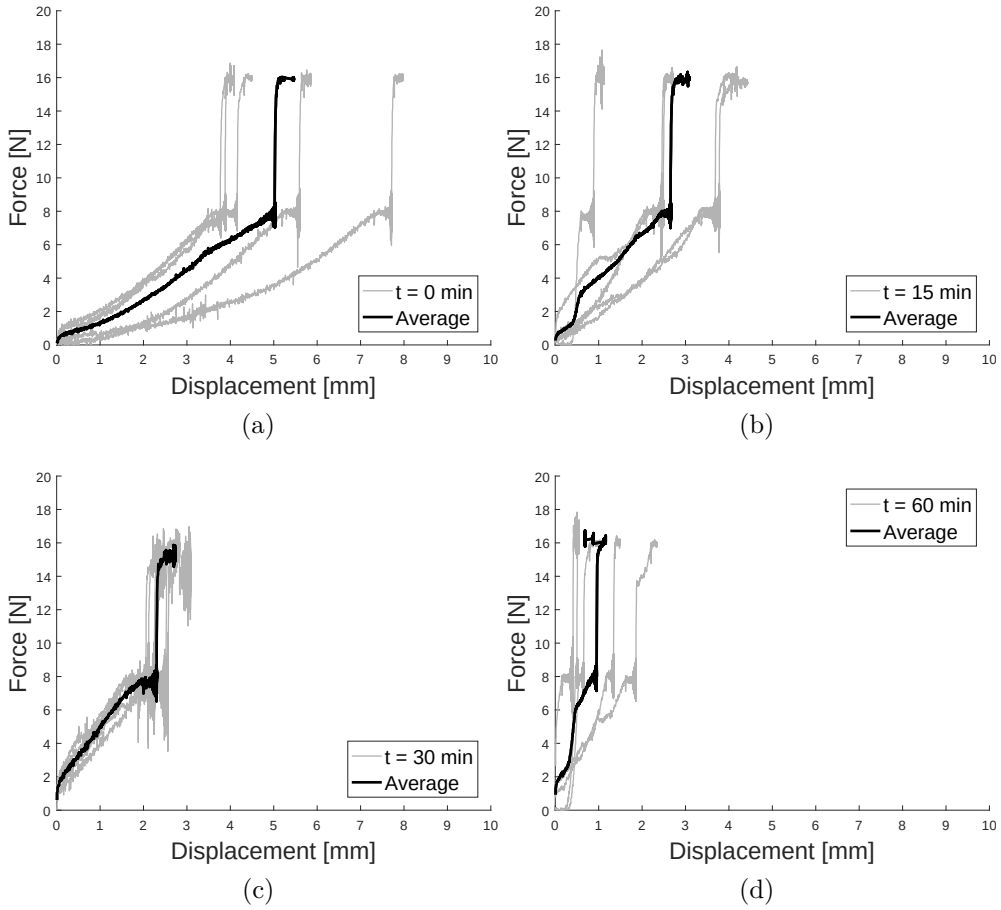

Figure 5.69: Long-term creep tests, 0.1% plasticizer with membrane. Average and individual results at different time - (a) 0 minutes, (b) 15 minutes, (c) 30 minutes, (d) 60 minutes.

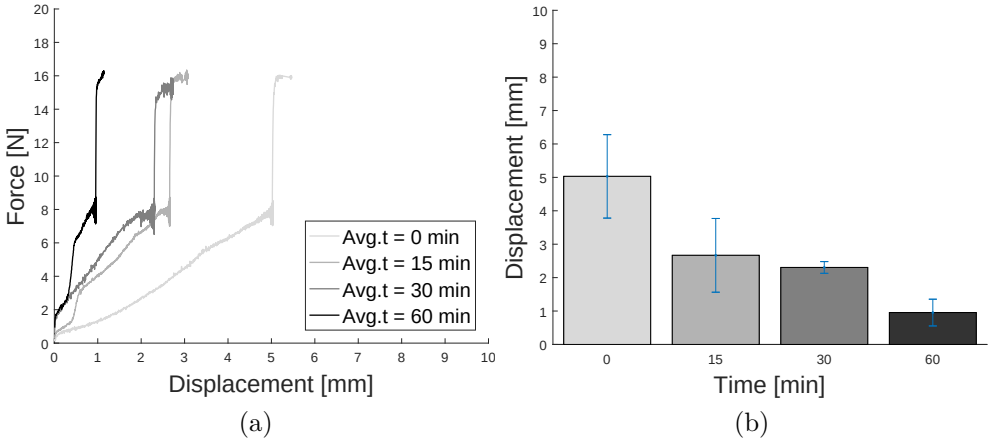

Figure 5.70: Long-term creep tests, 0.1% plasticizer with membrane. Average comparisons at different time - 0 minutes, 15 minutes, 30 minutes, 60 minutes - (a) trend & (b) peaks with standard deviation - REF-SP0.10-LC-DR3.

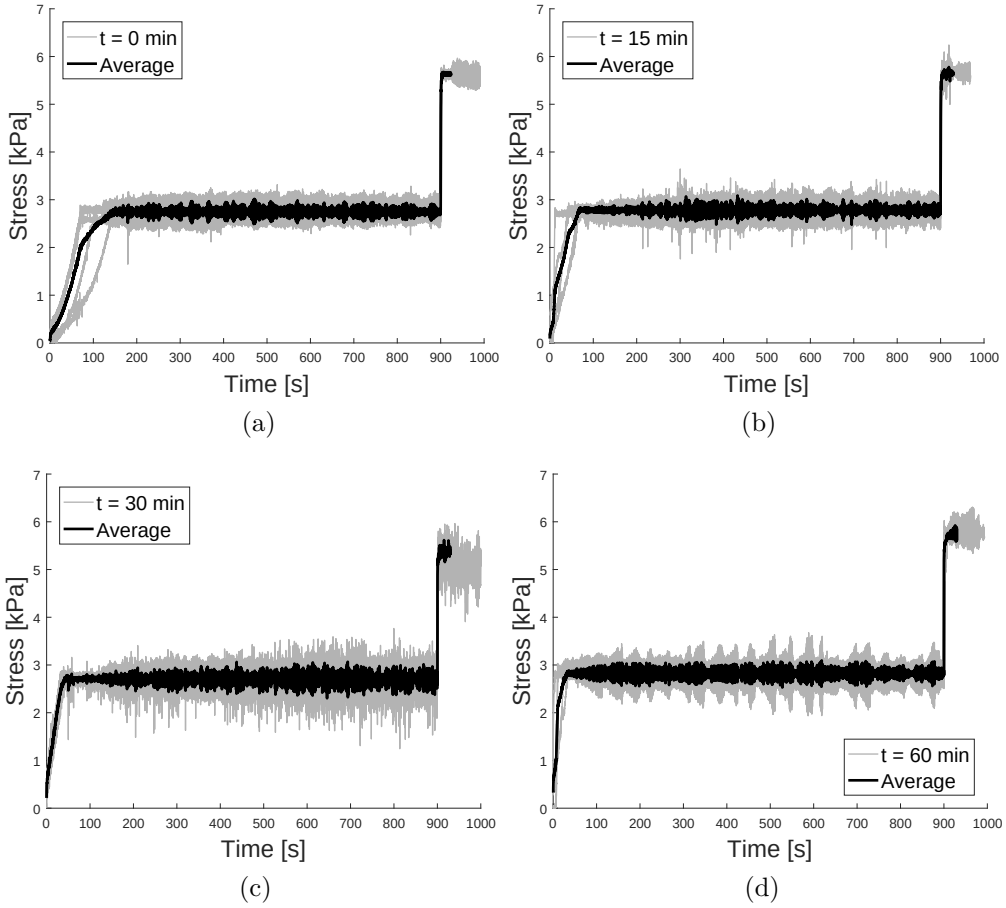

Figure 5.71: Long-term creep tests, 0.1% plasticizer with membrane. Average and individual results at different time - (a) 0 minutes, (b) 15 minutes, (c) 30 minutes, (d) 60 minutes.

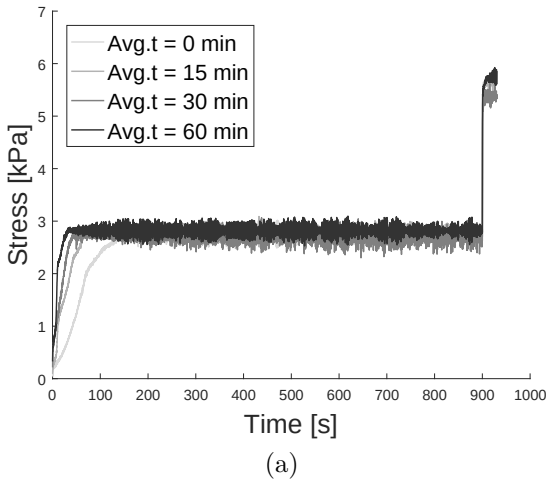

Figure 5.72: Long-term creep tests, 0.1% plasticizer with membrane. Average comparisons at different time - 0 minutes, 15 minutes, 30 minutes, 60 minutes - (a) trend - REF-SP0.10-LC-DR3.

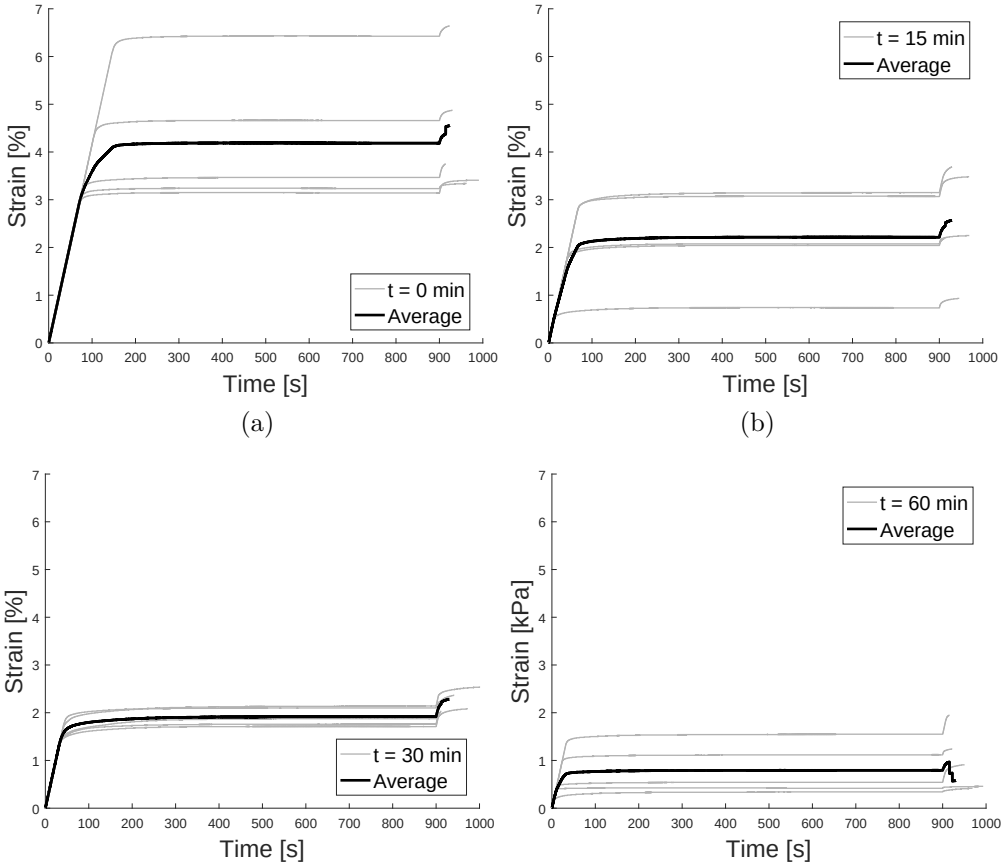

Figure 5.73: Long-term creep tests, 0.1% plasticizer with membrane. Average and individual results at different time - (a) 0 minutes, (b) 15 minutes, (c) 30 minutes, (d) 60 minutes.

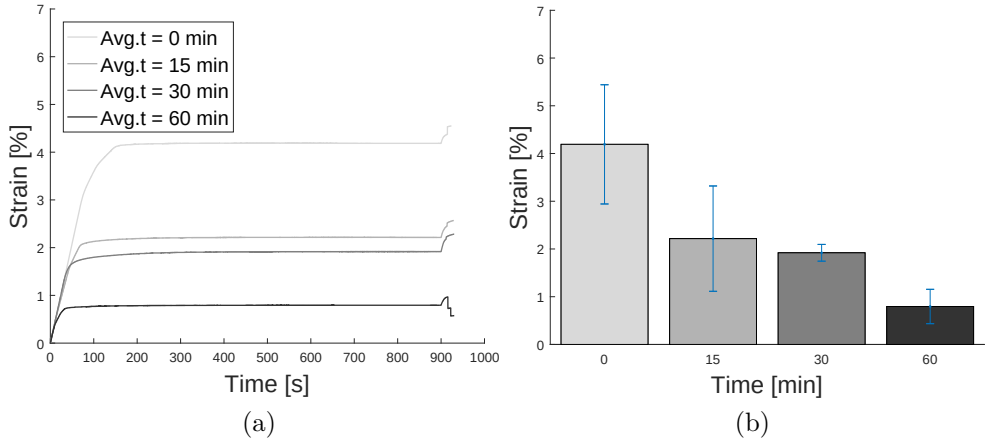

Figure 5.74: Long-term creep tests, 0.1% plasticizer with membrane. Average comparisons at different time - 0 minutes, 15 minutes, 30 minutes, 60 minutes - (a) trend & (b) peaks with standard deviation - REF-SP0.10-LC-DR3.

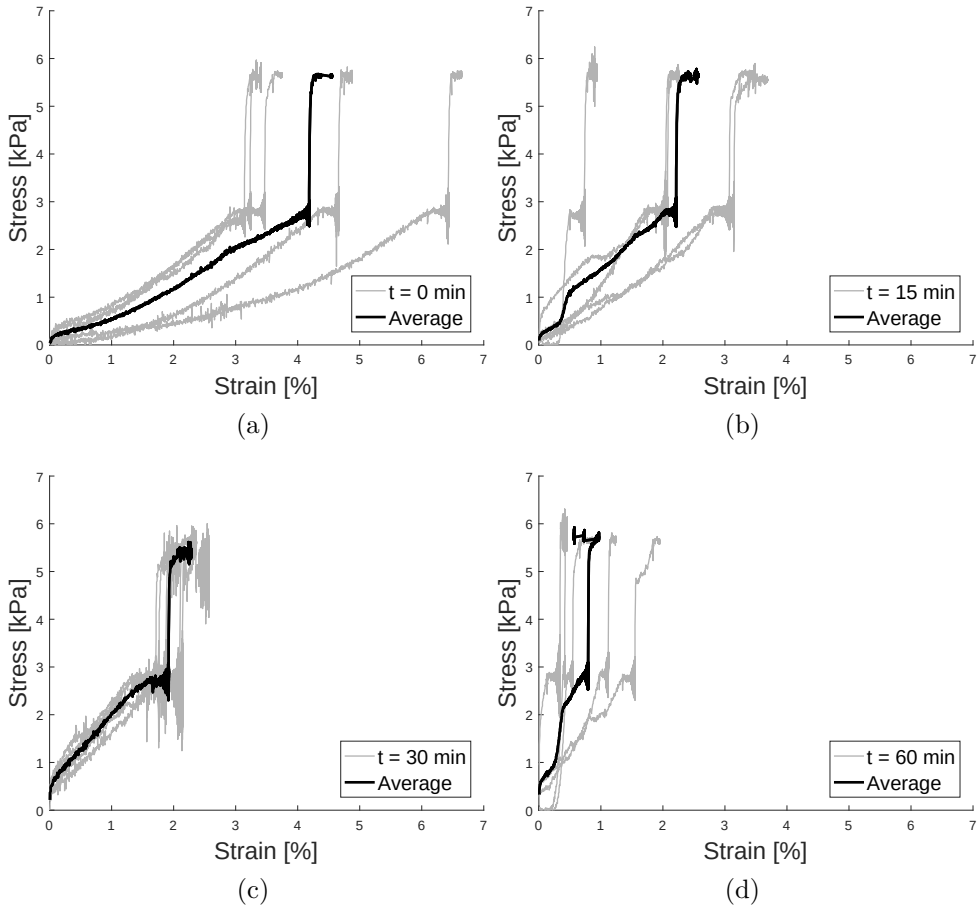

Figure 5.75: Long-term creep tests, 0.1% plasticizer with membrane. Average and individual results at different time - (a) 0 minutes, (b) 15 minutes, (c) 30 minutes, (d) 60 minutes.

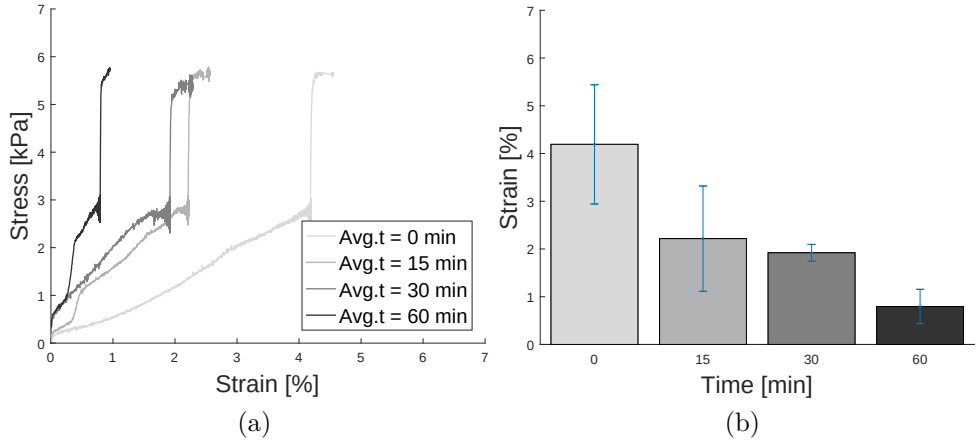

Figure 5.76: Long-term creep tests, 0.1% plasticizer with membrane. Average comparisons at different time - 0 minutes, 15 minutes, 30 minutes, 60 minutes - (a) trend & (b) peaks with standard deviation - REF-SP0.10-LC-DR3.

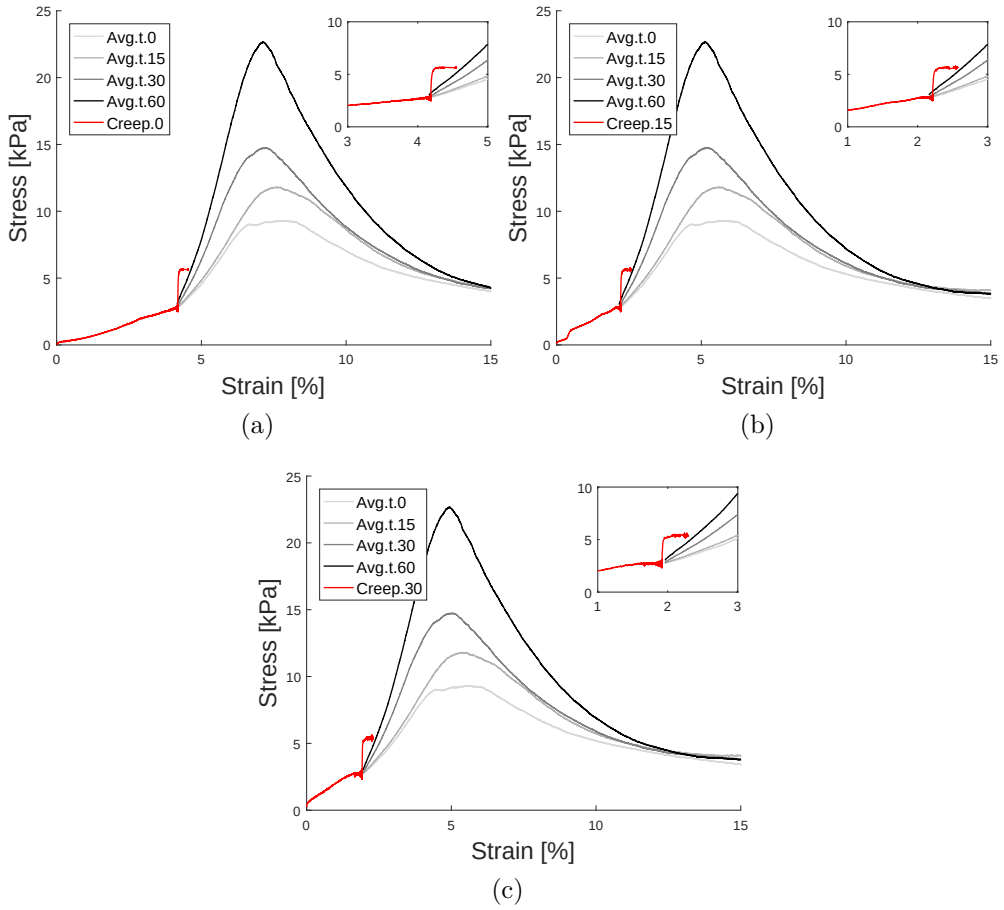

Figure 5.77: Creep tests compared with compression tests, 0.1% plasticizer with membrane. Average and individual results at different time - (a) 0 minutes, (b) 15 minutes, (c) 30 minutes

Comparing results in Figs. 5.67 and 5.73 it is clear that the early age mechanical response of concrete evolves between 0 and 60 min, showing a stiffness increase that conduces to lower displacements and strain (up to 5mm and 4%), congruently with unconfined compression test results (the stiffness increment can also be noticed in Figs. 5.69 and 5.75, where the force-displacement and the stress-strain response is depicted). In order to evaluate the potential transition among curing ages during the testing time (900 sec), i.e., if t = 0, 15 and 30 samples harden up to t = 15, 30 and 60, respectively, stress-strain diagrams are overlapped with compression test results, Fig. 5.77. Comparing stress-strain creep tests (red) with stress-strain compression test results (greyscale), we can evince that the first branch of stress-strain creep curves (corresponding to the initial increment of self weight, 8N) is congruent with the beginning of the compression test; however, the second branch (corresponding to the second increment of weight, 16N) is much more stiff than stress-strain compression curves. In order to have a deeper insight on this phenomena, please refer to Fig. 5.78: in this example the 0 min cured specimen is set in the testing machine. The stress-strain creep curve is depicted in red, while the stress-strain compression curve is marked in black. Initially, the sample is loaded with the self weight (first branch); subsequently, the load is maintained constant for 900 sec, and then loaded again to double the self weight (second branch).

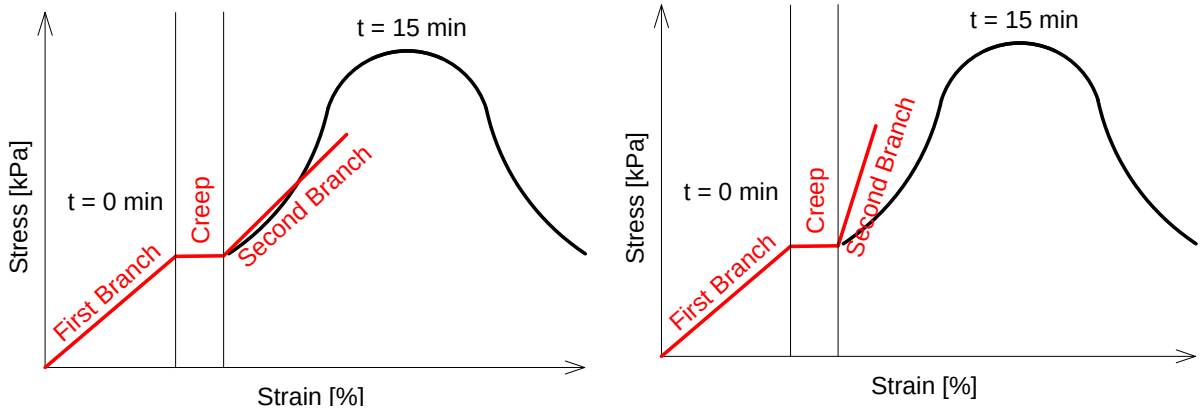

(a) (b)

Figure 5.78: Creep tests compared with compression tests, conceptual example of curing transition.

Therefore, the 0 min cured curve evolves in a 15 min cured curve during creep; however, instead to follow the 15 min cured compression curve (Fig. 5.78a) it develops stiffer (Fig. 5.78b). This interesting feature underlines that early age specimens cured under compression reach a higher stiffness and strength: as this condition simulates the layer-based 3D printing buildup process, i.e., where concrete layers cure sustaining the weight of higher layers, it follows that in such process concrete layers will tend to exhibit an improved performance in terms of stiffness and strength. In Tab. 5.15, peak values obtained during the long-term creep test are summarized. Note that in this case, the strain refers to the total strain (Fig. 5.98).

In Fig. 5.79, three illustrative time-dependent strain diagrams are shown: Fig. 5.79a shows typical deformations of hardened concrete, Fig. 5.79b represents idealized deformations of early age mixes and Fig. 5.79c depicts a real case obtained with fresh concrete. We want to highlight that, even if the theoretical application of the constant load is instantaneous, practically, the load is applied throughout a ramp law (therefore the first branch of the curve

	Curing Time			
	0 min	**15 min**	**30 min**	**60 min**
	peak averages	**peak averages**	**peak averages**	**peak averages**
Force [N]	8.53	8.73	8.67	8.75
Total Displacement [mm]	4.19	2.21	1.92	0.80
Stress [kPa]	3.02	3.09	3.07	3.10
Total Strain [%]	3.49	1.84	1.60	0.67
Force Standard Deviation [N]	0.30	0.37	0.55	0.39
Relative Force Standard Deviation [%]	3.52	4.24	6.34	4.46
Disp. Standard Deviation [mm]	1.25	0.88	0.18	0.47
Relative Disp. Standard Deviation [%]	29.83	39.81	9.83	58.75
Tot. number of samples	**5**	**5**	**5**	**5**

Table 5.15: Reference force-displacement and stress-strain results.

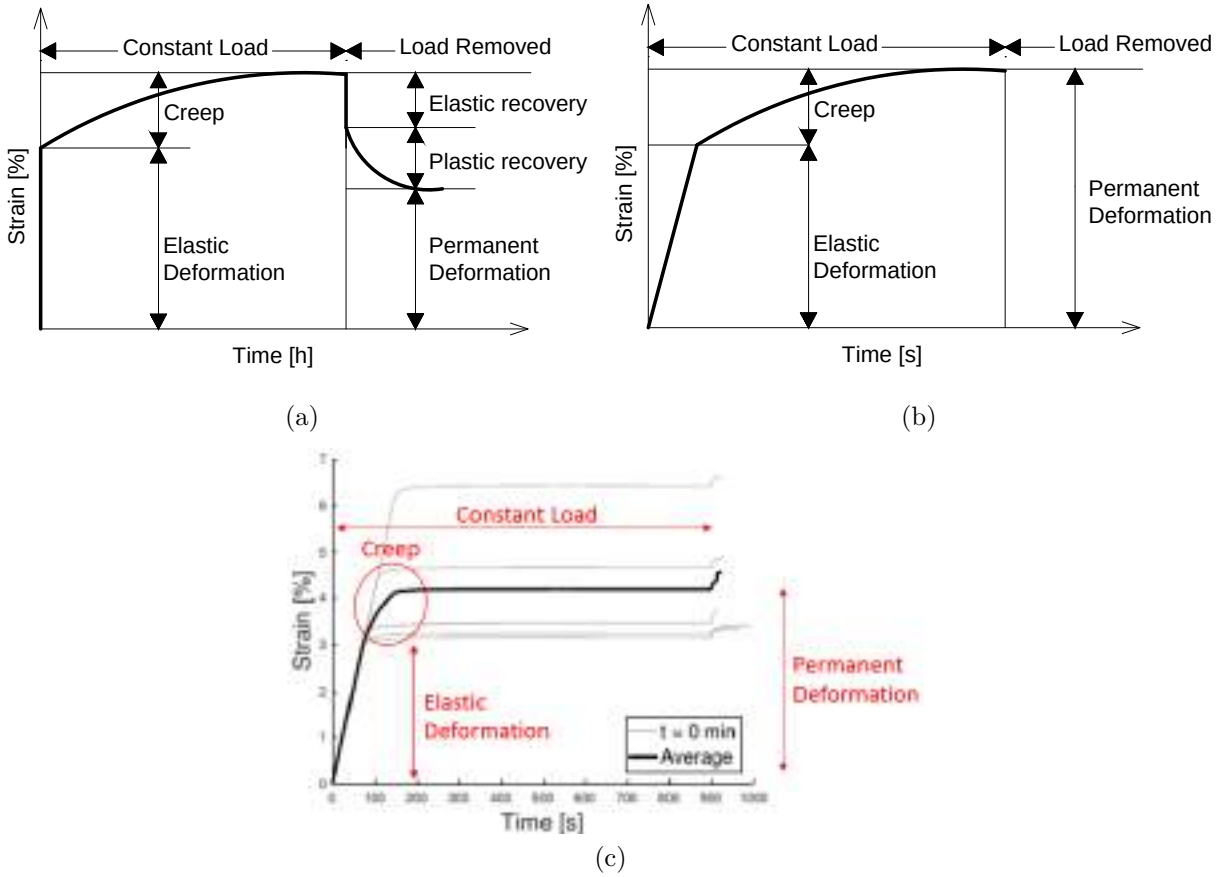

Figure 5.79: Creep in (a) hardened and (b) early age concrete; (c) real case.

is sloped). Moreover, new chemical bonds are created in the deformed configuration (during testing): elasto-plastic recovery is minimum and permanent deformations are maximum. As a result, we represent creep strains alone, i.e., obtained removing the elastic deformation from total strain curves (Fig. 5.79c). Fig. 5.80 represents the creep strain at different curing early ages (t = 0, 15, 30 and 60 min); for each measurement, the average, the maximum and the minimum value are represented: comparing average curves (Fig . 5.81) it is possible to notice that the creep strain decreases as the concrete harden (maintaining the same constant load at 8N), beginning with 0.21% (t = 0 minutes) and halving in one hour. In Tab. 5.16, the strain, the standard deviation and the relative standard deviation are summarized.

	Curing Time			
	0 min peak averages	**15 min peak averages**	**30 min peak averages**	**60 min peak averages**
Creep Strain [%]	0.21	0.19	0.15	0.10
Strain Standard Deviation [%]	0.0232	0.0178	0.0103	0.0252
Relative Strain Standard Deviation [%]	11.05	9.37	6.87	25.21
Tot. number of samples	**5**	**5**	**5**	**5**

Table 5.16: Reference long-term creep results.

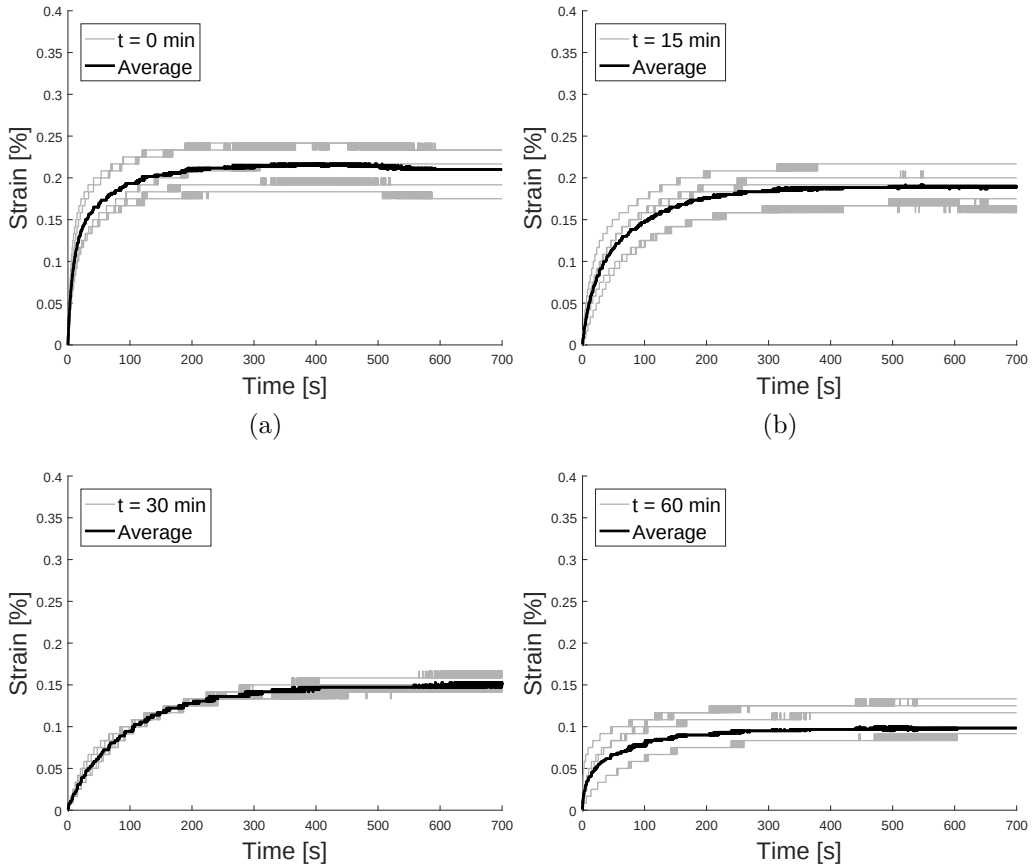

Figure 5.80: Creep tests, 0.1% plasticizer with membrane. Average and individual results at different time - (a) 0 minutes, (b) 15 minutes, (c) 30 minutes, (d) 60 minutes - creep strain.

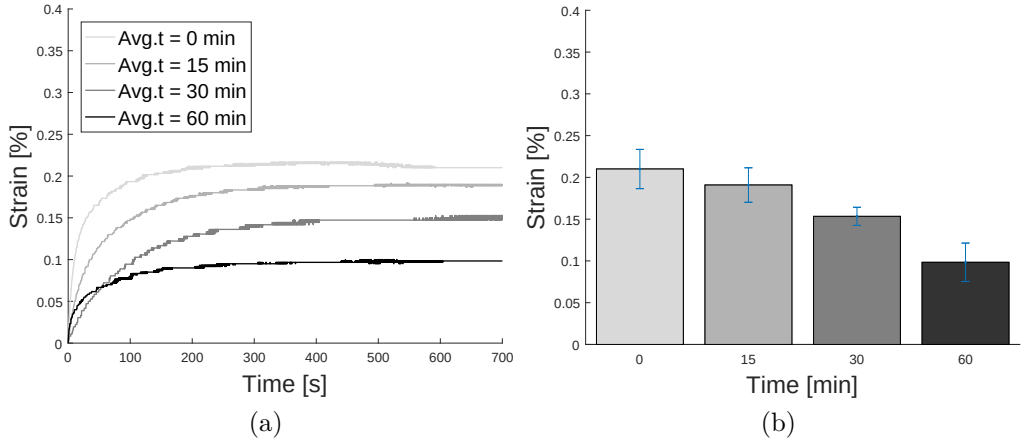

Figure 5.81: Creep tests, 0.1% plasticizer with membrane. Average comparisons at different time - 0 minutes, 15 minutes, 30 minutes, 60 minutes - (a) trend & (b) peaks with standard deviation - REF-SP0.10-LC-DR3.

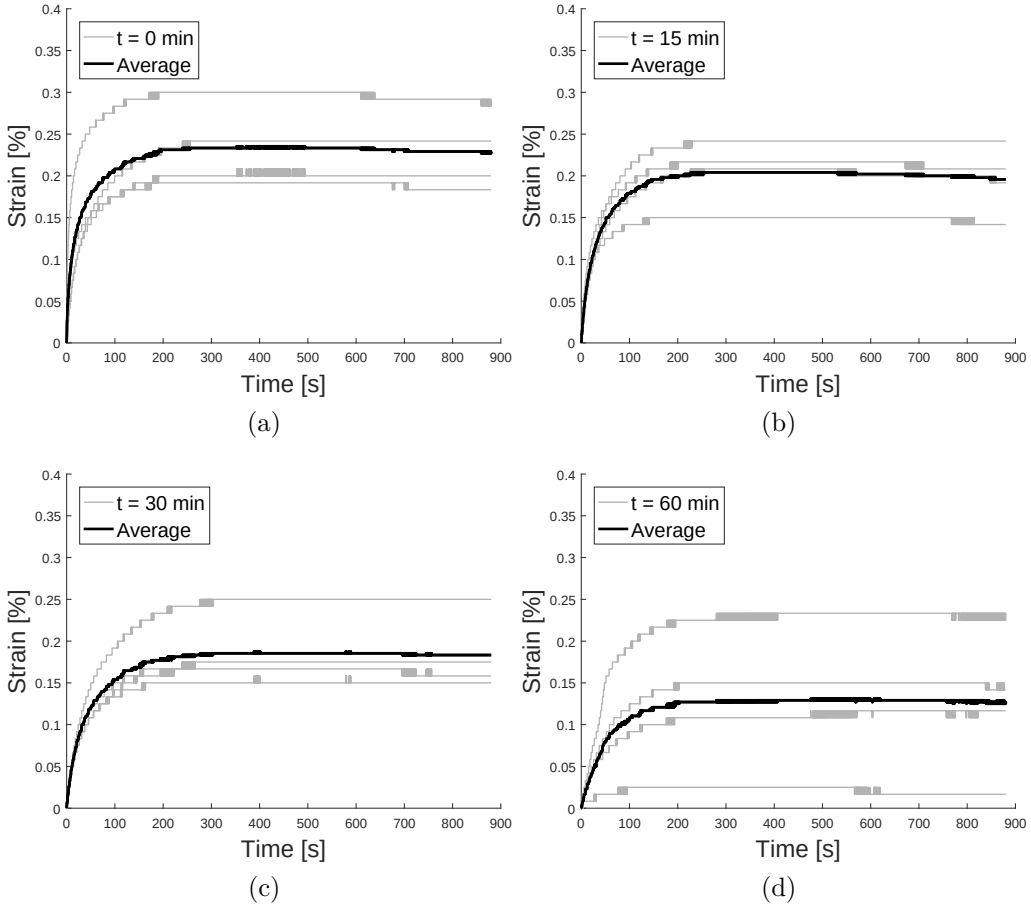

Figure 5.82: Creep tests, 0.1% plasticizer with membrane. Average and individual results at different time - (a) 0 minutes, (b) 15 minutes, (c) 30 minutes, (d) 60 minutes - creep strain.

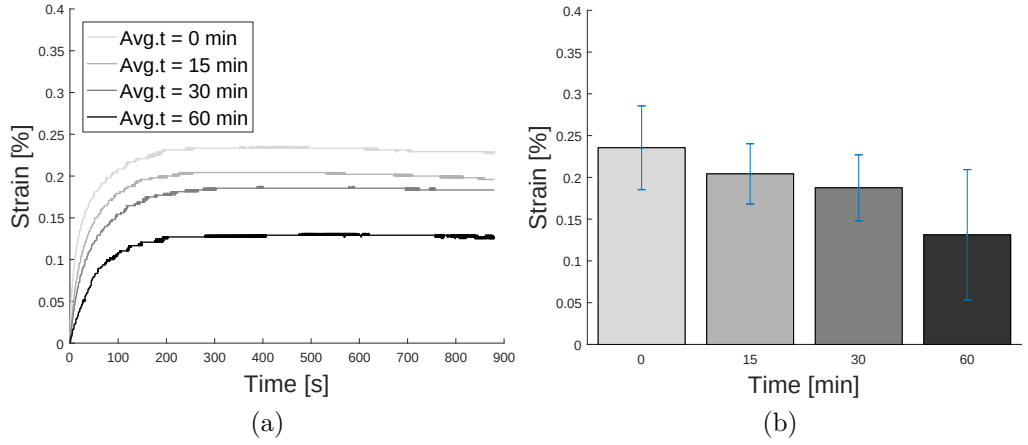

Figure 5.83: Creep tests, 0.1% plasticizer with membrane. Average comparisons at different time - 0 minutes, 15 minutes, 30 minutes, 60 minutes - (a) trend & (b) peaks with standard deviation - SP0.10-LC-DR30.

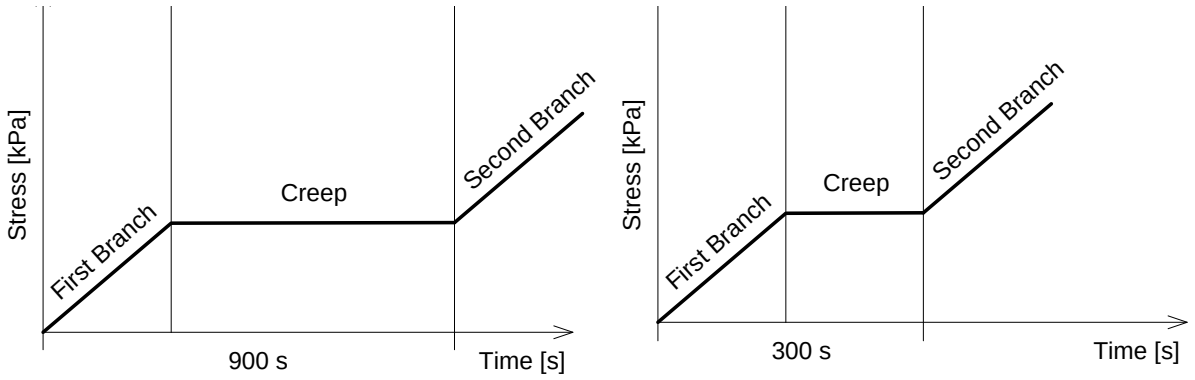

(a) (b)

Figure 5.84: Load application schematic of the for the reference long-term and short-term creep test.

Fig. 5.82 and 5.83 represent creep strain curves obtained with an increased displacement rate (30 mm/min): as expected, the creep remains approximately unvaried, reaching a peak of 0.23% with an increased RSD, nearly the 26%. Creep induced deformations can exacerbate the fresh state stability of 3D printed walls, representing, in our opinion, a specific challenge to be addressed in 3D concrete printing process. Furthermore, 0.23% is the maximum strain obtained applying the self weight to a single layer (i.e., simulating one-layer stacking): as the number of layer increases, the deformation accumulates, worsening the stability during the buildup process. Further analyses need to be carried out in order to quantify the amount of creep accumulated during the process.

From Fig. 5.81 it is possible to observe that average creep values stabilize after approximately 200 seconds, reaching a plateau: therefore, we introduce short-term creep tests, performed in 300 seconds (Fig. 5.84). In such tests we investigate on correlations between creep and the amount of superplasticizer, as well as on the accumulation of creep obtained increasing the number of layers. Accordingly, in Tab. 5.17 we outline the following tests under assessment.

	Curing Time			
	0 min	**15 min**	**30 min**	**60 min**
	n. samples	**n. samples**	**n. samples**	**n. samples**
SP0.00-SC-DR3	5	5	5	5
SP0.10-SC-DR3	5	5	5	5
SP0.15-SC-DR3	5	5	5	5
SP0.10-SC-DR3, 2 layers	5	5	5	5
SP0.10-SC-DR3, 3 layers	5	5	5	5
Tot. number of samples	**25**	**25**	**25**	**25**

Table 5.17: Test matrix.

5.4.3.2 Short-term creep

Results condensed in following pages are organized as follows: initially, each page displays a set of four diagrams that represents the time-dependent response (in terms of creep strain) at early age curing time, i.e., for t = 0, 15, 30 and 60 minutes.

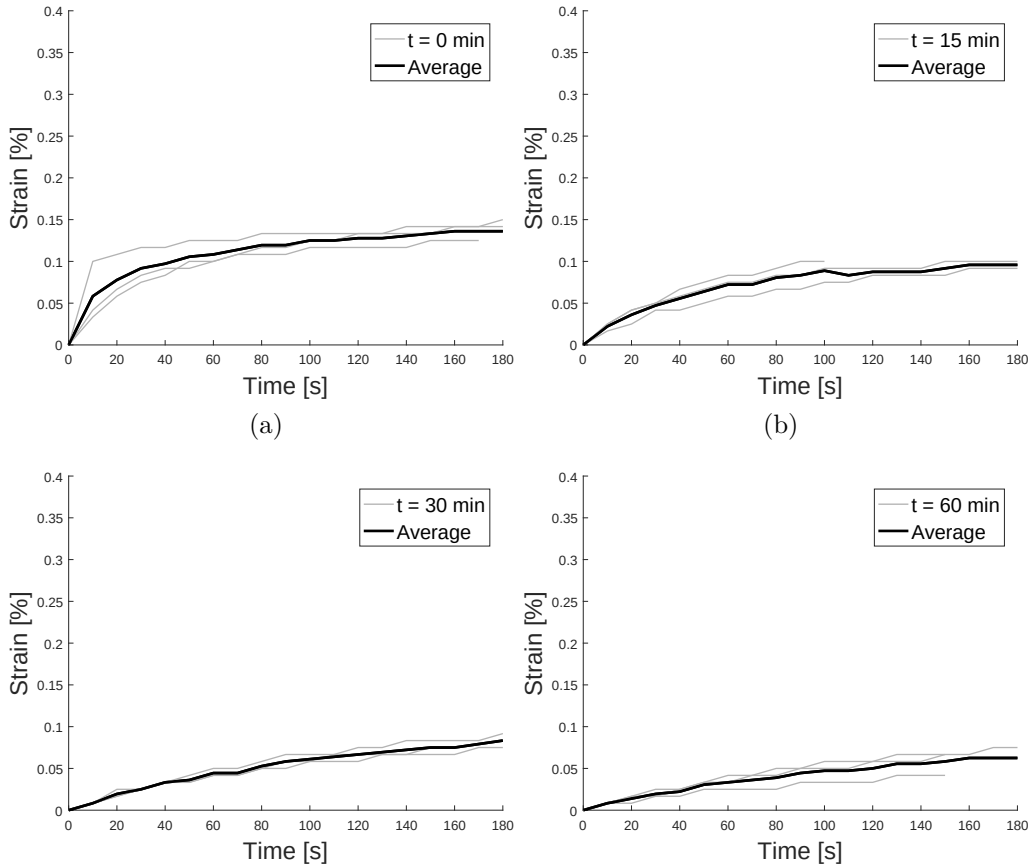

Figure 5.85: Creep tests, 0.0% plasticizer with membrane. Average and individual results at different time - (a) 0 minutes, (b) 15 minutes, (c) 30 minutes, (d) 60 minutes - creep strain.

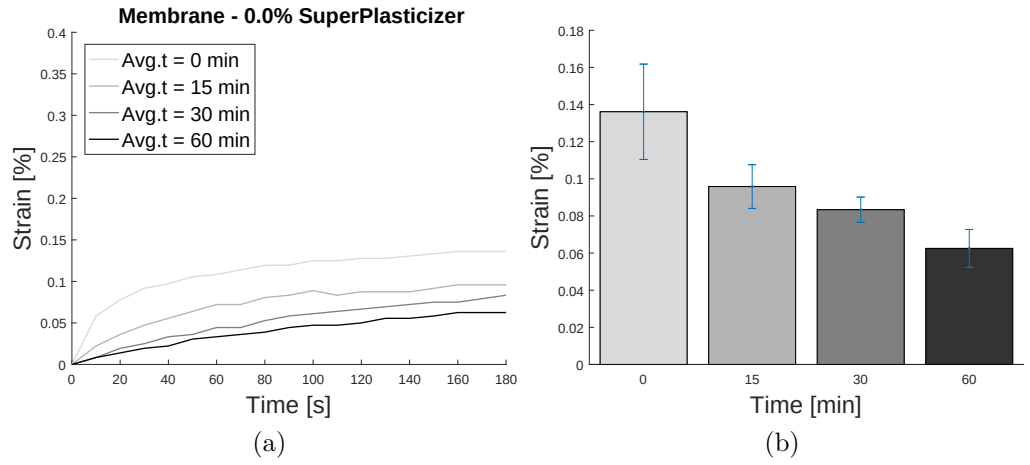

Figure 5.86: Creep tests, 0.0% plasticizer with membrane. Average comparisons at different time - 0 minutes, 15 minutes, 30 minutes, 60 minutes - (a) trend & (b) peaks with standard deviation - SP0.00-SC-DR3.

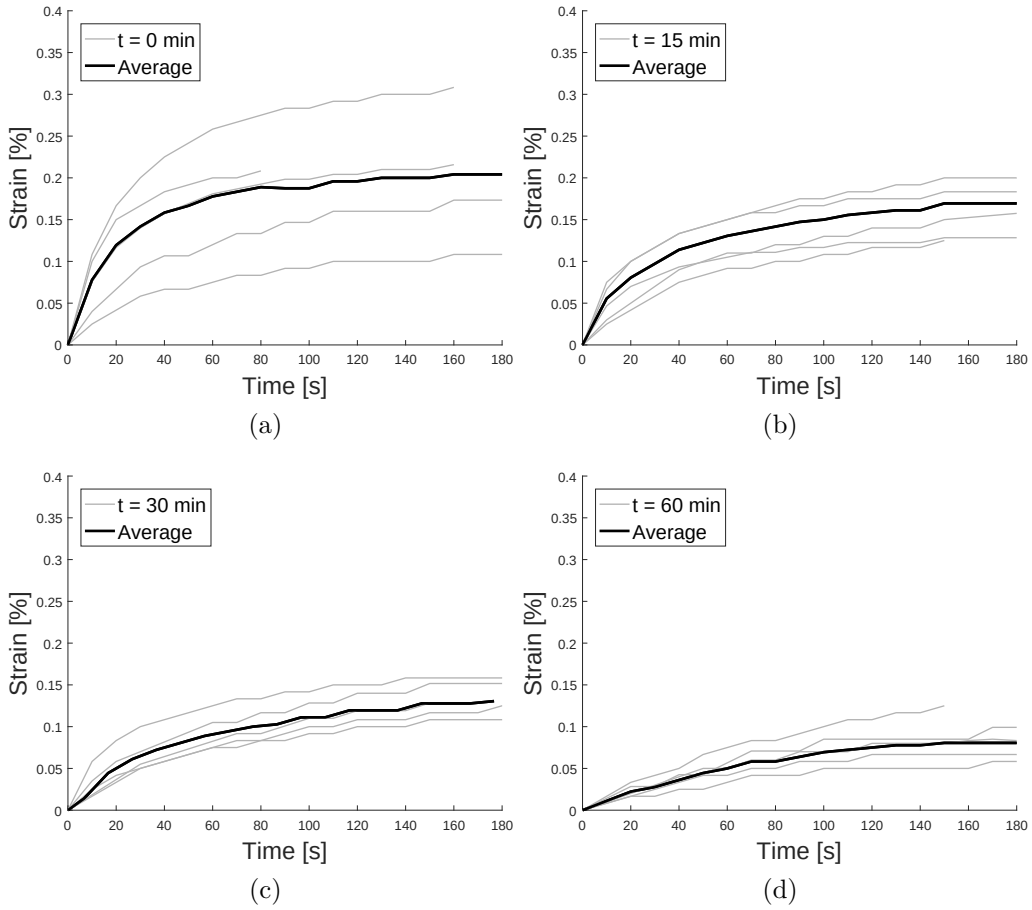

Figure 5.87: Creep tests, 0.1% plasticizer with membrane. Average and individual results at different time - (a) 0 minutes, (b) 15 minutes, (c) 30 minutes, (d) 60 minutes - creep strain.

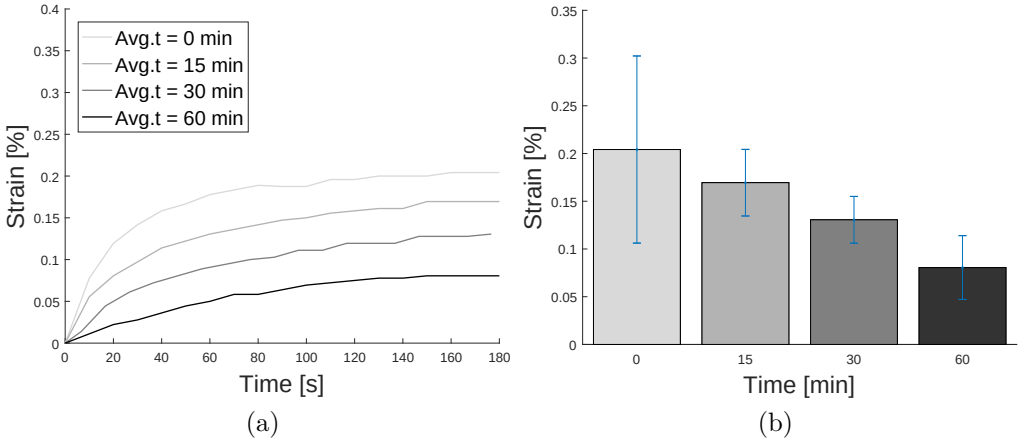

Figure 5.88: Creep tests, 0.1% plasticizer with membrane. Average comparisons at different time - 0 minutes, 15 minutes, 30 minutes, 60 minutes - (a) trend & (b) peaks with standard deviation - SP0.10-SC-DR3.

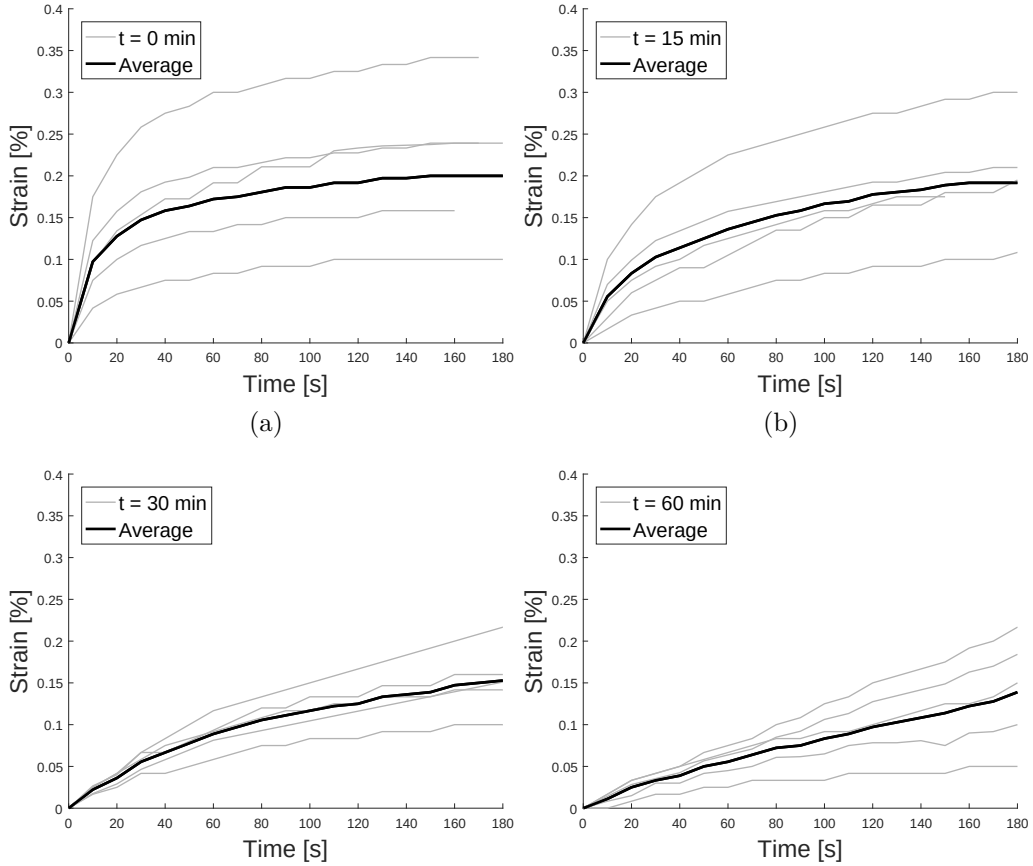

Figure 5.89: Creep tests, 0.15% plasticizer with membrane. Average and individual results at different time - (a) 0 minutes, (b) 15 minutes, (c) 30 minutes, (d) 60 minutes - creep strain.

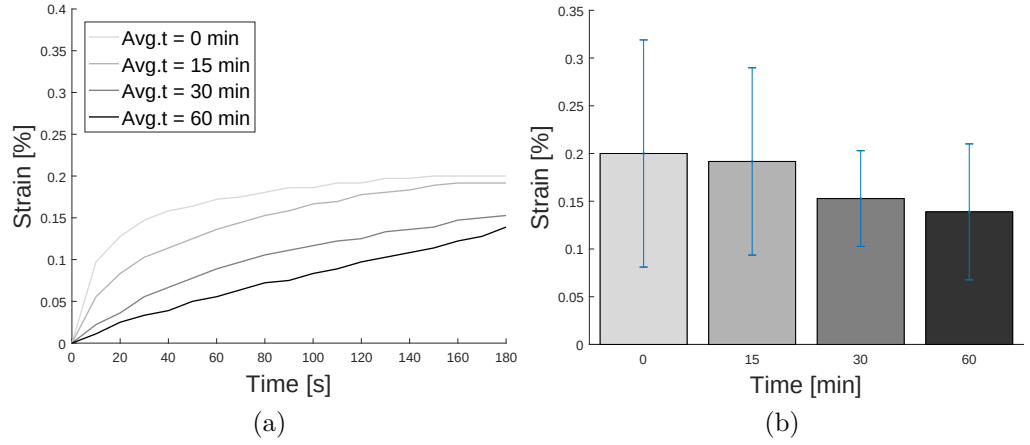

Figure 5.90: Creep tests, 0.15% plasticizer with membrane. Average comparisons at different time - 0 minutes, 15 minutes, 30 minutes, 60 minutes - (a) trend & (b) peaks with standard deviation - SP0.15-SC-DR3.

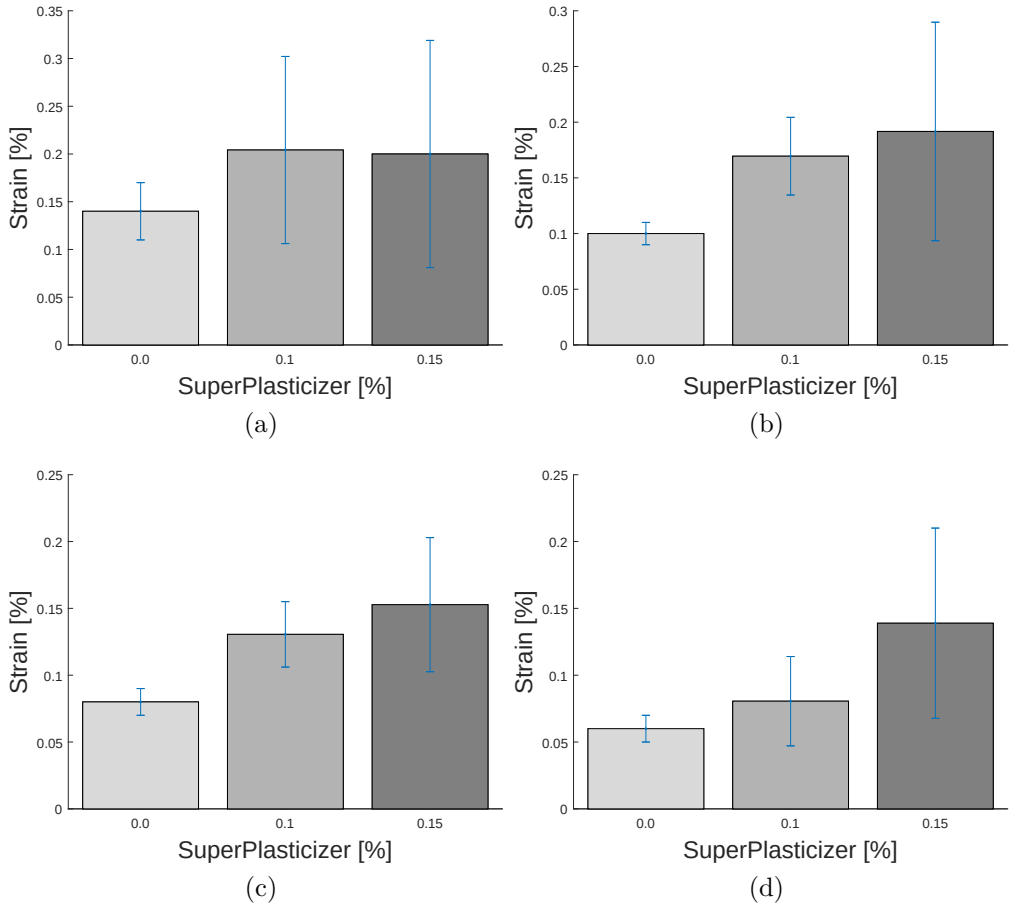

Figure 5.91: Creep tests, 0.00%, 0.1% and 0.15% plasticizer with membrane. Average peak results at different time - (a) 0 minutes, (b) 15 minutes, (c) 30 minutes, (d) 60 minutes.

Each diagram of this set depicts five individual test results (grey) along with their average (black). Afterwards, in the same page, comparison among averages is displayed in order to give insight on the extent of specimen response variation in curing time. Subsequently, average peak values are exhibited with their standard deviation, in order to measure the repeatability of the test. Finally, the correlation between creep strain and superplasticizer amounts is shown in Fig. 5.91, while test results are summarized in Tabs. 5.18-5.20. Analyzing Figs. 5.86, 5.88, 5.90 and Fig. 5.91, it is possible to observe that the creep strain decreases as the concrete harden and increase as the superplasticizer amount increase. As a result, maximum creep values are recorded for time 0 and 0.15% in cement weight of superplasticizer, reaching a peak average of 0.204%. In addition, superplasticizer affects test accuracy, that decreases for higher amounts of additive and roughly increases in curing time (Tab. 5.20). Indeed, SP0.15-SC-D3 is the most inaccurate reaching a maximum of 59.5% as RSD.

As aforementioned, to analyze creep during the buildup process, specimens are subjected to multiple of their self weight, simulating one, two and three upper layer deposition (Fig. 5.92). Accordingly, results are gathered in the following figures (Figs. 5.93-5.96) where two- and three-stage creep strain is highlighted.

	Curing Time			
	0 min peak averages	**15 min peak averages**	**30 min peak averages**	**60 min peak averages**
SP0.00-SC-DR3	0.136 [%]	0.096 [%]	0.083 [%]	0.063 [%]
SP0.10-SC-DR3	0.200 [%]	0.169 [%]	0.131 [%]	0.081 [%]
SP0.15-SC-DR3	0.204 [%]	0.192 [%]	0.153 [%]	0.139 [%]
Tot. number of samples	**15**	**15**	**15**	**15**

Table 5.18: Creep strain at different curing time and superplasticizer amounts.

	Curing Time			
	0 min peak averages	**15 min peak averages**	**30 min peak averages**	**60 min peak averages**
SP0.00-SC-DR3	0.026 [%]	0.012 [%]	0.007 [%]	0.01 [%]
SP0.10-SC-DR3	0.098 [%]	0.034 [%]	0.024 [%]	0.033 [%]
SP0.15-SC-DR3	0.119 [%]	0.098 [%]	0.048 [%]	0.071 [%]
Tot. number of samples	**15**	**15**	**15**	**15**

Table 5.19: Standard deviation at different curing time and superplasticizer amounts.

	Curing Time			
	0 min peak averages	**15 min peak averages**	**30 min peak averages**	**60 min peak averages**
SP0.00-SC-DR3	19.12 [%]	12.50 [%]	8.43 [%]	15.87 [%]
SP0.10-SC-DR3	48.04 [%]	20.12 [%]	18.32 [%]	40.74 [%]
SP0.15-SC-DR3	59.5 [%]	51.04 [%]	31.37 [%]	51.08 [%]
Tot. number of samples	**15**	**15**	**15**	**15**

Table 5.20: Relative standard deviation at different curing time and superplasticizer amounts.

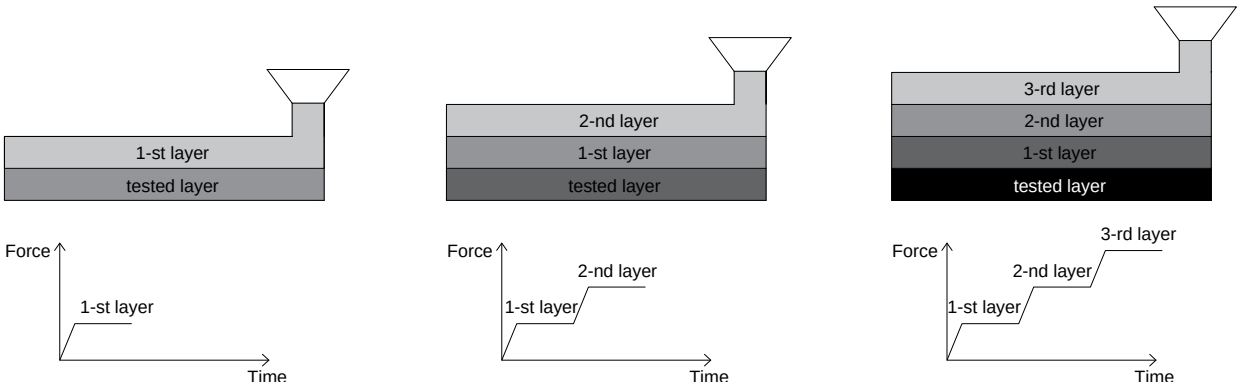

Figure 5.92: Simluation of one-, two- and three-layer stacking.

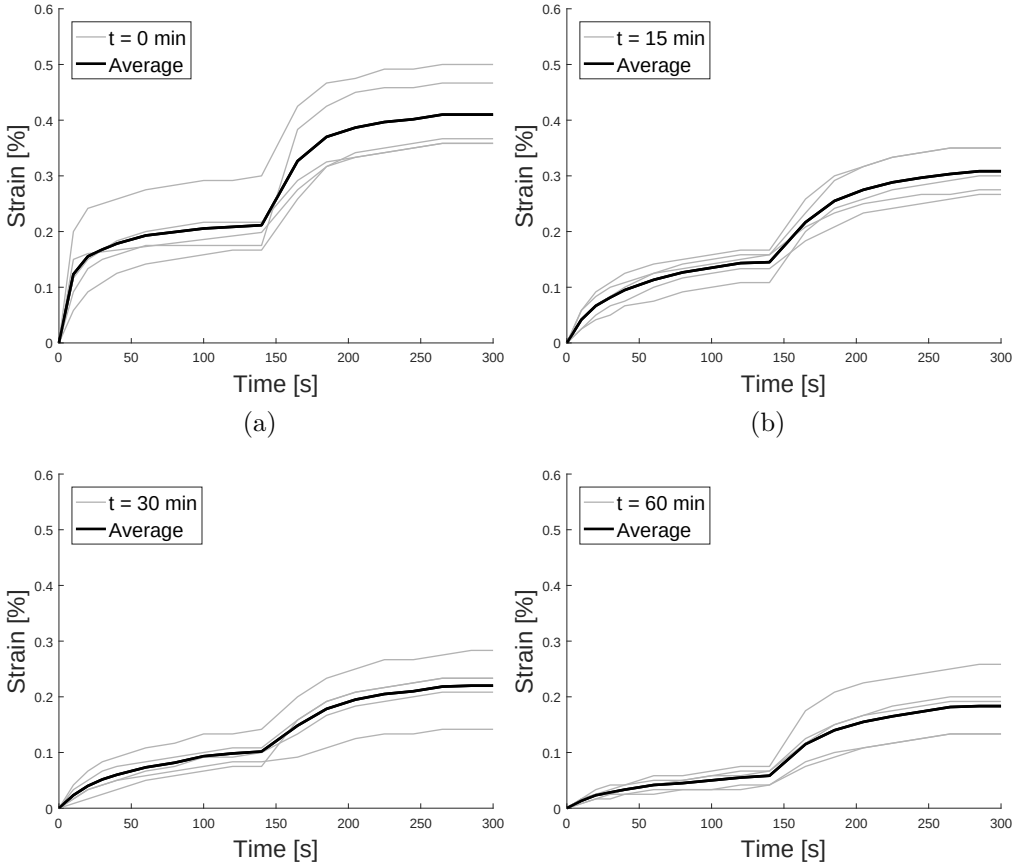

Figure 5.93: Creep tests, 0.1% plasticizer with membrane. Average and individual results at different time - (a) 0 minutes, (b) 15 minutes, (c) 30 minutes, (d) 60 minutes - creep strain.

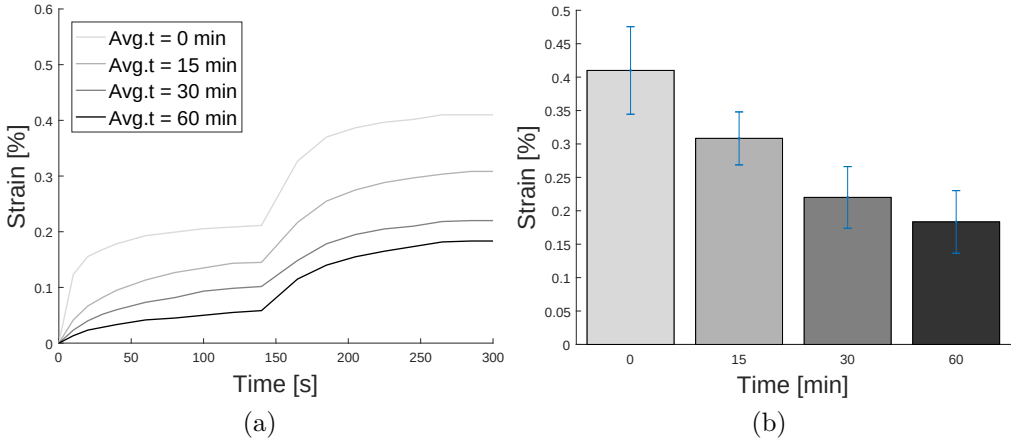

Figure 5.94: Creep tests, 0.1% plasticizer with membrane. Average comparisons at different time - 0 minutes, 15 minutes, 30 minutes, 60 minutes - (a) trend & (b) peaks with standard deviation - SP0.10-SC-DR3, 2 layers.

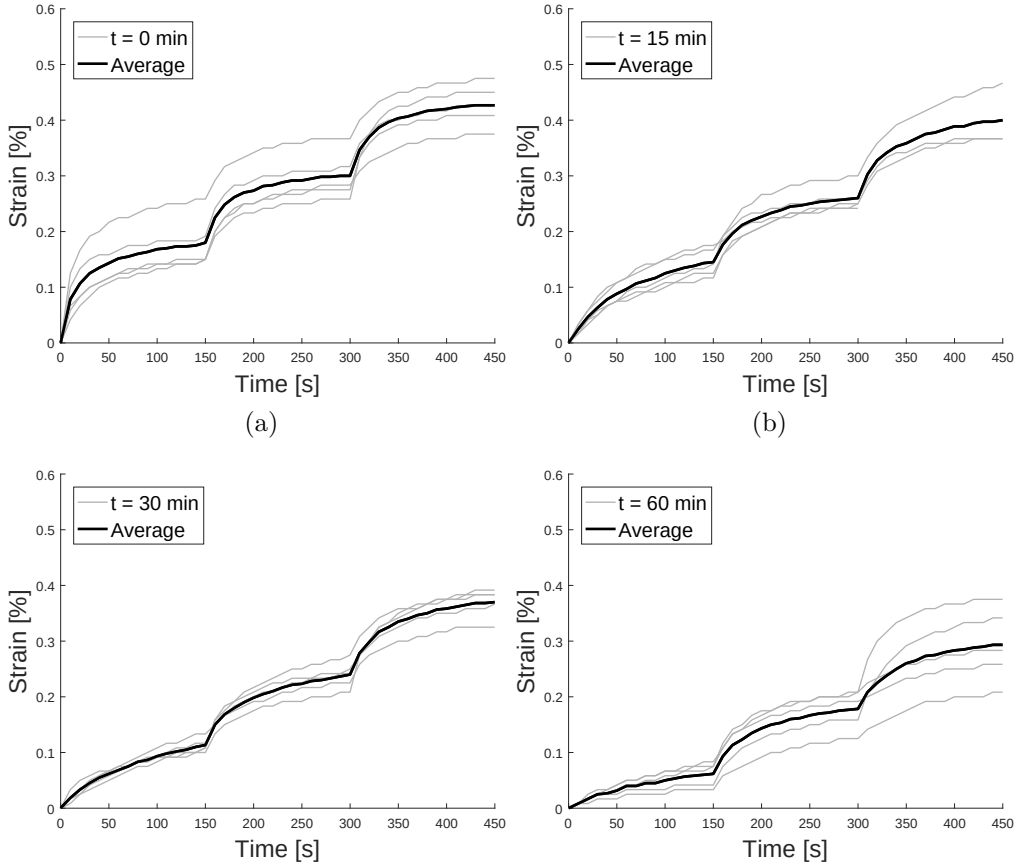

Figure 5.95: Creep tests, 0.1% plasticizer with membrane. Average and individual results at different time - (a) 0 minutes, (b) 15 minutes, (c) 30 minutes, (d) 60 minutes - creep strain.

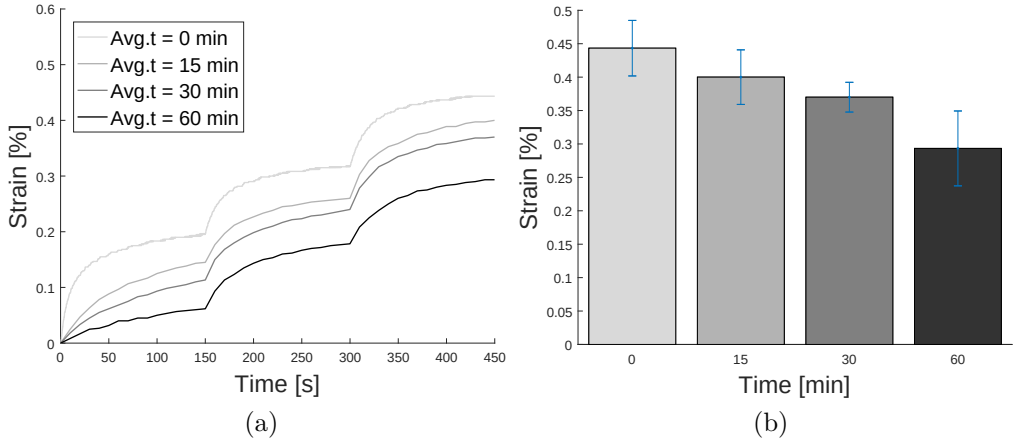

Figure 5.96: Creep tests, 0.1% plasticizer with membrane. Average comparisons at different time - 0 minutes, 15 minutes, 30 minutes, 60 minutes - (a) trend & (b) peaks with standard deviation - SP0.10-SC-DR3, 3 layers.

	Curing Time			
	0 min peak averages	**15 min peak averages**	**30 min peak averages**	**60 min peak averages**
SP0.10-SC-DR3, 2 layers	0.410 [%]	0.308 [%]	0.220 [%]	0.183 [%]
SP0.10-SC-DR3, 3 layers	0.443 [%]	0.400 [%]	0.370 [%]	0.293 [%]
Tot. number of samples	**10**	**10**	**10**	**10**

Table 5.21: Creep strain at different curing time and superplasticizer amounts.

	Curing Time			
	0 min peak averages	**15 min peak averages**	**30 min peak averages**	**60 min peak averages**
SP0.10-SC-DR3, 2 layers	0.065 [%]	0.040 [%]	0.046 [%]	0.047 [%]
SP0.10-SC-DR3, 3 layers	0.042 [%]	0.041 [%]	0.022 [%]	0.056 [%]
Tot. number of samples	**10**	**10**	**10**	**10**

Table 5.22: Standard deviation at different curing time and superplasticizer amounts.

	Curing Time			
	0 min peak averages	**15 min peak averages**	**30 min peak averages**	**60 min peak averages**
SP0.10-SC-DR3, 2 layers	15.97 [%]	12.86 [%]	20.97 [%]	25.52 [%]
SP0.10-SC-DR3, 3 layers	9.37 [%]	10.21 [%]	6.02 [%]	19.10 [%]
Tot. number of samples	**10**	**10**	**10**	**10**

Table 5.23: Relative standard deviation at different curing time and superplasticizer amounts.

	Curing Time			
	0 min peak averages	**15 min peak averages**	**30 min peak averages**	**60 min peak averages**
SP0.10-LC-DR3, total strain	4.19 [%]	2.22 [%]	1.97 [%]	0.80 [%]
SP0.00-SC-DR3, total strain	3.58 [%]	3.11 [%]	2.52 [%]	1.66 [%]
SP0.10-SC-DR3, total strain	4.49 [%]	3.51 [%]	2.74 [%]	2.08 [%]
SP0.15-SC-DR3, total strain	3.96 [%]	2.54 [%]	2.20 [%]	0.96 [%]
SP0.10-SC-DR3, 2 layers, total strain	7.38 [%]	4.59 [%]	4.07 [%]	2.34 [%]
SP0.10-SC-DR3, 3 layers, total strain	8.24 [%]	5.20 [%]	3.27 [%]	2.05 [%]
SP0.10-LC-DR3, ratio	5.00 [%]	8.65 [%]	7.81 [%]	12.57 [%]
SP0.00-SC-DR3, ratio	4.38 [%]	2.68 [%]	3.29 [%]	3.79 [%]
SP0.10-SC-DR3, ratio	4.45 [%]	7.66 [%]	4.79 [%]	3.90 [%]
SP0.15-SC-DR3, ratio	5.15 [%]	7.55 [%]	6.93 [%]	14.55 [%]
SP0.10-SC-DR3, 2 layers, ratio	5.56 [%]	6.71 [%]	5.40 [%]	7.84 [%]
SP0.10-SC-DR3, 3 layers, ratio	4.85 [%]	8.52 [%]	11.32 [%]	14.32 [%]
Tot. number of samples	**30**	**30**	**30**	**30**

Table 5.24: Creep to elastic strain ratios (according to Fig. 5.79).

In Tabs. 5.21-5.23 results are summarized: it is evident that the amount of creep strain rises during the buildup process with the number of layers, up to 0.443% on average and 0.501% as a peak. By means of a logarithmic regression it is possible to fit experimental results, obtaining:

$$C[\%] = 0.23ln(L) + 0.2136 \tag{5.8}$$

where C is the creep strain (in %) at the ground layer and L is the number of stacked layers. Fig. 5.97a depicts such correlation, showing that deformations rise rapidly at first and then slows over the number of layers; Fig. 5.97b associates the number of layers with the strain accumulated on top of the printed element (in terms of % of the layer height).

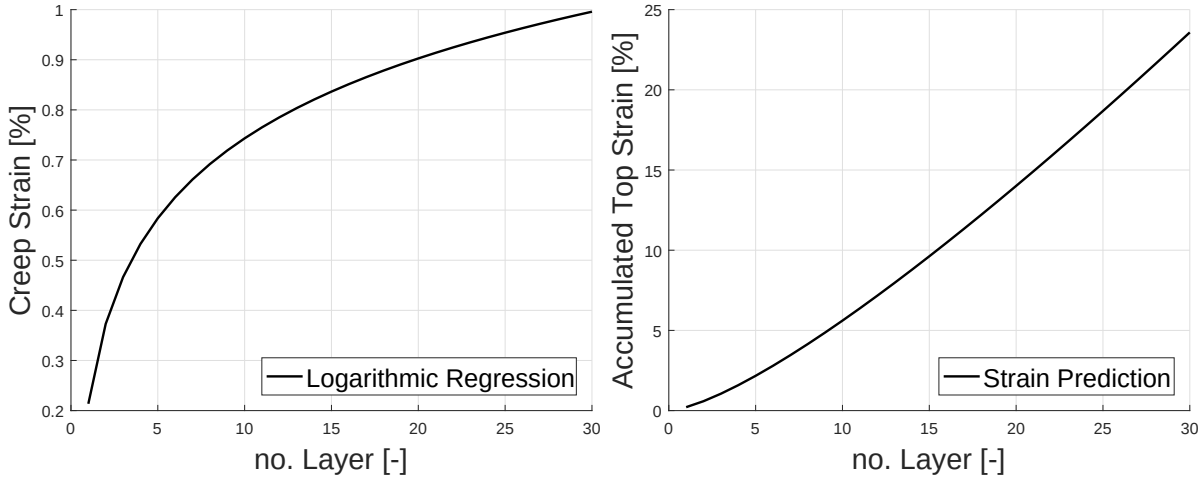

(a) (b)

Figure 5.97: Prediction of creep strain accumulated on top of 3D printed elements.

As a result, even if individual creep strains are small, the top displacement rapidly increases as the number of layer increases, being a potential cause for displacement-based failures.

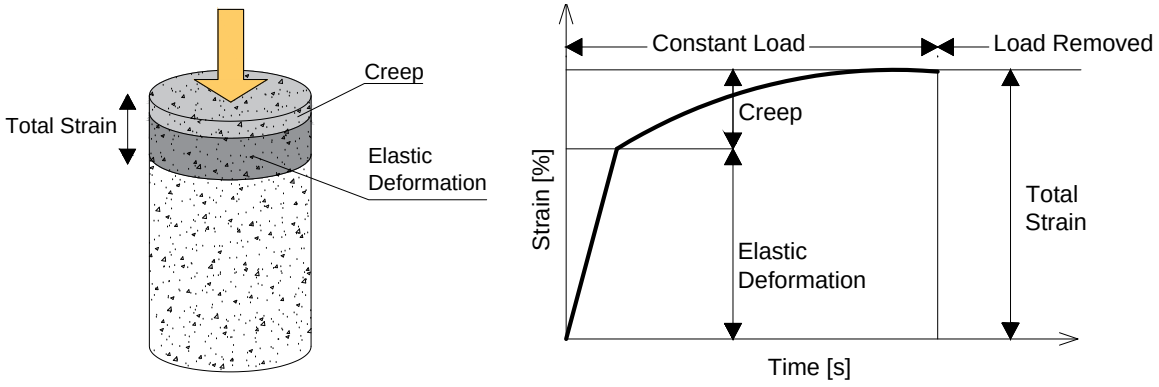

(a) (b)

Figure 5.98: Creep to elastic strain ratio.

The accuracy of the test, expressed by means of relative standard deviation, increases passing from two to three layers (corresponding to decrease in relative standard deviation up to 9.37%, Tab. 5.23).

Additionally, in Tab. 5.24, ratios between the amount of creep and the total strain (Fig. 5.98) are outlined. As expected, the total strain is maximum for three layers, especially at time 0 minutes, i.e., when concrete is in the fresh state. Elastic strain ratios behave with a roughly linear increasing trend, due to the hardening of concrete that imply a transition from the viscous to the elastic phase. Such transition modify the concrete compresive creep response, displaying an accentuated elastic strain.

5.5 Rheological tests

The Anton Paar RheolabQC cylindrical rheometer is used to determine the plastic viscosity and the yield stress, as defined by Bingham [87]. The plastic viscosity is the amount of increased shear stress when the shear rate increases; the static yield stress is defined as the maximum stress required to flow from the rest condition, while the dynamic is defined as the minimum stress required to maintain the flow [88]. Such parameters can not be directly measured by the rheometer, but only calculated from the Bingham model for non-Newtonian materials [87]. This kind of rheometer contains a probe in the form of a spindle (diameter 12 mm) that measures the torque: at the beginning, when the early age concrete is in rest state, higher torque is required for the spindle to start the rotation, and this value is considered the static torque [53]. Therefore, by imposing the shear rate and measuring the torque, it is possible to extrapolate both the yield stress and the plastic viscosity, as expressed in the adopted rheological protocol in Fig. 5.100. The reference mix and the specimen preparation are provided in Section 5.3.2. Multiple fresh concrete curing ages are considered, t = 0, 15, 30 and 60 min, while two amounts of superplasticizer are selected (0.1, 0.15%). After the preparation, specimens are left undisturbed before the test in order to onset the cement hydration. Once the sample is loaded in the container, flow curves are achieved for increasing shear rates (maximum 30 1/s) up to 180 seconds of constant rotation.

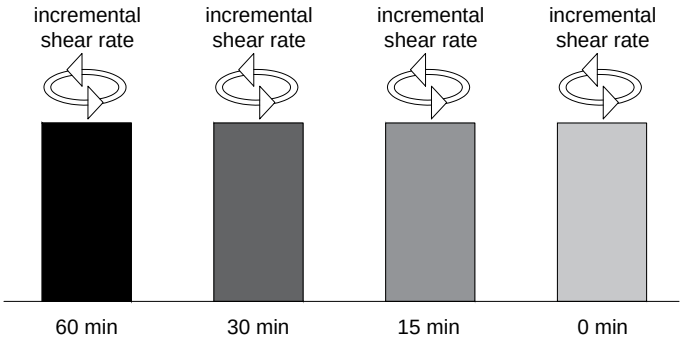

Figure 5.99: Schematic of early age sample set with different curing time.

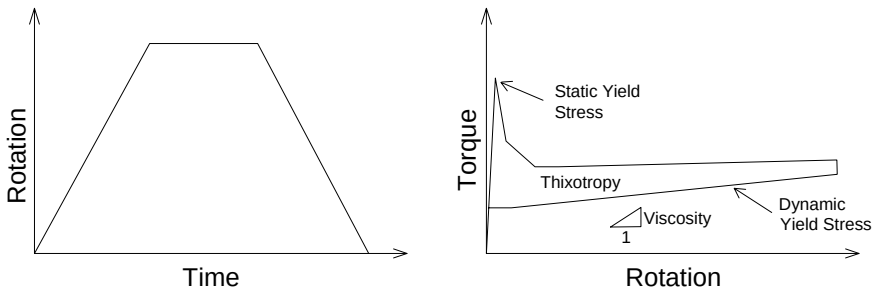

Figure 5.100: Rheological tests: flow curve protocol.

5.5.1 Results and Discussions

Rheological properties of cement pastes are difficult to measure with traditional rheometric procedures [88]. On one hand, challenges can be experienced when granular pastes show high solid fraction and low shear rates, since subjected to a frictional flow regime. On the other hand, particle segregation can be encountered for high shear rates and fluid pastes (for instance, by means of superplasticizer). Moreover, the compound behaves like a shear thinning material, i.e., the apparent viscosity usually drops increasing the shear rate (with consequences during the pumping process). As a result, we evaluate the possibility to consider early age concrete as a fluid, employing simple protocols to quantify the shear strength of the mix: initially, the shear stress and the plastic viscosity are determined by means of rotational spindle rheometers. Subsequently, from the flow curve it is possible to deduce both the static and the dynamic shear stress. Indeed, for thixotropic materials there is an initial (static) and an equilibrium (dynamic) state for each shear rate (Fig. 5.101); if no equilibrium is achieved, the plastic stress can be under- or over-estimated. Results are organized as follows: initially, each page contains a set of four curves that represent the time-dependent response (in terms of shear stress and viscosity) at early age curing time, i.e., for t = 0, 15, 30 and 60 minutes. Each curve of this set shows four individual test results achieved at four different shear rates (maximum 30 1/s). Subsequently, in the same page, comparison among averages is displayed.

Please consider that peak averages expressed in Figs. 5.103,5.105,5.107 and 5.109 refer to the equilibrium state; since we are treating the mixture as a fluid, we do not evaluate concrete without superplasticizer. Diagrams in Figs. 5.102 and 5.106 depict shear stress values: initially, a peak is needed to onset the flow (yield stress); consequently, the peak decreases stabilizing. Yield stress evolves in curing time, showing the lowest amounts for fresh mixes and the highest values at 60 minutes. Such values reside in the range of 0.12-1.05 kPa for 0.1% in cement weight of superplasticizer and 0.02-1.10 kPa for 0.15%. According to experimental findings [32], 0.3–0.9 KPa is the yield stress range that may prevent obstructions during pumping/extrusion. As a result, even if the selected compound is a suitable mix, particular care has to be payed extruding the material after 30 minutes.

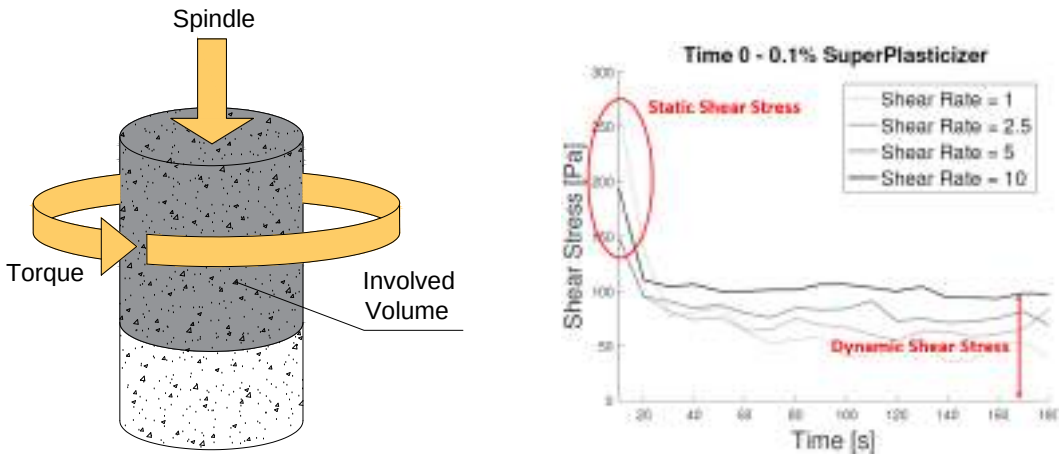

(a) (b)

Figure 5.101: Sketch of rheological test along with hints for result interpretation.

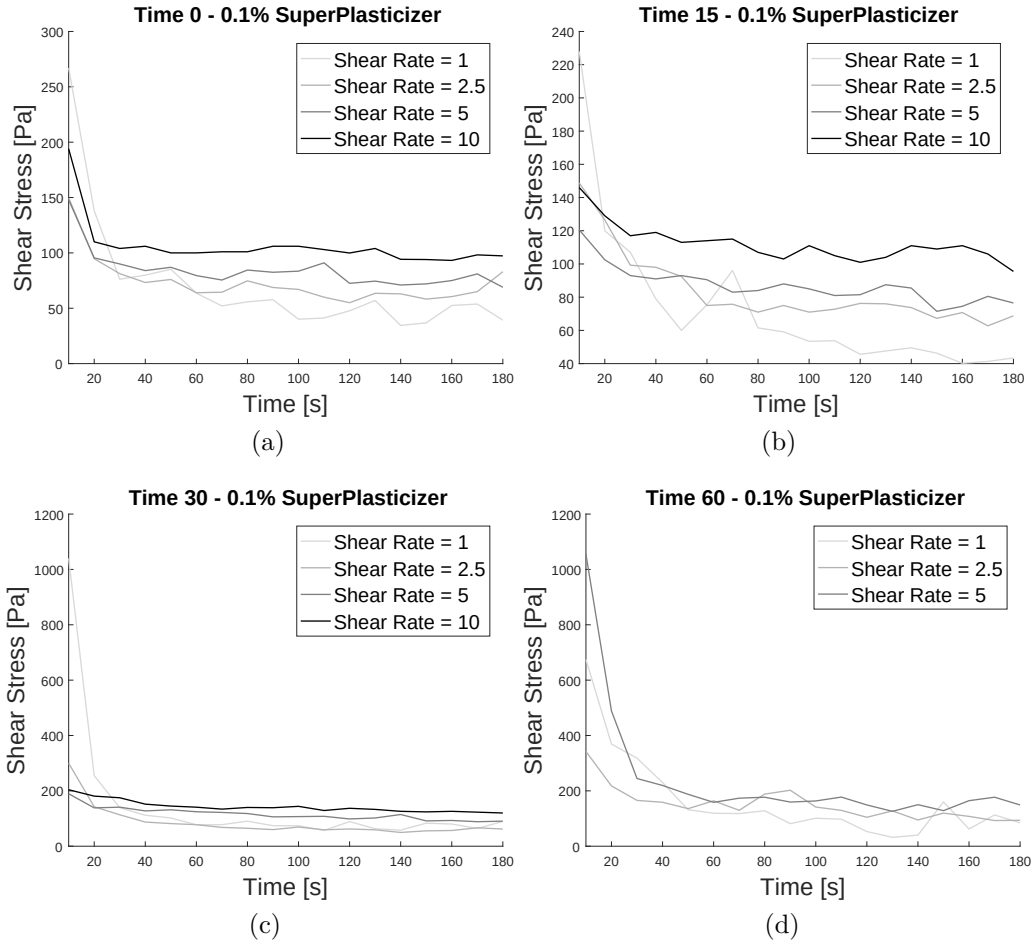

Figure 5.102: Rheological tests, individual results - 0.1% plasticizer, (a) 0 minutes, (b) 15 minutes, (c) 30 minutes, (d) 60 minutes.

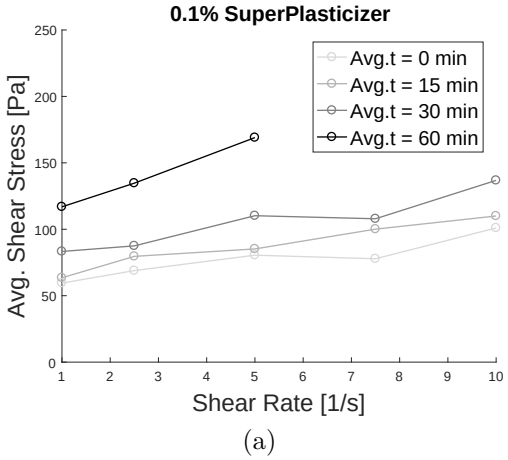

Figure 5.103: Rheological tests, average results - 0.1% plasticizer, (a) 0 minutes, (b) 15 minutes, (c) 30 minutes, (d) 60 minutes.

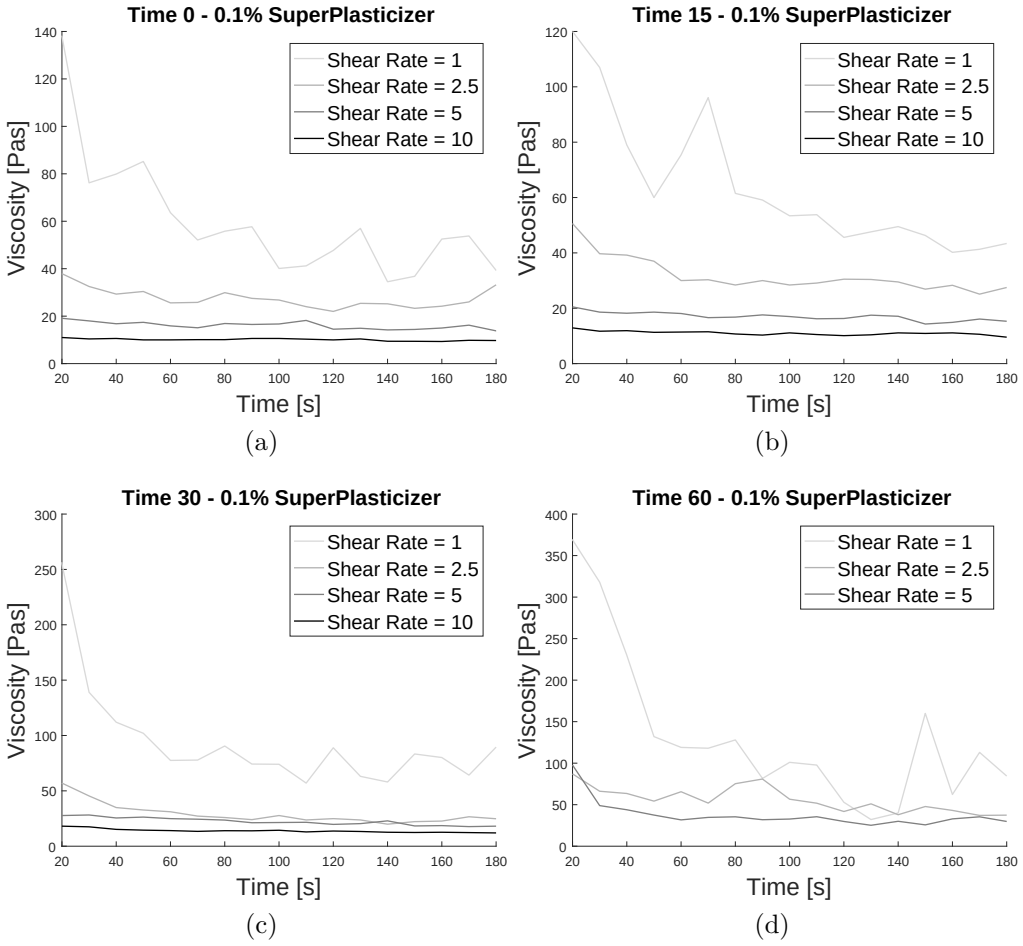

Figure 5.104: Rheological tests, individual results - 0.1% plasticizer, (a) 0 minutes, (b) 15 minutes, (c) 30 minutes, (d) 60 minutes.

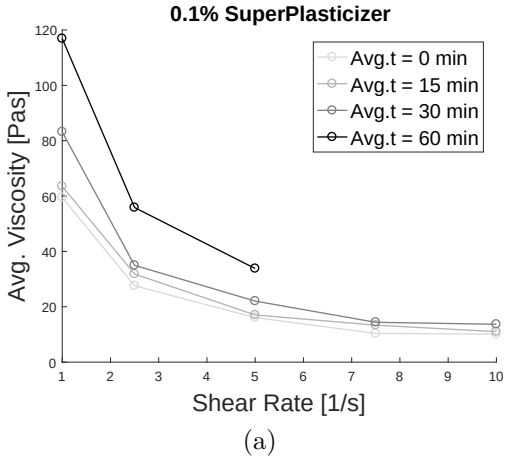

Figure 5.105: Rheological tests, average results - 0.1% plasticizer, (a) 0 minutes, (b) 15 minutes, (c) 30 minutes, (d) 60 minutes.

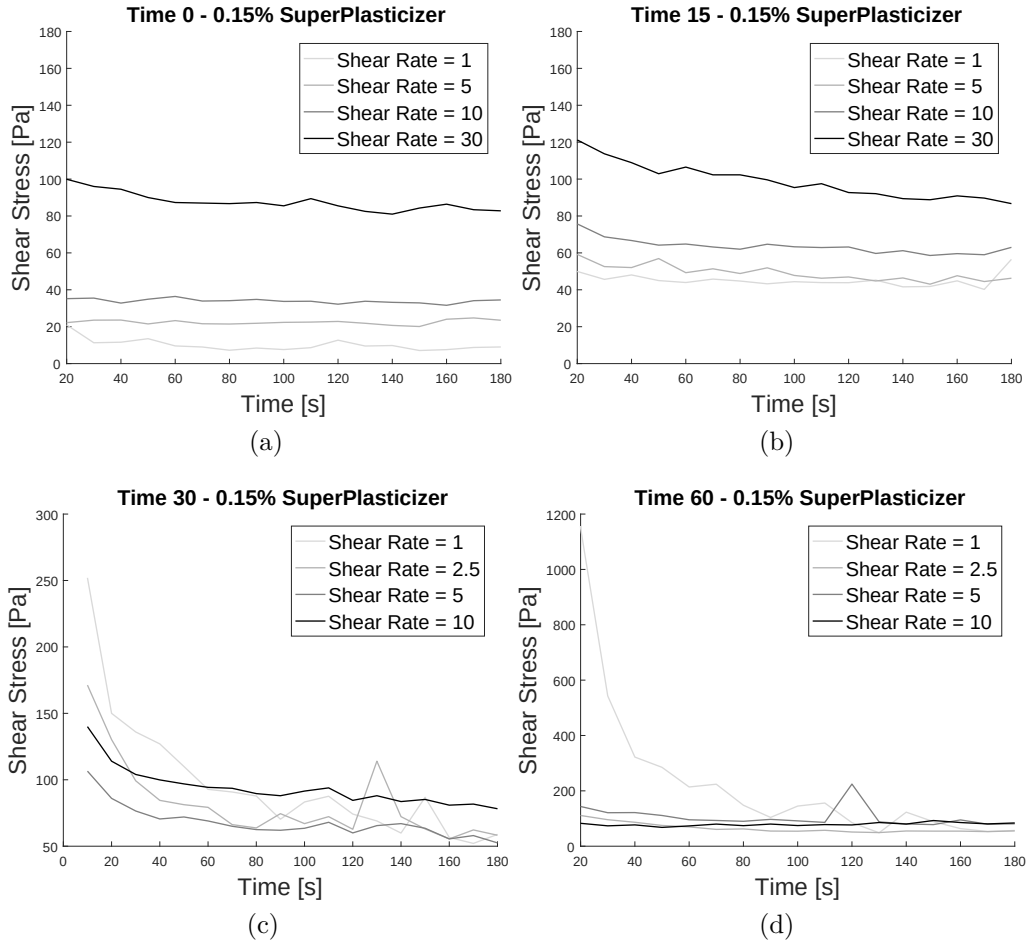

Figure 5.106: Rheological tests, individual results - 0.15% plasticizer, (a) 0 minutes, (b) 15 minutes, (c) 30 minutes, (d) 60 minutes.

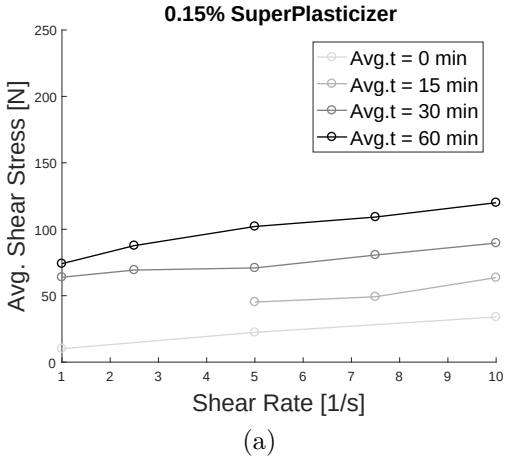

Figure 5.107: Rheological tests, average results - 0.15% plasticizer, (a) 0 minutes, (b) 15 minutes, (c) 30 minutes, (d) 60 minutes.

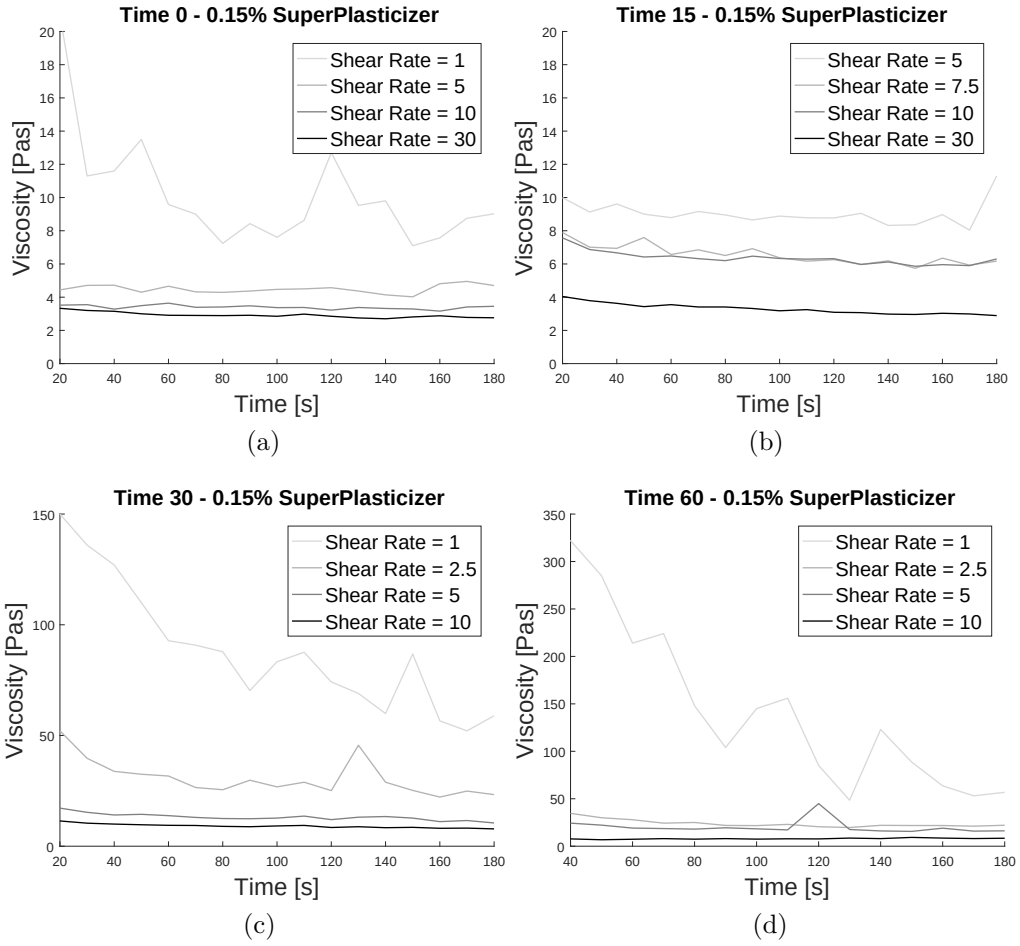

Figure 5.108: Rheological tests, individual results - 0.15% plasticizer, (a) 0 minutes, (b) 15 minutes, (c) 30 minutes, (d) 60 minutes.

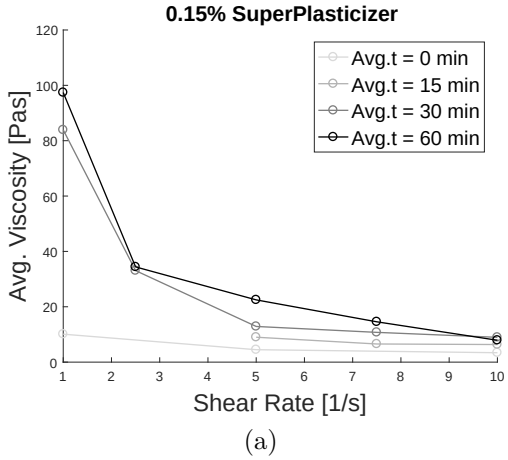

Figure 5.109: Rheological tests, average results - 0.15% plasticizer, (a) 0 minutes, (b) 15 minutes, (c) 30 minutes, (d) 60 minutes.

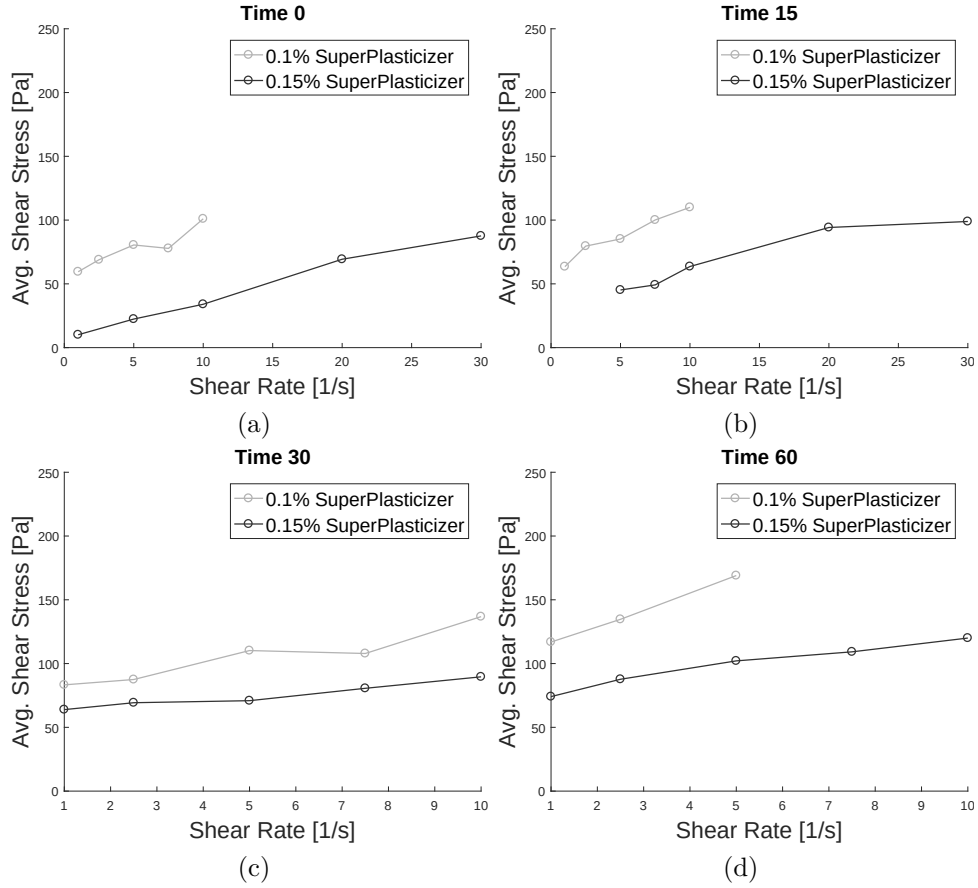

Figure 5.110: Rheological tests, comparisons - 0.1% plasticizer, (a) 0 minutes, (b) 15 minutes, (c) 30 minutes, (d) 60 minutes.

By contrast, Thrane et al. [64] found that to efficiently pump/extrude the mix, the appropriate plastic viscosity resides in the range of 21.1-38.8 Pas: as a result, only the mix with 0.15% of superplasticizer at t = 0 min can be easily pumped.

Comparing Figs. 5.103 and 5.107 it is possible to observe that shear strength is higher in samples with 0.1% of superplasticizer, reaching, in the dynamic state, 170 Pa. Coherently, the lowest value of shear strength is reached for fresh samples (0 minutes) with 0.15% of superplaasticizer, approximately 10 Pa, value that limits the buildability capacity. Once again, 0.1% of superplasticizer is selected as the most suitable mix.

It is also worth noting that the chosen compound can be represented by a Bingham and a shear thinning material (Fig. 5.112). Bingham fluids are viscoplastic materials that reacts as an elastic solid at low stress but flows as a viscous fluid at high stress. Shear thinning materials show reduction in apparent viscosity with increasing the shear rate.

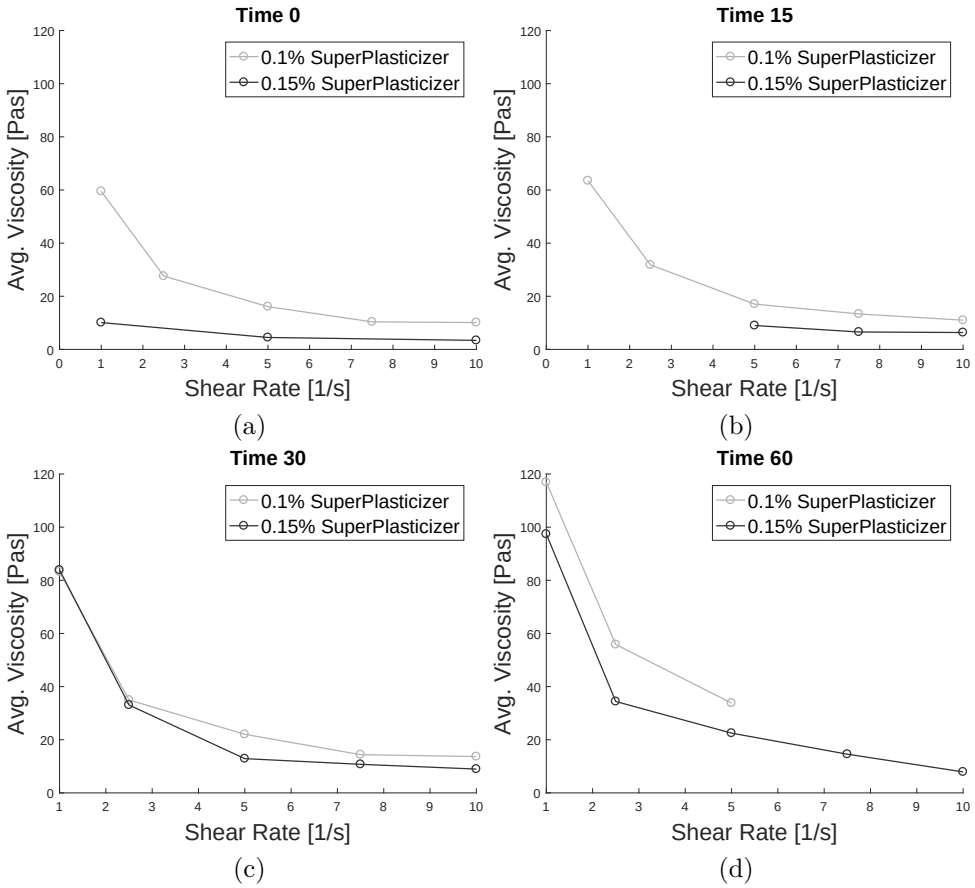

Figure 5.111: Rheological tests, comparisons - 0.1% plasticizer, (a) 0 minutes, (b) 15 minutes, (c) 30 minutes, (d) 60 minutes.

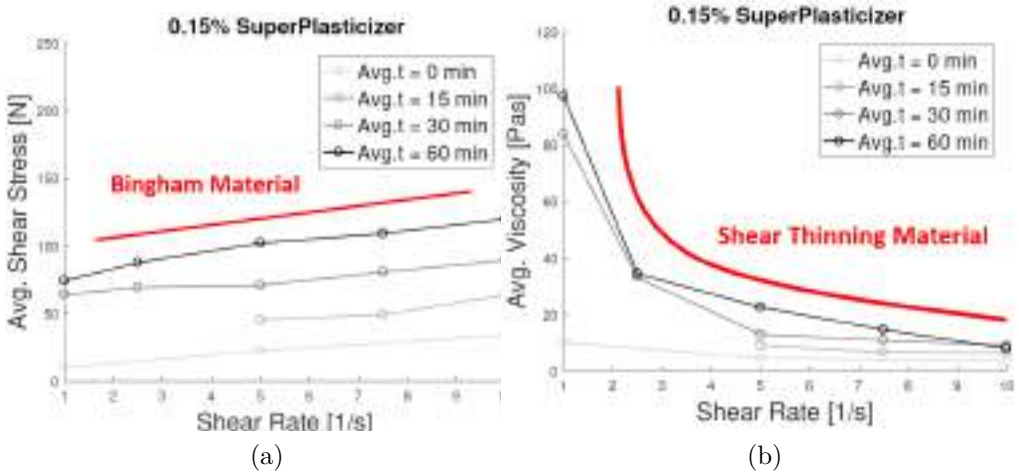

Figure 5.112: Hints for result interpretation: Bingham and shear thinning materials.

Part III

Future developments: Circular Economy for a sustainable environment.

Chapter 6

Conclusions and future perspectives

6.1 Conclusions

The central objective of the work was to present and discuss a standardized characterisation procedure for 3D-printable concrete mixes. Such characterization investigated the early-age response of 3D-printable mortars: in particular, considering that material properties evolve during the printing process, we focused on the time-dependent compressive, creep and rheological response, as well as on the efficiency of testing procedures that may affect the buildability.

Initially, we summarized chronological steps in digital fabrication with concrete, along with potentials and challenges of 3D concrete printing. Subsequently, we provided the composition of a 3D-printable concrete mix: on such mix we set up and performed an experimental campaign composed by unconfined uniaxial compression tests, unconfined uniaxial creep tests and rheological tests, by varying: (i) the concrete age, (ii) the material and sample preparation, and (iii) the adopted displacement rate. Finally, by means of such experimental results, we employed an analytical failure criterion to foresee either the strength or the self-buckling failure of the 3D printed component, focusing on the effect of particular testing procedure on the prediction of the structural performance. Tests highlighted that:

- the early age mechanical response is influenced by the concrete resting time; as the concrete age evolves, passing from the fresh to the hardened state, there is a transition from plastic to brittle behavior along with a compressive strength (from 8.32 to 21.69 kPa), stiffness (from 210 to 607 kPa), plastic viscosity (from 120 to 360 Pas) and static shear strength (from 0.27 to 1.07 kPa) enhancement. Even creep is affected by the concrete age, showing a reduction (from 0.21 to 0.10 %) as the mix matures. This behaviour is also experienced by modifying testing procedures;
- both increasing and decreasing the amount of superplasticizer (to simulate changes in material preparation) results vary, emerging in lowered strength, stiffness, viscosity and experimental precision (the relative standard deviation reached a peak of 44.86%). Creep grows increasing the SP and reduces decreasing the SP. This phenomena underlines the need to precisely reproduce the physical composition of the printing mix;
- the use of the membrane was considered to evaluate variations in sample preparation: results shows that without the membrane there is a decrease in strength (from 5.81 to 3.54 kPa) and stiffness (from 124 to 68 kPa), giving rise at the most inaccurate results

(the relative standard deviation reached a peak of 49.06%);
- the displacement rate influences the stress-strain response: when the rate rises it is possible to observe a significant increment in compressive strength (up to 33.25 kPa), despite a reduction in accuracy (the relative standard deviation reached 39.73%);
- the amount of creep strain rises during the buildup process; two- and three-stage simulations accumulate creep deformations with a logarithmic trend, up to 0.443% on average and 0.501% as a peak;

As supported by laboratory test results, we can conclude that the proposed experimental methodology is suitable for evaluating the properties of early age printed concrete; however, tests demonstrate that the reliability of the methodology strictly depends on the variability of the testing procedures. Indeed, achieved results clearly highlight the need to prescribe standardized procedures for the mechanical characterization of the material, in order to have greater confidence in analytical/predictive models (the failure prediction fluctuation is in the range of 30-40%). Some recommendations may be employed to enhance the reliability of the testing protocol: (i) the external membrane increases the repeatability of the test, (ii) 0.1% represents the optimal superplasticizer amount, (iii) a lower displacement rate increases the test accuracy. Such recommendations also permit a more reliable failure prediction.

6.2 Vision for future work

Computer-aided design and 3D printed fabrication of articulated multiscale structures is one of the most complex tasks of modern civil engineering [37]. Properly capturing the material response opens up new perspectives of importance for the applications of interest in 3D concrete printing, i.e., addressing those challenges which cannot be addressed with conventional casting. Accordingly, our vision is a concrete panel, optimized in terms of energy and mechanical properties, and generated by means of a suitable 3D printing process (based on ad hoc automated technologies) designed in conjunction with waste-based concrete materials, aiming to support affordable and sustainable nearly zero-emission residential housing solutions.

As a matter of fact, the prevailing limitation is in the choice and in the characterization of materials. However, given what illustrated in the previous sections of this work, the experimental plan may be represented by a multi-disciplinary approach, involving several methodologies and scientific fields, in order to: (i) develop proper mixtures, made of recycled materials, characterizing the final product by high added value; (ii) capture material responses of importance for the applications of interest, along with the development of robust and effective simulation techniques for proposed constitutive models; (iii) address current challenges in concrete additive manufacturing technologies, validate the employment of proposed concrete mixtures in printing processes and prove the methodological accuracy under effective conditions.

The proposed approach will generate a massive potential impact on industry and linear economy, specifically based on a triple thematic: **Resource Recycling**, **Waste Reduction** and **Production Reuse**; in this view, AM equipment may become a tool for tackling pollution and housing emissions. In the following, the approach is illustrated by means of its scientific context.

6.2.1 Scientific background and rationale

After water, concrete is the second most employed material worldwide [89], primarily used in the construction industry. Ordinary Portland Cement is the traditional binder, composed mainly by calcium silicate minerals: a fine powder is obtained from raw materials, before entering in a preheater and reaching 1400^oC [90]. Even if CO_2 emission-reduction technologies and their application in the market can be a turning point in the cement manufacturing industry, as one of the mid- and long-term climate change mitigation strategies, the demand for Portland cement is dangerously increasing (Fig 6.2).

Although growing worldwide environmental concerns have led to face this problem, the emission rate increases unmitigatedly, mainly due to the economic expansion of developing countries (such as Latin America, Africa, the Middle East, India and Asia) and since low-carbon technologies have not been commercialized yet [91].

On the contrary, manufactured materials are defined "green" or "sustainable" when the use of natural resources is more efficient, reducing energy and waste production, i.e., cutting their global impact on the environment [92]. As a result, given the compelling need to pollution control, the idea is to design and develop a circular-resource regeneration system, focused on the production of waste-based concrete, dealing with the agricultural and industrial residue footprint, through the following aforementioned aims:

(a) Transform waste products in alternatives for Ordinary Portland Cement;
(b) Substitute quarry virgin aggregates with high added value recycled ones, derived from constructions, demolitions and finishing materials;
(c) Reduce the construction waste, designing and developing ad hoc AM concrete processes based on the concept of disassemblability and modularity. Concrete fracture is mitigated with recycled fibers and additives reinforcement;
(d) Develop a sustainable organization model to face housing emissions, by employing concrete panels optimized towards the energy sustainability of housing in Lombardy.

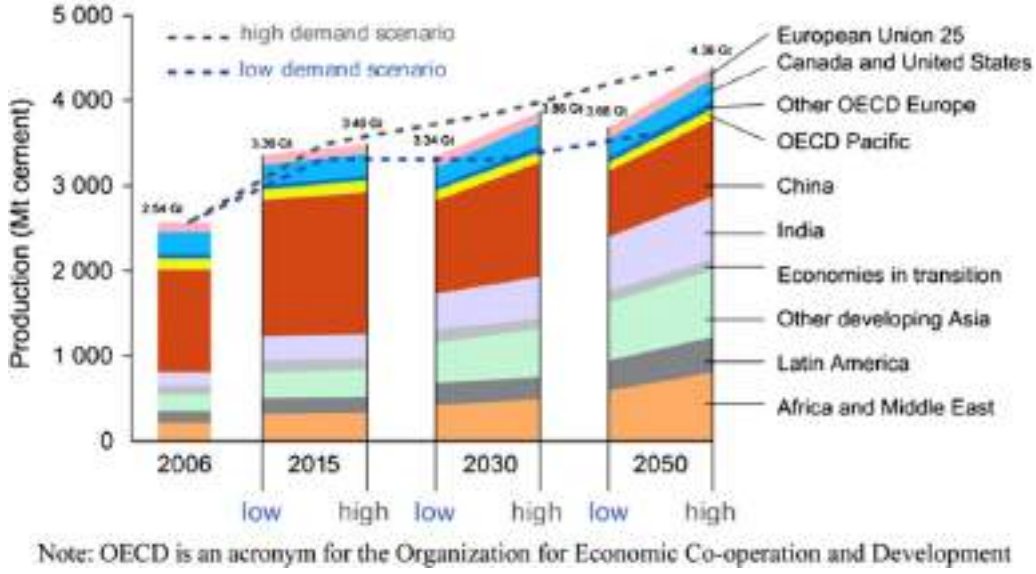

Figure 6.1: Annual world cement production, after [91].

6.2.1.1 OPC Alternatives

Various methods have been developed to shorten the use of OPC in cement industry, although the appropriateness of such methods is still under investigation. Some solid waste materials are rich in silica and alumina, showing cementitious properties [93]; however, the study of their mechanics, production and implementation is still at an early stage [61].

Resources from Agriculture

- **Rice husk ash (RHA)**: highly siliceous (90-95% SiO_2) compared to OPC (21% of SiO_2). RHA improves workability, strength, durability and prevents cracking [94]. Superior compressive features are obtained at 28 days [95]. RHA concrete is still at laboratory stage.
- **Saw dust ash (SDA)**: generated as a by-product of burning wood waste. The compressive strength of concrete increases replacing 20% of wood ash at 60 days [96]. SDA can be used as a partial replacement material to produce structural grade concrete [97].
- **Palm oil fuel ash (POFA)**: obtained by burning palm oil residue to generate electricity. Since POFA contains 21-22% of SiO_2, it can be used as an auxiliary cementitious material [98]: 20% substitution of POFA produces the highest strength in structural lightweight concrete [99].

Resources from Industries

- **Fly ash**: concrete exhibited improvements on compressive strength due to pozzolanic reaction [100]. Different OPC replacement levels of fly ash are tested, showing that 36%–43% of carbon footprint can be bypassed replacing 40% OPC with fly ash [101].
- **Ground-granulated blast-furnace slag (GGBFS)**: produced in blast furnaces, it can be used as a partial replacement of cement (up to 40%) [61], giving higher compressive and flexural strength [102], due to the high composition in silicates and aluminates.
- **Silica fumes**: derived from silicon metal and ferrosilicon alloy production. Due to the ultra-fine powder and to 85-90% silica content [103], they contribute to additional strength, reacting with the calcium hydroxide of OPC [104].

Geopolymer cement

A geopolymer cement is an inorganic polymer formed by polymerization of a source containing silica and alumina dissolved in alkaline medium. Geopolymers (GP) are attractive materials because their impact, measured as carbon dioxide equivalents, is reduced with respect to OPC. The starting materials are produced at lower temperatures compared to OPC. The main contribution to carbon dioxide production of GP is the preparation of sodium silicate [105], but this could be reduced in the future if the demand for this material increases. Furthermore, geopolymers could be produced from different starting materials, including wastes, and they are more fire-resistant compared to OPC [106]. The first step of their production is the reaction of an aluminosilicate source with an alkaline medium (sodium or potassium hydroxide and/or sodium silicate). The dissolution of the material give rise to an activated silica/alumina mixture. When the water evaporates, the mixture goes from the solution to the gel state and finally to the solid state, due to irreversible condensation reactions. Starting materials for the preparation of GP can be represented in the ternary diagram below:

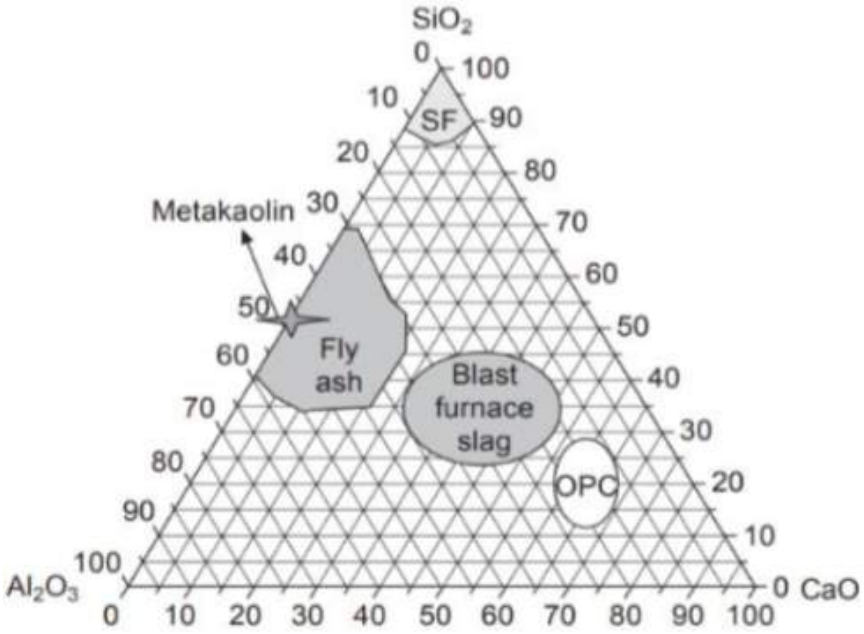

Figure 6.2: Range of raw materials composition used for the production of GP [107].

(SF stands for silica fume). As it is visible, OPC can be reused as a starting material for the production of GP. Geopolymers can be classified according also to their CaO content. As a matter of fact, the calcium content results in the improvement of an early strength by the extra precipitation of calcium compounds and also provides a latent heat during the setting reaction. As an example, a list of materials tested as GP are shown in the table below:

Materials	SiO_2	Al_2O_3	Fe_2O_3	CaO	MgO	Na_2O	K_2O	SO_3	FeO	Si/Al	% Si+Al	References
Low calcium Fly ash	50.0	28.2	13.50	1.79	0.89	0.32	0.46	0.38	-	1.77	78.25	(Nath & Sarker, 2012)
High calcium Fly ash	39.7	20.0	14.10	17.30	1.40	1.40	2.70	2.60	-	1.99	59.70	(Rattanasak, et al., 2011)
GBFS	32.5	14.3	0.61	43.10	3.94	0.24	0.33	4.58	-	2.27	46.76	(Nath & Sarker, 2012)
Silica Fume	92.0	0.46	1.60	0.29	0.28	0.51	0.61	0.19	-	200	92.46	(Dutta, et al., 2010)
Steel Slag	15.0	6.70	15.40	44.20	10.9	0.20	0.10	0.70	-	2.24	21.70	(Hu, et al., 2008)
Ferronickel Slag	32.7	8.32	0.76	-	2.76	-	-	-	38	3.94	41.06	(Komnitsas & Zaharaki, 2007)
Tungsten mine waste	53.5	16.7	12.33	-	1.27	0.67	7.65	-	-	3.21	70.14	(Pacheco-Torgal, et al., 2007)
Cement Kiln Dust	11.0	3.90	2.00	42.00	3.60	-	0.60	-	-	2.82	14.90	(Khater, 2012)
Waste paper sludge ash	26.2	17.50	4.40	23.40	0.90	0.10	0.20	4.63	-	1.50	43.75	(Anuar, et al., 2011)
Water Sludge	70.4	15.40	5.30	1.53	0.96	0.90	3.66	0.31	-	4.57	85.80	(Kongkaew, 2007)
Demolished Wall	76.4	1.88	1.28	9.84	0.26	0.22	0.08	2.09	-	40.65	78.30	(Khater, 2011)
Waste Concrete	71.5	2.14	2.43	12.76	0.39	1.04	1.13	0.33	-	33.43	73.67	(Khater, 2011)
Metakaolin	54.8	40.4	0.76	0.10	0.41	0.07	2.72	-	-	1.36	95.20	(Yip, et al., 2005)
Kaolin	48.1	36.9	0.26	0.20	0.17	0.20	1.90	-	-	1.30	85.00	(Hounsi, et al., 2013)
Rice husk ash (RHA)	86.1	0.17	2.87	1.03	0.84	-	4.65	0.41	-	506	86.27	(Nuruddin, et al., 2013b)
Silty Clay	20.1	7.55	32.89	26.15	0.47	-	3.17	4.92	-	2.66	27.65	(Sukmak, et al., 2013)
Diatomite	59.3	10.0	18.50	1.20	-	-	-	2.74	-	5.93	69.30	(Phoo-ngernkham & Sinsiri, 2013)
Volcanic Mud	38.5	14.2	23.76	5.62	-	-	4.31	0.78	-	2.71	52.70	(Al Bakri, et al., 2012)

Figure 6.3: Examples of GP composition, adapted from [108].

The compressive strength of the materials could be equal or superior of OPC:

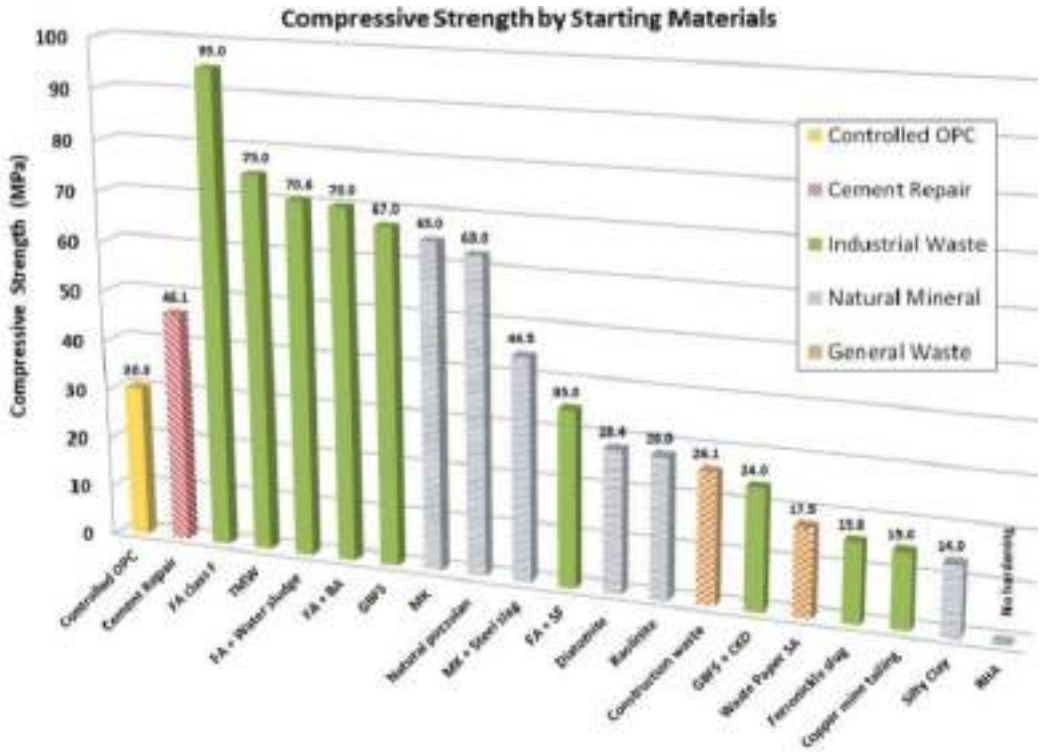

Figure 6.4: Compressive strength in function of starting materials [108].

6.2.1.2 Quarry Aggregate Alternatives

There is an increasing interest in recycled and industrial by-product aggregates: as a result, the American Concrete Institute (ACI) [109], the Department of the Environment and Water Resources in Australia, the Waste and Resources Action Programme (WRAP) in UK have developed guidelines on the use of recycled aggregates. European Standards do not discriminate between various sources of aggregate, but examine their potential use in concrete.

- **Waste foundry sand (WFS)**: with high concentration of silica, it is potentially capable to increase mechanical properties when partially substituted (up to 30%) as fine aggregate [110]. Different structural grades can be achieved adopting higher WFS percentages [111].
- **Rubber waste**: can be adopted as aggregate, showing inferior splitting-tensile and compressive strength than ordinary concrete. However, it has higher ductile performances as it absorbs a larger quantity of plastic energy under dynamic actions [112].
- **Plastic waste**: plastic bottles and polythene bags can replace fine aggregate in lightweight concrete mixture. On one hand, sand-substitution reduces the compressive strength by 10-20% [113]; on the other hand, the workability improves [114].
- **Recycled coarse aggregate (RCA)**: derived from construction and demolition, can replace 100% of virgin quarry aggregates [115], but also improve the durability and the microstructure of traditional concrete. However, current use of RCA for structural applications is scarce [116].

6.2.1.3 3D Printing

Digital fabrication techniques combined with suitable cementitious materials have successfully led to the implementation of innovative manufacturing processes for concrete-like products [70]. We focus on the Layered Extrusion (LE) technology, since this technique has been already successful in the production of polymeric customized parts. LE is expected to revolutionize the concrete construction industry, mainly due to the following reasons [70]:

- freedom in terms of the design of shapes (enabling new aesthetic and functional features)
- reduction in construction time and expenses
- improved worker safety
- better quality and reliability
- material savings, and, consequently, sustainability

On the other hand, engineering challenges are several:

- larger machines requirements [32]
- design and characterization of materials
- implementation of reinforcement
- surface finishing
- formation of cold joints [41].

Moreover, fresh printed materials should satisfy specific rheological requirements in order to achieve an optimized balance between workability and extrudability, on the one hand – which would require reduced pumping forces – and the need for buildability (i.e. ability to stacked concrete layers) on the other – which would require an increased strength.

For small batch production (up to 10,000 items), the AM cost/production relationship is more affordable than injection molding (Fig. 6.5) [30]. Potential Layered Extrusion business areas related to construction sector are several as well, and are highlighted in Fig. 6.5.

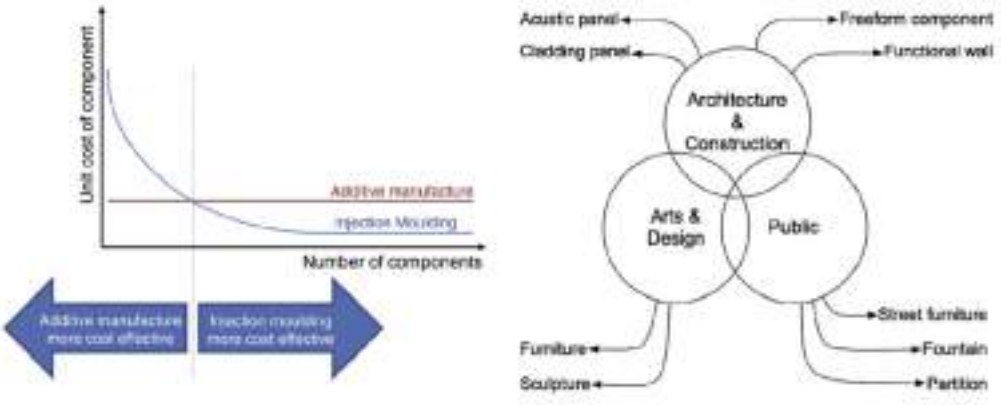

Figure 6.5: Diagram of cost case and applications for additive manufacturing, after [30].

In general, the equipment (Fig. 6.6) for LE technology is composed by [40]: 0. System command; 1. Robot controller; 2. Printing controller; 3. Robotic arm (Fig. 6.7, left) or Overhead crane (Fig. 6.7, right); 4. Printing head; 5. Accelerating agent; 6. Peristaltic pump for accelerating agent; 7. Peristaltic pump for premix; 8. Premix mixer; 9. 3D printed object.

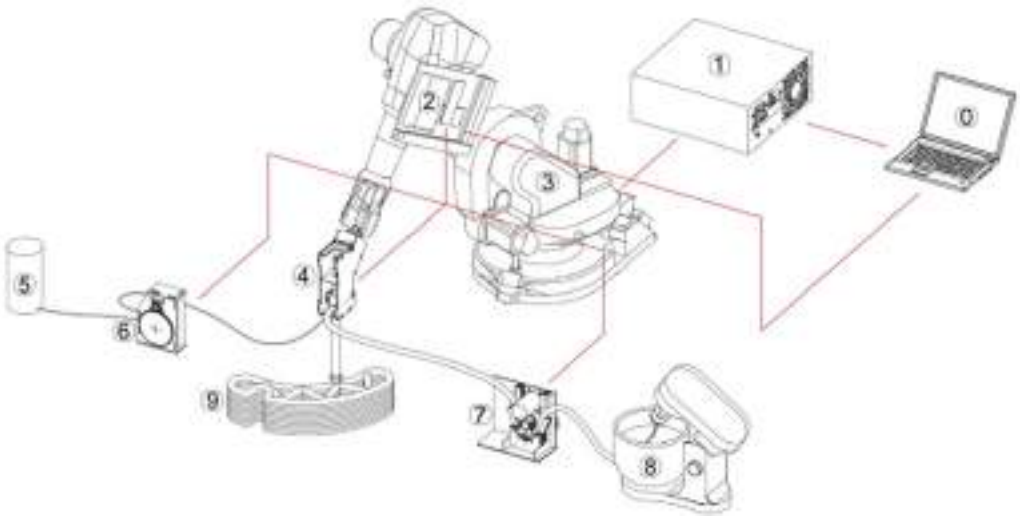

Figure 6.6: Schematic of the 3D printing setup, after [40].

3D printing of geopolymers

Several additives are studied to act as plasticizers (or superplasticizers). They can be divided into organic (charged particles) such as lignosulfonate (LS), polynaphthalene sulfonate (PNS), polycarboxylate ether (PCE), polymelamine sulphonates and vinyl copolymers; inorganic additives, namely clays (bentonite, montmorillonite, kaolinite, sepiolite, organic nanoclays...), polymeric fibers, either natural or artificial such as cellulose, polyvinyl acetate, polypropylene or polyethylene fibers. The latter group exhibits shear thinning (i.e. decrease of the apparent viscosity by increasing the shear rate) due to their opposing surface charges, which gives rise to a house of cards structure that can form at rest and break down under shear, whereas after extrusion they can be expected to help the material to remain in place. Just to mention the widespread possibilities of GP, the 3D printing of geopolymers are considered also by NASA for Moon and Mars construction building with lunar and Martian regolith [117].

Figure 6.7: Robotic arm (left, after [37]), Overhead crane (right, after [30].

6.2.1.4 Optimized Concrete Panels

European goals for the year 2030 show an increased interest in sustainability in general [118] with a major focus on energy efficiency of buildings, responsible for about 40% of the primary energy consumption [119]. As a response to this sustainability issue, EU measures introduced by Energy Performance Building Directive (EPBD) 2010/31/EU (as modified by Directive 2018/884) establish that new buildings should meet minimum energy performance requirements, introducing the concept of nearly zero-energy buildings (n-ZEB) identified as the reference target for new buildings starting from 2020. In Italy, residential buildings accounts for 57% of primary energy consumption, where space heating alone is responsible for 66% of the national energy balance in this sector. Specifically, in Lombardy, most of the primary energy demand comes from the residential sector (in particular, 68% for winter heating, 18% for electric uses, 9% for hot water supply and 5% for cooking [119]). Therefore, high energy-performance buildings are one of the challenges for regional public attention in terms of investments among key players of the building sector.

Source description	B(a)P (kg year−1)	(%)	Cumulative (%)
Residential heating, traditional stove–wood	1185	32%	32%
Residential heating, closed fireplaces–wood	853	23%	54%
Residential heating, open fireplaces–wood	708	19%	73%
Industrial combustion–biomass	282	7.50%	81%
Open burning of agriculture residue	204	5.40%	86%
Institutional and commercial heating, pizza oven–wood	110	2.90%	89%
Road transport–diesel	87	2.30%	91%
Residential heating, automatic pellets stove–wood	75	2.00%	93%
Residential heating, innovative stove–wood	58	1.60%	95%
Industrial combustion–coal	58	1.50%	96%
Secondary aluminum smelting	35	0.90%	97%
Forest fires	31	0.80%	98%
Industrial combustion–fuel oil	23	0.60%	99%
Other machinery–diesel	11	0.30%	99%
Fluid catalytic cracking	10	0.26%	99%
Road transport–gasoline	8.2	0.22%	100%
Tire and break wear	7.6	0.20%	100%
Steel production	4.9	0.13%	100%
Other metallurgical processes	1.9	0.05%	100%
Industrial waste incineration	1.4	0.04%	100%
Residential heating, small boilers–gas oil	1.2	0.03%	100%
Energy production, district heating–biomass	0.56	0.01%	100%
Off road transport–diesel	0.34	0.01%	100%
Institutional and commercial heating, small boilers–gas oil	0.2	0.01%	100%
Energy production–natural gas	0.16	0.00%	100%
Secondary lead smelting	0.12	0.00%	100%
Residential heating, small boilers–natural gas	0.12	0.00%	100%
Institutional and commercial heating, small boilers–natural gas	0.035	0.00%	100%
Agriculture waste incineration	0.016	0.00%	100%
Road transport–LPG	0.0079	0.00%	100%
Municipal solid waste incineration	0.0076	0.00%	100%
Road transport–natural gas	0.00023	0.00%	100%
TOTAL	**3758**	**100%**	

Figure 6.8: Emission of B(a)P pollutant in Lombardy, year 2008, after [120].

The idea is based on a multidisciplinary approach that starts from the following considerations:

- 3D concrete printing will transform today's architecture. This development has to consider sustainability issues, both for material and construction methods;
- Waste material and industrial by-product recycling is feasible and documented in construction mixings. However, no AM technologies are applied to waste-based concretes;
- Italian atmospheric particulate matter emission due to residential heating reaches its peak in Lombardy (Fig. 6.8, [120]);
- Advantages arising from 3D printing technology in construction can be employed to deal with Lombardy environmental challenges.

The key role for improving energy performances of buildings is played by their envelope; in this regard, it is widely recognized that outer walls mostly contribute to the envelope efficiency. We want face Lombardy's sustainability challenges through the development of optimized wall panels, to be integrated in low impact and highly efficient buildings, i.e. suitable for n-ZEB like buildings. In detail, the optimization will target the sustainable design of the printable mix; the shape of wall panels in terms of energy (i.e. by minimizing heat transmittance) and mechanical performances (i.e. by topological optimization) which will be produced through a 3D printing process and employed as units in customized walls for constructions. By monitoring the thermal flux at the internal/external surfaces of the wall, the shape optimization will improve the thermal resistance of the panels, by iterating the evolving topology of the panel itself. At the same time, the optimization will be completed with a number of topology changes, in order to get an improvement in construction technology and load bearing behavior. As an example, Fig. 6.9 shows the conceptual application of optimized concrete panels to the structure, designed to be long-lasting due to the foundational principles of modularity, disassemblability, recyclability and reparability.

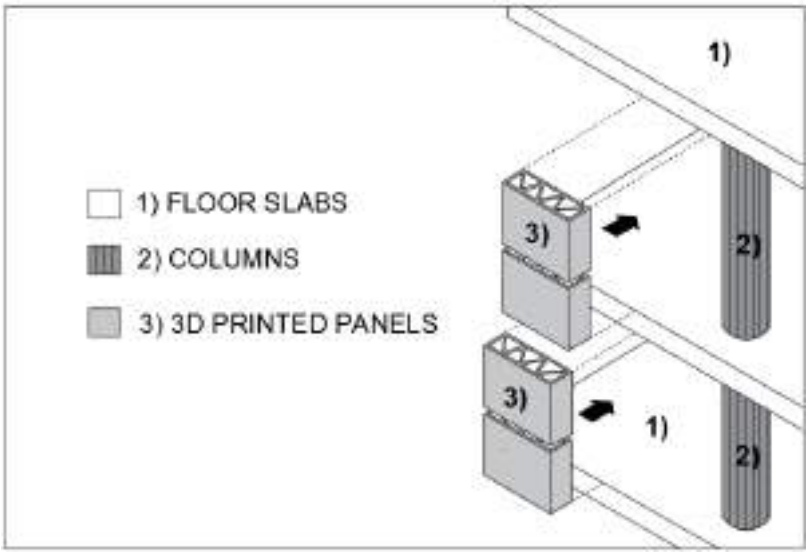

Figure 6.9: Sketch of optimized concrete panels and their application.

6.2.2 Impact

Circular economy reformulates economic activities through the 3Rs principle, i.e. Recycle (regenerating renewable resources), Reduce (decreasing residues and industrial by-products in the production and consumption processes) and Reuse (extending product and service life-cycle and lifespan). Therefore, shifting from the traditional one-way linear economy, defined by the "resource – product – waste" model, to the circular "resource – product – waste – renewable resource" model, maximal economic and social benefits are pursued through the minimal resource consumption and environmental costs. We shows an attractive application of circular economy principles, locally recycling available inputs (industrial by-products and waste) and integrating waste-reducing manufacturing technologies (3D printing) to reproduce physical artifacts (optimized concrete panels) that can be reused due to their modularity and disassemblability. The production of waste-based concrete composites, converting residues in revenues and opening to highly added-value activities in existing businesses, can be interesting for the virtuous industrial cluster in Lombardy. Indeed, Lombardy is a suitable area for developing scientifically and technologically cutting-edge initiatives due to the presence of academic and financial key actors, generating academic and non-academic spin-offs and increasing the potential of small and medium-size enterprises.

Recycle

Recycling of municipal waste in the EU, during the period 2008-2016 has increased, and the contribution of recycled materials to the demand of the overall material shows continuous improvements. However, on average, recycled materials only meet less than 12% of the EU demand for materials (source: COM(2019) n.190). For this reason, EU encourages the use of recycled materials and green concrete fulfills this requirement for two reasons: the use of waste material for the construction of the new product and the recyclability of the product at the end-of-life. Italy is the greatest rice producer in the EU-28 (Sorce: Ente Nazionale Risi - http://enterisi.it) and Lombardy is the second Italian Region (after Piedmont, with 105.000 ha), especially in Pavia, Milano and Vercelli areas (Fig. 6.10). Considering that husks represent the 20% of the rice refining chain waste products, Lombardy is also one of the main producers of rice husk ashes (RHA).

The sawmills of northern Lombardy may assure the Saw Dust Ash (SDA), as waste from wood use, as well as carpentry and construction, and products for wood packaging. Moreover, in Lombardy several plants could provide fly ash and the other secondary raw materials. The region is also a territory with a high number of waste-processing plants per capita (Fig. 6.11):

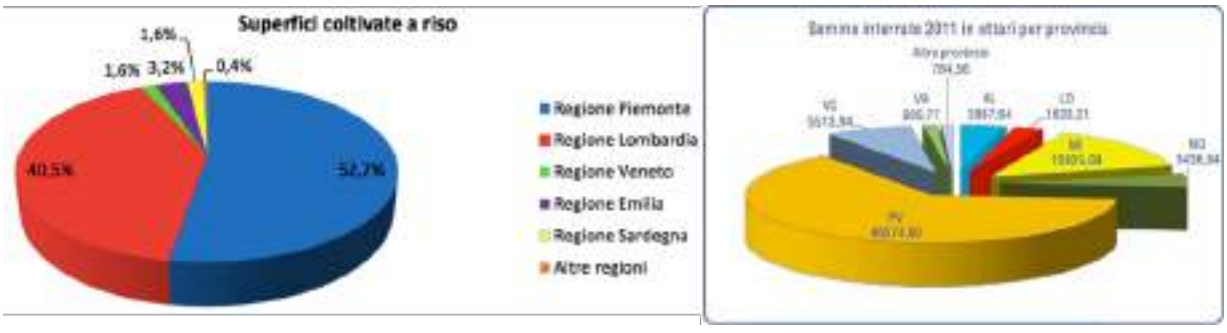

Figure 6.10: Italian rice cultivation – regional breakdown (2013). Source: Ente risi.

in detail 3279 waste-processing plants, of which 46 landfills, 45 incinerators and 618 waste-storage plants (Source: Ente Regione Lombardia - http:// www.cgrweb.servizirl.it), thus, solid waste incineration fly ash can be used for the cement production.

Moreover, although Lombardy has the biggest Italian recycling plant capacity (Fig. 6.12, left), it strongly contributes to exporting special waste outside the national borders. In this specific context, the impact on the waste-processing chain can be significative, promoting recycling of production residues (through a more efficient use of raw materials and dangerous waste cause of contamination) and a reduction in carbon emissions (as the production site

Figure 6.11: Lombardy waste-processing plants (2018). Source: Regione Lombardia.

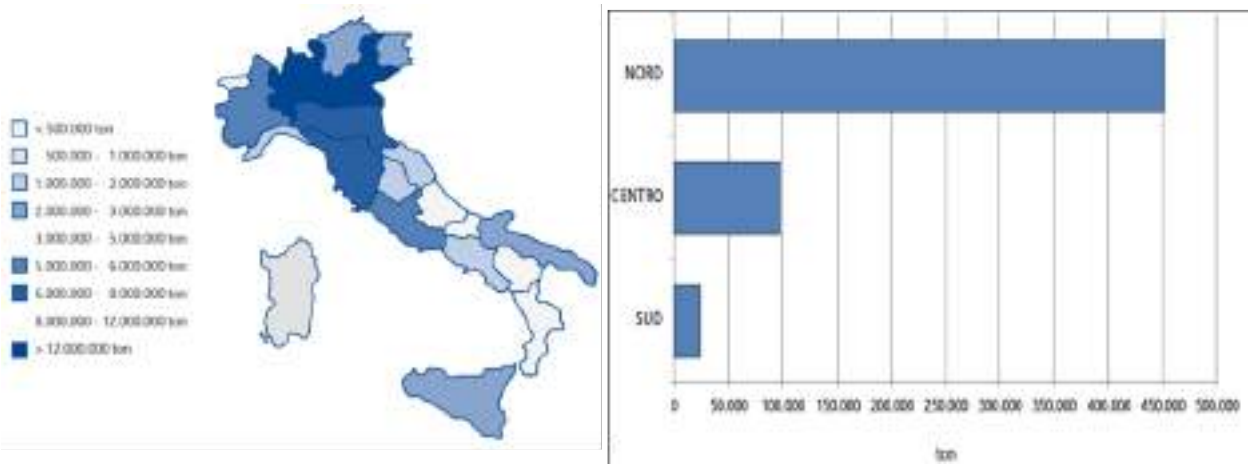

Figure 6.12: Italian recycling plant capacity (left) – Special waste export from Italy (right). Source: Ministero dell'Ambiente (2008).

will be closer to the consumer). In Northern Italy, even if the scenario is prosperous, the waste theme is divisive; however, interesting start-ups and commercial players are investing in the recycling sector, supporting sustainable and cheaper technologies currently generating profits and producing revenues for shareholders. In general, the active involvement of high-potential research players will be encouraged, in order to make leading-edge technologies more diffused, collaborative and closer to the society. The implementation of a green supply chain management can maximize the resource utilization, reduce the resource consumption and enhance Lombardy's national and international reputation, improving and promoting the compatibility between enterprises toward long-term economic and social benefits. According to the eco-design principle, panels can be designed as disassemblably products in order to reuse valuable materials and components of the products at the end-of-life. In this way, the circle of the recycle will not be stopped.

Reduce

Innovative manufacturing processes will be designed to adapt the most common and widespread 3D printing technologies (the Layered Extrusion) to the synthesis of advanced waste-based concrete materials. 3D printing technologies are progressively having massive impacts on manufacturing processes worldwide, representing a new industrial revolution for the mass customization of industrial products (Fig. 6.13). Even in construction engineering processes, digital fabrication techniques offer several competitive advantages respect to the more traditional ones, mainly due to reduction in: construction time and cost (for labor and formwork), geometrical shape restraints (freeform architectures), material waste (due to its intrinsic nature and especially with respect to formwork, optimizing the shape complexity) and unexpected events [37]. Moreover, since production of the modular parts will be localized and moved closer to the market, the carbon footprint of the whole production process will be reduced, as greenhouse gas emissions due to transport distribution and imports. Not to mention that the use of the 3D printing technology can lead, on the health and social side, to a reduction of accidents and deaths at work.

The production of 3D-printed waste-based concrete objects certainly represents a radically

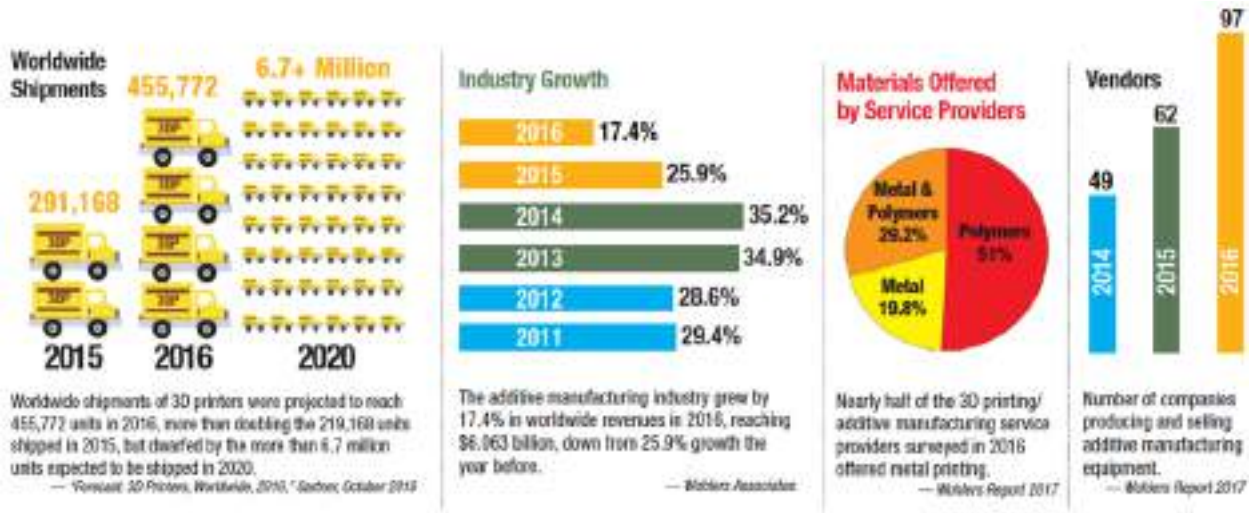

Figure 6.13: 3D Printing market snapshot, Source: Digital Engineering (2017).

new line of process. This project will provide the Proof-of-Principle of such a new scientific opportunity, completely defining the synthesis process and improving 3D printing facilities through the development of dedicated equipment.

Reuse

Our ambition is a concrete panel optimized in terms of energy and mechanical properties and generated by means of a 3D printing process, in conjunction with waste-based concrete materials, aiming to provide affordable and sustainable housing solutions. We will demonstrate to have a deep impact on manufacturing processes, through the fabrication of economic and customized parts that will be assembled in a customized living module, behind a simple idea: optimized design, recycled local materials, designed to be rapidly 3D printed and easy to assemble, compensating costs with mass production, toward a nearly zero-emission building. The panel is designed to transfer its housing role, due to the foundational principles of modularity, disassemblability, recyclability, reparability, maintenance, substitution and reuse. Once a product has been produced and located for the building construction, its lifetime can be extended through reuse and repair, hence avoiding wastage.

Bibliography

[1] J. Pegna, "Application of cementitious bulk materials to site processed solid freeform construction," in *1995 International Solid Freeform Fabrication Symposium*, 1995.

[2] J. Pegna, "Exploratory investigation of layered fabrication applied to construction automation," *Advances in design automation*, vol. 1, no. 21, pp. 219–226, 1995.

[3] X. Yan and P. Gu, "A review of rapid prototyping technologies and systems," *Computer-aided design*, vol. 28, no. 4, pp. 307–318, 1996.

[4] B. Khoshnevis, "Contour crafting a new rapid prototyping process," in *1997 Proceedings of The Seventh International Conference on Rapid Prototyping*, 1997.

[5] J. Pegna, "Exploratory investigation of solid freeform construction," *Automation in construction*, vol. 5, no. 5, pp. 427–437, 1997.

[6] D. T. Pham and R. S. Gault, "A comparison of rapid prototyping technologies," *International Journal of machine tools and manufacture*, vol. 38, no. 10-11, pp. 1257–1287, 1998.

[7] A. Warszawski and R. Navon, "Implementation of robotics in building: Current status and future prospects," *Journal of Construction Engineering and Management*, vol. 124, no. 1, pp. 31–41, 1998.

[8] J. Pegna, S. Pattofatto, R. Berge, C. Bangalan, H. Herring, M. LeSaux, and J. Engler, "The sand painter: two dimensional powder deposition," in *Proceedings on the Solid Freeform Fabrication Symposium, Austin, TX*, pp. 695–709, 1999.

[9] B. Kolarevic, "Digital fabrication: manufacturing architecture in the information age," 2001.

[10] B. Khoshnevis, S. Bukkapatnam, H. Kwon, and J. Saito, "Experimental investigation of contour crafting using ceramics materials," *Rapid Prototyping Journal*, vol. 7, no. 1, pp. 32–42, 2001.

[11] B. Khoshnevis and G. Bekey, "Automated construction using contour crafting – applications on earth and beyond," in *2002 Proceedings of the 19th ISARC, Washington, U.S.A*, pp. 489–495, 2002.

[12] B. Khoshnevis, "Toward total automation of on-site construction an integrated approach based on contour crafting," *Proceedings of ISARC*, pp. 61–66, 2003.

[13] D. Hwang, B. Khoshnevis, and E. Daniel, "Concrete wall fabrication by contour crafting," in *21st International Symposium on Automation and Robotics in Construction (ISARC 2004), Jeju, South Korea*, pp. 301–307, 2004.

[14] B. Khoshnevis, "Automated construction by contour crafting—related robotics and information technologies," *Automation in construction*, vol. 13, no. 1, pp. 5–19, 2004.

[15] B. Khoshnevis, M. Bodiford, K. Burks, E. Ethridge, D. Tucker, W. Kim, H. Toutanji, and M. Fiske, "Lunar contour crafting-a novel technique for isru-based habitat development," in *43rd AIAA Aerospace Sciences Meeting and Exhibit*, p. 538, 2005.

[16] D. Hwang and B. Khoshnevis, "An innovative construction process-contour crafting (cc)," in *22nd International Symposium on Automation and Robotics in Construction*, vol. 90111, 2005.

[17] B. Khoshnevis, D. Hwang, K.-T. Yao, Z. Yeh, *et al.*, "Mega-scale fabrication by contour crafting," *International Journal of Industrial and Systems Engineering*, vol. 1, no. 3, pp. 301–320, 2006.

[18] M. P. Bodiford, K. Burks, M. Perry, R. Cooper, and M. Fiske, "Lunar in situ materials-based habitat technology development efforts at nasa/msfc," in *Earth & Space 2006: Engineering, Construction, and Operations in Challenging Environment*, pp. 1–8, 2006.

[19] A. K. Kamrani and E. A. Nasr, *Rapid prototyping: theory and practice*, vol. 6. Springer Science & Business Media, 2006.

[20] J. Bassler, M. Bodiford, M. Hammond, R. King, C. Mclemore, N. Hall, M. Fiske, and J. Ray, "In situ fabrication and repair (isfr) technologies; new challenges for exploration," in *44th AIAA Aerospace Sciences Meeting and Exhibit*, p. 350, 2006.

[21] N. Hopkinson, R. Hague, and P. Dickens, "Rapid manufacturing," *An Industrial Revolution for the Digital Age. Chichister, England: John Wiley and Sons, Ltd*, 2006.

[22] R. A. Buswell, R. C. Soar, A. G. Gibb, and A. Thorpe, "Freeform construction: mega-scale rapid manufacturing for construction," *Automation in construction*, vol. 16, no. 2, pp. 224–231, 2007.

[23] R. A. Buswell, A. Thorpe, R. C. Soar, and A. G. Gibb, "Design, data and process issues for mega-scale rapid manufacturing machines used for construction," *Automation in Construction*, vol. 17, no. 8, pp. 923–929, 2008.

[24] D. M. L. Thrane, T. Andersen, and D. Mathiesen, "The use of robots and self-compacting concrete for unique concrete structures," *Tailor Made Concrete Structures-Walraven & Stoelhorst (eds)*, pp. 801–806, 2008.

[25] X. De Kestelier and R. Buswell, "A digital design environment for large- scale rapid manufacturing," in *Building a Better Tomorrow: Proceedings of the 29th Annual Conference of the Association for Computer Aided Design in Architecture (ACADIA)*, pp. 201–208, 2009.

[26] S. Lim, T. Le, J. Webster, R. Buswell, A. Austin, A. Gibb, and T. Thorpe, "Fabricating construction components using layered manufacturing technology," in *Global Innovation in Construction Conference*, pp. 512–520, 2009.

[27] J. Gardiner and M. Burry, "Dshape- construction scale additive manufacturing, reflection on current projects and the state of technology development," in *6th International Conference on Innovation in AEC 2009*, p. 305, 2009.

[28] S. Lim, R. A. Buswell, T. T. Le, R. Wackrow, S. A. Austin, A. G. Gibb, and T. Thorpe, "Development of a viable concrete printing process," 2011.

[29] J. Gardiner, "Exploring the emerging design territory of construction 3d printing-project led architectural research," 2011.

[30] S. Lim, R. A. Buswell, T. T. Le, S. A. Austin, A. G. Gibb, and T. Thorpe, "Developments in construction-scale additive manufacturing processes," *Automation in construction*, vol. 21, pp. 262–268, 2012.

[31] T. T. Le, S. A. Austin, S. Lim, R. A. Buswell, R. Law, A. G. Gibb, and T. Thorpe, "Hardened properties of high-performance printing concrete," *Cement and Concrete Research*, vol. 42, no. 3, pp. 558–566, 2012.

[32] T. T. Le, S. A. Austin, S. Lim, R. A. Buswell, A. G. F. Gibb, and A. Thorpe, "Mix design and fresh properties for high-performance printing concrete," *RILEM Materials & Structures*, vol. 45, no. 8, pp. 1221–1232, 2012.

[33] H. Lipson and M. Kurman, *Fabricated: The New World of 3D Printing*. Wiley Publishing, 1st ed., 2013.

[34] G. Cesaretti, E. Dini, X. D. Kestelier, V. Colla, and L. Pambaguian, "Building components for an outpost on the lunar soil by means of a novel 3d printing technology," *Acta Astronautica*, vol. 93, pp. 430 – 450, 2014.

[35] R. Wolfs, T. Salet, and B. Hendriks, "3d printing of sustainable concrete structures," *Proceedings of IASS Annual Symposia*, vol. 2015, no. 2, pp. 1–8, 2015.

[36] E. Lloret, A. R. Shahab, M. Linus, R. J. Flatt, F. Gramazio, M. Kohler, and S. Langenberg, "Complex concrete structures: merging existing casting techniques with digital fabrication," *Computer-Aided Design*, vol. 60, pp. 40–49, 2015.

[37] T. Wangler, E. Lloret, L. Reiter, N. Hack, F. Gramazio, M. Kohler, M. Bernhard, B. Dillenburger, J. Buchli, N. Roussel, *et al.*, "Digital concrete: opportunities and challenges," *RILEM Technical Letters*, vol. 1, pp. 67–75, 2016.

[38] I. Hager, A. Golonka, and R. Putanowicz, "3d printing of buildings and building components as the future of sustainable construction?," *Procedia Engineering*, vol. 151, pp. 292–299, 2016.

[39] F. Bos, R. Wolfs, Z. Ahmed, and T. Salet, "Additive manufacturing of concrete in construction: potentials and challenges of 3d concrete printing," *Virtual and Physical Prototyping*, vol. 11, no. 3, pp. 209–225, 2016.

[40] C. Gosselin, R. Duballet, P. Roux, N. Gaudillière, J. Dirrenberger, and P. Morel, "Large-scale 3d printing of ultra-high performance concrete–a new processing route for architects and builders," *Materials & Design*, vol. 100, pp. 102–109, 2016.

[41] A. Perrot, D. Rangeard, and A. Pierre, "Structural built-up of cement-based materials used for 3d-printing extrusion techniques," *Materials and Structures*, vol. 49, no. 4, pp. 1213–1220, 2016.

[42] S. Lim, R. A. Buswell, P. J. Valentine, D. Piker, S. A. Austin, and X. De Kestelier, "Modelling curved-layered printing paths for fabricating large-scale construction components," *Additive Manufacturing*, vol. 12, pp. 216–230, 2016.

[43] A. Kazemian, X. Yuan, E. Cochran, and B. Khoshnevis, "Cementitious materials for construction-scale 3d printing: Laboratory testing of fresh printing mixture," *Construction and Building Materials*, vol. 145, pp. 639–647, 2017.

[44] Y. W. D. Tay, B. Panda, S. C. Paul, N. A. Noor Mohamed, M. J. Tan, and K. F. Leong, "3d printing trends in building and construction industry: a review," *Virtual and Physical Prototyping*, vol. 12, no. 3, pp. 261–276, 2017.

[45] B. Panda, S. C. Paul, and M. J. Tan, "Anisotropic mechanical performance of 3d printed fiber reinforced sustainable construction material," *Materials Letters*, vol. 209, pp. 146–149, 2017.

[46] R. Duballet, O. Baverel, and J. Dirrenberger, "Classification of building systems for concrete 3d printing," *Automation in Construction*, vol. 83, pp. 247–258, 2017.

[47] F. Bos, Z. Ahmed, E. Jutinov, and T. Salet, "Experimental exploration of metal cable as reinforcement in 3d printed concrete," *Materials*, vol. 10, no. 11, p. 1314, 2017.

[48] A. Kazemian, X. Yuan, R. Meier, E. Cochran, and B. Khoshnevis, "Construction-scale 3d printing: shape stability of fresh printing concrete," in *ASME 2017 12th International Manufacturing Science and Engineering Conference collocated with the JSME/ASME 2017 6th International Conference on Materials and Processing*, pp. V002T01A011–V002T01A011, American Society of Mechanical Engineers, 2017.

[49] R. A. Buswell, W. L. de Silva, S. Jones, and J. Dirrenberger, "3d printing using concrete extrusion: A roadmap for research," *Cement and Concrete Research*, vol. 112, pp. 37–49, 2018.

[50] R. Wolfs, F. Bos, and T. Salet, "Early age mechanical behaviour of 3d printed concrete: Numerical modelling and experimental testing," *Cement and Concrete Research*, vol. 106, pp. 103–116, 2018.

[51] B. Panda and M. J. Tan, "Experimental study on mix proportion and fresh properties of fly ash based geopolymer for 3d concrete printing," *Ceramics International*, vol. 44, no. 9, pp. 10258–10265, 2018.

[52] B. Panda, S. C. Paul, N. A. N. Mohamed, Y. W. D. Tay, and M. J. Tan, "Measurement of tensile bond strength of 3d printed geopolymer mortar," *Measurement*, vol. 113, pp. 108–116, 2018.

[53] S. C. Paul, Y. W. D. Tay, B. Panda, and M. J. Tan, "Fresh and hardened properties of 3d printable cementitious materials for building and construction," *Archives of civil and mechanical engineering*, vol. 18, no. 1, pp. 311–319, 2018.

[54] G. De Schutter, K. Lesage, V. Mechtcherine, V. N. Nerella, G. Habert, and I. Agusti-Juan, "Vision of 3d printing with concrete—technical, economic and environmental potentials," *Cement and Concrete Research*, vol. 112, pp. 25–36, 2018.

[55] M. Comstock, C. Garrigan, S. Pouffary, T. d. Feraudy, J. Halcomb, and J. Hartke, "Building design and construction: Forging resource efficiency and sustainable development," *United National Environmental Program (UNEP)*, p. 1, 2012.

[56] S. Ford and M. Despeisse, "Additive manufacturing and sustainability: an exploratory study of the advantages and challenges," *Journal of Cleaner Production*, vol. 137, pp. 1573–1587, 2016.

[57] N. Roussel, "Rheological requirements for printable concretes," *Cement and Concrete Research*, vol. 112, pp. 76–85, 2018.

[58] G. Ma and L. Wang, "A critical review of preparation design and workability measurement of concrete material for largescale 3d printing," *Frontiers of Structural and Civil Engineering*, vol. 12, no. 3, pp. 382–400, 2018.

[59] Z. Zhang, B. Zhang, and P. Yan, "Comparative study of effect of raw and densified silica fume in the paste, mortar and concrete," *Construction and Building Materials*, vol. 105, pp. 82–93, 2016.

[60] E. Güneyisi, "Fresh properties of self-compacting rubberized concrete incorporated with fly ash," *Materials and structures*, vol. 43, no. 8, pp. 1037–1048, 2010.

[61] V. Vishwakarma and D. Ramachandran, "Green concrete mix using solid waste and nanoparticles as alternatives–a review," *Construction and Building Materials*, vol. 162, pp. 96–103, 2018.

[62] M. Bouasker, P. Mounanga, P. Turcry, A. Loukili, and A. Khelidj, "Chemical shrinkage of cement pastes and mortars at very early age: Effect of limestone filler and granular inclusions," *Cement and Concrete Composites*, vol. 30, no. 1, pp. 13–22, 2008.

[63] J. Björnström, A. Martinelli, A. Matic, L. Börjesson, and I. Panas, "Accelerating effects of colloidal nano-silica for beneficial calcium–silicate–hydrate formation in cement," *Chemical Physics Letters*, vol. 392, no. 1-3, pp. 242–248, 2004.

[64] L. N. Thrane, C. Pade, and C. V. Nielsen, "Determination of rheology of self-consolidating concrete using the 4c-rheometer and how to make use of the results," *Journal of ASTM International*, vol. 7, no. 1, pp. 1–10, 2009.

[65] T. Voigt, T. Malonn, and S. P. Shah, "Green and early age compressive strength of extruded cement mortar monitored with compression tests and ultrasonic techniques," *Cement and Concrete Research*, vol. 36, no. 5, pp. 858–867, 2006.

[66] V. N. Nerella, M. Krause, and V. Mechtcherine, "Practice-oriented buildability criteria for developing 3d-printable concretes in the context of digital construction," 2018.

[67] P. Feng, X. Meng, J.-F. Chen, and L. Ye, "Mechanical properties of structures 3d printed with cementitious powders," *Construction and Building Materials*, vol. 93, pp. 486–497, 2015.

[68] R. Wolfs, F. Bos, and T. Salet, "Hardened properties of 3d printed concrete: The influence of process parameters on interlayer adhesion," *Cement and Concrete Research*, vol. 119, pp. 132–140, 2019.

[69] R. Wolfs, F. Bos, and T. Salet, "Triaxial compression testing on early age concrete for numerical analysis of 3d concrete printing," *Cement and Concrete Composites*, p. 103344, 2019.

[70] D. Asprone, F. Auricchio, C. Menna, and V. Mercuri, "3d printing of reinforced concrete elements: Technology and design approach," *Construction and Building Materials*, vol. 165, pp. 218–231, 2018.

[71] R. J. Thomas and A. D. Sorensen, "Review of strain rate effects for uhpc in tension," *Construction and Building Materials*, vol. 153, pp. 846–856, 2017.

[72] H. Schuler, C. Mayrhofer, and K. Thoma, "Spall experiments for the measurement of the tensile strength and fracture energy of concrete at high strain rates," *International Journal of Impact Engineering*, vol. 32, no. 10, pp. 1635–1650, 2006.

[73] Z. P. Bazant, *Mathematical modeling of creep and shrinkage of concrete*. Wiley, 1988.

[74] S. Shh, M. Krguller, and M. Sarigaphuti, "Effects of shrinkage-reducing admixtures on restrained shrinkage cracking of concrete," *Materials Journal*, vol. 89, no. 3, pp. 289–295, 1992.

[75] E. E. Holt, *Early age autogenous shrinkage of concrete*, vol. 446. Technical Research Centre of Finland Espoo, Finland, 2001.

[76] M. Briffaut, F. Benboudjema, J.-M. Torrenti, and G. Nahas, "Concrete early age basic creep: Experiments and test of rheological modelling approaches," *Construction and Building Materials*, vol. 36, pp. 373–380, 2012.

[77] L. Maia and J. Figueiras, "Early-age creep deformation of a high strength self-compacting concrete," *Construction and Building Materials*, vol. 34, pp. 602–610, 2012.

[78] B. Han, H.-B. Xie, L. Zhu, and P. Jiang, "Nonlinear model for early age creep of concrete under compression strains," *Construction and Building Materials*, vol. 147, pp. 203–211, 2017.

[79] D. S. Atrushi, *Tensile and compressive creep of young concrete: Testing and modelling*. Fakultet for ingeniørvitenskap og teknologi, 2003.

[80] I. Khan, T. Xu, A. Castel, and R. I. Gilbert, "Early-age tensile creep and shrinkage induced cracking in internally restrained concrete members," *Magazine of Concrete Research*, pp. 1–13, 2018.

[81] A. Leemann, P. Lura, and R. Loser, "Shrinkage and creep of scc–the influence of paste volume and binder composition," *Construction and Building Materials*, vol. 25, no. 5, pp. 2283–2289, 2011.

[82] E. Rozière, S. Granger, P. Turcry, and A. Loukili, "Influence of paste volume on shrinkage cracking and fracture properties of self-compacting concrete," *Cement and concrete composites*, vol. 29, no. 8, pp. 626–636, 2007.

[83] G. De Schutter, "Degree of hydration based kelvin model for the basic creep of early age concrete," *Materials and Structures*, vol. 32, no. 4, p. 260, 1999.

[84] A. Niyogi, P. Hsu, and B. Meyers, "The influence of age at time of loading on basic and drying creep," *Cement and Concrete Research*, vol. 3, no. 5, pp. 633–644, 1973.

[85] L. Østergaard, D. A. Lange, S. A. Altoubat, and H. Stang, "Tensile basic creep of early-age concrete under constant load," *Cement and concrete research*, vol. 31, no. 12, pp. 1895–1899, 2001.

[86] R. Ghosh, "Creep of portland cement paste at early ages," *Matériaux et Construction*, vol. 5, no. 2, pp. 93–97, 1972.

[87] F. De Larrard, C. Ferraris, and T. Sedran, "Fresh concrete: a herschel-bulkley material," *Materials and structures*, vol. 31, no. 7, pp. 494–498, 1998.

[88] G. H. Tattersall and P. F. Banfill, *The rheology of fresh concrete*. No. Monograph, 1983.

[89] B. Sabir, S. Wild, and J. Bai, "Metakaolin and calcined clays as pozzolans for concrete: a review," *Cement and concrete composites*, vol. 23, no. 6, pp. 441–454, 2001.

[90] D. N. Huntzinger and T. D. Eatmon, "A life-cycle assessment of portland cement manufacturing: comparing the traditional process with alternative technologies," *Journal of Cleaner Production*, vol. 17, no. 7, pp. 668–675, 2009.

[91] A. Hasanbeigi, L. Price, and E. Lin, "Emerging energy-efficiency and co2 emission-reduction technologies for cement and concrete production: A technical review," *Renewable and Sustainable Energy Reviews*, vol. 16, no. 8, pp. 6220–6238, 2012.

[92] C. Meyer, "The greening of the concrete industry," *Cement and concrete composites*, vol. 31, no. 8, pp. 601–605, 2009.

[93] V. M. Malhotra and P. K. Mehta, *Pozzolanic and cementitious materials*. Crc Press, 2004.

[94] M. N. Al-Khalaf and H. A. Yousif, "Use of rice husk ash in concrete," *International Journal of Cement Composites and Lightweight Concrete*, vol. 6, no. 4, pp. 241–248, 1984.

[95] J. Rajput, R. Yadav, and R. Chandak, "The effect of rice husk ash used as supplementary cementing material on strength of mortar," *International Journal of Engineering Research and Applications*, vol. 3, no. 3, pp. 133–136, 2013.

[96] F. F. Udoeyo, H. Inyang, D. T. Young, and E. E. Oparadu, "Potential of wood waste ash as an additive in concrete," *Journal of materials in civil engineering*, vol. 18, no. 4, pp. 605–611, 2006.

[97] C. B. Cheah and M. Ramli, "The implementation of wood waste ash as a partial cement replacement material in the production of structural grade concrete and mortar: An overview," *Resources, Conservation and Recycling*, vol. 55, no. 7, pp. 669–685, 2011.

[98] M. M. Johari, A. Zeyad, N. M. Bunnori, and K. Ariffin, "Engineering and transport properties of high-strength green concrete containing high volume of ultrafine palm oil fuel ash," *Construction and Building Materials*, vol. 30, pp. 281–288, 2012.

[99] S. K. Lim, C. S. Tan, O. Y. Lim, and Y. L. Lee, "Fresh and hardened properties of lightweight foamed concrete with palm oil fuel ash as filler," *Construction and Building Materials*, vol. 46, pp. 39–47, 2013.

[100] A. K. Saha, "Effect of class f fly ash on the durability properties of concrete," *Sustainable Environment Research*, vol. 28, no. 1, pp. 25–31, 2018.

[101] P. Nath, P. K. Sarker, and W. K. Biswas, "Effect of fly ash on the service life, carbon footprint and embodied energy of high strength concrete in the marine environment," *Energy and Buildings*, vol. 158, pp. 1694–1702, 2018.

[102] R. Siddique and D. Kaur, "Properties of concrete containing ground granulated blast furnace slag (ggbfs) at elevated temperatures," *Journal of Advanced Research*, vol. 3, no. 1, pp. 45–51, 2012.

[103] C.-S. Poon, S. Kou, and L. Lam, "Compressive strength, chloride diffusivity and pore structure of high performance metakaolin and silica fume concrete," *Construction and building materials*, vol. 20, no. 10, pp. 858–865, 2006.

[104] S. Bhanja and B. Sengupta, "Influence of silica fume on the tensile strength of concrete," *Cement and Concrete Research*, vol. 35, no. 4, pp. 743–747, 2005.

[105] L. K. Turner and F. G. Collins, "Carbon dioxide equivalent (co2-e) emissions: A comparison between geopolymer and opc cement concrete," *Construction and Building Materials*, vol. 43, pp. 125–130, 2013.

[106] H. Cheng Yong, Y. M. Liew, M. M. Al Bakri Abdullah, and K. Hussin, "Fire resistant properties of geopolymers: A review," in *Key Engineering Materials*, vol. 660, pp. 39–43, Trans Tech Publ, 2015.

[107] F. Pacheco-Torgal, "Introduction to handbook of alkali-activated cements, mortars and concretes," in *Handbook of alkali-activated cements, mortars and concretes*, pp. 1–16, Elsevier, 2015.

[108] T. Suwan, M. Fan, and N. Braimah, "Internal heat liberation and strength development of self-cured geopolymers in ambient curing conditions," *Construction and Building Materials*, vol. 114, pp. 297–306, 2016.

[109] T. C. Hansen and H. Narud, "Strength of recycled concrete made from crushed concrete coarse aggregate," *Concrete International*, vol. 5, no. 1, pp. 79–83, 1983.

[110] Y. Aggarwal and R. Siddique, "Microstructure and properties of concrete using bottom ash and waste foundry sand as partial replacement of fine aggregates," *Construction and Building Materials*, vol. 54, pp. 210–223, 2014.

[111] E. P. Salokhe and D. Desai, "Application of foundry waste sand in manufacture of concrete," *IOSRJMCE, ISSN*, pp. 2278–1684, 2013.

[112] M. Bignozzi and F. Sandrolini, "Tyre rubber waste recycling in self-compacting concrete," *Cement and concrete research*, vol. 36, no. 4, pp. 735–739, 2006.

[113] Z. Z. Ismail and E. A. Al-Hashmi, "Use of waste plastic in concrete mixture as aggregate replacement," *Waste management*, vol. 28, no. 11, pp. 2041–2047, 2008.

[114] P. Asokan, M. Osmani, and A. D. Price, "Assessing the recycling potential of glass fibre reinforced plastic waste in concrete and cement composites," *Journal of Cleaner Production*, vol. 17, no. 9, pp. 821–829, 2009.

[115] S. B. Huda and M. S. Alam, "Mechanical behavior of three generations of 100% repeated recycled coarse aggregate concrete," *Construction and Building Materials*, vol. 65, pp. 574–582, 2014.

[116] E. Güneyisi, M. Gesoglu, Z. Algın, and H. Yazıcı, "Rheological and fresh properties of self-compacting concretes containing coarse and fine recycled concrete aggregates," *Construction and Building Materials*, vol. 113, pp. 622–630, 2016.

[117] A. Alexiadis, F. Alberini, and M. E. Meyer, "Geopolymers from lunar and martian soil simulants," *Advances in Space Research*, vol. 59, no. 1, pp. 490–495, 2017.

[118] W. Colglazier, "Sustainable development agenda: 2030," *Science*, vol. 349, no. 6252, pp. 1048–1050, 2015.

[119] L. Sarto, A. Galante, G. Pasetti, *et al.*, "Comparison between predicted and actual energy performance for winter heating in high-performance residential buildings in the lombardy region (italy)," *Energy and buildings*, vol. 47, pp. 247–253, 2012.

[120] V. Gianelle, C. Colombi, S. Caserini, S. Ozgen, S. Galante, A. Marongiu, and G. Lanzani, "Benzo (a) pyrene air concentrations and emission inventory in lombardy region, italy," *Atmospheric Pollution Research*, vol. 4, no. 3, pp. 257–266, 2013.

[121] A. Papagiannakis, A. Abbas, and E. Masad, "Micromechanical analysis of viscoelastic properties of asphalt concretes," *Transportation Research Record*, vol. 1789, no. 1, pp. 113–120, 2002.